Investigations of the Origin of Stereocontrol in Syndiospecific Ziegler-Natta Polymerizations

Thesis by

Deanna Lynn Zubris

In Partial Fulfillment of the Requirements for the
Degree of Doctor of Philosophy

Division of Chemistry and Chemical Engineering
California Institute of Technology
Pasadena, California

2001
(Submitted July 10, 2000)

For Mom and Dad

Acknowledgments

My five years at Caltech have been a huge learning experience for me on both a scientific and personal level. This brief section expresses some of my gratitude for those who have helped me along the way.

John Bercaw has helped me to learn a great deal of chemistry and really enjoy doing it by providing a challenging intellectual environment. Throughout my time at Caltech he has been a compassionate listener and friend and for this I will always be grateful. My committee members Bob Grubbs, Harry Gray, and Doug Rees have also provided helpful suggestions and advice. It was especially fun to organize Organometallics talks with Harry around to spice things up. I would also like to thank Gui Bazan, Rich Eisenberg and Bill Jones for urging me to consider Caltech for graduate school while I was an undergraduate at the University of Rochester.

Starting out in the Bercaw group I was very fortunate to get teamed up with Tim Herzog. He showed me the ropes on the vacuum line and despite his tendency to store items out of my reach he was a great line mate and friend. Talking chemistry with Tim and Dario Veghini was invaluable to me as a new graduate student. Dario's charm, honesty, and sense of humor made him a wonderful confidant. Although I enjoyed having Shannon Stahl around for late night chats and his strong convictions regarding birthday celebrations, I admit that I was excited to assume his prime desk location when he finished at Caltech. And while Mike Abrams was initially apprehensive about sharing the Nook™ with a "chick", he seemed to really warm up to my lists of "things to be happy about". Mike also did a great job of helping me to pick out a monstrous pair of hiking boots and related gear for the group hike I attended with John, Dario, Chris and Jennifer Levy, and Arnel Fajardo.

My labmates really defined my experience in the Bercaw group. I'm glad that Steve Miller was there to provide me with back-up on the softball field, as a fellow TA, and in the lab. Most of my ups and downs at Caltech were shared with Paul Chirik and I'm thankful for his genuine support and encouragement. Susan Schofer has been a great linemate and I'm pretty sure she doesn't realize how important her friendship was for maintaining my sanity in the lab. Chris Jones (Boss #3) was a fun addition to the lab and hopefully he won't tease my sister too much at Georgia Tech. Best of luck to my newest labmates, Sara Klamo and Endy Min. Also, best wishes to Lily Ackermann in her admirable

pursuit of group 5 *ansa*-metallocenes. Their fresh enthusiasm was a boost to me as I was in the home stretch of my thesis work.

My time in the Bercaw group has been shared with a very diverse group of people and I would like to acknowledge some of them here. I'm grateful for Chris (Theory) Brandow's upbeat attitude and ability to bring out the best in people. I appreciate John Scollard giving me a shoulder to cry on (often literally) and for supporting my love of Snoopy. Antek Wong-Foy was also there to lend me a hand when I needed it. Andy Kiely, Cory Nelson, Jim Gilchrist, Matt Holtcamp, Jeff Yoder, Shigenobu Miyake, Ola Wendt, Seva Rostovstev, and Chris Levy are other "Hogs" who have helped me along the way. While not technically a "Hog" (due to an apparent aversion to softball) I've also had helpful talks with Joseph Sadighi.

Caltech is a pretty incredible place to be a graduate student in part due to a few people who work hard to keep things running smoothly. Dian Buchness and Pat Anderson have both been very helpful and especially understanding when I needed to vent my frustrations. My time in the lab was a lot easier due to Rick Gerhart's ability to compensate for my clumsiness with a glass blowing torch and Mike Roy's assistance with blue box repairs. Larry Henling and Mike Day were helpful for obtaining X-ray diffraction data. Despite many ugly, misshapen crystals Larry still managed to provide me with all of the information I needed when I needed it along with well-timed, free snacks.

I'm very grateful to my friends who have provided me with much needed breaks from the laboratory and helped to keep me grounded. The Caltech Masters Swim Club was a welcome reprieve after many tough days in the lab; Laurie and Dan Stein and coaches Kenny Grace and Mo Salama provided me with laughs and friendship. I've shared many of my grad school experiences with the "chick lunch" gang Aileen Kua, Claudine Chen, and Liz Krider. Aileen's thoughtful and kind nature and Liz's encouragement to "let my light shine" helped to keep me going. Magali Billen has been a caring friend through many of my tough times at Caltech and I hope that our paths cross again in the future. Fred Miller, Sarah Lorenz, and Kary Caccamise have been my constant cheerleaders and their friendship has helped me to believe in myself. Even though our lives are always moving in different directions I know they will always be my friends.

Lastly I would like to acknowledge my parents, Donald and Sharon Zubris, and my sister Melissa for their constant support and love. I can't thank them enough for helping to me make it this far.

Abstract

In order to expand our understanding of the mechanism of stereocontrol in syndiospecific α-olefin polymerization, a family of *Cs*-symmetric, *ansa*-group 3 metallocenes was targeted as polymerization catalysts. The syntheses of new *ansa*-yttrocene and scandocene derivatives that employ the doubly [$SiMe_2$]-bridged ligand array (1,2-$SiMe_2$)$_2${C_5H_2-4-R}{C_5H-3,5-($CHMe_2$)$_2$} (where R = *t*-butyl, tBuThp; where R = *i*-propyl, iPrThp) are described. The structures of tBuThpY(μ-Cl)$_2$K(THF)$_2$, tBuThpSc(μ-Cl)$_2$K(Et_2O)$_2$, tBuThpYCH($SiMe_3$)$_2$, Y$_2${μ$_2$-(tBuThp)$_2$}$_2$(μ$_2$-H)$_2$, and tBuThpSc(μ-CH_3)$_2$Al(CH_3)$_2$ have been examined by single crystal X-ray diffraction methods. *Ansa*-yttrocenes and scandocenes that incorporate the singly [CPh_2]-bridged ligand array (CPh_2)(C_5H_4)($C_{13}H_8$) (where C_5H_4 = Cp, cyclopentadienyl; where $C_{13}H_8$ = Flu, fluorenyl) have also been prepared. Select metallocene alkyl complexes are active single component catalysts for homopolymerization of propylene and 1-pentene. The scandocene tetramethylaluminate complexes generate polymers with the highest molecular weights of the series. Under all conditions examined atactic polymer microstructures are observed, suggesting a chain-end mechanism for stereocontrol.

A series of *ansa*-tantalocenes have been prepared as models for Ziegler-Natta polymerization catalysts. A singly bridged *ansa*-tantalocene trimethyl complex, $Me_2Si(\eta^5\text{-}C_5H_4)_2TaMe_3$, has been prepared and used for the synthesis of a tantalocene ethylene-methyl complex. Addition of propylene to this ethylene-methyl adduct results in olefin exchange to give a mixture of *endo* and *exo* propylene isomers. Doubly-silylene bridged *ansa*-tantalocene complexes have been prepared with the tBuThp ligand; a tantalocene trimethyl complex and a tantalocene methylidene-methyl complex have been synthesized and characterized by X-ray diffraction. Thermolysis of the methylidene-methyl complex affords the corresponding ethylene-hydride complex. Addition of either propylene or styrene to this ethylene-hydride compound results in olefin exchange. In both cases, only one product isomer is observed. Studies of olefin exchange with *ansa*-tantalocene olefin-hydride and olefin-methyl complexes have provided information about the important steric influences for olefin coordination in Ziegler-Natta polymerization.

Investigations of the Origin of Stereocontrol in Syndiospecific Ziegler-Natta Polymerizations

TABLE OF CONTENTS

List of Figures

Chapter 1:

List of Tables

Chapter 1:

Chapter 2:

Chapter 1

Synthesis of C_S- Symmetric Group 3 Metallocenes as Catalysts for α-Olefin Polymerization

Abstract

The preparation of a series of C_s-symmetric yttrocene and scandocene complexes incorporating the doubly (silylene-bridged) ligand array, (1,2-$SiMe_2)_2$[4-R-C_5H_2][3,5-$(CHMe_2)_2$-C_5H] (RThp), is described. Reaction of K_2RThp (where R = *t*-butyl or *i*-propyl) with $MCl_3(THF)_n$ (where M = Y, n = 3.5; M = Sc, n = 3) affords the corresponding metallocene chloride complexes tBuThpY(μ-$Cl)_2K(THF)_n$, tBuThpSc(μ-$Cl)_2K(THF)_n$, and iPrThpY(μ-$Cl)_2K(THF)_n$ (where $0 \leq n \leq 2$). The analogous scandocene bromide complex, iPrThpSc(μ-$Br)_2K(THF)_n$, has also been prepared. Reaction of tBuThpY(μ-$Cl)_2K(THF)_n$ with NaI and subsequent metathesis with $KCH(SiMe_3)_2$ provides a bis(trimethylsilyl)methyl yttrocene complex, tBuThpYCH$(TMS)_2$. Hydrogenation of tBuThpYCH$(TMS)_2$ provides a mixture of two dimeric yttrocene hydride complexes, Y{μ-$(tBuThp)_2(\mu\text{-}H)_2$}Y. One of these hydride complexes has been characterized by X-ray diffraction; each ligand array spans two metal centers in a "fly-over" dimeric structure. Combination of RThpM(μ-$X)_2K(THF)_n$ (where M = Y, Sc; R = tBu, iPr; X = Cl , Br) with $LiAlMe_4$ affords the corresponding tetramethylaluminate complexes RThpM(μ-$Me)_2AlMe_2$ (where M = Y, Sc; R = tBu, iPr). Scandocene and yttrocene tetramethylaluminate complexes that employ a singly linked cyclopentadienyl-fluorenyl ligand, $[(C_6H_5)_2C\{(\eta^5\text{-}C_5H_4)(\eta^5\text{-fluorenyl})\}]M(\mu\text{-}Me)_2AlMe_2$ (where M = Y, Sc), have been prepared via a similar methodology.

Select tetramethylaluminate complexes serve as single component polymerization catalysts for the polymerization of 1-pentene and propylene. Use of these catalysts under a variety of conditions yields polymers with essentially atactic microstructures with a continuum of tacticities that range from a slight syndiotactic preference ($[r] \approx 68\%$) to a slight isotactic preference ($[m] \approx 67\%$). This data is consistent with a chain-end control mechanism. These C_s-symmetric group 3 catalysts follow a stereocontrol mechanism unlike what has been observed for analogous zirconocene catalysts.

Introduction

The use of metallocenes as catalysts for ethylene and α-olefin polymerization is an area of intense investigation for academic and industrial chemists alike.[1] Homogeneous Ziegler-Natta catalysts (neutral group 3 and cationic group 4 metallocenes and their derivatives, see Figure 1) excel at the homopolymerization and copolymerization of these monomers.

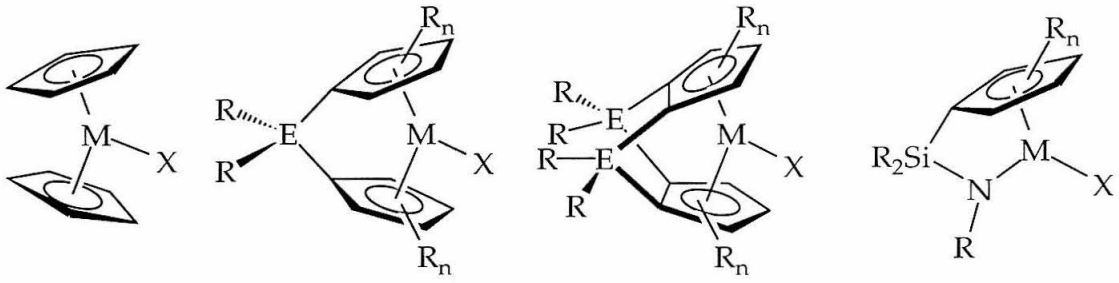

where M = Ti^+, Zr^+, Sc, Y, La

X = alkyl, H; E = C, Si; R = alkyl, aryl

Figure 1: Various metallocenes (unlinked, singly bridged, and doubly bridged) and an *ansa*-monocyclopentadienyl-amido complex can be utilized as α-olefin polymerization catalysts.

The predictable correlation between metallocene structure and polypropylene tacticity is one of the most striking features of these polymerization catalysts.[1] In general, C_{2v}-symmetric metallocenes produce atactic polypropylene, C_2-symmetric metallocenes provide isotactic polypropylene, and select C_1-symmetric metallocenes yield isotactic polypropylene, generally with less stereospecificity than what is observed with C_2-symmetric catalysts.

While a variety of metallocene catalysts have been reported for generation of isotactic polypropylene, the number of catalysts for production of syndiotactic polypropylene is limited. Ewen and Razavi first described the preparation of C_s-symmetric, singly-linked cyclopentadienyl-fluorenyl zirconocenes as syndiospecific polymerization catalysts.[2] Following this discovery a family of C_s-symmetric catalysts were synthesized for the production of syndiotactic polypropylene, as illustrated in Figure 2.[2,3]

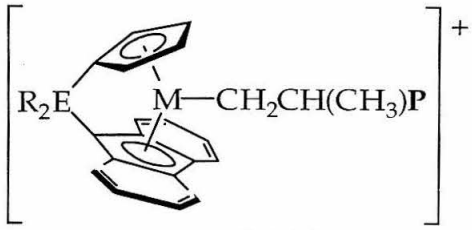

where M = Zr, Hf; E = C, Si; R = CH_3, C_6H_5

Figure 2: C_S-symmetric singly linked cyclopentadienyl-fluorenyl cationic group 4 metallocenes serve as catalysts for the production of syndiotactic polypropylene.

The mechanism first proposed by Ewen and Razavi[2] for formation of syndiotactic polypropylene requires olefin insertions from alternating (enantiotopic) sides of the metallocene wedge. The authors also suggested that the methyl substituent of the propylene monomer would be directed away from the larger fluorenyl ligand. This mechanism is depicted in Figure 3.

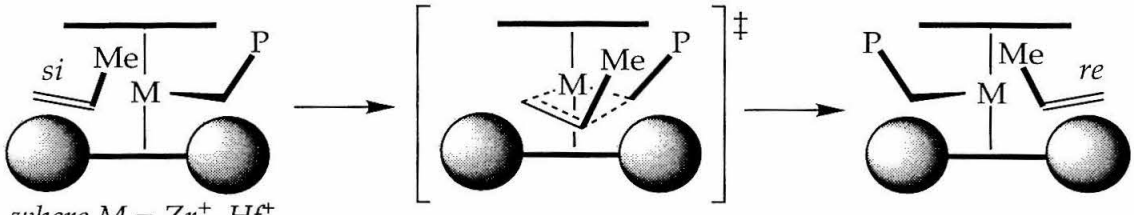

where M = Zr^+, Hf^+

Figure 3: Original proposed mechanism for formation of syndiotactic polypropylene.

Recent efforts in our group have helped to delineate the essential requirements for syndiospecific α-olefin polymerization catalysts. Two features of the singly linked cyclopentadienyl-fluorenyl catalysts, their C_S-symmetry and cyclopentadienyl ligands of differing sizes, were adopted in the zirconocene pictured in Figure 4.[4] These two features were not sufficient for creation of a syndiospecific catalyst. Activation of this zirconocene with methylaluminoxane (MAO, 10^3 equivalents) in liquid propylene at 0°C provides essentially atactic polypropylene ([*r*] ≈ 55%).

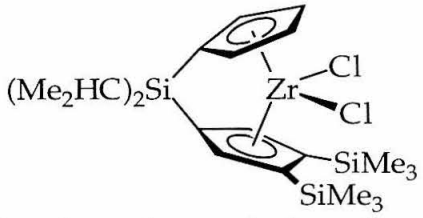

Figure 4: C_S-symmetry is not the only requirement for formation of syndiotactic polypropylene.

Further consideration of the olefin insertion transition state described in Figure 3 suggested that the alkyl substituent of the incoming monomer may be oriented *trans* with respect to the β-carbon of the polymer chain, as illustrated in Figure 5.[4] This stereochemical assignment is supported by theoretical[5] and experimental[6] measurements of transition state geometry in related C_2-symmetric metallocenes. Incorporation of α C-H agostic assistance in the olefin insertion transition state[7] is also consistent with this stereochemical assignment.

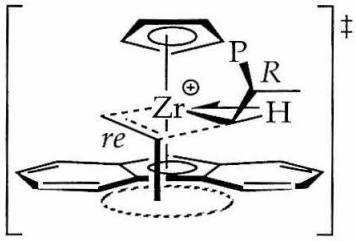

Figure 5: Proposed transition state for propylene insertion into a growing polymer chain for a syndiospecific zirconocene catalyst.

These observations were implemented in the design of a family of C_s-symmetric, doubly-silylene bridged *ansa*-zirconocenes, [(1,2-$SiMe_2$)$_2$(η^5-4-R-C_5H_2)(η^5-3,5-$(CHMe_2)_2$-C_5H)]$ZrCl_2$ (RThpZrCl_2, where R = H, iPr, tBu, TMS) for the production of highly syndiotactic polypropylene (Figure 6).[4] These catalysts are notable for their high syndiospecificity, activity, and polymer molecular weights. For example, ThpZrCl_2 (R = H) produces highly syndiospecific polypropylene ([*rrrr*] = 93.4% for ThpZrCl_2/MAO = 1 : 2000, in liquid propylene at 20°C) with high molecular weight (M_w = 1,300,000, PDI = 1.9). The highest syndiospecificity is found using iPrThpZrCl_2 (iPrThpZrCl_2/MAO = 1 : 2000, in liquid propylene at 20°C) where a [*rrrr*] value of 97.5% has been observed.

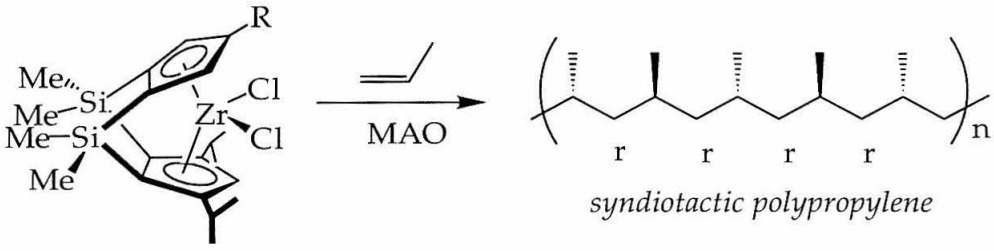

where R = H, i-Pr, t-Bu, TMS

Figure 6: C_s-symmetric RThp zirconocene dichlorides, when activated with MAO, serve as highly active catalysts for the production of syndiotactic polypropylene.

From this work it appears that syndiospecific propylene polymerization catalysts operate via the general mechanism illustrated in Figure 7. Since both sides of the metallocene wedge are enantiotopic for a C_s-symmetric metallocene, regular migratory insertions from opposite sides of the metallocene wedge are required for syndiospecificity via enantiomorphic site control. One of the cyclopentadienyl ligands must have steric bulk flanking the metallocene wedge; this provides an open region to accommodate a propylene methyl group for olefin coordination and insertion. An α-agostic interaction in the transition state for olefin insertion may help enforce a *trans* relationship between the propylene methyl substituent and the β-carbon of the polymer chain.

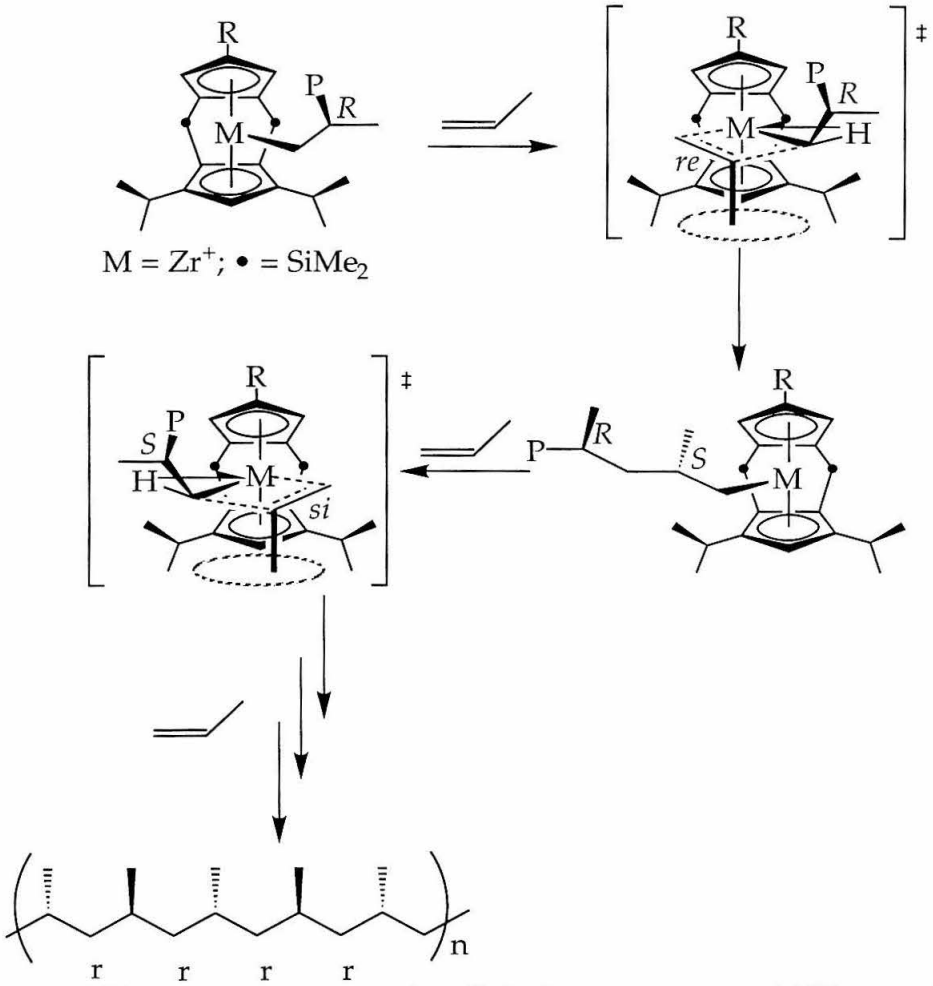

Figure 7: Essential features for formation of syndiotactic polypropylene. A RThp metallocene has been used for illustrative purposes.

While these doubly-silylene bridged zirconocenes produce highly syndiotactic poly(α-olefins) under high olefin pressure and low temperature conditions, polymerization under other conditions produces stereoerrors in the polymer microstructure. Examination of these errors reveals that site epimerization, polymer chain migration without insertion, is the predominant stereoerror forming mechanism (Scheme 1).[8] Site epimerization disrupts regular migratory insertions from opposite sides of the metallocene wedge, and as a result syndiospecificity is lost.

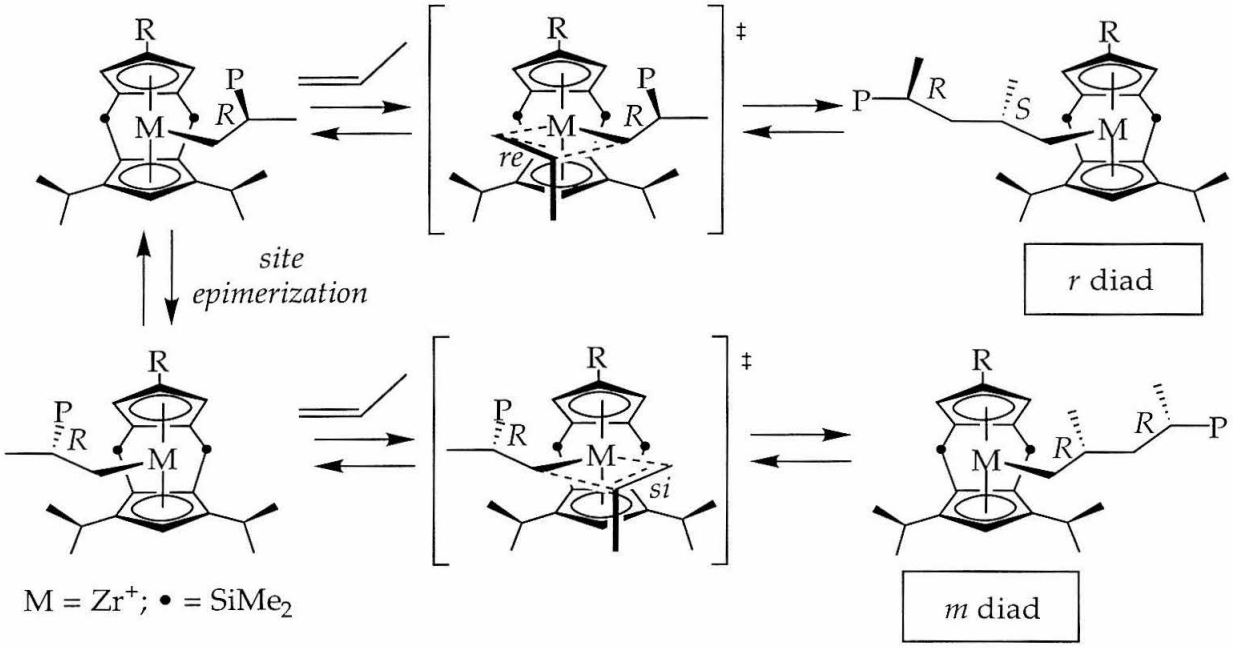

Scheme 1: Site epimerization is the principle stereoerror mechanism for RThp zirconocenes.

In order to expand our understanding of the source of stereoerrors and mechanism of stereocontrol in syndiospecific α-olefin polymerization, we targeted a family of C_s-symmetric, *ansa*-group 3 metallocenes as polymerization catalysts (Figure 8). These target molecules are isoelectronic with cationic zirconocene catalysts. While group 3 metallocenes are typically less active polymerization catalysts than the analogous zirconocene cations, they have the advantage of being single component catalysts.

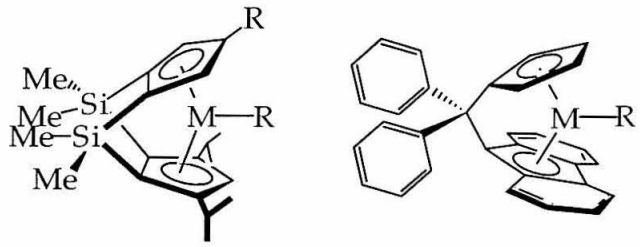

where M is Y or Sc and R is H or alkyl

Figure 8: C_s-symmetric yttrocenes and scandocenes are desired as catalysts for Ziegler-Natta polymerization.

In contrast to cationic C_s-symmetric zirconocenes, theoretical studies predict that neutral C_s-symmetric yttrocene and scandocene complexes will not generate syndiotactic poly(α-olefins).[9] Calculations indicate that a pendant alkyl substituent, such as a growing polymer chain, has an energetic preference to rest in a lateral position of the metallocene wedge for cationic group 4 metallocenes and rest in the central position of the wedge for neutral group 3 metallocenes (Figure 9). Isoelectronic compounds with the general formula X_2M-R were examined in this study (where X = Cl, (η^5-C_5H_5); M = Sc, Ti+; R = H, CH_3, SiH_3).

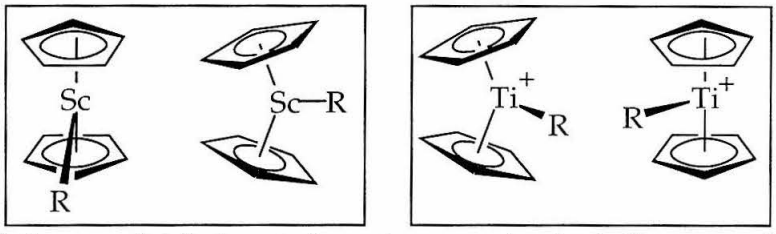

Figure 9: Calculations predict that neutral scandocene and cationic titanocene alkyl complexes have different preferences for the location of the alkyl substituent in the metallocene wedge.

By extension, after each monomer insertion with a group 3 metallocene the growing polymer chain will relax to the central position of the metallocene wedge. The difference in transition state energies for olefin insertion may produce stereoregularity in the polymer microstructure if one transition state is energetically favored (Figure 10). Stereoregularity arising from a chain-end control mechanism contrasts our current understanding for generation of syndiotactic poly(α-olefins) with zirconocene catalysts, where regular alternation of monomer approach from different sides of the metallocene wedge yields syndiotactic polymer. These theoretical predictions provided further impetus for

preparation of C_s-symmetric group 3 metallocenes to expand our understanding of stereocontrol in Ziegler-Natta polymerization.

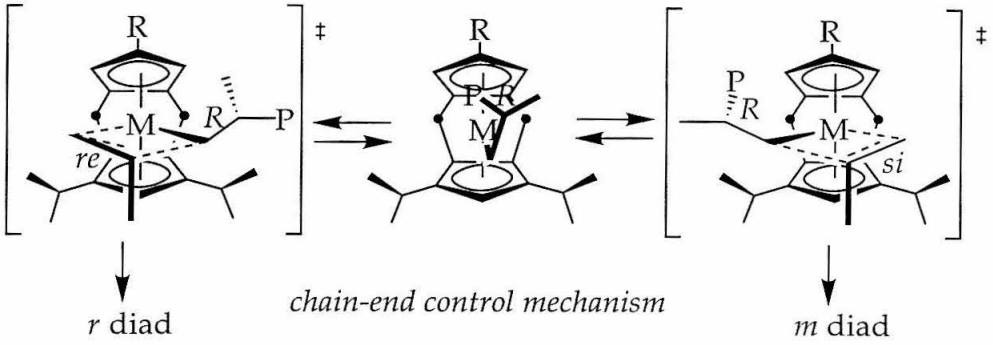

Figure 10: A chain-end control mechanism may operate for C_s-symmetric group 3 metallocenes.

Results and Discussion

Preparation of yttrocene and scandocene RThp chloride complexes

The *tert*-butyl substituted Thp ligand, [(1,2-$SiMe_2$)$_2$(4-CMe_3-C_5H_2)(3,5-($CHMe_2$)$_2$-C_5H)] (tBuThp), was first targeted for the preparation of scandocene and yttrocene halide complexes. It was hoped that the bulky *tert*-butyl substituent would help prevent intermolecular C-H activation of the cyclopentadienyl ring by the electrophilic metal center, as has been observed previously (eq. 1).[10]

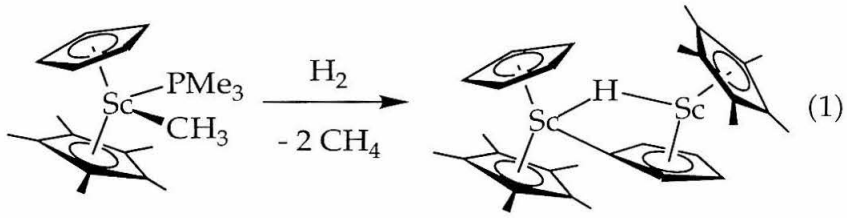

The most common synthetic route for the preparation of group 3 (Sc, Y, La) metallocenes is the reaction of deprotonated ligand salts with metal halides.[11] For this reason, the dilithio and dipotassio tBuThp ligand salts, Li_2[(1,2-$SiMe_2$)$_2$(4-CMe_3-C_5H_2)(3,5-($CHMe_2$)$_2$-C_5H)] (**2**, Li_2tBuThp) and K_2[(1,2-$SiMe_2$)$_2$(4-CMe_3-C_5H_2)(3,5-($CHMe_2$)$_2$-C_5H)] (**3**, K_2tBuThp), have been synthesized (eq. 2). The dilithio ligand salt was prepared by addition of 2.2 equivalents of *n*-BuLi to a 0°C

diethyl ether solution of **1**; complex **2** was isolated as a white powder in high yield. Combination of **1** and 1.90 equivalents of $KN(SiMe_3)_2$ in diethyl ether at -78°C and slow warming to 25°C affords the dipotassio ligand salt, **3**; this compound has been isolated as an off-white powder in high yield. Examination of THF-d_8 solutions of **2** and **3** by ^1H NMR spectroscopy reveals that variable amounts of diethyl ether may be present in these samples; this coordinated solvent is taken into account for calculation of molecular weight.

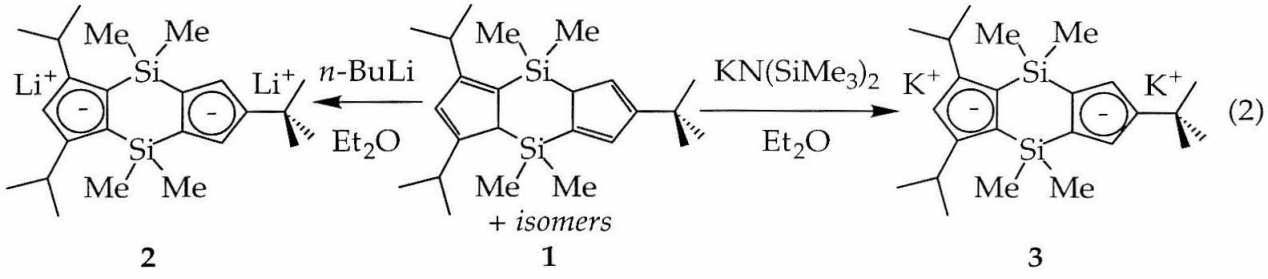

In a similar fashion, K_2iPrThp {$K_2[(1,2\text{-}SiMe_2)_2(4\text{-}CHMe_2\text{-}C_5H_2)(3,5\text{-}(CHMe_2)_2\text{-}C_5H)]$, **4**} has been prepared by reaction of protio iPrThp with 1.90 equivalents of $KN(SiMe_3)_2$ (eq. 3). This ligand salt may be isolated as an off-white powder in high yield.

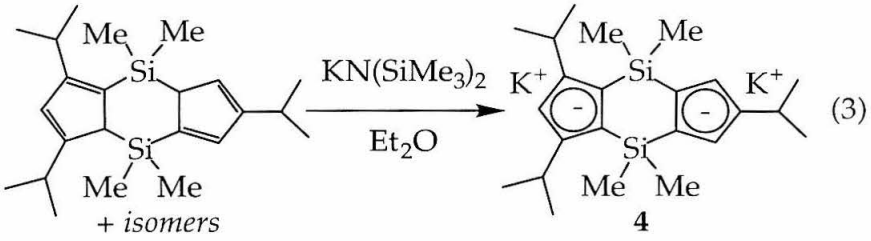

Metallation of **2** was attempted by addition of THF to a mixture of **2** and $YCl_3(THF)_{3.5}$ at -78°C followed by slow warming to 25°C. Examination of the reaction product in THF-d_8 by ^1H NMR spectroscopy reveals that two C_s-symmetric compounds are present. A variety of products are possible, such as solvent adducts ($L_nMCl(THF)_x$), dimeric complexes (($L_nMCl)_2$), or salt adducts ($L_nM(\mu\text{-}Cl)_2Li(THF)_x$).[11] Selective crystallization of one component of the reaction mixture has not been achieved.

In contrast, the dipotassio ligand salt **3** may be metallated with $YCl_3(THF)_{3.5}$ to provide one isolated yttrocene product. Combination of **3** and $YCl_3(THF)_{3.5}$ and addition of THF at -78°C followed by slow warming to 25°C provides the salt adduct, $[(1,2\text{-}SiMe_2)_2(\eta^5\text{-}4\text{-}CMe_3\text{-}C_5H_2)(\eta^5\text{-}3,5\text{-}(CHMe_2)_2\text{-}C_5H)]Y(\mu\text{-}Cl)_2K(THF)_n$ ($tBuThpY(\mu\text{-}Cl)_2K(THF)_n$, **5**), as the sole yttrocene product (eq. 4). Compound **5** has been analyzed by ^1H NMR spectroscopy in THF-d_8 and displays characteristic resonances for a C_s-symmetric, doubly-silylene bridged metallocene. Two cyclopentadienyl resonances are present (in a 2 : 1 ratio); two isopropyl methyl and two dimethylsilyl resonance are also observed. Variable amounts of protio THF are observed for different batches of **5** ($0 \leq n \leq 2$ equivalents); the amount of coordinated solvent may be quantified by comparison to integrations for ligand resonances.

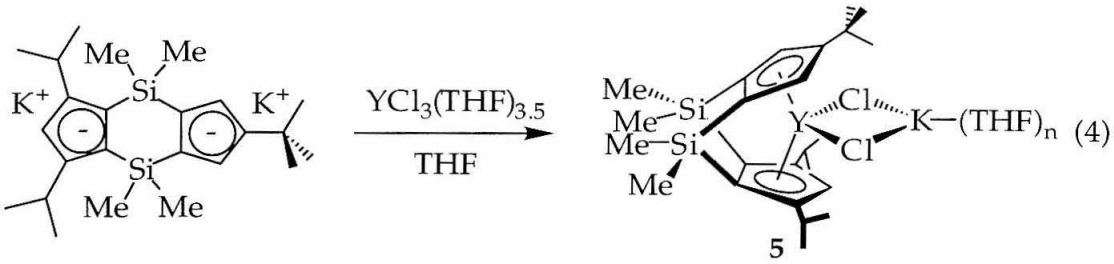

(4)

The presence of potassium in **5** has been supported by addition of 18-crown-6 to a THF-d_8 solution of **5**. This crown ether is known for its ability to solubilize cationic potassium. In the presence of 18-crown-6, the ^1H NMR resonances of **5** are shifted, suggesting coordination of potassium.

The structural assignment of **5** has been confirmed by X-ray crystallography. Diffusion of pentane into a diethyl ether/tetrahydrofuran solution of **5** with slow cooling to -20°C affords colorless crystals that are suitable for X-ray diffraction, as illustrated in Figure 11. This structure is monoclinic and fits the $P2_1/n$ space group. The ligand exhibits η^5,η^5 cyclopentadienyl coordination with yttrium-cyclopentadienyl distances that are typical of RThp metallocenes.[12] The potassium atom coordinates two molecules of THF, two bridging chlorides, and also displays η^3-coordination to a *t*-butyl substituted cyclopentadienyl ring of another molecule in the unit cell. The THF molecules have been modeled isotropically but their disorder appears to have little effect

on the remainder of the structure. Select bond distances and angles are given in Table 1.

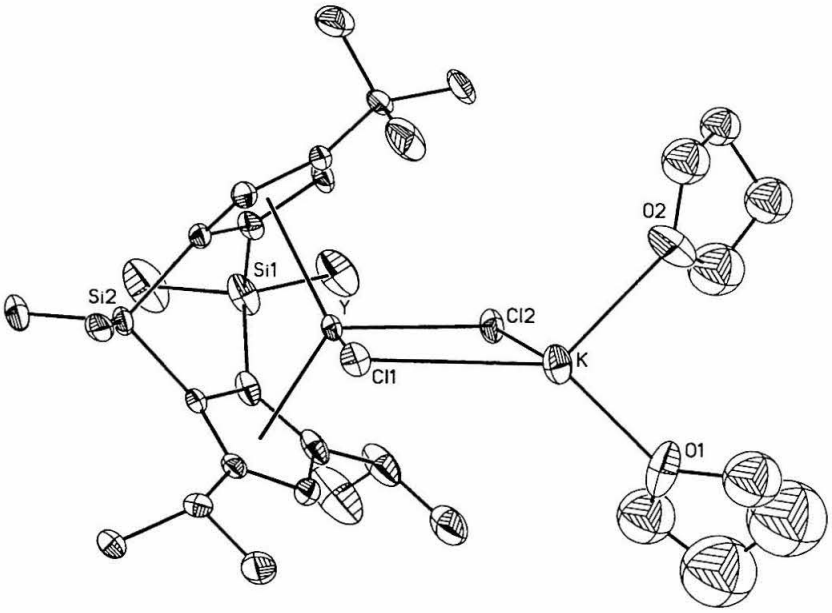

Figure 11: Molecular structure of **5** with selected atoms labeled (50% probability ellipsoids).

Group 3 metallocene potassium chloride adducts are more rare than lithium chloride adducts.[11] For example, prior work in our group suggested that use of dipotassio ligand salts, such as $K_2[(1\text{-}SiMe_2)(2\text{-}SiMe_3\text{-}4\text{-}CMe_3\text{-}C_5H_2)_2]$ (K_2Bp), may prevent formation a salt adduct upon metallation with $YCl_3(THF)_{3.5}$.[13] Formation of a yttrocene potassium chloride adduct has been implicated previously, e.g., $(\eta^5\text{-}C_5Me_5)_2Y(\mu\text{-}Cl)_2K(THF)_2$, but an X-ray crystal structure is not available.[14] The analogous cerium compound, $(\eta^5\text{-}C_5Me_5)_2Ce(\mu\text{-}Cl)_2K(THF)_2$, has been analyzed by X-ray diffraction; in this structure each potassium atom coordinates four chlorides and one THF molecule.[15]

Similar experiments were examined for preparation of tBuThp scandocene chloride complexes. Combination of $ScCl_3(THF)_3$ and the dilithio ligand salt **2** provides a mixture of products, as evidenced by ^1H NMR spectroscopy. Attempts to selectively crystallize one component of the reaction mixture have not been successful to date.

The dipotassio ligand salt **3** may be employed for metallation with $ScCl_3(THF)_3$ to provide a single isolated scandocene product. Combination of **3** and $ScCl_3(THF)_3$ and addition of THF at -78°C followed by slow warming to 25°C provides the salt adduct, $[(1,2\text{-}SiMe_2)_2(\eta^5\text{-}4\text{-}CMe_3\text{-}C_5H_2)(\eta^5\text{-}3,5\text{-}(CHMe_2)_2\text{-}C_5H)]Sc(\mu\text{-}Cl)_2K(THF)_n$ ($tBuThpSc(\mu\text{-}Cl)_2K(THF)_n$, **6**) (eq. 5). Analysis of **6** by ^1H NMR spectroscopy in THF-d_8 reveals characteristic resonances for a C_s-symmetric, doubly-silylene bridged metallocene. Variable amounts of protio THF are observed for different batches of **6** ($0 \leq n \leq 2$ equivalents) and the amount of solvent may be quantified by comparison to integrations for ligand resonances. Addition of 18-crown-6 to a THF-d_8 solution of **6** causes the ^1H NMR resonances to shift, thus supporting the presence of potassium in **6**.

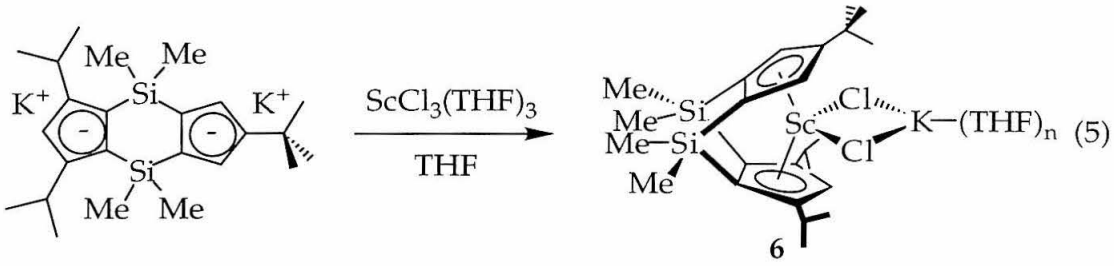

(5)

Compound **6** has been analyzed by X-ray crystallography. Diffusion of petroleum ether into a diethyl ether solution of **6** with slow cooling to -20°C affords colorless crystals that are suitable for X-ray diffraction, as illustrated in Figure 12. This structure is triclinic and fits the P_{-1} space group. Standard η^5,η^5 cyclopentadienyl coordination for RThp metallocenes is observed. The conditions for crystal growth appear to displace the coordinated THF (observed by ^1H NMR spectroscopy) with two coordinated diethyl ether molecules. The potassium atom coordinates two molecules of Et_2O and three bridging chlorides; one of these chlorides is from another molecule in the unit cell. The diethyl ether molecules are disordered, but their disorder appears to have little effect on the remainder of the structure. Select bond distances and angles are given in Table 1.

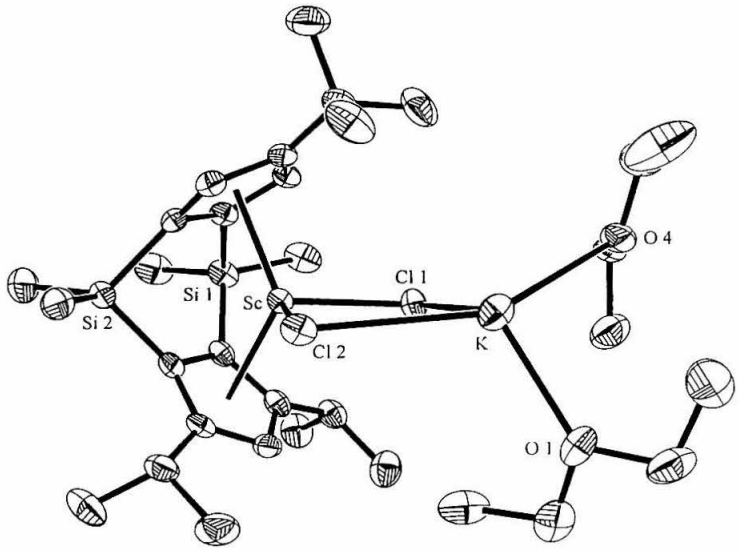

Figure 12: Molecular structure of **6•Et$_2$O** with selected atoms labeled (50% probability ellipsoids).

select bond distances (Å) *and bond angles* (°)	tBuThpY(μ-Cl)$_2$K(THF)$_2$	tBuThpSc(μ-Cl)$_2$K(Et$_2$O)$_2$
M-CpA	2.403	2.351(8)
M-CpB	2.391	2.2830(9)
M-Cl1	2.587(2)	2.4488(10)
M-Cl2	2.579(2)	2.5070(13)
CpA-M-CpB	115.0	122.71(3)
PlnA-PlnB	80.7(3)	66.74(10)
Cl1-M-Cl2	95.7(1)	94.52(4)

Table 1: Select bond distances and bond angles for potassium chloride adducts tBuThpY(μ-Cl)$_2$K(THF)$_2$ and tBuThpSc(μ-Cl)$_2$K(Et$_2$O)$_2$.

An isopropyl functionalized Thp yttrocene chloride complex has been prepared by combination of the dipotassio ligand salt, K$_2$iPrThp {K$_2$[(1,2-SiMe$_2$)$_2$(4-CHMe$_2$-C$_5$H$_2$)(3,5-(CHMe$_2$)$_2$-C$_5$H)], **4**} with YCl$_3$(THF)$_{3.5}$ in THF. After two days of reaction at 25°C, the desired yttrocene chloride complex may be isolated (eq. 6). Characterization by ^{1}H NMR spectroscopy in THF-*d*$_8$ solvent reveals that the complex has C_s-symmetry and that a non-stoichiometric amount of protio THF is present. The amount of coordinated protio THF may be

quantified by comparison to integrations of ligand resonances. This compound appears to be the potassium chloride adduct, [(1,2-$SiMe_2$)$_2$(η^5-4-$CHMe_2$-C_5H_2)(η^5-3,5-$(CHMe_2)_2$-C_5H)]Y(μ-Cl)$_2$K$(THF)_n$ (iPrThpY(μ-Cl)$_2$K$(THF)_n$, **7**).

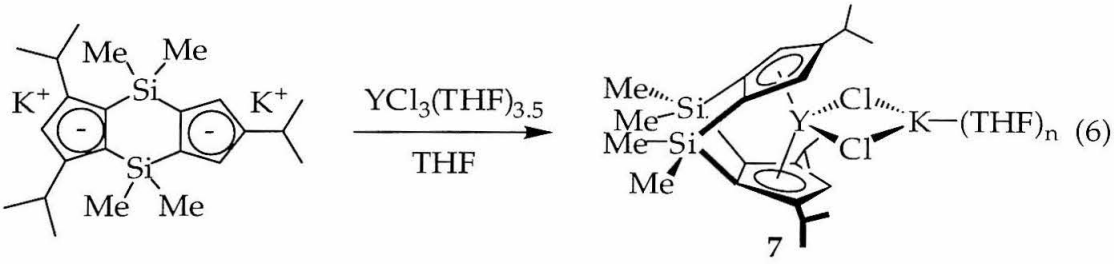

(6)

Protio THF may be removed from yttrocenes **5** and **7** via a modified Soxhlet extraction, as described in the experimental section. Analysis of the products by ^{1}H NMR spectroscopy reveals that all protio solvent is absent following this procedure.

Metallation of K_2iPrThp with $ScCl_3(THF)_3$ in THF does not provide the corresponding scandocene chloride under reaction conditions analogous to those for the preparation of **6**. As a result, a related scandocene bromide complex has been synthesized (*vide infra*).

Isolation of an unsubstituted Thp scandocene halide complex has not been achieved to date. Reaction of K_2[(1,2-$SiMe_2$)$_2$(C_5H_3)(3,5-$(CHMe_2)_2$-C_5H)] (K_2Thp) with $ScCl_3(THF)_3$ in THF-d_8 at 87°C provides a mixture of products and decomposition, as evidenced by ^{1}H NMR spectroscopy (eq. 7). Addition of excess NaI or NaBr to the reaction mixture also leads to decomposition. It is likely that intermolecular C-H activation of the unsubstituted cyclopentadienyl ring by scandium forms undesired products (e.g., eq. 1).

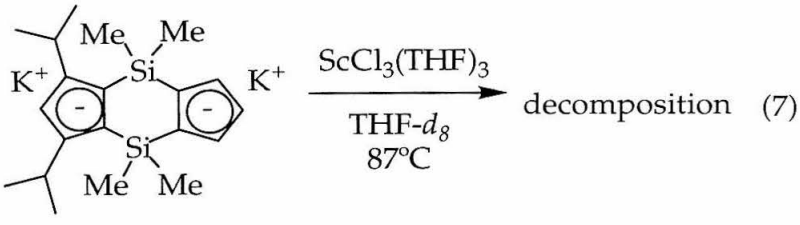

(7)

Preparation of yttrocene and scandocene RThp iodide and bromide complexes

While yttrocene and scandocene chloride complexes tend to be synthesized most frequently, analogous bromide and iodide complexes have been reported.[11] In some cases, bromide and iodide complexes may be prepared by chemical modification of known chloride complexes. For example, $[(\eta^5\text{-}1,3\text{-}SiMe_3\text{-}C_5H_3)_2]YI(THF)$ has been synthesized by addition of 2 equivalents of NaI to $\{[(\eta^5\text{-}1,3\text{-}SiMe_3\text{-}C_5H_3)_2]YCl\}_2$ in THF (eq. 8).[16] Alternatively, deprotonated ligand salt (e.g., Li_2tBuThp), $MCl_3(THF)_3$ (where M = Y, Sc) and excess NaX (where X = Br, I) may be combined in one pot to yield the desired metallocene bromide or iodide complex.

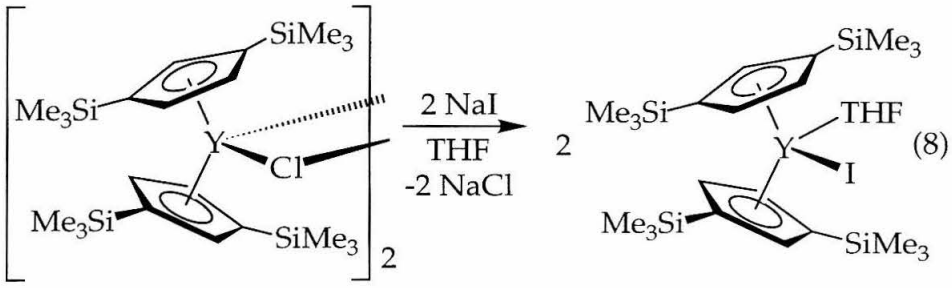

(8)

Addition of THF to a mixture of $tBuThpY(\mu\text{-}Cl)_2K(THF)_n$ and 2 equivalents of NaI results in halide exchange after two days of stirring at 25°C (eq. 9). Analysis by ^1H NMR spectroscopy in THF-d_8 solvent reveals a 1 : 1 mixture of a C_1-symmetric product and a C_s-symmetric product. The presence of approximately 1 equivalent of protio THF suggests that the C_1-symmetric product is an iodo-THF complex, $[(1,2\text{-}SiMe_2)_2(\eta^5\text{-}4\text{-}CMe_3\text{-}C_5H_2)(\eta^5\text{-}3,5\text{-}(CHMe_2)_2\text{-}C_5H)]YI(THF)$ (tBuThpYI(THF), **8a**). The C_s-symmetric product may be assigned as a dimeric yttrocene iodide complex with bridging iodide ligands, $\{[(1,2\text{-}SiMe_2)_2(\eta^5\text{-}4\text{-}CMe_3\text{-}C_5H_2)(\eta^5\text{-}3,5\text{-}(CHMe_2)_2\text{-}C_5H)]Y(\mu\text{-}I)\}_2$ {$[tBuThpY(\mu\text{-}I)]_2$, **8b**}.

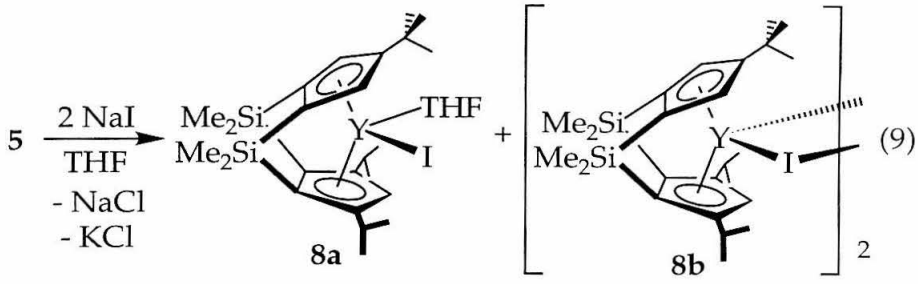

Other methods for preparation of tBuThp yttrocene iodide complexes are not as efficient as the procedure described in eq. 9. Heating a mixture of tBuThpY(μ-Cl)$_2$K(THF)$_n$ and NaI in THF to 87°C induces some decomposition; similar results are obtained if dioxane-*d*$_8$ is used as a solvent. Combination of K$_2$tBuThp, YCl$_3$(THF)$_{3.5}$, and excess NaI in THF-*d*$_8$ also provides some decomposition. Analogous reactions with NaBr as a halide source do not produce yttrocene bromide products.

Further experimentation suggests that halide interconversion is highly dependent on the ligand and metal identity. Scandocene bromide or iodide complexes that employ the tBuThp ligand array cannot be isolated through the procedures described above. Addition of NaX to tBuThpSc(μ-Cl)$_2$K(THF)$_n$ in THF or combination of K$_2$tBuThp, ScCl$_3$(THF)$_3$, and excess NaX in THF-*d*$_8$ does not yield the desired halide complexes. Boron triiodide is also ineffective for conversion of tBuThpSc(μ-Cl)$_2$K(THF)$_n$ to the corresponding iodide complex.

Curiously, reaction of K$_2$iPrThp, ScCl$_3$(THF)$_3$, and excess NaBr in refluxing THF for four hours allows isolation of a scandocene bromide complex as an off-white powder (eq. 10). Analysis of the reaction product by ^{1}H NMR spectroscopy in THF-*d*$_8$ reveals *C*$_s$-symmetry of the product and the presence of protio THF. This is consistent with formation of a potassium bromide adduct, [(1,2-SiMe$_2$)$_2$(η^5-4-CHMe$_2$-C$_5$H$_2$)(η^5-3,5-(CHMe$_2$)$_2$-C$_5$H)]Sc(μ-Br)$_2$K(THF)$_n$ (iPrThpSc(μ-Br)$_2$K(THF)$_n$, **9**).

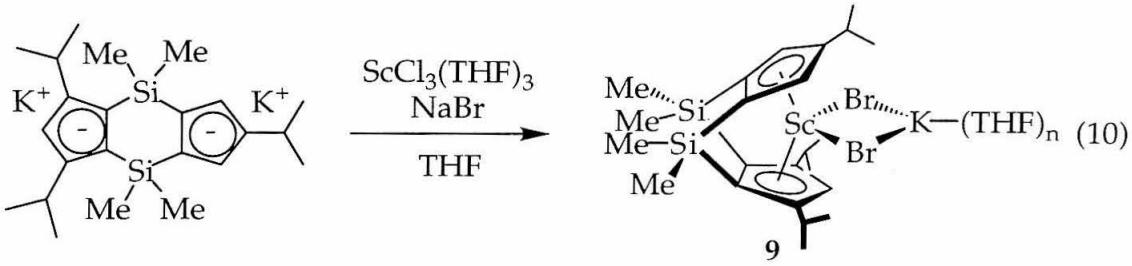

(10)

9

Preparation of yttrocene alkyl and hydride complexes

Alkyl substituents with significant steric bulk, such as bis(trimethylsilyl)-methyl, are commonly used for the preparation of monomeric yttrocene and scandocene alkyls.[11] The significant steric bulk prevents formation of dimeric alkyls which tend to be less reactive towards dihydrogen or α-olefins. The lack of β hydrogens prevents decomposition of the alkyl complex via a β-hydrogen elimination pathway.

Addition of either $LiCH(SiMe_3)_2$ or $KCH(SiMe_3)_2$ to $tBuThpY(\mu\text{-}Cl)_2K(THF)_n$ in toluene-d_8 provides decomposition, as evidenced by ^1H NMR spectroscopy. Slow addition of a toluene solution of $LiCH(SiMe_3)_2$ to a toluene solution of $tBuThpY(\mu\text{-}Cl)_2K(THF)_n$ at -78°C, followed by slow warming to 25°C, also provides extensive decomposition.

In contrast, combination of $tBuThpYI(THF)/[tBuThpY(\mu\text{-}I)]_2$ (**8a**/**8b**) and $KCH(SiMe_3)_2$, addition of toluene at -78°C, and slow warming to 25°C affords the desired monomeric alkyl complex, $[(1,2\text{-}SiMe_2)_2(\eta^5\text{-}4\text{-}CMe_3\text{-}C_5H_2)(\eta^5\text{-}3,5\text{-}(CHMe_2)_2\text{-}C_5H)]YCH(SiMe_3)_2$ ($tBuThpYCH(TMS)_2$, **10**) (eq. 11). The product is isolated as an off-white powder by recrystallization from cold pentane.

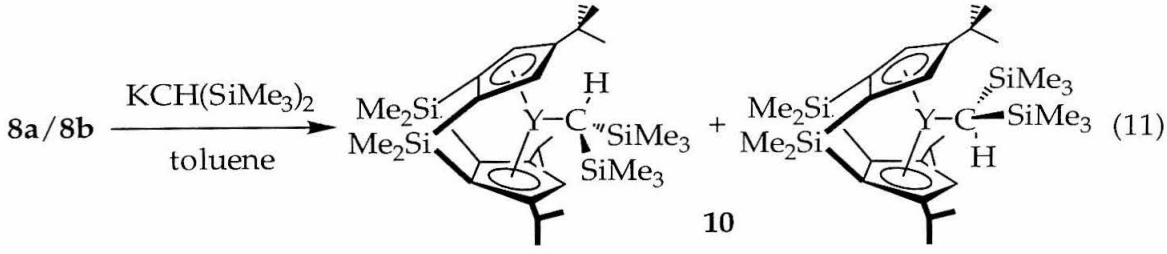

(11)

10

Compound **10** has been analyzed by ^1H and ^{13}C NMR spectroscopy in both benzene-d_6 and toluene-d_8 solvent. Two C_s-symmetric species are evident. Variable temperature ^1H NMR spectroscopy from 196 to 356 K reveals that these two species are maintained in this temperature range. Two energetically preferred rotamers of the bis(trimethylsilyl)methyl substituent may be used to rationalize this observation, as illustrated in equation 11. This implies hindered rotation about the Y-C sigma bond.

This phenomena has been observed for other singly-linked yttrocenes, such as $[Me_2Si(\eta^5\text{-}C_5Me_4)_2]YCH(SiMe_3)_2$ [OpYCH(TMS)$_2$][17] and $[Me_2Si(\eta^5\text{-}C_5Me_4)(\eta^5\text{-}C_5H_4)]YCH(SiMe_3)_2$.[18] For example, examination of OpYCH(TMS)$_2$ by ^1H NMR spectroscopy reveals a single resonance for all six Si-CH_3 groups of the $CH(SiMe_3)_2$ ligand and two sets of (η^5-C_5Me_4) resonances at 25°C (300 MHz, benzene-d_6). Again this signifies hindered rotation about the Y-C sigma bond.

Colorless six-sided plates suitable for X-ray diffraction were precipitated from a toluene-d_8 solution of **10**. This compound crystallized in the $P2_1/n$ space group and its molecular structure appears in Figure 13. Atoms C25 and C26 exhibited some disorder during refinement. In fact C25 exists in two distinct conformations, with its attached hydrogen either up or down with respect to the metallocene wedge. The relative populations of C25A and C25B are 0.719(11) and 0.281(11), respectively. This contributes to the disorder of C26; it was most effectively modeled as a single anisotropic atom. The partial atom, C25A, was refined isotropically and is included in Figure 13.

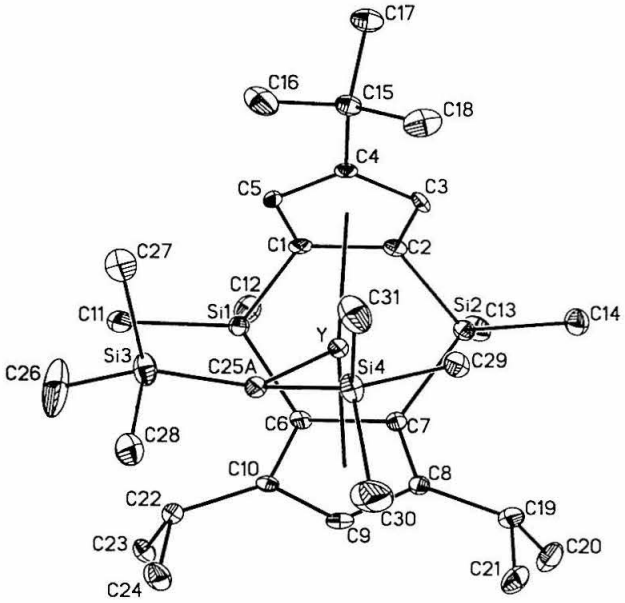

Figure 13: Molecular structure of **10** with selected atoms labeled (50% probability ellipsoids). Hydrogens omitted for clarity.

The bonding of the bis(trimethylsilyl)methyl group in **10** is notable (Figure 14). There appears to be an interaction between the yttrium atom and a silicon carbon bond (Si4-C29). C25A seems to be shifted to the side of the metallocene wedge to facilitate this interaction. Select bond angles and bond distances for **10** are given in Table 2.

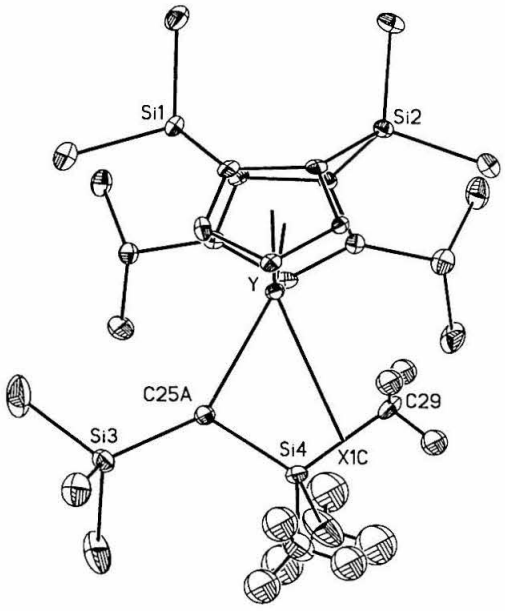

Figure 14: Molecular structure of **10** with selected atoms labeled (50% probability ellipsoids). Select hydrogens omitted for clarity.

select bond distances (Å) *and bond angles* (°)	tBuThpYCH(TMS)$_2$	OpYCH(TMS)$_2$
Y-CpA	2.394	2.377
Y-CpB	2.386	2.377
Y-X1C	2.806	—
Y-C25A/Y-C3	2.437(4)	2.418(7)
Y...C29/Y...C4	2.751(4)	2.816(7)
Si3-C25A-Si4/Si3-C3-Si2	118.5(2)	122.8(3)
CpA-Y-CpB	116.1	124.3
PlnA-PlnB	80.7(1)	—

Table 2: Select bond distances and bond angles for tBuThpYCH(TMS)$_2$ and OpYCH(TMS)$_2$. The centroid of Si4 and C29 is assigned as X1C.

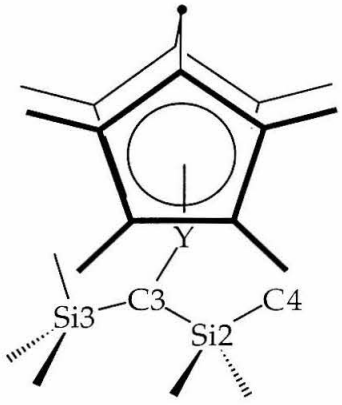

Figure 15: Select atom labels for $[Me_2Si(\eta^5\text{-}C_5Me_4)_2]YCH(SiMe_3)_2$ [OpYCH(TMS)$_2$].[17]

Related singly-linked bis(trimethylsilyl)methyl complex $[Me_2Si(\eta^5\text{-}C_5Me_4)_2]YCH(SiMe_3)_2$ [OpYCH(TMS)$_2$][17](Figure 15) and the lutetium analog of $[Me_2Si(\eta^5\text{-}C_5Me_4)(\eta^5\text{-}C_5H_4)]YCH(SiMe_3)_2$[18] have been analyzed by X-ray diffraction. Both complexes display a bridging M-(CH_3)-Si interaction (where M = Y, Lu). This type of three center, two electron bridging interaction has been studied by Schaverien for other metallocenes.[19]

Hydrogenation of **10** in benzene-d_6 solvent induces liberation of bis(trimethylsilyl)methane and generation of a mixture of two dimeric hydride complexes, as evidenced by ^{1}H NMR spectroscopy (eq. 12). The bridging yttrium hydrides of **11a** and **11b** resonate as 1 : 2 : 1 triplets at 2.78 and 2.51 ppm with $^1J_{Y\text{-}H}$ values of 32.7 and 31.6 Hz, respectively. Each bridging hydride is coupled to two equivalent ^{89}Y nuclei (I = 1/2; 100% natural abundance) producing this characteristic splitting pattern.

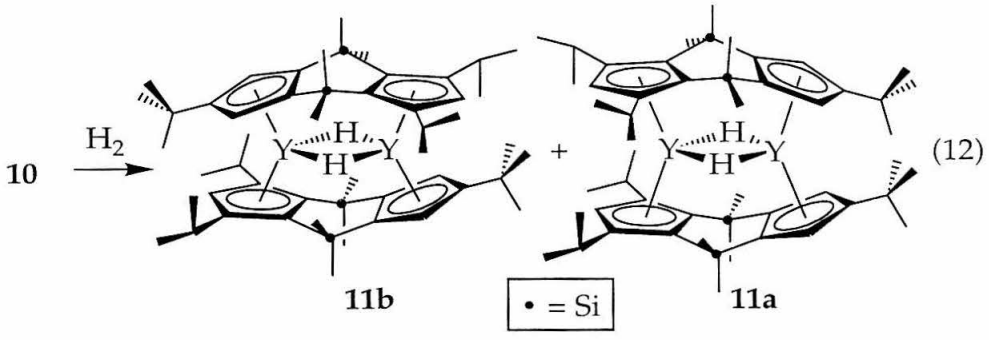

(12)

Dimeric *ansa*-yttrocene hydride complexes of two types have been reported in the literature (Figure 16). Type I is more common that type II; the latter is often referred to as a "flyover" dimer.[11] Marks has described the preparation of $[Et_2Si(\eta^5\text{-}C_5Me_4)(\eta^5\text{-}C_5H_4)YH]_2$ and suggests that it is a type II dimer.[18] The analogous lutetium complex, $Lu\{\mu\text{-}[Et_2Si(\eta^5\text{-}C_5Me_4)(\eta^5\text{-}C_5H_4)]_2(\mu\text{-}H)_2\}Lu$ has been characterized by X-ray diffraction and possesses a type II coordination environment.[18] Conversion of the type I complex, $[Me_2Si(\eta^5\text{-}C_5Me_4)_2YH]_2$, to the type II complex, $Y\{\mu_2\text{-}[Me_2Si(\eta^5\text{-}C_5Me_4)(\eta^5\text{-}C_5Me_4)]_2(\mu_2\text{-}H)_2\}Y$ through a "facile ligand redistribution" has been reported.[17] Our group has also reported type I compounds that do not generate the corresponding type II compounds over time, such as *meso* and *rac*-$[Me_2Si(\eta^5\text{-}2\text{-}SiMe_3\text{-}4\text{-}Ad\text{-}C_5H_2)_2Y(\mu\text{-}H)]_2$ ($[AbpYH]_2$),[20] $[Me_2Si(\eta^5\text{-}2\text{-}SiMe_3\text{-}4\text{-}CMe_3\text{-}C_5H_2)_2Y(\mu\text{-}H)]_2$ ($[BpYH]_2$),[21] and homo- and heterochiral $[(OC_{10}H_6C_{10}H_6O)Si(\eta^5\text{-}2\text{-}SiMe_3\text{-}4\text{-}CMe_3\text{-}C_5H_2)_2Y(\mu\text{-}H)]_2$ ($[BnBpYH]_2$).[22] Proton NMR chemical shifts and $^1J_{Y\text{-}H}$ coupling constants for these yttrocene hydrides are listed in Table 3. Bridging hydride ligands of both Type I and Type II complexes appear as 1 : 2 : 1 triplets due to coupling to two equivalent ^{89}Y nuclei.

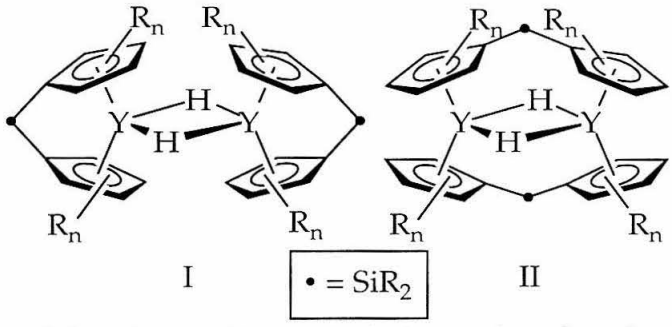

Figure 16: Two types of dimeric *ansa*-yttrocene hydride complexes have been observed previously.

compound	type	^{1}H: δ (Y-H)	$^1J_{Y-H}$	reference
$[Et_2Si(\eta^5\text{-}C_5Me_4)(\eta^5\text{-}C_5H_4)YH]_2$	II	3.03	35.3	18
$[Me_2Si(\eta^5\text{-}C_5Me_4)_2YH]_2$	I	5.286	33.3	17
$[Me_2Si(\eta^5\text{-}C_5Me_4)_2YH]_2$	II	3.867	34.4	17
11a	II ?	2.78	32.7	*
11b	II	2.51	31.6	*
[*meso*-AbpYH]$_2$	I	4.65	31.1	20
[*rac*-AbpYH]$_2$	I	4.76	31.3	20
[BpYH]$_2$	I	4.87	31	21
homochiral [BnBpYH]$_2$	I	4.98	31.4	22
heterochiral [BnBpYH]$_2$	I	5.97	31.4	22

Table 3: Select bond distances and bond angles for dimeric yttrocene hydride complexes. * denotes data from this work.

Key structural information has been obtained from X-ray diffraction studies. X-ray quality crystals of **11b** were deposited from a benzene-d_6 solution of **11a** and **11b**. The space group for these colorless square column crystals is $P2_1/c$. The molecule sits on a center of symmetry, so the unique bridging hydride was located by Direct methods. The yttrium hydride distance is 2.11(2) Å. Notably, **11b** possesses a Type II, "flyover" dimeric structure where each tBuThp ligand array spans two yttrium atoms (Figure 17). The yttrium centroid distances are 2.2775(13) and 2.3594(15) Å, respectively, and the centroid-yttrium-centroid angle for a single tBuThp ligand is 146.24(3)°.

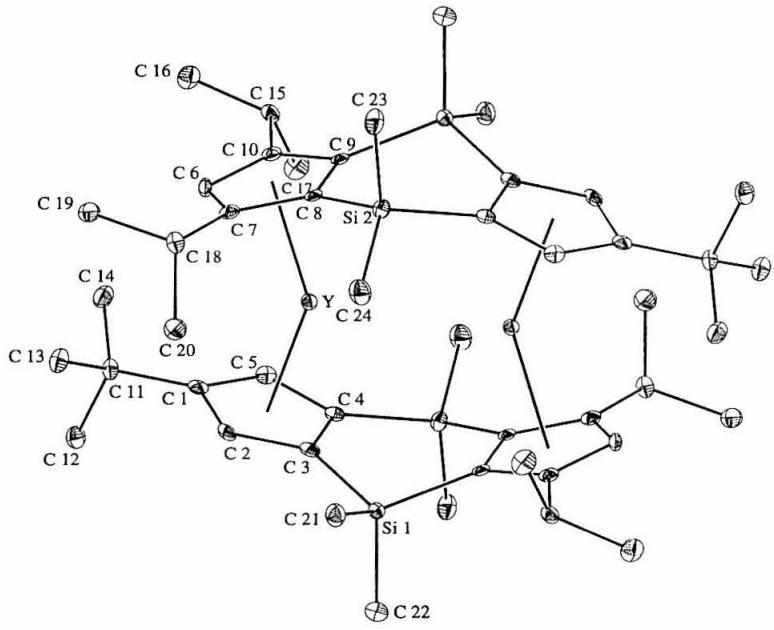

Figure 17: Molecular structure of **11b** with selected atoms labeled (50% probability ellipsoids). Hydrogens omitted for clarity.

Dissolution of crystals of **11b** in toluene-d_8 and examination by ^{1}H NMR spectroscopy reveals that this "flyover" structure corresponds to the upfield hydride resonance at 2.51 ppm. Further NMR experiments have been directed at determining the structural identity of **11a**. Comparison of the bridging hydride ^{1}H chemical shifts listed in Table 3 suggests that **11a** may be a Type II, "flyover" dimer; Type I dimers tend to have more downfield chemical shifts for their hydrides. However, since **11a** incorporates a doubly-silylene bridged ligand comparison to singly-silylene bridged yttrocenes may not be valid. Additional structural evidence for both yttrocene hydride complexes has been obtained by NOE difference NMR spectroscopy. These studies provided additional support for the "flyover" nature of both **11a** and **11b**.

The relative amounts of **11a** and **11b** formed during the course of hydrogenation (eq. 12) and subsequent equilibration of these dimers has been monitored by ^{1}H NMR spectroscopy. In related experiments other reagents have been added, such as dideuterium, trimethylphosphine, tetrahydrofuran, and α-olefins, to examine the effect on equilibration of **11a** and **11b**.

Hydrogenation of tBuThpYCH(TMS)$_2$ has been examined by variable temperature NMR spectroscopy. Both yttrocene hydride compounds appear in approximately a 50 : 50 ratio after 1 hour at 0°C. Over the course of 4 hours at this temperature, these compounds grow in intensity but maintain the same relative ratio. The yttrocene alkyl starting material is still present at this point. Upon warming the sample to 25°C for 1 week, an equilibrium ratio of yttrocene hydride compounds is reached (38 : 62 ratio, **11a** : **11b**). When excess dihydrogen is removed, the product ratio remains the same. These results provide further support for a "flyover" structure of both **11a** and **11b**.

Addition of dideuterium to an equilibrium mixture of **11a** and **11b** (38 : 62 ratio) results in approximately 65% deuterium incorporation over the course of 48 hours, as evidenced by ^{1}H NMR spectroscopy. Removal of dideuterium and addition of dihydrogen provides complete restoration of the bridging hydride resonances.

When 22 equivalents of ethylene is added to a benzene-d_6 solution of **11a** and **11b** (38 : 62 ratio), olefin is not consumed over the course of 12 hours at 25°C. The relative amount of **11b** increases upon ethylene addition, suggesting an associative pathway for the interconversion of **11a** and **11b**. Ethylene does not appear to react with these complexes since their ^{1}H NMR resonances are not altered in the presence of ethylene. Similar behavior is observed upon addition of excess PMe_3 or THF to **11a** and **11b** (38 : 62 ratio) in toluene-d_8 solvent; these reagents promote formation of **11b**. Upon removal of PMe_3 or THF the altered **11a** : **11b** ratio is maintained with no observed chemical modification of either compound.

Heating a benzene-d_6 solution of **11a** and **11b** to 87°C also promotes equilibration of these compounds to generate increased amounts of **11b**. Since each yttrium of **11a** and **11b** has sixteen valence electrons, it is unclear why addition of σ-donor ligands such as PMe_3 and THF promotes this equilibration.

Synthesis of tetramethylaluminate complexes

Unlinked group 3 metallocene tetramethylaluminate complexes of the form $(\eta^5\text{-}C_5H_5)_2M(\mu\text{-}CH_3)_2Al(CH_3)_2$ ($Cp_2MMe_2AlMe_2$, where M = Y, Sc[23]) and

$(\eta^5\text{-}C_5Me_5)_2M(\mu\text{-}CH_3)_2Al(CH_3)_2$ ($Cp^*_2MMe_2AlMe_2$, where M = Sm,[24] Yb, Y[25,26]) have been reported previously. The unsubstituted complexes, $Cp_2MMe_2AlMe_2$ (where M = Y, Sc), are prepared by reaction of $[Cp_2MCl]_2$ and $LiAlMe_4$ in toluene (eq. 13). The monomeric yttrocene tetramethylaluminate complex, $Cp_2YMe_2AlMe_2$, has been analyzed by X-ray diffraction.[23a] The ^1H NMR resonances for bridging and terminal methyl substituents are diagnostic for tetramethylaluminate complexes. For the yttrocene compound, spectra acquired at -40°C reveal distinct bridging and terminal methyl resonances and at 40°C a single broad resonance is present for all methyl substituents. In contrast, the scandocene compound is static at 25°C, and distinct bridging and terminal methyl resonances are observed.

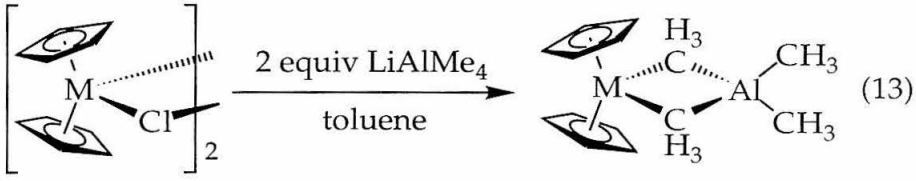

(13)

Use of the more sterically hindered bis-pentamethylcyclopentadienyl ligand array leads to formation of mixtures of monomeric and dimeric tetramethylaluminates. For example, Watson has described an equilibrium between monomeric $Cp^*_2YMe_2AlMe_2$ and dimeric $(Cp^*_2YMe_2AlMe_2)_2$, as illustrated in equation 14.[25c] Reaction of $Cp^*_2YMe_2Li$ with $AlMe_3$ affords these products. Teuben has also reported the preparation of these complexes via reaction of $Cp^*_2YCl\bullet THF$ and $LiAlMe_4$ in toluene.[26] At 20°C the monomer is dominant in solution; the monomer to dimer ratio is 4 : 1. Watson has characterized this dimeric yttrocene by X-ray crystallography.

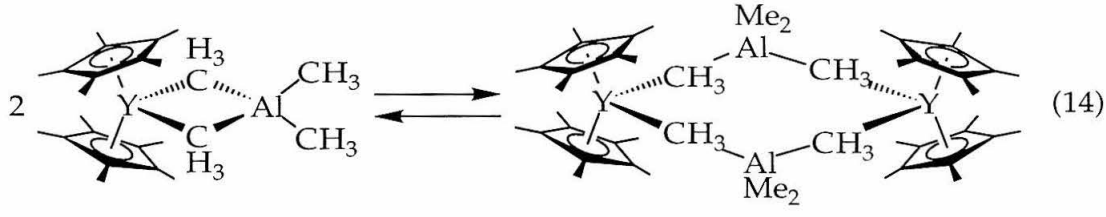

(14)

Lithium tetramethylaluminate has been utilized for conversion of the chloride complexes, **5** and **6**, to the corresponding tetramethylaluminate complexes. Combination of either **5** or **6** with $LiAlMe_4$ in toluene results in

alkylation; removal of toluene and extraction with pentane allows isolation of $[(1,2\text{-}SiMe_2)_2(\eta^5\text{-}4\text{-}CMe_3\text{-}C_5H_2)(\eta^5\text{-}3,5\text{-}(CHMe_2)_2\text{-}C_5H)]M(\mu\text{-}CH_3)_2Al(CH_3)_2$ ($tBuThpMMe_2AlMe_2$, where M = Y, **12**; where M = Sc, **13**) (eq. 15). Both **12** and **13** may be purified via recrystallization from pentane followed by addition of benzene and lyophilization.

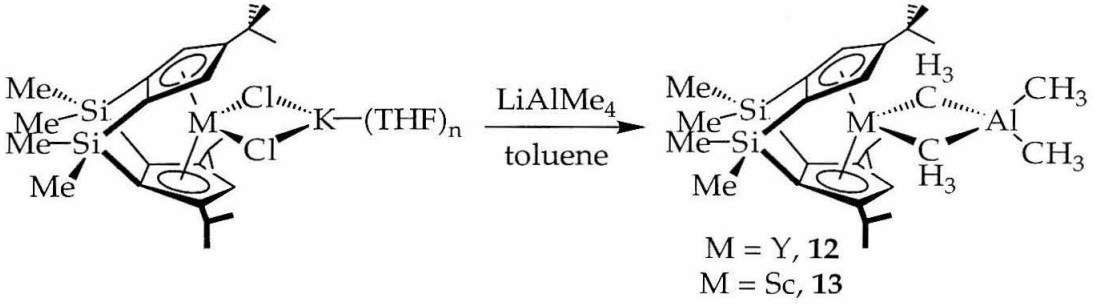

M = Y, **12**
M = Sc, **13**

(15)

These tetramethylaluminate complexes have been analyzed by ^1H and ^{13}C NMR spectroscopy. Due to the C_s-symmetry of these compounds, the bridging methyl substituents are chemically equivalent and the terminal methyl substituents are distinct. These methyl resonances are listed in Table 4 along with comparisons to previously reported tetramethylaluminate data.

compound	bridging Me	terminal Me	solvent	temp.	ref.
$tBuThpYMe_2AlMe_2$	-0.32	-0.33, -0.41	benzene-d_6	25°C	*
$tBuThpScMe_2AlMe_2$	-0.35	-0.23, -0.38	benzene-d_6	25°C	*
$Cp_2YMe_2AlMe_2$	-0.2	-0.09	toluene-d_8	-45°C	23
$Cp_2YMe_2AlMe_2$	-0.32	-0.98	CD_2Cl_2	-45°C	23
$Cp_2ScMe_2AlMe_2$	-0.29	-0.84	CD_2Cl_2	25°C	23
$Cp^*_2SmMe_2AlMe_2$	-17.6	1.63	benzene-d_6	25°C	24
$[Cp^*_2SmMe_2AlMe_2]_2$	-14.3	-2.26	benzene-d_6	25°C	24
$Cp^*_2YMe_2AlMe_2$	-0.61	-0.47	toluene-d_8	20°C	26
$[Cp^*_2YMe_2AlMe_2]_2$	-1.08	-0.29	toluene-d_8	20°C	26
$Cp^*_2YMe_2AlMe_2$	-0.506	-0.218	toluene-d_8	-40°C	25
$[Cp^*_2YMe_2AlMe_2]_2$	-0.982	-0.038	toluene-d_8	-40°C	25

Table 4: ^1H NMR resonances for bridging and terminal methyl substituents of select metallocene tetramethyaluminate complexes. Both monomeric and dimeric complexes are tabulated where appropriate. * denotes data from this work.

As previously noted, metallocene tetramethylaluminate complexes may exist in monomeric or dimeric form. To probe the molecularity of **12** and **13** variable temperature ^{1}H NMR spectroscopy was used for characterization. NMR spectra were acquired in a temperature range from 200 to 340 K; no evidence was obtained for a monomer-dimer equilibrium in either case. For yttrocene **12**, the three chemically distinct methyl resonances coalesce at -0.45 ppm at 338 K. This has also been observed for $Cp_2YMe_2AlMe_2$.[23c] Coalescence of bridging and terminal methyl resonances may be attributed to dissociation of a bridging methyl substituent, rotation about the remaining yttrium-methyl bond, and recoordination of an aluminum bound methyl substituent. This sequence for equilibration of methyl substituents is illustrated in Scheme 2.

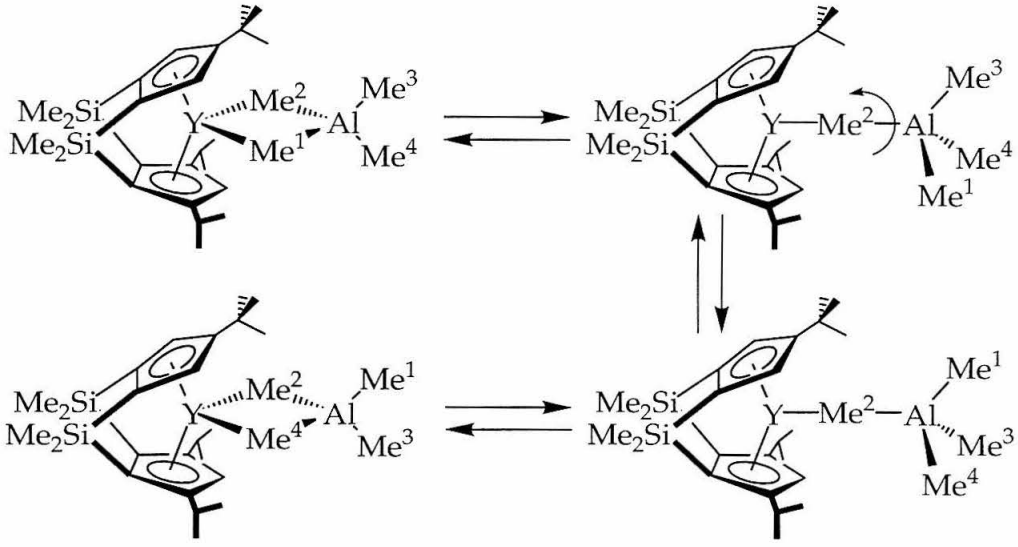

Scheme 2: Bridging and terminal methyl substituents may be equivalenced by this series of equilibrium reactions.

In contrast, scandocene **13** displays three methyl resonances that remain distinct throughout the temperature range examined. Equilibration of bridging and terminal methyl resonances is not observed on the NMR time scale.

Further evidence for the monomeric nature of **13** has been obtained by X-ray crystallography. Slow cooling of a solution of **13** afforded colorless crystals that were suitable for X-ray diffraction, as illustrated in Figure 18. The space group is $P\bar{1}$. The aluminum displays a nearly tetrahedral arrangement of methyl substituents. The *tert*-butyl substituent appears to exert a small steric influence

on the coordination environment of aluminum; the aluminum is found 0.1 Å below the plane formed by scandium and the bridging carbon atoms (C25 and C26). Select bond distances and bond angles are given in Table 5.

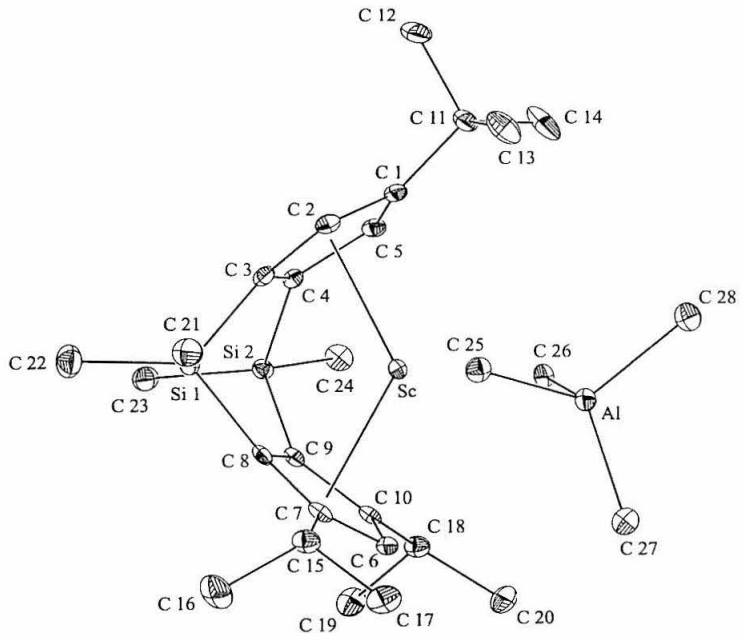

Figure 18: Molecular structure of **13** with selected atoms labeled (50% probability ellipsoids). Hydrogen atoms are omitted for clarity.

select bond distances (Å) *and bond angles* (°)	tBuThpSc(μ-Me)$_2$AlMe$_2$	Cp$_2$Y(μ-Me)$_2$AlMe$_2$
M-CpA	2.239(1)	2.62(2) (average)
M-CpB	2.233(1)	2.62(2) (average)
M-C25/M-C1	2.442(2)	2.57(2)
M-C26/M-C2	2.414(2)	2.60(2)
C25-M-C26/C1-M-C2	88.48(8)	85(1)
C25-Al-C26/C1-Al-C2	108.73(9)	112(1)
C27-Al-C28/C3-Al-C4	113.13(10)	111(1)
CpA-M-CpB	123.53(3)	—
PlnA-PlnB	75.68(7)	—

Table 5: Select bond distances and bond angles for monomeric tetramethylaluminates tBuThpSc(μ-Me)$_2$AlMe$_2$ and Cp$_2$Y(μ-Me)$_2$AlMe$_2$.[23b]

Hydrogen atoms H25C and H26C are 2.21(2) and 2.19(2) Å from scandium, respectively, suggesting bonding interactions (see Figure 19). These agostic C-H interactions have been observed in other metallocenes[7] but have not been noted for tetramethylaluminate complexes to date.

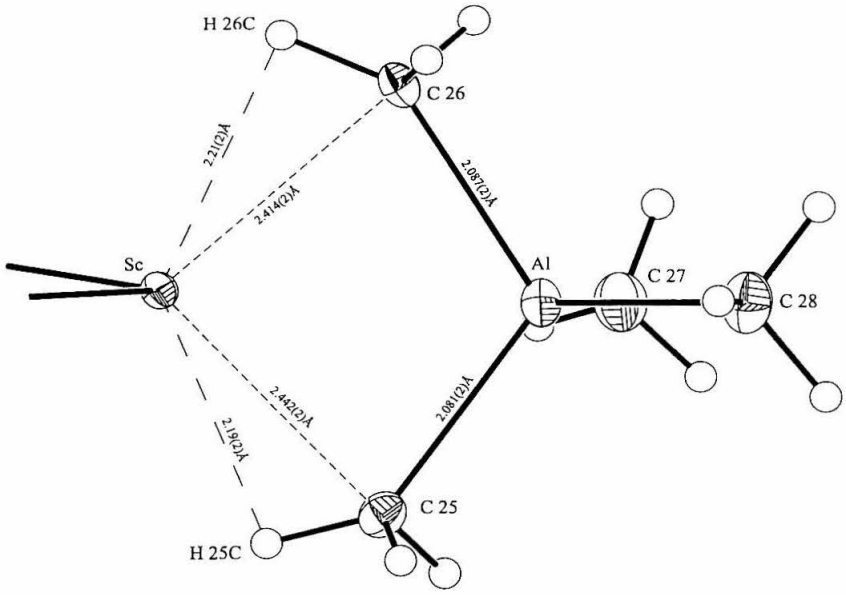

Figure 19: Molecular structure of **13** with selected atoms labeled (50% probability ellipsoids).

The analogous iPrThp scandium tetramethylaluminate complex may be prepared from combination of the scandocene bromide precursor, iPrThpSc(μ-Br)$_2$K(THF)$_n$, with LiAlMe$_4$ in toluene (eq. 16). Removal of toluene and extraction with pentane allows isolation of [(1,2-SiMe$_2$)$_2$(η^5-4-CHMe$_2$-C$_5$H$_2$)(η^5-3,5-(CHMe$_2$)$_2$-C$_5$H)]Sc(μ-CH$_3$)$_2$Al(CH$_3$)$_2$ (iPrThpScMe$_2$AlMe$_2$, **14**). Like **12** and **13**, complex **14** may be purified via recrystallization from pentane followed by addition of benzene and lyophilization.

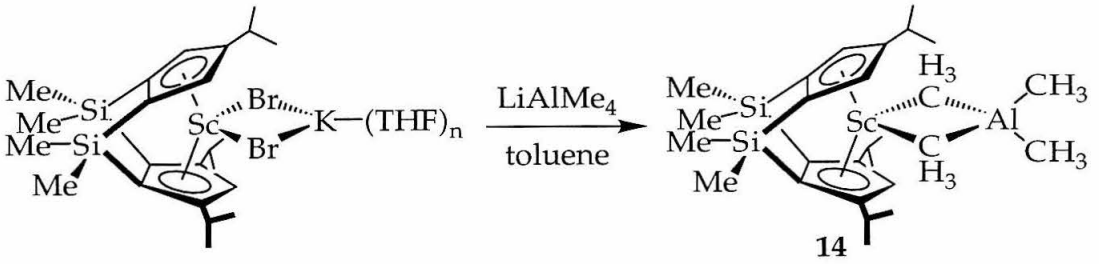

14 (16)

Reactivity of tetramethylaluminate complexes

Addition of pyridine to $Cp_2MMe_2AlMe_2$ (where M = Y, Sc) has been reported previously.[27] When 1 equivalent of pyridine (pyr) is added to $Cp_2YMe_2AlMe_2$, it coordinates $AlMe_3$, and a dimeric yttrocene methyl compound is formed. In contrast, 1 equivalent of pyridine coordinates the scandium of $Cp_2ScMe_2AlMe_2$ yielding a scandocene methyl-pyridine complex and 0.5 equivalents of $[Al_2Me_6]$ (Figure 20). Similarly, addition of THF to $Cp_2ScMe_2AlMe_2$ affords the corresponding methyl-THF compound. Removal of pyridine from $Cp_2ScMe(pyr)$ *in vacuo* provides an unidentified product.

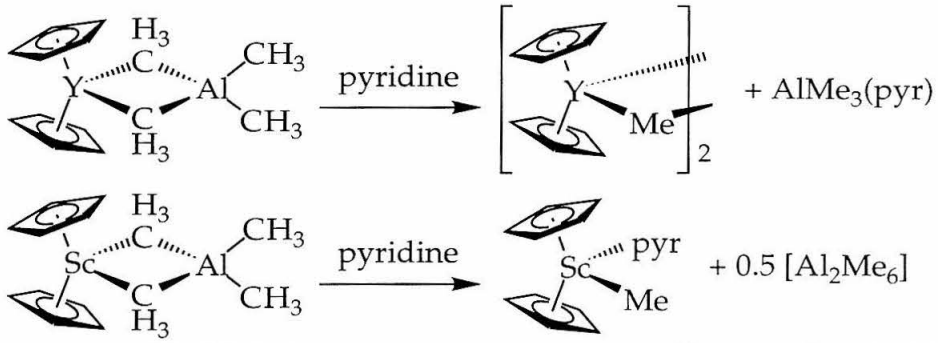

Figure 20: Reaction of $Cp_2MMe_2AlMe_2$ with pyridine provides different products for M = Y versus M = Sc.

Addition of 1 equivalent of pyridine to $tBuThpYMe_2AlMe_2$ in benzene-d_6 provides approximately 66% conversion to a C_1-symmetric species, as evidenced by ^1H NMR spectroscopy. The ligand and pyridine resonances are consistent with formation of a methyl-pyridine compound, as illustrated in eq. 17. When additional pyridine is added to drive this reaction to completion, decomposition occurs.

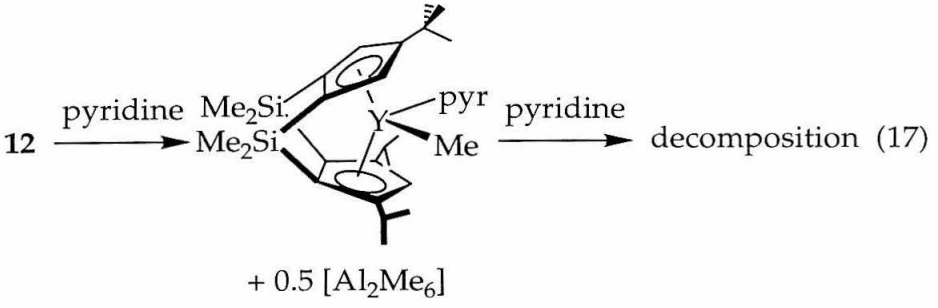

When 1 equivalent of pyridine is added to tBuThpScMe$_2$AlMe$_2$ in benzene-d_6, a C_1-symmetric species forms initially and a C_s-symmetric species grows in over the course of 24 hours. Analysis by ^{1}H NMR spectroscopy reveals that the initial product may be a methyl-pyridine adduct and the second product a dimeric methyl complex (eq. 18).

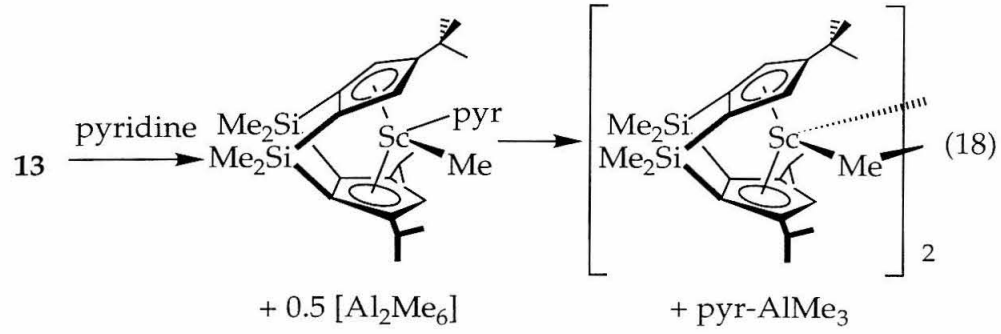

(18)

Strauss and Grubbs have utilized 4-dimethylaminopyridine (DMAP) as a stoichiometric trap for AlMe$_2$Cl.[28] The insolubility of DMAP-AlMe$_2$Cl in pentane was designed as a driving force for the reaction described in equation 19.

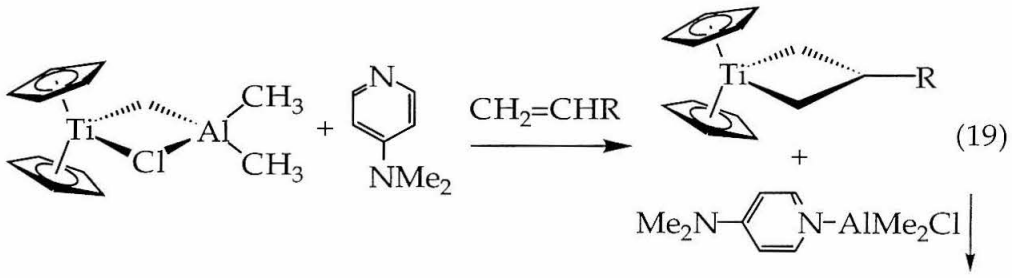

(19)

Addition of approximately 1 equivalent of DMAP to tBuThpYMe$_2$AlMe$_2$ in benzene-d_6 solution provides a mixture of products, as evidenced by ^{1}H NMR spectroscopy. At least one C_1- and one C_s- symmetric product are present. Notably, all of the starting yttrocene was consumed. However, when this reaction was attempted on a preparative scale, extensive decomposition occurred.

The reactivity of the yttrocene and scandocene products described in eq. 17 and eq. 18 towards propylene has been examined. Addition of 1 equivalent of pyridine and 10 equivalents of propylene to tBuThpMMe$_2$AlMe$_2$ (where M = Y,

Sc) in benzene-d_6, does not lead to olefin consumption, as evidenced by ^{1}H NMR spectroscopy (eq. 20). Over the course of three days at 25°C, negligible propylene is consumed and additional metallocene products are formed that were not observed in the propylene-free reactions. Addition of stoichiometric pyridine does not enhance the reactivity of tBuThpMMe$_2$AlMe$_2$ (where M = Y, Sc) towards α-olefins, such as propylene.

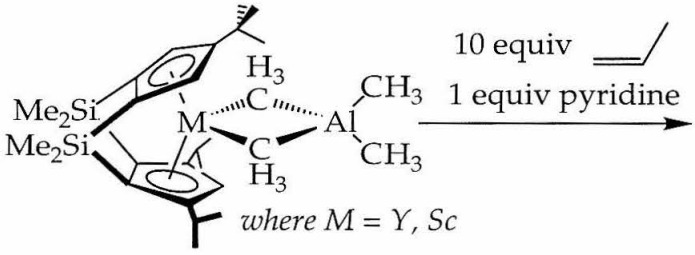

(20)

Methylaluminoxane has also been examined as a potential additive to enhance the reactivity of tBuThpMMe$_2$AlMe$_2$ (where M = Y, Sc) towards α-olefins. However, addition of MAO (≈ 100 equivalents) to tBuThpMMe$_2$AlMe$_2$ (where M = Y, Sc) in combination with propylene (in benzene-d_6) or 1-pentene (neat) does not lead to olefin consumption.

Preparation of linked cyclopentadienyl-fluorenyl complexes

The dilithio ligand salt, Li$_2$[Ph$_2$C(C$_5$H$_4$)(C$_{13}$H$_8$)] (Li$_2$Ep)[29] has been utilized for the preparation of C_s-symmetric yttrocene and scandocene complexes. Metallation of Li$_2$Ep with YCl$_3$(THF)$_{3.5}$ in THF affords the dimeric yttrocene chloride complex, {[Ph$_2$C(η^5-C$_5$H$_4$)(η^5-C$_{13}$H$_8$)]YCl}$_2$ [(EpYCl)$_2$, **15**] as a bright yellow solid (eq. 21). The ^{1}H NMR spectrum of **15** is consistent with this structural assignment; no protio THF is present and the product exhibits C_s-symmetry.

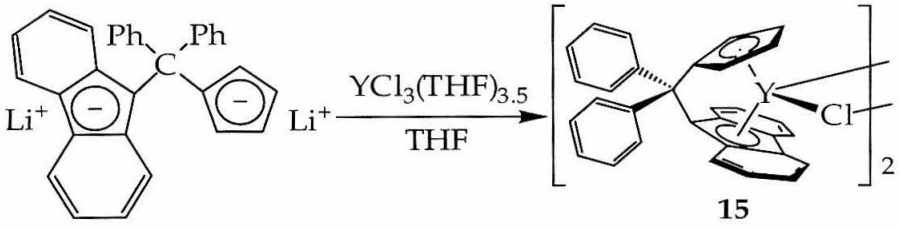

(21)

15

Metallation of Li_2Ep with $ScCl_3(THF)_3$ in THF provides the monomeric scandocene complex, $[Ph_2C(\eta^5\text{-}C_5H_4)(\eta^5\text{-}C_{13}H_8)]ScCl(THF)$ [EpScCl(THF), **16**] as a bright yellow solid (eq. 22). Analysis of **16** by ^1H NMR spectroscopy in THF-d_8 reveals that one equivalent of protio THF is present. Since **16** appears to be C_s-symmetric, the THF may be dissociating and recoordinating to scandium at a rate that is fast relative to the NMR time scale.

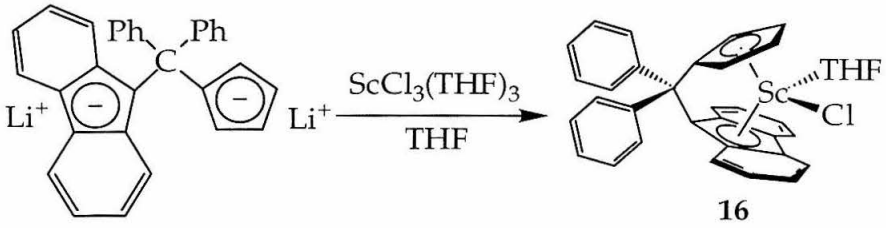

(22)

16

Combination of either **15** or **16** with excess $LiAlMe_4$ provides the corresponding tetramethylaluminate complexes, $[Ph_2C(\eta^5\text{-}C_5H_4)(\eta^5\text{-}C_{13}H_8)]M(\mu\text{-}CH_3)_2Al(CH_3)_2$ (where M = Y, $EpYMe_2AlMe_2$, **17**; where M = Sc, $EpScMe_2AlMe_2$, **18**], respectively (eq. 23). These complexes have been isolated via Soxhlet extraction with pentane solvent; low solubility of **17** and **18** in pentane results in low isolated yields.

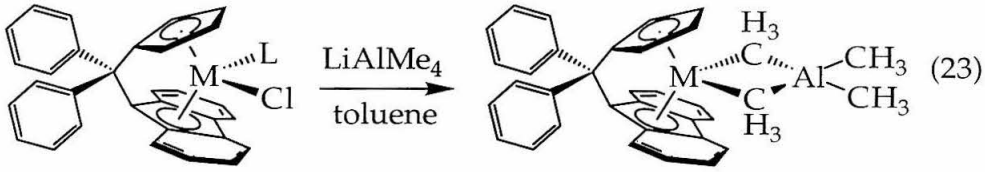

(23)

M = Y, **17**
M = Sc, **18**

Both **17** and **18** have been characterized by ^1H NMR spectroscopy in benzene-d_6 solution at 25°C. Yttrocene **17** displays a broad resonance at -1.2 ppm that corresponds to all four yttrium-methyl resonances, both bridging and terminal. Scandocene **20** displays three distinct scandium methyl resonances; the bridging methyls are found at -1.83 ppm and the terminal methyls are found at -0.52 and -0.55 ppm.

Polymerization of α-olefins

The yttrocene and scandocene alkyl and hydride complexes described above have been tested as potential catalysts for α-olefin polymerization. Both small scale (≈ 15 mg metallocene) and preparative scale (≈ 300 mg metallocene) reactions have been carried out to examine the efficiency of olefin consumption.

When ethylene (≈ 100 equivalents) is added to a benzene-d_6 solution of the yttrium tetramethylaluminate compound, tBuThpYMe$_2$AlMe$_2$ (**12**), it is consumed rapidly as evidenced by ^{1}H NMR spectroscopy. The increased viscosity of the solution and the ^{1}H NMR spectrum suggest formation of polyethylene. Addition of α-olefins such as propylene or 1-hexene (≈ 100 equivalents) to this yttrocene yields no measurable olefin consumption after weeks at 25°C. In contrast, when 1-hexene (≈ 40 equivalents) is added to a benzene-d_6 solution of the related scandocene compound, tBuThpScMe$_2$AlMe$_2$ (**13**), olefin is completely consumed within 4 hours at 25°C. Analysis by ^{1}H NMR spectroscopy reveals that 1-hexene oligomers have formed. From these experiments it appears that **13** is more reactive towards α-olefins than **12**.

A proposed mechanism for α-olefin insertion into a tetramethylaluminate complex of the form RThpMMe$_2$AlMe$_2$ (where M = Y, Sc) is given in Scheme 3. Presumably when aluminum does not share bridging methyl substituents with the metallocene, trimethylaluminum may dissociate readily. This dissociation is shown in Scheme 3 when the olefin CH$_2$=CHR' coordinates to the metallocene. Throughout the course of polymerization, AlMe$_3$ may be associated with the metallocene between olefin insertions. These mechanistic issues are currently under investigation with singly-linked and unlinked scandium tetramethylaluminate complexes.[30]

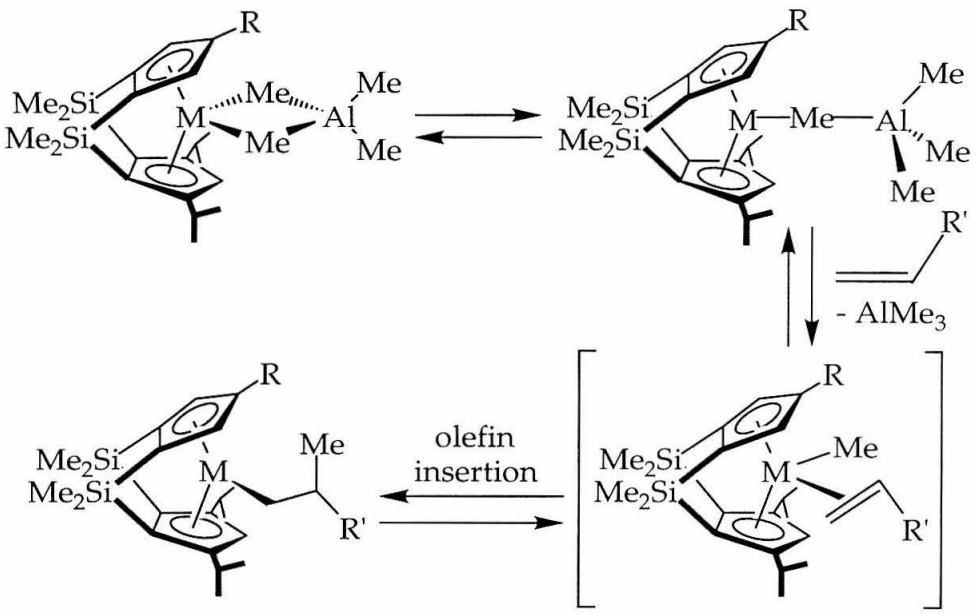

Scheme 3: Proposed mechanism for α-olefin insertion with compounds of the form RThpMMe2AlMe2.

Compound **13** also serves as an effective hydrocyclization catalyst for α-ω dienes. Addition of 1,5-hexadiene (≈ 50 equivalents) to a toluene-d_8 solution of **13** under dihydrogen affords a mixture of cyclized and uncyclized products (eq. 24). The relative amounts of methylcyclopentane and hexane were ascertained by gas chromatography. Combination of 1,6-heptadiene (≈ 50 equivalents) and **13** in benzene-d_6 under dihydrogen affords a mixture of cyclized and uncyclized products (eq. 25). The relative amounts of methylcyclohexane and heptane were measured by gas chromatography. For both reactions, conversion to products is complete within approximately 24 hours.

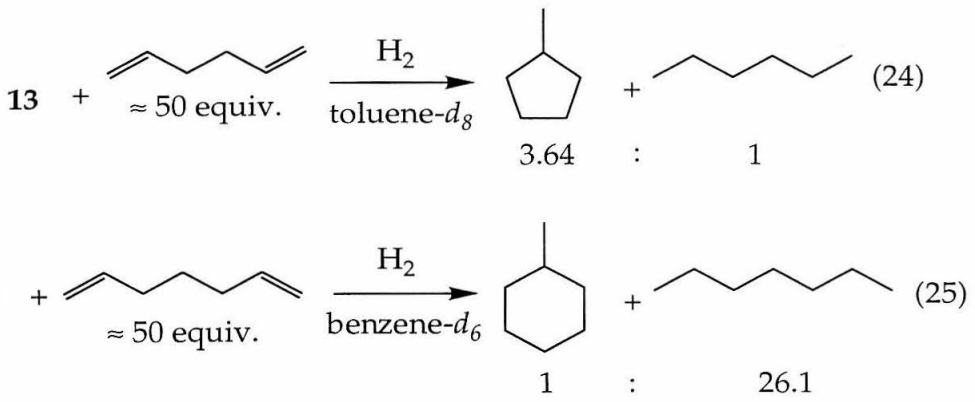

Yttrocene compounds tBuThpYCH(TMS)$_2$ (**10**) and [tBuThpYH]$_2$ (**11a/11b**) are less reactive towards ethylene and α-olefins than their tetramethylaluminate counterparts. When ethylene (≈ 5 equivalents) is added to a benzene-d_6 solution of **10** no olefin consumption is observed over the course of 12 hours at 25°C. Similarly, addition of ethylene (≈ 5 equivalents) to a benzene-d_6 solution of **11a/11b** results in no olefin consumption over the course of 12 hours at 25°C. Addition of α-olefins such as propylene or 1-pentene (100 equivalents) to **11a/11b** yields no measurable olefin consumption after weeks at 25°C. When **11a/11b** are exposed to neat 1-butene (≈ 860 equivalents) for five days at 25°C, no isolable polymer is formed. Combination of **10** and approximately 5200 equivalents of neat 1-pentene does not provide isolable polymer after one week at 25°C. Successful polymerization of 1-pentene was achieved by *in situ* generation of the corresponding yttrium hydride species; when **10** is exposed to neat 1-pentene (≈ 8100 equivalents) under a dihydrogen atmosphere, poly(pentene) is isolated after 7.5 days at 25°C.

The observed lack of reactivity of **10** and **11a/11b** towards α-olefins and the requirement for *in situ* generation of a yttrium hydride species may be rationalized by Schemes 4 and 5. Scheme 4 delineates a mechanism for α-olefin insertion into the bis(trimethylsilyl)methyl complex, **10**. Unfavorable steric interactions between the bulky bis(trimethylsilyl)methyl substituent and an incoming α-olefin (CH_2=CHR') may hinder olefin coordination and subsequent insertion. Coordination and insertion of CH_2=CHR' may be more facile for related tetramethylaluminate complexes since loss of trimethylaluminum may reduce the steric hindrance at the metal center (Scheme 3).

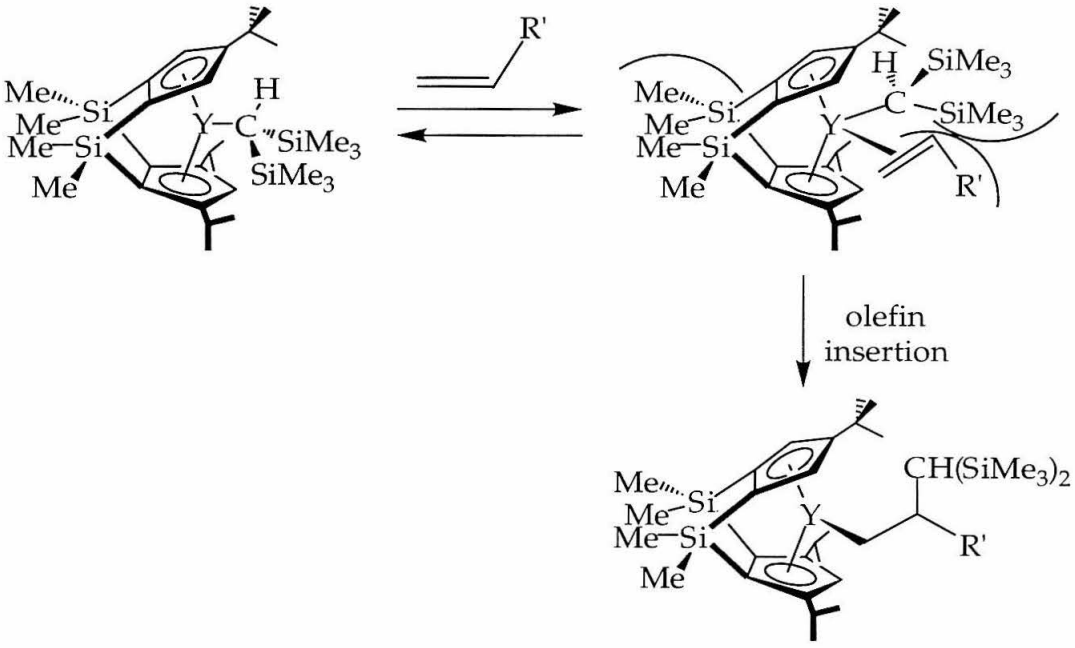

Scheme 4: Proposed mechanism for α-olefin insertion for tBuThpYCH(TMS)$_2$.

Scheme 5 describes α-olefin coordination and insertion with a monomeric yttrocene hydride intermediate. Previous studies have suggested that a monomeric hydride species is required for polymerization of α-olefins.[31] The steric hindrance for olefin coordination and insertion is negligible as compared to what is described in both Scheme 3 and Scheme 4. However, dimerization of the monomeric yttrocene hydride may compete with olefin insertion, thus reducing the rate of propagation. *In situ* hydrogenation of **10** may be necessary to generate a working concentration of monomeric [tBuThpYH] that is necessary for propagation.

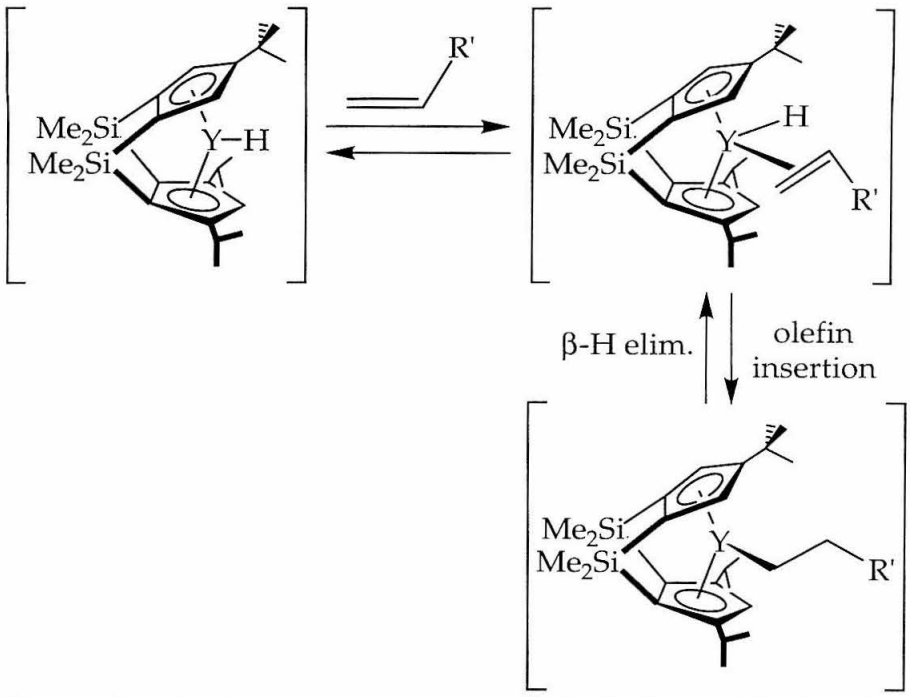

Scheme 5: Proposed mechanism for α-olefin insertion for *in situ* formed [tBuThpYH].

The metallocenes illustrated in Figure 21 have been utilized for polymerization of 1-pentene and propylene. Tetramethylaluminate complexes **12**, **13**, **14**, and **18** serve as single component polymerization catalysts. Dihydrogen gas (4 atm) was added to **10** to promote the polymerization of 1-pentene (*vide supra*). Select reaction conditions and full pentad distributions for these polymers are listed in Tables 6 and 7.

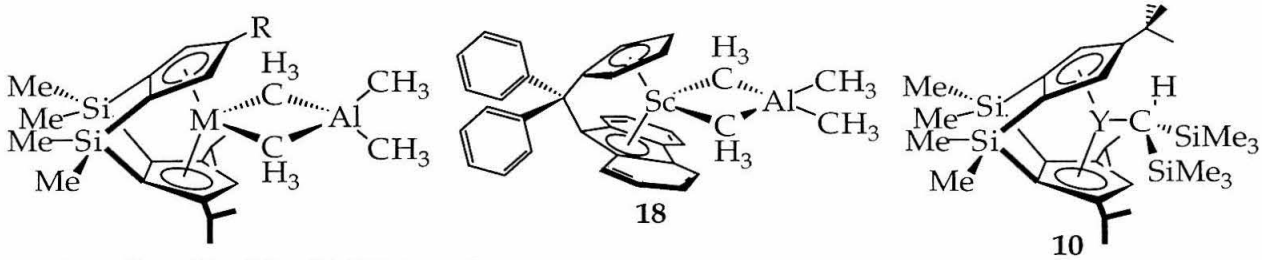

where R = tBu: M = Y, **12**; M = Sc, **13**
where R = iPr: M = Sc, **14**

Figure 21: Compounds **12**, **13**, **14**, **18**, and (**10** + H_2) may be used as catalysts for α-olefin polymerization.

entry	catalyst	T(°C)	duration	% yield by mass	[*mmmm*]	[*mmmr*] [*rmmr*] [*mmrr*]	[*mmrm*] [*rmmr*]	[*mrmr*] [*rrrr*]	[*mrrr*]	[*mrrm*]	[*m*]	[*r*]
1	**13**	0	10.75 hr	50.7	9.49	23.84	25.26	25.03	11.78	4.52	48.31	51.73
2	**13**	20	2 hr	37.5	8.90	24.68	26.22	21.29	12.57	6.35	47.92	52.12
3	**14**	0	9 hr	89.0	22.64	29.03	28.17	7.30	8.30	4.55	62.76	37.26
4	**14**	21	2 hr	64.5	20.81	30.20	27.24	8.28	9.15	4.60	61.69	38.62
5	**12**	22	7.5 d	4.8	25.39	28.40	27.36	6.54	8.38	3.80	64.39	35.51
6	**10** + H_2	22	7.5 d	8.6	21.62	25.40	27.68	10.34	7.79	7.18	59.23	40.81
7	**18**	21	24 hr	49.9	29.45	27.85	25.79	5.16	7.84	3.92	66.86	33.18

Table 6: 1-pentene polymerizations.

entry	cat.	duration	[*mmmm*]	[*mmmr*]	[*rmmr*]	[*mmrr*]	[*mrmm*] [*rmrr*]	[*mrmr*]	[*rrrr*]	[*mrrr*]	[*mrrm*]	[*m*]	[*r*]
1	**18**	10.67 hr	0.62	4.24	4.87	8.6	21.58	13.83	16.4	19.41	10.45	31.74	68.26
2	**13**	1 hr	1.9	6.56	6.35	9.78	24.39	13.97	12	17.64	7.42	38.88	61.13
3	**13**	3 hr	1.44	6.93	6.98	10.92	27.12	13.96	11.34	16.23	5.09	41.35	58.66
4	**13**	4 hr*	2.07	7.96	7.43	10.62	25.82	14.21	11.19	15.48	5.21	42.79	57.21
5	**14**	2.5 hr	3.76	11.17	8.35	12.02	28.1	14.48	5.38	11.22	5.52	50.58	49.42
6	**14**	1 hr	4.97	11.91	7.85	11.7	26.93	14.19	5.18	11.02	6.23	51.14	48.84
7	**14**	4 hr*	3.72	11.1	9.4	12.37	27.28	14.35	5.9	11.49	4.38	51.22	48.77

Table 7: Propylene polymerizations. * denotes polymerization with a 50/50 (v/v) mixture of propylene and toluene.

entry	catalyst	monomer	T(°C)	duration	[*m*]	[*r*]	M_n (x 10^3)	M_w (x 10^3)	M_w/M_n
1	**18**	propylene	-5	10.67 hr	31.74	68.26	86.0	195	2.3
2	**13**	propylene	-5	1 hr	38.88	61.13	—	—	—
3	**13**	propylene	-5	3 hr	41.35	58.66	—	—	—
4	**13**	propylene	-5	4 hr*	42.79	57.21	13.4	34.0	2.5
5	**13**	1-pentene	20	2 hr	47.92	52.12	4.5	11.6	2.6
6	**13**	1-pentene	0	10.75 hr	48.31	51.73	9.3	26.7	2.9
7	**14**	propylene	-5	2.5 hr	50.58	49.42	—	—	—
8	**14**	propylene	-5	1 hr	51.14	48.84	—	—	—
9	**14**	propylene	-5	4 hr*	51.22	48.77	16.0	32.1	2.0
10	**10** + H_2	1-pentene	22	7.5 d	59.23	40.81	—	—	—
11	**14**	1-pentene	21	2 hr	61.69	38.62	3.9	7.5	1.9
12	**14**	1-pentene	0	9 hr	62.76	37.26	—	—	—
13	**12**	1-pentene	22	7.5 d	64.39	35.51	2.9	5.5	1.9
14	**18**	1-pentene	21	24 hr	66.86	33.18	5.3	10.5	2.0

Table 8: Polymerizations of 1-pentene and propylene.
* denotes polymerization with a 50/50 (v/v) mixture of propylene and toluene.

A comparison of the [*m*] and [*r*] diad content for these 1-pentene and propylene polymerizations is summarized in Table 8. Polymer molecular weight information is also provided when available. The scandium tetramethylaluminate complexes **13**, **14**, and **18** display the highest polymer molecular weights of the series; this is notable since scandocene complexes generally dimerize α-olefins.[32] In general, the scandocenes, **13**, **14**, and **18**, are more active polymerization catalysts than yttrocenes, **12** and (**10** + H_2). A proposed mechanism for α-olefin insertion, chain propagation, and termination with tetramethylaluminate compounds of the form RThpMMe_2AlMe_2 (where M = Y, Sc) is provided in Scheme 6.

Use of these catalysts under a variety of conditions yields polymers with essentially atactic microstructures with a continuum of tacticities that range from a slight syndiotactic preference ([*r*] ≈ 68%) to a slight isotactic preference ([*m*] ≈ 67%). Changes in polymerization temperature or monomer dilution appear to exert little influence on polymer tacticity, within experimental error. For a given catalyst, the [*r*] diad content is larger for the polypropylene it produces versus polypentene. This effect is most striking for catalyst **18**; it forms the most syndiospecific polypropylene and the most isospecific polypentene of the series.

This tacticity data is consistent with the chain-end control mechanism depicted in Scheme 7, where small differences in transition state energies for olefin insertion may provide some stereoregularity in the polymer microstructure. Since relaxation of the polymer chain to the central position of the metallocene wedge appears to be fast relative to olefin insertion, stereocontrol is not derived from regular alternating olefin insertion. These C_s-symmetric group 3 catalysts appear to follow a chain-end control mechanism unlike the mechanism of stereocontrol for analogous zirconocene catalysts.

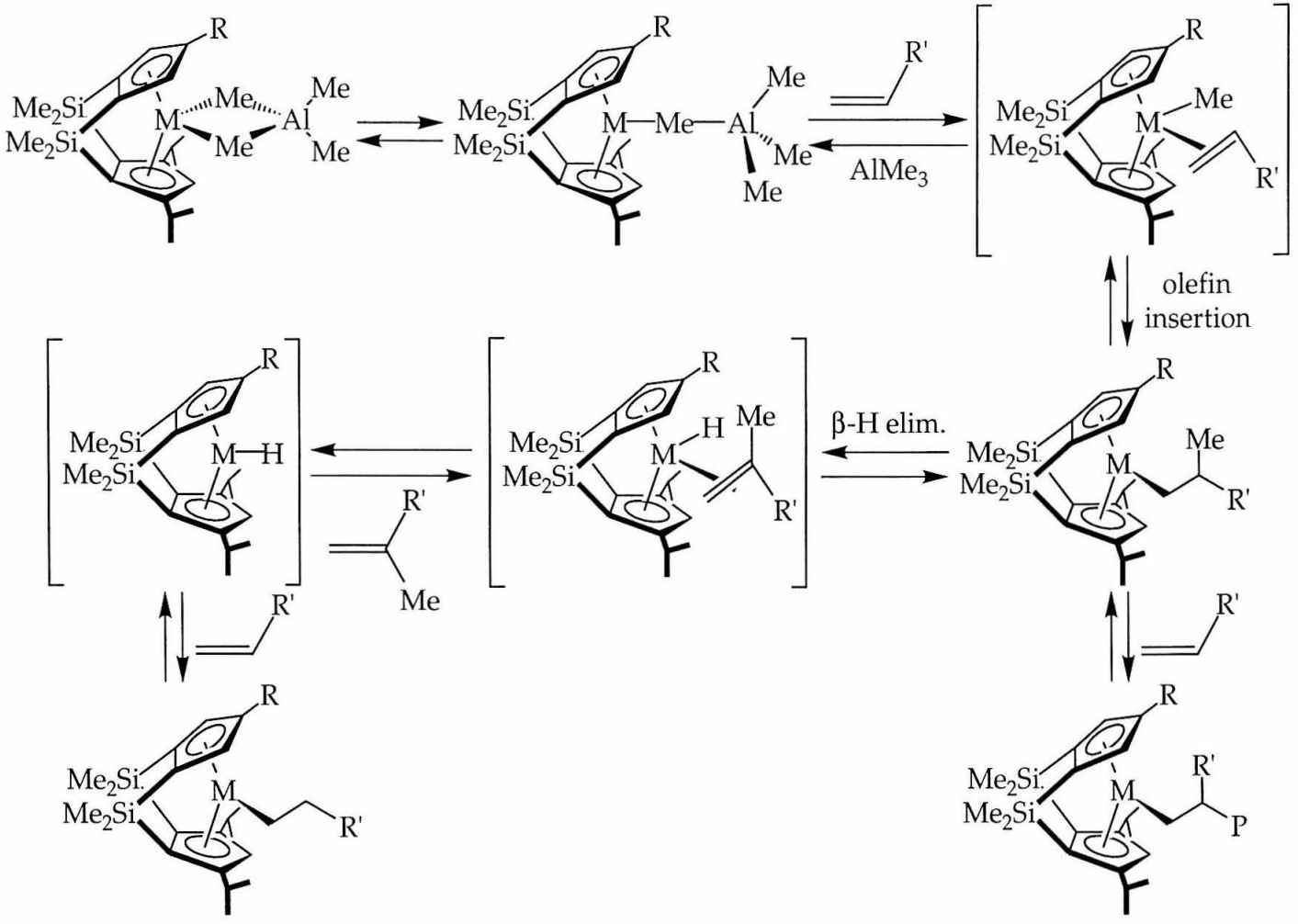

Scheme 6: Proposed mechanism for α-olefin polymerization with tetramethylaluminate compounds of the form RThpMMe2AlMe2.

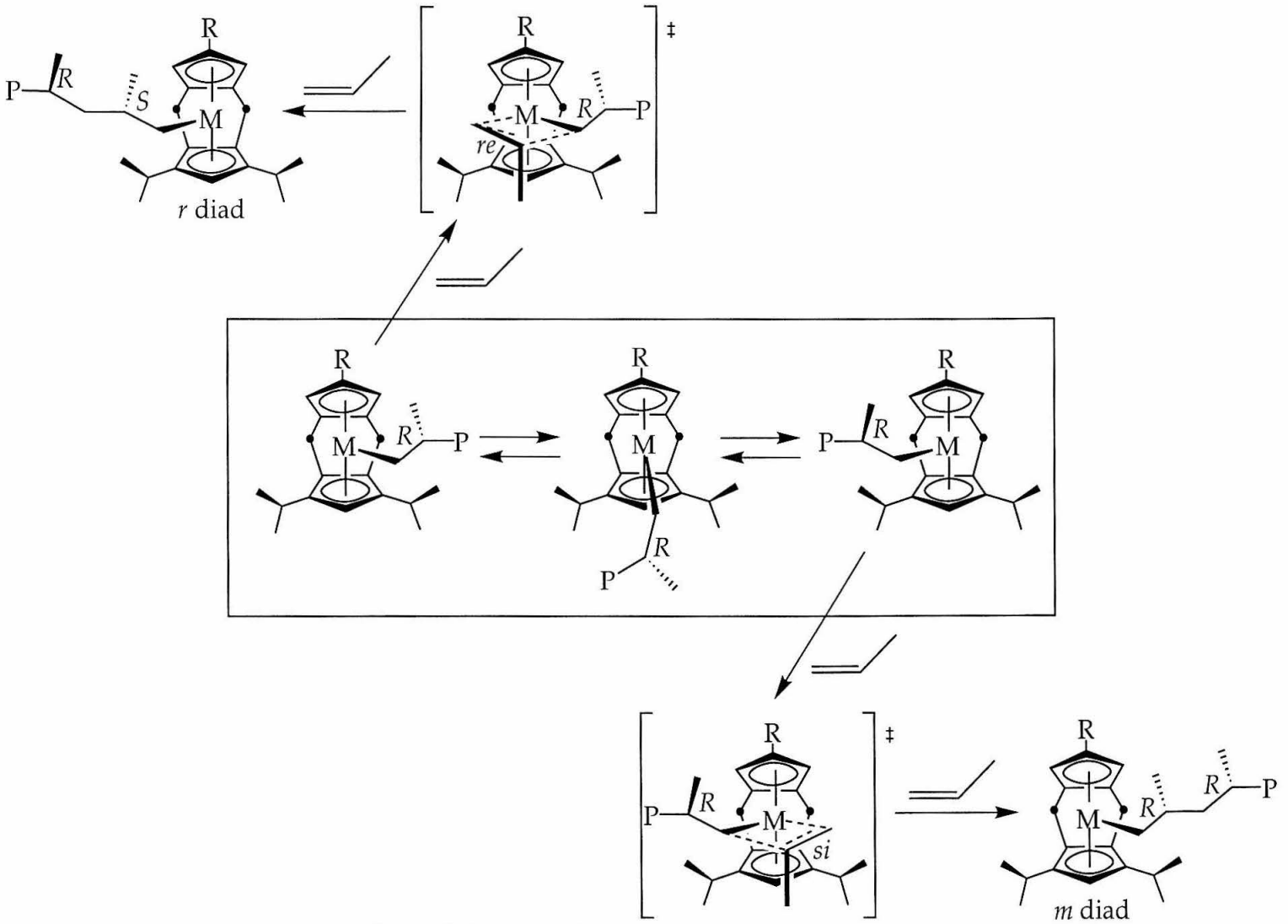

Scheme 7: Rapid site epimerization may induce a chain-end mechanism for stereocontrol.

Conclusions

A series of C_s-symmetric yttrocene and scandocene hydride and alkyl complexes have been prepared as single component catalysts for α-olefin polymerization. Yttrocene and scandocene chloride complexes that employ the doubly-silylene bridged ligand array, [(1,2-$SiMe_2$)$_2$(4-$CHMe_2$-C_5H_2)(3,5-($CHMe_2$)$_2$-C_5H)] (tBuThp), have been synthesized and characterized by X-ray diffraction. Both compounds exist as potassium chloride adducts with ethereal solvent coordinated to potassium (tetrahydrofuran or diethyl ether, respectively). The related complexes iPrThpY(μ-Cl)$_2$K(THF)$_n$ and iPrThpSc(μ-Br)$_2$K(THF)$_n$ have been prepared as well. A yttrocene alkyl complex, tBuThpYCH(TMS)$_2$, has been synthesized by combination of tBuThpY(μ-Cl)$_2$K(THF)$_n$ with NaI and subsequent metathesis with KCH($SiMe_3$)$_2$. This yttrocene alkyl compound has been characterized by X-ray crystallography; its structure displays an interaction between yttrium and one of the silicon-carbon bonds of the bis(trimethylsilyl)methyl substituent. Hydrogenation of tBuThpYCH(TMS)$_2$ provides a mixture of two dimeric yttrocene hydride complexes, Y{μ-(tBuThp)$_2$(μ-H)$_2$}Y. One of these hydride complexes has been analyzed by X-ray diffraction; each ligand array spans two metal centers in a "fly-over" dimeric structure. Reaction of RThpM(μ-X)$_2$K(THF)$_n$ (where M = Y, Sc; R = tBu, iPr; X = Cl , Br) with $LiAlMe_4$ affords the corresponding tetramethylaluminate complexes RThpM(μ-Me)$_2$$AlMe_2$ (where M = Y, Sc; R = tBu, iPr). Scandocene and yttrocene tetramethylaluminate complexes that employ a singly linked cyclopentadienyl-fluorenyl ligand, [(C_6H_5)$_2$C{(η^5-C_5H_4)(η^5-fluorenyl)}]M(μ-Me)$_2$$AlMe_2$ (where M = Y, Sc), have been synthesized using a similar methodology.

Select tetramethylaluminate complexes serve as single component catalysts for polymerization of propylene and 1-pentene. *In situ* generation of [tBuThpYH] provides an active species for polymerization of 1-pentene. The scandium tetramethylaluminate complexes display higher polymerization activities and produce higher polymer molecular weights than the yttrocene catalysts. Overall these catalysts produce polymers with essentially atactic microstructures under a variety of conditions. Polymer tacticities range from a slight syndiotactic preference ([*r*] ≈ 68%) to a slight isotactic preference ([*m*] ≈ 67%). This tacticity data is consistent with a chain-end control mechanism. The

polymer chain appears to relax to the central position of the metallocene wedge at a rate faster than olefin insertion. Therefore, stereocontrol is not derived from regular alternating olefin insertion. The C_s-symmetric group 3 catalysts described herein follow a stereocontrol mechanism unlike that of analogous zirconocene catalysts. These metallocenes have expanded our understanding of stereocontrol for syndiospecific α-olefin polymerizations.

Experimental

General Considerations. All air or moisture sensitive chemistry was performed using standard high vacuum line or Schlenk techniques, or in a dry box under a nitrogen atmosphere as described previously.[33] Dinitrogen, dihydrogen, and argon were purified by passage over MnO on vermiculite and activated molecular sieves. Petroleum ether and toluene were distilled from sodium and stored under vacuum over titanocene.[34] Tetrahydrofuran and diethyl ether were distilled from sodium benzophenone ketyl. Pyridine was distilled from CaH_2 immediately before use. 1-hexadiene and 1-heptadiene were distilled from $LiAlH_4$ immediately before use. Benzene-d_6 was distilled from $LiAlH_4$ and then distilled from sodium sand before use. Tetrahydrofuran-d_8 was distilled from sodium benzophenone ketyl and stored over 4Å molecular sieves. Methylene chloride-d_2 was distilled from calcium hydride. Ethylene was purchased from Matheson and passed through a dry ice/acetone trap before use. Propylene was purchased from Aldrich and stored under vacuum over triisobutylaluminum. MAO (methylaluminoxane, Albemarle) was prepared by removing toluene *in vacuo*; the white MAO solid was dried at 25°C for 48 hours at high vacuum. $LiCH(TMS)_2$ was prepared by the method of Cowley.[35] Potassium bis(trimethylsilyl)amide ($KN(TMS)_2$) was sublimed before use. $Li_2[Ph_2C(C_5H_4)(C_{13}H_8)]$ (Li_2Ep) was prepared as described by Razavi.[29] $ScCl_3(THF)_3$ and $YCl_3(THF)_{3.5}$ were prepared according to literature methods.[36] Protio RThp ligands, $(1,2\text{-}SiMe_2)_2(4\text{-}R\text{-}C_5H_3)(3,5\text{-}(CHMe_2)_2\text{-}C_5H_2)$ (where R = tBu, iPr), were synthesized as described previously.[4] All dilithio and dipotassio ligand salts were prepared via standard procedures[37] unless otherwise noted. All other reagents were purchased from Aldrich and used as received or purified using standard methods.[38]

Instrumentation. NMR spectra were recorded on a Bruker AM500 (^{1}H, 500.13 MHz; ^{13}C, 125.77 MHz) spectrometer, a Joel GX-400 (^{1}H, 399.78 MHz; ^{13}C 100.53 MHz; ^{19}F, 376.1 MHz) spectrometer, a G.E. QE300 (^{1}H, 300.1 MHz) spectrometer, a Varian INOVA 500 (^{1}H, 500.13 MHz; ^{13}C, 125.77 MHz) spectrometer, or a Varian 300 (^{1}H , 300 MHz) spectrometer. All chemical shifts are relative to TMS for ^{1}H (residual) and ^{13}C NMR (solvent used as a secondary standard). Nuclear Overhauser (NOE) difference experiments were conducted using a Varian INOVA 500 MHz spectrometer. Elemental analysis was performed at the California Institute of Technology Elemental Analysis Facility by Fenton I. Harvey or at Midwest Microlab in Indianapolis, Indiana. X-ray crystallography was carried out by Dr. Michael W. Day and Lawrence M. Henling using an Enraf-Nonius CAD-4 diffractometer. Small crystalline fragments were cut under Paratone-N oil and mounted on the diffractometer under a stream of cold N_2 gas.

$Li_2[(1,2\text{-}SiMe_2)_2(4\text{-}CMe_3\text{-}C_5H_2)(3,5\text{-}(CHMe_2)_2\text{-}C_5H)]$ (2). (Li_2tBuThp). In the dry box a 100 mL round bottom flask was charged with $[(1,2\text{-}SiMe_2)_2(4\text{-}CMe_3\text{-}C_5H_3)(3,5\text{-}(CHMe_2)_2\text{-}C_5H_2)]$ (2.21 g, 5.74 mmol) and attached to a fine porosity swivel frit assembly. On the vacuum line, diethyl ether (50 mL) was added by vacuum transfer. The -78°C cold bath was replaced with a 0°C ice water bath and the apparatus was backfilled with argon. A cannula was threaded through the side arm of the swivel frit and then *n*-BuLi (9.0 mL, 12.60 mmol, 2.2 equiv, 1.4 M in hexanes) was added dropwise via a syringe. When addition was complete, the cannula was removed and replaced with the Kontes valve and the reaction was left open to the mercury bubbler to slowly warm to 25°C. After 24 hr of stirring, diethyl ether was removed *in vacuo*, petroleum ether (50 mL) was added by vacuum transfer, and the reaction mixture was stirred for 30 minutes. Petroleum ether was removed *in vacuo*, then fresh petroleum ether (50 mL) was added by vacuum transfer. A yellow supernatent was filtered away from a white solid and washed with recycled petroleum ether (2 x 40 mL). The petroleum ether was removed *in vacuo* and the white solid was dried under high vacuum for 4 hr; 2.49 g (89.7%). ^{1}H NMR (THF-d_8): δ = 0.27 (s, 12H, broad $(CH_3)_2Si$), 1.21 (d, 12H, $(CH_3)_2CH$, J = 6.8), 1.27 (s, 9H, $(CH_3)_3C$), 3.13 (m, 2H, $(CH_3)_2CH$, J = 6.8), 5.92 (s, 1H, Cp-*H*), 6.12 (s, 2H, Cp-*H*).

$K_2[(1,2\text{-}SiMe_2)_2(4\text{-}CMe_3\text{-}C_5H_2)(3,5\text{-}(CHMe_2)_2\text{-}C_5H)]$ (3). (K_2tBuThp). In the dry box a 250 mL round bottom flask was charged with $[(1,2\text{-}SiMe_2)_2(4\text{-}CMe_3\text{-}C_5H_3)(3,5\text{-}(CHMe_2)_2\text{-}C_5H_2)]$ (3.55 g, 9.20 mmol) and $KN(TMS)_2$ (3.49 g, 17.5 mmol, 1.90 eq) and attached to a fine porosity swivel frit assembly. On the vacuum line, diethyl ether (150 mL) was added by vacuum transfer. A few minutes after the addition of diethyl ether, the solution becomes cloudy. The -78°C cold bath was removed to allow the reaction to slowly warm to 25°C. The apparatus was backfilled with argon and stirred for 12 hr. A yellow supernatent was filtered away from an off-white solid and washed with recycled diethyl ether (4 x 100 mL). After removing diethyl ether *in vacuo*, petroleum ether (75 mL) was added by vacuum transfer and used to wash the solid three additional times. Petroleum ether was removed *in vacuo* and the off-white solid was dried under high vacuum for 6 hr with heating to 50°C; 3.80 g (89.6%). ^{1}H NMR (THF-d_8): δ = 0.13 (s, 12H, broad $(CH_3)_2Si$), 1.14 (d, 12H, $(CH_3)_2CH$, J = 6.77), 1.27 (s, 9H, $(CH_3)_3C$), 3.05 (m, 2H, $(CH_3)_2CH$, J = 6.30), 5.71 (s, 1H, Cp-*H*), 5.97 (s, 2H, Cp-*H*).

$K_2[(1,2\text{-}SiMe_2)_2(4\text{-}CHMe_2\text{-}C_5H_2)(3,5\text{-}(CHMe_2)_2\text{-}C_5H)]$ (4). (K_2iPrThp). Compound **4** is prepared in an analogous manner to **3** by the reaction of $[(1,2\text{-}SiMe_2)_2(4\text{-}CHMe_2\text{-}C_5H_4)(3,5\text{-}(CHMe_2)_2\text{-}C_5H_3)]$ (4.69 g, 12.6 mmol) with $KN(SiMe_3)_2$ (4.78 g, 23.9 mmol, 1.90 equiv) in diethyl ether (125 mL). The resulting suspension was allowed to slowly warm to 25°C while stirring for 12 hr. The white solid was isolated on a fine frit and washed with diethyl ether (3 x 50 mL) and then with petroleum ether (3 x 50 mL). The solvent was removed *in vacuo* and the solid dried under high vacuum for 6 hr with heating to 50°C to provide a white powder; 4.87 g (86.5%).

$[(1,2\text{-}SiMe_2)_2(\eta^5\text{-}4\text{-}CMe_3\text{-}C_5H_2)(\eta^5\text{-}3,5\text{-}(CHMe_2)_2\text{-}C_5H)]Y(\mu\text{-}Cl)_2K(THF)_n$ (5). (tBuThpY(μ-Cl)$_2$K(THF)$_n$). In the glove box, a 200 mL flask was charged with **3** (3.49 g, 7.58 mmol) and $YCl_3(THF)_{3.5}$ (3.39 g, 7.58 mmol) and attached to a fine porosity swivel frit assembly. On the vacuum line, tetrahydrofuran (125 mL) was added by vacuum transfer while stirring at -78°C, and then this cold bath was replaced by a 0°C ice water bath and the reaction was allowed to slowly warm to 25°C while stirring. After 72 hr of reaction, solvent was removed *in vacuo* and the solid dried under high vacuum for 12 hr. Diethyl ether (100 mL) was added to the reaction flask via vacuum transfer to give a pale tan slurry; a pale tan solid was filtered away from the orange supernatant and washed with

recycled solvent (3 x 75 mL). Solvent was removed *in vacuo* and the solids dried under high vacuum for 12 hr. Petroleum ether (100 mL) was added to the flask containing the orange diethyl ether soluble material by vacuum transfer to yield an off-white solid precipitate and a pale yellow solution. This off-white solid was filtered away from the supernatant and washed with recycled petroleum ether (4 x 75 mL). Solvent was removed *in vacuo* and hexane (50 mL) was added for two additional solid washings. Solvent was removed *in vacuo* and the off-white product was dried under high vacuum for 12 hr; 2.44 g (51.3%). ^{1}H NMR (THF-d_8): δ = 0.56 (s, 6H, $(CH_3)_2Si$), 0.69 (s, 6H, $(CH_3)_2Si$), 0.99 (d, 6H, $(CH_3)_2CH$, J = 6.9), 1.21 (d, 6H, $(CH_3)_2CH$, J = 6.6), 1.27 (s, 9H, $(CH_3)_3C$), 1.78 (m, ~0.25H, protio THF), 2.90 (m, 2H, $(CH_3)_2CH$, J = 6.7), 3.62 (m, ~0.25H, protio THF), 5.75 (s, 1H, Cp-*H*), 6.32 (s, 2H, Cp-*H*). ^{1}H NMR (CD_2Cl_2): δ = 0.54 (s, 6H, $(CH_3)_2Si$), 0.76 (s, 6H, $(CH_3)_2Si$), 1.02 (d, 6H, $(CH_3)_2CH$, J = 6.8), 1.18 (d, 6H, $(CH_3)_2CH$, J = 5.7), 1.23 (s, 9H, $(CH_3)_3C$), 1.82 (broad, ~2H, protio THF), 2.75 (broad, 2H, $(CH_3)_2CH$), 3.68 (broad, protio THF), 5.83 (s, 1H, Cp-*H*), 6.34 (s, 2H, Cp-*H*). ^{13}H NMR (THF-d_8): δ = 0.68, 5.29 ($(CH_3)_2Si$), 22.75, 30.42 ($(CH_3)_2CH$, $(CH_3)_2CH$, overlapping peaks), 33.33, 33.98 ($(CH_3)_3C$, $(CH_3)_3C$), 106.46, 116.77, 121.61, 139.61, 154.23 (Cp). Analysis Calculated (Found) C: 52.91 (53.04); H: 7.03 (7.63). Note regarding preparation- amount of protio THF present in product varies from run to run, and is quantified by integration of protio THF resonances as compared to ligand resonances in the ^{1}H NMR spectrum.
Addition of 18-crown-6 (excess) to this sample yields: ^{1}H NMR (THF-d_8): δ = 0.59 (s, 6H, $(CH_3)_2Si$), 0.65 (s, 6H, $(CH_3)_2Si$), 0.99 (d, 6H, $(CH_3)_2CH$, J = 6.9), 1.21 (d, 6H, $(CH_3)_2CH$, J = 6.6), 1.27 (s, 9H, $(CH_3)_3C$), 2.97 (m, 2H, $(CH_3)_2CH$, J = 6.77), 5.70 (s, 1H, Cp-*H*), 6.33 (s, 2H, Cp-*H*).

Removal of protio THF from 5. Tetrahydrofuran was removed from **5** via a modified Soxhlet extraction, similar to a method utilized previously.[39] In the glove box, **5** (0.80 g) was placed in a 150 mL round bottom flask and attached to a Soxhlet extractor. A glass thimble (fitted with coarse frit) was filled 3/4 full with 10 Å activated molecular sieves and carefully placed inside the Soxhlet extractor. A condenser and 180° needle valve were attached and the apparatus was removed from the glove box. Toluene (100 mL) was added to the round bottom flask by vacuum transfer and then the apparatus was closed to dynamic vacuum. The solution was stirred at 25°C and the condenser cooled to -30°C with a methanol cooling unit to begin the Soxhlet extraction. After 24 hr, the

flask was attached to a fine porosity swivel frit assembly, toluene was removed and hexane (50 mL) was added via vacuum transfer to provide a white slurry. A white solid was filtered away from a yellow supernatant; the product was washed with recycled hexane (2 x 30 mL) and dried under high vacuum for 12 hr; 0.49 g. ^{1}H NMR (THF-d_8): same chemical shifts as **5** but no protio THF present.

[(1,2-SiMe$_2$)$_2$(η^5-4-CMe$_3$-C$_5$H$_2$)(η^5-3,5-(CHMe$_2$)$_2$-C$_5$H)]Sc(μ-Cl)$_2$K(THF)$_n$ (6). (tBuThpSc(μ-Cl)$_2$K(THF)$_n$). In the glove box, a 100 mL flask was charged with **3** (2.80 g, 6.07 mmol) and $ScCl_3(THF)_3$ (2.23 g, 1 equiv) and a fine swivel frit assembly was attached. On the vacuum line, tetrahydrofuran (60 mL) was added by vacuum transfer while stirring at -78°C, and then this cold bath was replaced by a 0°C ice water bath and the reaction was allowed to slowly warm to 25°C while stirring. After 4.5 days of reaction at 25°C, solvent was removed *in vacuo* to leave a brown sludge which was dried under high vacuum for 12 hr. Diethyl ether (60 mL) added to the reaction flask by vacuum transfer to provide a pale brown slurry. A pale tan solid was filtered away from a red-orange supernatant and the solid washed with recycled solvent (6 x 30 mL). Diethyl ether was removed *in vacuo* and petroleum ether (50 mL) was added by vacuum transfer. The slurry was stirred for 1 hr and then the solvent was removed *in vacuo* and the solid dried under high vacuum for 12 hr. Petroleum ether (50 mL) was added by vacuum transfer to the flask containing the orange diethyl ether soluble material. Next, a pale tan precipitate was filtered away from the supernatant and washed with recycled petroleum ether (3 x 30 mL). Solvent was removed *in vacuo* and hexane was added for three additional solid washings. Solvent was removed *in vacuo* and the pale tan product was dried under high vacuum for 12 hr; 1.21 g (36.0%). ^{1}H NMR (THF-d_8): δ = 0.54 (s, 6H, $(CH_3)_2Si$), 0.68 (s, 6H, $(CH_3)_2Si$), 0.98 (d, 6H, $(CH_3)_2CH$, J = 7.0), 1.19 (d, 6H, $(CH_3)_2CH$, J = 6.6), 1.28 (s, 9H, $(CH_3)_3C$), 1.77 (m, ~1H, protio THF), 2.86 (m, 2H, $(CH_3)_2CH$, J = 6.72), 3.62 (m, ~1H, protio THF), 5.81 (s, 1H, Cp-*H*), 6.29 (s, 2H, Cp-*H*). ^{13}H NMR (THF-d_8): δ = -0.55, 4.33 ($(CH_3)_2Si$), 21.82, 26.43, 28.99, 29.17, 32.77 ($(CH_3)_2CH$, $(CH_3)_3C$), 110.11, 113.56, 119.94, 128.03, 140.31, 156.54 (Cp). Note regarding preparation- amount of protio THF present in product varies from run to run, and is quantified by integration of protio THF resonances as compared to ligand resonances in the ^{1}H NMR spectrum.

Addition of 18-crown-6 (excess) to this sample yields: ^{1}H NMR (THF-d_8): δ = 0.57 (s, 6H, $(CH_3)_2Si$), 0.65 (s, 6H, $(CH_3)_2Si$), 0.98 (d, 6H, $(CH_3)_2CH$, J = 7.0), 1.22 (d, 6H,

(CH_3)$_2$CH, J = 6.6), 1.29 (s, 9H, (CH_3)$_3$C), 2.91 (m, 2H, (CH_3)$_2$C*H*, J = 4.66), 5.79 (s, 1H, Cp-*H*), 6.31 (s, 2H, Cp-*H*).

[(1,2-SiMe$_2$)$_2$(η^5-4-CHMe$_2$-C$_5$H$_2$)(η^5-3,5-(CHMe$_2$)$_2$-C$_5$H)]Y(μ-Cl)$_2$K(THF)$_n$ (7). (iPrThpY(μ-Cl)$_2$K(THF)$_n$). Compound **7** is prepared in an analogous manner to **5** by the reaction of **4** (824 mg, 1.84 mmol) with $YCl_3(THF)_{3.5}$ (826 mg, 1 equiv) in tetrahydrofuran (50 mL). After 48 hr of reaction at 25°C, solvent was removed *in vacuo*, petroleum ether (50 mL) was added by vacuum transfer, and the resulting slurry was stirred for 2 hr. The solvent was removed *in vacuo* and the solid dried under high vacuum for 12 hr. Diethyl ether (40 mL) was added by vacuum transfer to provide a pale tan slurry; a pale tan solid was filtered away from an orange supernatant and washed with recycled solvent (3 x 30 mL). Solvent was removed *in vacuo* and the solids dried under high vacuum for 12 hr. Petroleum ether (25 mL) was added via vacuum transfer to the flask containing the orange diethyl ether soluble material, resulting in precipitation of an off-white solid from the yellow-orange solution. This off-white solid was filtered away from the supernatant and washed with recycled petroleum ether (3 x 20 mL). Solvent was removed *in vacuo* and hexane (20 mL) was added by vacuum transfer for two additional solid washings. Hexane was removed *in vacuo* and the off-white product was dried under high vacuum for 9 hr; 0.70 g (65.0%). ^{1}H NMR (THF-d_8): δ = 0.56 (s, 6H, (CH_3)$_2$Si), 0.70 (s, 6H, (CH_3)$_2$Si), 0.99 (d, 6H, (CH_3)$_2$CH, J = 6.9), 1.78 (m, ~0.8H, protio THF), 1.97 (d, 12H, (CH_3)$_2$CH, J = 6.8), 2.83 (m, 1H, (CH_3)$_2$C*H*, J = 6.86), 2.89 (m, 2H, (CH_3)$_2$C*H*, J = 6.79), 5.75 (s, 1H, Cp-*H*), 3.62 (m, ~0.8H, protio THF), 6.26 (s, 2H, Cp-*H*). ^{13}H NMR (THF-d_8): δ = 5.19, 9.72 ((CH_3)$_2$Si), 27.22, 34.83 ((CH_3)$_2$CH, (CH_3)$_2$CH, overlapping peaks), 112.08, 121.57, 126.40, 139.89, 158.64 (Cp).

Removal of protio THF from 7. Tetrahydrofuran was removed from **7** with an analogous procedure to that used for **5**. In the glove box, **7** (0.35 g) was placed in a 50 mL round bottom flask and the Soxhlet apparatus was assembled as for **5**. Toluene (30 mL) was added to the round bottom flask and the Soxhlet extraction was carried out for 30 hr. The flask was attached to a fine porosity swivel frit assembly, toluene was removed and hexane (20 mL) was added via vacuum transfer to provide a white slurry. A white solid was filtered away from a yellow supernatant; the product was washed with recycled hexane (2 x 10 mL) and dried

under high vacuum for 12 hr; 0.49 g. ^{1}H NMR (THF-d_8): same chemical shifts as **7** but no protio THF present.

[(1,2-SiMe$_2$)$_2$(η^5-4-CMe$_3$-C$_5$H$_2$)(η^5-3,5-(CHMe$_2$)$_2$-C$_5$H)]YI(THF) (tBuThpYI(THF), 8a), {[(1,2-SiMe$_2$)$_2$(η^5-4-CMe$_3$-C$_5$H$_2$)(η^5-3,5-(CHMe$_2$)$_2$-C$_5$H)]Y(μ-I)}$_2$ {[tBuThpY(μ-I)]$_2$, 8b} In the glove box, a 100 mL round bottom flask equipped with stir bar was charged with **5** (678 mg, 1.13 mmol) and NaI (381 mg, 2.54 mmol, 2.2 equiv) and a fine swivel frit assembly attached. On the vacuum line, tetrahydrofuran (50 mL) was added by vacuum transfer while stirring at -78°C, and then this cold bath was replaced by a 0°C ice water bath and the reaction was allowed to slowly warm to 25°C. After 48 hr of reaction at 25°C, solvent was removed *in vacuo*, petroleum ether (20 mL) was added by vacuum transfer, and the resulting slurry was stirred for 30 minutes. The solvent was removed *in vacuo* and the solid dried under high vacuum for 4 hr. Diethyl ether (25 mL) was added by vacuum transfer to provide a yellow slurry; this slurry was stirred for 12 hr. A yellow-orange solution was filtered away from a white solid and the solid washed with recycled solvent (3 x 15 mL). Solvent was removed *in vacuo* and pentane (25 mL) was added to the collection flask via vacuum transfer. An orange solution was filtered away from a white solid, solvent was removed *in vacuo*, and this white solid was dried under high vacuum for 4 hr. **8a/8b** was isolated as a white solid; 470 mg (44.5%). **8a:** ^{1}H NMR (THF-d_8): δ = 0.55 (s, 6H, (C*H*$_3$)$_2$Si), 0.66 (s, 3H, (C*H*$_3$)$_2$Si), 0.70 (s, 3H, (C*H*$_3$)$_2$Si), 0.99 (d, 3H, (C*H*$_3$)$_2$CH, J = 7.0), 1.20 (d, 3H, (C*H*$_3$)$_2$CH, J = 6.6), 1.23 (d, 3H, (C*H*$_3$)$_2$CH), 1.33 (s, 9H, (C*H*$_3$)$_3$C), 1.39 (d, 3H, (C*H*$_3$)$_2$CH), 1.78 (m, 4H, protio THF), 2.97 (m, 1H, (CH$_3$)$_2$C*H*, J = 5.6), 3.05 (m, 1H, (CH$_3$)$_2$C*H*, J = 5.6), 3.62 (m, 4H, protio THF), 5.98 (s, 1H, Cp-*H*), 6.46 (s, 1H, Cp-*H*), 6.52 (s, 1H, Cp-*H*). **8b:** ^{1}H NMR (THF-d_8): δ = 0.54 (s, 6H, (C*H*$_3$)$_2$Si), 0.70 (s, 6H, (C*H*$_3$)$_2$Si), 0.98 (d, 6H, (C*H*$_3$)$_2$CH, J = 7.0), 1.20 (d, 6H, (C*H*$_3$)$_2$CH, J = 6.6), 1.27 (s, 9H, (C*H*$_3$)$_3$C), 2.83 (m, 2H, (CH$_3$)$_2$C*H*, J = 6.8), 5.86 (s, 1H, Cp-*H*), 6.30 (s, 2H, Cp-*H*).

[(1,2-SiMe$_2$)$_2$(η^5-4-CHMe$_2$-C$_5$H$_2$)(η^5-3,5-(CHMe$_2$)$_2$-C$_5$H)]Sc(μ-Br)$_2$K(THF)$_n$ (iPrThpSc(μ-Br)$_2$K(THF)$_n$, 9). In the glove box, a 100 mL round bottom flask equipped with stir bar was charged with **4** (971 mg, 2.17 mmol), ScCl$_3$(THF)$_3$ (798 mg, 1 equiv), and NaBr (849 mg, 8.25 mmol, 3.8 equiv) and a 14/20 reflux condensor and 180° needle valve attached. On the vacuum line, tetrahydrofuran (30 mL) was added by vacuum transfer and the reaction mixture was heated to

reflux under an argon atmosphere. After 4 hr of reaction, solvent was removed *in vacuo* and the solid was dried under high vacuum for 2 hr. In the glove box, a medium swivel frit assembly was attached. Petroleum ether (30 mL) was added by vacuum transfer, and the resulting yellow-white slurry was stirred for 12 hr. Solvent was removed *in vacuo* and diethyl ether (25 mL) was added by vacuum transfer to provide a yellow slurry. This slurry was stirred for 3 hr, and then a yellow solution was filtered away from a white solid. The solid was washed with recycled solvent (5 x 15 mL) and then solvent was removed *in vacuo* to provide a pale yellow foam in the collection flask. Petroleum ether (25 mL) was added to the collection flask via vacuum transfer, the slurry was stirred for 1 hr, and then solvent was removed *in vacuo*. The resulting pale yellow solid was dried under high vacuum for 12 hr. **9** was isolated as a pale yellow solid; 898 mg (65.7%). ^{1}H NMR (THF-d_8): δ = 0.54 (s, 6H, $(CH_3)_2Si$), 0.70 (s, 6H, $(CH_3)_2Si$), 0.98 (d, 6H, $(CH_3)_2CH$, J = 6.9), 1.20 (d, 6H, $(CH_3)_2CH$, J = 6.6), 1.21 (d, 6H, $(CH_3)_2CH$, J = 6.9), 1.78 (m, ~0.5H, protio THF), 2.84 (m, 1H, $(CH_3)_2CH$, overlapping), 2.85 (m, 2H, $(CH_3)_2CH$, overlapping), 3.62 (m, ~0.5H, protio THF), 5.82 (s, 1H, Cp-*H*), 6.21 (s, 2H, Cp-*H*).

[(1,2-SiMe$_2$)$_2$(η^5-4-CMe$_3$-C$_5$H$_2$)(η^5-3,5-(CHMe$_2$)$_2$-C$_5$H)]YCH(SiMe$_3$)$_2$ (10). (tBuThpYCH(TMS)$_2$). In the glove box, a 100 mL flask was charged with **8a/8b** (422 mg, 0.70 mmol) and KCH(TMS)$_2$ (154 mg, 1.1 equiv) and a fine swivel frit assembly was attached. On the vacuum line, toluene (50 mL) was added by vacuum transfer while stirring at -78°C, and then this cold bath was replaced by a 0°C ice water bath and the reaction was allowed to slowly warm to 25°C while stirring. After 23 hr of reaction, a yellow solution was filtered away from an off-white solid and the solid was washed with recycled solvent (3 x 25 mL). Toluene was removed *in vacuo* and then pentane was added by vacuum transfer (10 mL). After stirring for 6 hr, pentane was removed *in vacuo* and then added again (20 mL). This pentane slurry was stirred for 12 hr, and then a pale yellow solution was filtered away from an off-white solid. Solvent was removed *in vacuo* and the apparatus was left open to dynamic vacuum for 4 hr. In the dry box, the off-white powder (from the collection flask) was collected as a first crop of the desired product. A new collection flask was attached to the swivel frit assembly in order to collect a second crop of the desired product. The extraction procedure was repeated with toluene and pentane as described, but the final filtration was carried out at -78°C to maximize the product yield. Two crops of

an off-white powder were collected; 211 mg (47.8%). Major isomer ^{1}H NMR (benzene-d_6): δ = -0.19 (s, 1H, C*H*(Si(CH$_3$)$_3$)$_2$), 0.14 (s, 18H, CH(Si(C*H*$_3$)$_3$)$_2$), 0.48 (s, 6H, (C*H*$_3$)$_2$Si), 0.89 (s, 6H, (C*H*$_3$)$_2$Si), 1.06 (d, 6H, (C*H*$_3$)$_2$CH, J = 6.8), 1.28 (d, 6H, (C*H*$_3$)$_2$CH, J = 6.7), 1.35 (s, 9H, (C*H*$_3$)$_3$C), 2.70 (m, 2H, (CH$_3$)$_2$C*H*, J = 6.7), 6.40 (s, 1H, Cp-*H*), 6.42 (s, 2H, Cp-*H*). Minor isomer ^{1}H NMR (benzene-d_6): δ = -0.18 (s, 1H, C*H*(Si(CH$_3$)$_3$)$_2$), 0.15 (s, 18H, CH(Si(C*H*$_3$)$_3$)$_2$), 0.50 (s, 6H, (C*H*$_3$)$_2$Si), 0.89 (s, 6H, (C*H*$_3$)$_2$Si), 1.08 (d, 6H, (C*H*$_3$)$_2$CH, J = 6.4), 1.28 (d, 6H, (C*H*$_3$)$_2$CH, J = 6.7), 1.35 (s, 9H, (C*H*$_3$)$_3$C), 2.74 (m, 2H, (CH$_3$)$_2$C*H*, J = 6.7), 6.21 (s, 1H, Cp-*H*), 6.34 (s, 2H, Cp-*H*). Major and minor isomers ^{13}H NMR (benzene-d_6): δ = 0.05, 1.78, 3.76, 3.95, 4.08, 4.11, 4.42, 4.61 ((*C*H$_3$)$_2$Si, *C*H(Si(CH$_3$)$_3$)$_2$), 21.81, 22.13, 24.63, 24.88, 29.17, 29.26, 29.78, 29.85, 30.58, 31.92, 32.20, 32.58, 33.05, 33.33 ((*C*H$_3$)$_2$CH, (*C*H$_3$)$_3$C), 109.02, 110.68, 119.79, 120.85, 124.38, 125.16, 125.33, 125.55, 144.76, 145.93, 154.61, 154.78 (Cp).

{[(1,2-SiMe$_2$)$_2$(η^5-4-CMe$_3$-C$_5$H$_2$)(η^5-3,5-(CHMe$_2$)$_2$-C$_5$H)]YH }$_2$ (11a/11b). ((tBuThpYH)$_2$). In the glove box, a thick walled reaction vessel equipped with stir bar was charged with **10** (57 mg, 0.90 mmol) and benzene (2 mL). The apparatus was degassed on the vacuum line using two freeze-pump-thaw cycles. The vessel was cooled to -78°C and dihydrogen was admitted. After 5 minutes of exposure to dihydrogen, the Kontes valve of the vessel was closed and the reaction was warmed to 25°C with vigorous stirring. After 20 hr of reaction, the pale yellow solution was frozen and the benzene was removed by lyophilization. The resulting pale yellow powder was dissolved in toluene-d_8 and cooled slowly to encourage growth of X-ray quality crystals. As a consequence a product yield was not determined. Major product (**11b**) ^{1}H NMR (benzene-d_6): δ = 0.52 (s, 6H, (C*H*$_3$)$_2$Si), 0.54 (s, 6H, (C*H*$_3$)$_2$Si), 1.18 (d, 6H, (C*H*$_3$)$_2$CH, J = 6.7), 1.38 (d, 6H, (C*H*$_3$)$_2$CH, J = 6.7), 1.46 (s, 9H, (C*H*$_3$)$_3$C), 2.78 (t, 2H, Y-(μ-H), J = 32.0), 2.86 (m, 2H, (CH$_3$)$_2$C*H*, J = 6.7), 6.10 (s, 2H, Cp-*H*), 6.76 (s, 1H, Cp-*H*). ^{13}H NMR (toluene-d_8): δ = 2.09, 5.77 ((CH$_3$)$_2$Si), 23.74, 25.58, 29.65, 30.31, 33.53 ((CH$_3$)$_2$CH, (CH$_3$)$_3$C), 107.71, 116.47, 123.05, 126.21, 143.53, 147.89 (Cp). Minor product (**11a**) ^{1}H NMR (benzene-d_6): δ = 0.49 (s, 6H, (C*H*$_3$)$_2$Si), 0.58 (s, 6H, (C*H*$_3$)$_2$Si), 1.07 (d, 6H, (C*H*$_3$)$_2$CH, J = 7.0), 1.24 (d, 6H, (C*H*$_3$)$_2$CH, J = 6.9), 1.54 (s, 9H, (C*H*$_3$)$_3$C), 2.51 (t, 2H, Y-(μ-H), J = 31.5), 2.84 (m, 2H, (CH$_3$)$_2$C*H*), 6.19 (s, 2H, Cp-*H*), 6.59 (s, 1H, Cp-*H*). ^{13}H NMR (toluene-d_8): δ = 4.29, 6.13 ((CH$_3$)$_2$Si), 23.12, 27.78, 28.89, 33.10, 33.37 ((*C*H$_3$)$_2$CH, (CH$_3$)$_3$C), 109.00, 112.58, 126.00, 127.08, 144.32, 153.75 (Cp).

[(1,2-$SiMe_2$)$_2$(η^5-4-CMe_3-C_5H_2)(η^5-3,5-$(CHMe_2)_2$-C_5H)]Y(μ-(CH_3))$_2$Al$(CH_3)_2$ (12). (tBuThpYMe_2AlMe_2). In the dry box a 100 mL round bottom flask equipped with stir bar was charged with **5** (501 mg, 0.83 mmol) and $LiAlMe_4$ (149 mg, 1.58 mmol, 1.9 equiv) and a fine swivel frit assembly was attached. On the vacuum line, toluene (75 mL) was added to the flask by vacuum transfer, and the dry ice/acetone bath was left intact to allow the reaction to slowly warm to 25°C while stirring. After 24 hr of reaction, toluene was removed *in vacuo* and pentane (40 mL) was added by vacuum transfer. The pale yellow slurry was stirred for 12 hr, and then a pale yellow solution was filtered away from a white solid. The solid was washed with recyled pentane (10 x 20 mL) and the pentane was removed *in vacuo* to provide an off-white residue in the collection flask that was dried under high vacuum for 4 hr. Complex **12** was isolated as an off-white powder; 322 mg (58.9%). ^{1}H NMR (benzene-d_6): δ = -0.41 (s, 3H, (μ-$CH_3)_2$Al($CH_3)_2$), -0.33 (s, 3H, (μ-$CH_3)_2$Al($CH_3)_2$), -0.32 (s, 6H, (μ-$CH_3)_2$Al$(CH_3)_2$), 0.40 (s, 6H, $(CH_3)_2$Si), 0.87 (s, 6H, $(CH_3)_2$Si), 1.03 (d, 6H, $(CH_3)_2$CH, J = 6.8), 1.23 (d, 6H, $(CH_3)_2$CH, J = 6.7), 1.27 (s, 9H, $(CH_3)_3$C), 2.63 (m, 2H, $(CH_3)_2CH$, J = 6.7), 6.32 (s, 1H, Cp-*H*), 6.33 (s, 2H, Cp-*H*). ^{13}H NMR (toluene-d_8): δ = -0.41, 3.45 ($(CH_3)_2$Si), 20.96, 29.04, 29.35, 32.08, 32.53 ($(CH_3)_2CH$, $(CH_3)_3C$), 109.91, 124.01, 125.22, 143.40, 154.95, 158.19 (Cp). (μ-$CH_3)_2$Al$(CH_3)_2$ resonances not located.

[(1,2-$SiMe_2$)$_2$(η^5-4-CMe_3-C_5H_2)(η^5-3,5-$(CHMe_2)_2$-C_5H)]Sc(μ-(CH_3))$_2$Al$(CH_3)_2$ (13). (tBuThpScMe_2AlMe_2). In the dry box a 100 mL round bottom flask equipped with stir bar was charged with **6** (297 mg, 0.39 mmol) and $LiAlMe_4$ (369 mg, 3.72 mmol, 3.5 equiv) and a fine swivel frit assembly was attached. On the vacuum line, toluene (50 mL) was added to the flask by vacuum transfer, and the dry ice/acetone bath was removed to allow the reaction to slowly warm to 25°C while stirring. After 24 hr of reaction, toluene was removed *in vacuo* and pentane (40 mL) was added by vacuum transfer. The pale yellow slurry was stirred for 12 hr, and then a yellow solution was filtered away from a white solid. The solid was washed with recyled pentane (5 x 20 mL) and the pentane was removed *in vacuo* to provide a yellow solid that was dried under high vacuum for 4 hr. In the dry box, this yellow solid was dissolved in benzene (2.5 mL) and transferred to a 10 mL round bottom flask equipped with stir bar. A 180° needle valve was attached. On the vacuum line, the solution was frozen and the benzene lyophilized away *in vacuo*. Complex **13** was isolated as a pale tan powder; 215 mg (78.6%). ^{1}H NMR (benzene-d_6): δ = -0.38 (s, 3H, (μ-

$CH_3)_2Al(CH_3)_2$), -0.35 (s, 6H, (μ-$CH_3)_2Al(CH_3)_2$), -0.23 (s, 3H, (μ-$CH_3)_2Al(CH_3)_2$), 0.39 (s, 6H, $(CH_3)_2Si$), 0.81 (s, 6H, $(CH_3)_2Si$), 0.99 (d, 6H, $(CH_3)_2CH$, J = 6.8), 1.24 (d, 6H, $(CH_3)_2CH$, J = 6.6), 1.31 (s, 9H, $(CH_3)_3C$), 2.55 (m, 2H, $(CH_3)_2CH$, J = 6.7), 6.24 (s, 2H, Cp-*H*), 6.49 (s, 1H, Cp-*H*). ^{13}H NMR (toluene-d_8): δ = -6.28, -4.38 ((μ-$CH_3)_2Al(CH_3)_2$, broad singlets), -0.92, 3.52 ($(CH_3)_2Si$), 30.27 ((μ-$CH_3)_2Al(CH_3)_2$), 20.83, 29.07, 29.14, 31.49, 33.26 ($(CH_3)_2CH$, $(CH_3)_3C$), 113.55, 116.14, 121.05, 126.67, 137.37, 155.87 (Cp).

[(1,2-SiMe$_2$)$_2$(η^5-4-CHMe$_2$-C$_5$H$_2$)(η^5-3,5-(CHMe$_2$)$_2$-C$_5$H)]Sc(μ-(CH$_3$)$_2$)Al(CH$_3$)$_2$ (14). (iPrThpScMe$_2$AlMe$_2$). In the dry box a 100 mL round bottom flask equipped with stir bar was charged with **9** (606 mg, 0.97 mmol) and $LiAlMe_4$ (369 mg, 3.72 mmol, 3.8 equiv) and a fine swivel frit assembly was attached. On the vacuum line, toluene (50 mL) was added to the flask by vacuum transfer, and the dry ice/acetone bath was removed to allow the reaction to slowly warm to 25°C while stirring. After 28 hr of reaction, toluene was removed *in vacuo* and pentane (40 mL) was added by vacuum transfer. The pale yellow slurry was stirred for 12 hr, and then a yellow-orange solution was filtered away from a white solid. The solid was washed with recyled pentane (5 x 20 mL) and the pentane was removed *in vacuo* to provide a yellow solid that was dried under high vacuum for 4 hr. In the dry box, this yellow solid was dissolved in benzene (2.5 mL) and transferred to a 10 mL round bottom flask equipped with stir bar. A 180° needle valve was attached. On the vacuum line, the solution was frozen and the benzene lyophilized away *in vacuo*. Complex **14** was isolated as a pale yellow solid; 407 mg (83.8%). ^{1}H NMR (benzene-d_6): δ = -0.45 (s, 3H, (μ-$CH_3)_2Al(CH_3)_2$), -0.44 (s, 6H, (μ-$CH_3)_2Al(CH_3)_2$), -0.25 (s, 3H, (μ-$CH_3)_2Al(CH_3)_2$), 0.36 (s, 6H, $(CH_3)_2Si$), 0.81 (s, 6H, $(CH_3)_2Si$), 0.97 (d, 6H, $(CH_3)_2CH$, J = 6.8), 1.20 (d, 6H, $(CH_3)_2CH$, J = 6.7), 1.21 (d, 6H, $(CH_3)_2CH$, J = 6.4), 2.53 (m, 2H, $(CH_3)_2CH$, J = 6.7), 3.03 (m, 1H, $(CH_3)_2CH$, J = 6.6), 6.06 (s, 2H, Cp-*H*), 6.43 (s, 1H, Cp-*H*). ^{13}H NMR (toluene-d_8): δ = -0.94, 3.51 ($(CH_3)_2Si$), 24.12, 27.58, 29.11 ($(CH_3)_2CH$), 112.31, 116.27, 120.99, 134.40, 139.15, 155.70 (Cp). (μ-$CH_3)_2Al(CH_3)_2$ resonances not located.

[{(C$_6$H$_5$)$_2$C[(η^5-C$_5$H$_4$)(η^5-C$_{13}$H$_8$)]}YCl]$_2$ (15). ([EpYCl]$_2$). In the dry box a 100 mL round bottom flask equipped with stir bar was charged with Li_2Ep (2.01 g, 4.94 mmol) and $YCl_3(THF)_{3.5}$ (2.21 g, 1 equiv) and a fine swivel frit assembly was attached. On the vacuum line, tetrahydrofuran (50 mL) was added to the flask

by vacuum transfer, and the dry ice/acetone bath was removed to allow the reaction to slowly warm to 25°C while stirring. The reaction mixture begins as cherry-red solution and slowly changes to brick-red in color. After 72 hr of reaction, tetrahydrofuran was removed *in vacuo* and petroleum ether (50 mL) was added by vacuum transfer. The slurry was stirred for 12 hr and then solvent was removed *in vacuo*. Diethyl ether (50 mL) was added by vacuum transfer and subsequent filtration provided a bright yellow solution in the collection flask. The solid was washed with recycled solvent (18 x 30 mL) until the solid remaining on the frit was no longer yellow in color. Solvent was removed *in vacuo* to leave a bright yellow solid in the collection flask. In the dry box, the collection flask was attached to a fine swivel frit assembly. Petroleum ether (40 mL) was added via vacuum transfer, and a yellow solution was filtered away from a bright yellow solid. The solid was washed with recycled solvent (5 x 20 mL), solvent was removed *in vacuo*, and the bright yellow solid that was dried under high vacuum for 4 hr. Complex **15** was isolated as an bright yellow powder; 2.27 g; (44.5%). ^{1}H NMR (THF-d_8): δ = 5.82 (s, 2H, Cp-*H*), 5.91 (s, 2H, Cp-*H*), 6.57 (d, 2H, Flu-*H*, J = 8.7), 6.78 (t, 2H, Ph-*H*, J = 7.7), 6.94 (t, 2H, Ph-*H*, J = 7.2), 7.09 (t, 2H, Flu-*H*, J = 7.2), 7.13 (t, 2H, Flu-*H*, J = 7.5), 7.27 (t, 2H, Ph-*H*, J = 8.0), 7.87 (d, 2H, Ph-*H*, J = 7.4), 8.03 (d, 2H, Flu-*H*, J = 8.3), 8.06 (d, 2H, Ph-*H*, J = 7.4).

[{$(C_6H_5)_2C[(\eta^5\text{-}C_5H_4)(\eta^5\text{-}C_{13}H_8)]$}ScCl(THF) (16). (EpScCl(THF)). In the dry box a 100 mL round bottom flask equipped with stir bar was charged with Li_2Ep (3.00 g, 7.37 mmol) and $ScCl_3(THF)_3$ (2.71 g, 1 equiv) and a fine swivel frit assembly was attached. On the vacuum line, tetrahydrofuran (75 mL) was added to the flask by vacuum transfer, and the dry ice/acetone bath was removed to allow the reaction to slowly warm to 25°C while stirring. The reaction mixture begins as red-brown slurry and slowly changes to a red-orange transparent solution. After 96 hr of reaction, tetrahydrofuran was removed *in vacuo* and petroleum ether (50 mL) was added by vacuum transfer. The slurry was stirred for 9 hr and then solvent was removed *in vacuo*. The solid was dried under high vacuum for 12 hr. Next, diethyl ether (50 mL) was added by vacuum transfer to provide a bright orange slurry. An orange solution was filtered from a red-orange solid, and this solid was washed with recycled solvent (8x 30 mL) until the solid remaining on the frit was no longer orange in color. Solvent was removed *in vacuo* to leave an orange-yellow solid in the collection flask. In the dry box,

the collection flask was attached to a new fine swivel frit assembly. Diethyl ether (40 mL) was added via vacuum transfer and then the swivel frit assembly was cooled to -78°C for a cold filtration. A red-orange solution was filtered away from a bright yellow solid. The solid was washed with recycled solvent at -78°C (1 x 20 mL) and then solvent was removed *in vacuo*. Petroleum ether (30 mL) was added by vacuum transfer and the bright yellow solid was washed with recycled solvent (4 x 20 mL). The solvent was removed *in vacuo* and then the solid was dried under high vacuum for 4 hr. Complex **16** was isolated as an bright yellow powder; 1.01 g (24.9%). ^{1}H NMR (THF-d_8): δ = 1.78 (m, 4H, protio THF), 3.62 (m, 4H, protio THF), 5.75 (s, 2H, Cp-*H*), 5.87 (s, 2H, Cp-*H*), 6.45 (d, 2H, Flu-*H*, J = 8.7), 6.71 (t, 2H, Ph-*H*, J = 7.3), 7.00 (t, 2H, Ph-*H*, J = 7.5), 7.13 (t, 2H, Flu-*H*, J = 6.2), 7.18 (t, 2H, Flu-*H*, J = 7.2), 7.31 (t, 2H, Ph-*H*, J = 6.9), 7.88 (d, 2H, Ph-*H*, J = 6.3), 7.90 (d, 2H, Ph-*H*, J = 7.7), 8.06 (d, 2H, Ph-*H*, J = 7.6).

{$(C_6H_5)_2C[(\eta^5\text{-}C_5H_4)(\eta^5\text{-}C_{13}H_8)]$}$Y(\mu\text{-}(CH_3)_2)Al(CH_3)_2$ (17). (EpYMe$_2$AlMe$_2$). In the dry box a 100 mL round bottom flask equipped with stir bar was charged with **15** (511 mg, 0.492 mmol) and $LiAlMe_4$ (162 mg, 1.72 mmol, 3.5 equiv) and a fine swivel frit assembly was attached. On the vacuum line, toluene (50 mL) was added to the flask by vacuum transfer, and the dry ice/acetone bath was removed to allow the reaction to slowly warm to 25°C while stirring. After 21.5 hr of reaction, toluene was removed *in vacuo* and petroleum ether (50 mL) was added by vacuum transfer. The slurry was stirred for 1 hr and then solvent was removed *in vacuo*. In the dry box, the contents of the reaction flask were transferred to a small Soxhlet thimble, and a Soxhlet apparatus was assembled with a small Soxhlet extractor, 14/20 condensor, 180° needle valve, and 25 mL collection flask. On the vacuum line, pentane (15 mL) was added by vacuum transfer, the apparatus was backfilled with argon, and the toluene solution was heated to reflux to begin the extraction. After 8 hr, the solution that passed through the thimble was colorless and the extraction was terminated. Pentane was removed *in vacuo* to provide a bright yellow solid that was dried under high vacuum for 4 hr. Complex **17** was isolated as an bright yellow powder; 44 mg (7.8%). ^{1}H NMR (benzene-d_6): δ = -1.22 (s, 12H, (μ-CH_3)$_2$Al(CH_3)$_2$, broad), 5.74 (s, 2H, Cp-*H*), 5.78 (s, 2H, Cp-*H*), 6.60 (d, 2H, Flu-*H*, J = 8.6), 6.75 (t, 2H, Ph-*H*, J = 7.4), 6.96 (t, 2H, Ph-*H*, J = 7.4), 7.00 (t, 2H, Flu-*H*, J = 7.3), 7.03 (t, 2H, Flu-*H*, J = 6.8), 7.15 (t, 2H, Ph-*H*, J = 7.5), 7.75 (d, 2H, Flu-*H*, J = 7.8), 7.94 (d, 2H, Ph-*H*, J = 7.4), 8.01 (d, 2H, Ph-*H*, J = 8.2). ^{13}C NMR (benzene-d_6): δ = 30.58, 37.31, 60.30,

90.68, 106.24, 112.83, 120.09, 120.67, 121.16, 121.63, 123.96, 125.84, 126.77, 126.94, 127.90, 129.09, 129.30, 130.28, 147.75.

{$(C_6H_5)_2C[(\eta^5\text{-}C_5H_4)(\eta^5\text{-}C_{13}H_8)]$}$Sc(\mu\text{-}(CH_3)_2)Al(CH_3)_2$ (18). (EpScMe$_2$AlMe$_2$). In the dry box a 100 mL round bottom flask equipped with stir bar was charged with **16** (492 mg, 0.90 mmol) and $LiAlMe_4$ (296 mg, 3.15 mmol, 3.5 equiv) and a fine swivel frit assembly was attached. On the vacuum line, toluene (50 mL) was added to the flask by vacuum transfer, and the dry ice/acetone bath was removed to allow the reaction to slowly warm to 25°C while stirring. After 8 hr of reaction, toluene was removed *in vacuo* and pentane (40 mL) was added by vacuum transfer. The reaction mixture was stirred for 12 hr and then solvent was removed *in vacuo*. In the dry box, the contents of the reaction flask were transferred to a small Soxhlet thimble, and a Soxhlet apparatus was assembled with a small Soxhlet extractor, 14/20 condensor, 180° needle valve, and 25 mL collection flask. On the vacuum line, pentane (15 mL) was added by vacuum transfer, the apparatus was backfilled with argon, and the toluene solution was heated to reflux to begin the extraction. The extraction was terminated after 6 hr. Pentane was removed *in vacuo* to provide an orange powder that was dried under high vacuum for 4 hr. Complex **18** was isolated as an bright orange solid; 57 mg (12.1%). ^{1}H NMR (benzene-d_6): δ = -1.83 (s, 6H, (μ-CH_3)$_2$Al(CH$_3$)$_2$), -0.55 (s, 3H, (μ-CH$_3$)$_2$Al(CH_3)$_2$), -0.52 (s, 3H, (μ-CH$_3$)$_2$Al(CH_3)$_2$), 5.46 (s, 2H, Cp-*H*), 5.78 (s, 2H, Cp-*H*), 6.50 (d, 2H, Flu-*H*, J = 8.8), 6.59 (t, 2H, Ph-*H*, J = 6.9), 6.97 (t, 2H, Ph-*H*, J = 7.4), 7.03 (t, 2H, Flu-*H*, J = 7.4), 7.06 (t, 2H, Flu-*H*, J = 8.6), 7.15 (t, 2H, Ph-*H*, J = 7.7), 7.77 (d, 2H, Flu-*H*, J = 7.9), 7.89 (d, 2H, Ph-*H*, J = 8.1), 7.91 (d, 2H, Ph-*H*, J = 6.0). ^{13}C NMR (benzene-d_6): δ = 10.27, 25.15, 30.59, 60.58, 70.41, 87.76, 106.27, 116.16, 117.12, 121.71, 122.43, 123.38, 123.80, 123.93, 126.18, 127.06, 127.73, 129.18, 129.35, 130.40, 147.29.

Polymerizations of 1-pentene using 12, 13, 14, 18, and 10 + H_2 as catalysts. 1-pentene polymerizations were executed in neat monomer; this reagent was stored under vacuum over lithium aluminum hydride and freshly distilled immediately prior to use. Approximately 5 mg ($\approx$ 0.010 mmol) of metallocene and 5000 equivalents of 1-pentene were used for each polymerization. The specific conditions for these polymerizations, such as temperature, duration, and percent yield (by mass), as well as pentad information[40] are given in Table 6. Measurements of polymer molecular weight were made elsewhere.[41]

Representative polymerization: In the dry box a thick walled reaction vessel equipped with stir bar was charged with **18** (5.4 mg, 0.010 mmol). The vessel was cooled to -78°C and 1-pentene (5.6 mL, 5000 equiv) was added by vacuum transfer. The reaction was warmed to 21°C with vigorous stirring. After 24 hr of reaction, the solution was slightly viscous. In the fume hood, the reaction solution was rinsed into a flask with diethyl ether (10 mL). While stirring rapidly, methanol (6 mL), dilute methanol-HCl (6 mL, 3 :1, v/v), and additional methanol (50 mL) were added to quench the reaction. A white semi-solid precipitates out this solution; it was removed and dried in vacuo at 50°C for 4 hr. The product was obtained in 49.9% yield by mass (1.79 g). A small sample was dissolved in 1,2-dichlorobenzene-benzene-d_6 (9 : 7, v/v) and analyzed by ^{13}C NMR spectroscopy at 323 K to determine the polymer pentad distribution.

Polymerizations of propylene using 12, 13, 14, and 18 as catalysts. Most propylene polymerizations were carried out in neat monomer at -5°C in a thick walled glass vessel. A 5 mm Kontes needle valve with an extended tip was used to seal the vessel. Approximately 10 mg (≈ 0.020 mmol) of metallocene and 4 mL of propylene (at 77 K) (≈ 3000 equiv) were used for each polymerization. Propylene was stored under vacuum over triisobutylaluminum (≈ 1:1 v/v at 77 K) and distilled immediately prior to use. Monomer was first distilled into a calibrated trap for volume measurement and then distilled into the liquid nitrogen cooled reaction vessel. The reaction mixture was warmed to -5°C with rapid stirring in a sodium chloride/ice water cold bath. Multiple blast shields were used as a precaution due to the elevated pressure in the reaction vessel. Two polymerizations were carried out using a 50/50 (v/v) mixture of propylene and toluene; these experiments were run to evaluate the effect of monomer concentration on polymer tacticity. The pentad distributions[42] for these polymerizations are provided in Table 7. Measurements of polymer molecular weight were made elsewhere.[41]

Representative polymerization: In the dry box a thick walled reaction vessel equipped with stir bar was charged with **18** (6.6 mg, 0.0125 mmol). The vessel was cooled to with liquid nitrogen and propylene (3.1 mL at 77 K, ≈ 3100 equiv) was added by vacuum transfer. In the fume hood behind multiple blast shields, the reaction was warmed to -5°C in a sodium chloride/ice water cold bath with vigorous stirring. After 10.67 hr of reaction, the solution was slightly viscous. The reaction was slowly vented to release excess propylene. The reaction

contents were dissolved in a minimal amount of diethyl ether (10 mL) and transferred to a flask. While stirring rapidly, methanol (10 mL), dilute methanol-HCl (10 mL. 3 :1, v/v), and additional methanol (50 mL) were added to quench the reaction. A white semi-solid precipitates out this solution; it was removed and dried in vacuo at 50°C for 4 hr. The product was obtained in 44.7% yield by mass (0.72 g). A small sample was dissolved in 1,2-dichlorobenzene-benzene-d_6 (9 : 7, v/v) and analyzed by ^{13}C NMR spectroscopy at 323 K to determine the polymer pentad distribution.

References

1. Brintzinger, H.H.; Fischer, D.; Mülhaupt, R.; Rieger, B.; Waymouth, R.M. *Angew. Chem. Int. Ed. Engl.* **1995**, *34*, 1143.

2. Ewen, J.A.; Jones, R.L.; Razavi, A.; Ferrara, J.D. *J. Am. Chem. Soc.*, **1988**, *110*, 6255.

3. (a) Patsidis, K.; Alt, H. G.; Milius, W.; Palackal, S. J. *J. Organomet. Chem.* **1996**, *509*, 63. (b) Razavi, A.; Atwood, J. L. *J. Organomet. Chem.* **1993**, *459*, 117. (c) Winter, J.; Rohrmann, M.; Dolle, V.; Spaleck, W. *Eur. Pat. Appl.* 0,387,690 and 0,387,691, 1991. (d) Spaleck, W.; Aulbach, M.; Bachmann, B.; Kuber, F.; Winter, A. *Macromol. Symp.* **1995**, *89*, 237. (e) Ewen, J. A. *Macromol. Symp.* **1995**, *89*, 181. (f) Alt, H. G.; Zenk, R. *J. Organomet. Chem.* **1996**, *518*, 7.

4. Herzog, T.A.; Zubris, D.L.; Bercaw, J.E. *J. Am. Chem. Soc.*, **1996**, *118*, 11988.

5. (a) Longo, P.; Grassi, A.; Pellecchia, C.; Zambelli, A. *Macromolecules* **1987**, *20*, 1015-1018. (b) Pino, P.; Galimberti, M. *J. Organomet. Chem.* **1989**, *370*, 1.

6. Gilchrist, J. H.; Bercaw, J. E. *J. Am. Chem. Soc.* **1996**, *118*, 12021.

7. (a) Piers. W.E.; Bercaw, J.E. *J. Am. Chem. Soc.* **1990**, *112*, 9406. (b) Grubbs, R.H.; Coates, G.W. *Acc. Chem. Res.* **1996**, *29*, 85.

8. Veghini, D.; Henling, L.M.; Burkhardt, T.J.; Bercaw, J.E. *J. Am. Chem. Soc.*, **1999**, *121*, 564.

9. Bierwagen, E.P.; Bercaw, J.E.; Goddard, W.A. *J. Am. Chem. Soc.*, **1994**, *116*, 1481.

10. Bunel, E. E. *Ph.D. Thesis*, California Institute of Technology, **1989**.

11. (a) Chirik, P.J.; Bercaw, J.E. in *Metallocenes: Synthesis, Reactivity, Applications, Vol. 1*; Togni, A.; Halterman, R.L. Eds.; Wiley-VCH: Weinheim, Germany, 1998, pp. 111-152. (b) Schumann, H.; Meese-Marktscheffel, J.A.; Esser, L. *Chem. Rev.* **1995**, *95*, 865.

12. (a) Henling, L.M.; Herzog, T.A.; Bercaw, J.E. *Acta Crystallogr., Sect. C 52*, **1996**, *submitted*. (b) Veghini, D.; Day, M.W.; Bercaw, J.E. *Inorganica Chimica Acta* **1998**, *280*, 226.

13. Coughlin, E.B. *Ph.D. Thesis*, California Institute of Technology, **1994**.

14. Evans, W.J.; Peterson, T.T.; Rausch, M.D.; Hunter, W.E.; Zhang, H.; Atwood, J.L. *Organometallics* **1985**, *4*, 554.

15. Evans, W.J.; Olofson, J.M.; Zhang, H.; Atwood, J.L. *Organometallics* **1988**, *7*, 629.

16. Xie, Z.; Liu, Z.; Zhang, Z.; Mak, T.C. W. *J. Organomet. Chem.* **1997**, *542*, 285.

17. Coughlin, E.B.; Henling, L.M.; Bercaw, J.E. *Inorg. Chimica Acta* **1996**, *242*, 205.

18. Stern, D.; Sabat, M.; Marks, T.J. *J. Am. Chem. Soc.* **1990**, *112*, 9558.

19. Schaverien, C.L. *Adv. Organometallic. Chem.* **1994**, *36*, 283.

20. Abrams, M.A. *Ph.D. Thesis* California Institute of Technology, **1998**.

21. Coughlin, E.B. *Ph.D. Thesis* California Institute of Technology, **1994**.

22. Mitchell, J.P.; Hajela, S.; Brookhart, S.K.; Hardcastle, K.I.; Henling, L.M.; Bercaw, J.E. *J. Am. Chem. Soc.* **1996**, *118*, 1045.

23. (a) Ballard, D.G.H.; Pearce, R. *J.C.S. Chem. Comm.* **1975**, 621. (b) Holton, J.; Lappert, M.F.; Scollary, G.R.; Ballard, D.G.H.; Pearce, R.; Atwood, J.L.; Hunter, W.E. *J.C.S. Chem. Comm.* **1976**, *12*, 425. (c) Holton, J.; Lappert, M.F.; Ballard, D.G.H.; Pearce, R.; Atwood, J.L.; Hunter, W.E. *J.C.S. Dalton.* **1979**, 45. (d) Holton, J.; Lappert, M.F.; Ballard, D.G.H.; Pearce, R.; Atwood, J.L.; Hunter, W.E. *J.C.S. Dalton.* **1979**, 54.

24. Evans, W.J.; Chamberlain, L.R.; Ulibarri, T.A.; Ziller, J.W. *J. Am. Chem. Soc.* **1988**, *110*, 6432.

25. (a) Watson, P.L. *J. Am. Chem. Soc.* **1982**, *104*, 337. (b) Watson, P.L.; Parshall, G.W. *Acc. Chem. Res.* **1985**, *18*, 51. (c) Busch, M.A.; Harlow, R.; Watson, P.L. *Inorganica Chimica Acta* **1987**, *140*, 15.

26. den Haan, K.H.; Wielstra, Y.; Eshuis, J.J.W.; Teuben, J.H. *J. Organomet. Chem.* **1987**, *323*, 181.

27. Holton, J.; Lappert, M.F.; Ballard, D.G.H.; Pearce, R.; Atwood, J.L.; Hunter, W.E. *J.C.S. Dalton.* **1979**, 54.

28. Strauss, D.A.; Grubbs, R.H. *J. Mol. Cat.* **1985**, *28*, 9.

29. Razavi, A.; Atwood, J.L. *J. Organomet. Chem.* **1993**, *459*, 117.

30. Schofer, S.J.; Bercaw, J.E. *unpublished results*.

31. Coughlin, E.B.; Bercaw, J.E. *J. Am. Chem. Soc.* **1992**, *114*, 7606.

32. Piers, W.E.; Shapiro, P.J.; Bunel, E.E.; Bercaw, J.E. *Synlett*, **1990**, *2*, 74.

33. Burger, B. J.; Bercaw, J. E. *New Developments in the Synthesis, Manipulation, and Characterization of Organometallic Compounds*, **1987**; Vol. 357. ACS Symposium Series.

34. Marvich, R. H.; Brintzinger, H. H. *J. Am. Chem. Soc.* **1971**, *93*, 203.

35. Cowley, A. H.; Kemp, R. A. *Synth. React. Inorg. Metal-Org. Chem.* **1981**, *11*, 591.

36. Manzer, L.E. *Inorg. Synth.* **1982**, *21*, 135.

37. Herzog, T.A. *Ph.D. Thesis*, California Institute of Technology, **1997**.

38. Perrin, D. D.; Armagrego, W. L. F. *Purification of Laboratory Chemicals*, 3rd ed.; Pergamon Press: New York, NY, 1988.

39. Herzog, T.A.; Bercaw, J.E. *unpublished results*.

40. Asakura, T.; Demura, M.; Nishiyama, Y. *Macromolecules* **1991**, *24*, 2334.

41. DLZ thanks Dr. Steve A. Cohen at BP Amoco Chemical for his assistance in obtaining molecular weight data.

42. Zambelli, A.; Locatelli, P.; Bajo, G.; Bovey, M.A. *Macromolecules* **1975**, *8*, 687.

Chapter 2

Group 5 *Ansa*-Metallocenes as Models for Ziegler-Natta Polymerization Catalysts

Abstract

To further elucidate the origin of stereocontrol in *ansa*-metallocene Ziegler-Natta polymerization catalysts, a family of *ansa*-tantalocene complexes has been prepared. The dipotassio ligand salt, $K_2[Me_2Si(C_5H_4)_2]$, has been utilized for preparation of the tantalocene trimethyl complex, $Me_2Si(\eta^5\text{-}C_5H_4)_2TaMe_3$ ($SpTaMe_3$). This complex has been characterized by X-ray crystallography. $SpTaMe_3$ may be used as a synthetic precursor for the corresponding tantalocene ethylene-methyl complex, $SpTa(\eta^2\text{-}CH_2{=}CH_2)Me$. Excess propylene may be added to this ethylene-methyl complex to induce olefin exchange; a mixture of *endo* and *exo* propylene-methyl isomers is observed.

Metallation of the doubly-silylene bridged ligand, $M_2[(1,2\text{-}SiMe_2)_2(C_5H_3)_2]$ (M_2Rp) with $TaCl_2Me_3$ yields a bridged dinuclear complex, $Rp(TaMe_3Cl)_2$. In contrast, metallation of $M_2[(1,2\text{-}SiMe_2)_2(4\text{-}CMe_3\text{-}C_5H_2)(C_5H_3)]$ (M_2tBuRp) with $TaCl_2Me_3$ allows isolation of an *ansa*-tantalocene methylidene-methyl complex, $tBuRpTa(CH_2)CH_3$, as a minor product. The dipotassio ligand salt, $K_2[(1,2\text{-}SiMe_2)_2(4\text{-}CMe_3\text{-}C_5H_2)(3,5\text{-}(CHMe_2)_2\text{-}C_5H)]$ ($K_2tBuThp$) when combined with $TaCl_2Me_3$ yields a mixture of $[(1,2\text{-}SiMe_2)_2(\eta^5\text{-}4\text{-}CMe_3\text{-}C_5H_2)(\eta^2\text{-}3,5\text{-}(CHMe_2)_2\text{-}C_5H)]TaMe_3$ and $[(1,2\text{-}SiMe_2)_2(\eta^5\text{-}4\text{-}CMe_3\text{-}C_5H_2)(\eta^5\text{-}3,5\text{-}(CHMe_2)_2\text{-}C_5H)]Ta(CH_2)CH_3$. Both complexes have been characterized by X-ray crystallography. Thermolysis of this methylidene-methyl complex promotes conversion to the corresponding ethylene-hydride complex, $tBuThpTa(\eta^2\text{-}CH_2{=}CH_2)H$. This ethylene-hydride complex undergoes olefin exchange with propylene and styrene to form the olefin-hydride complexes, $tBuThpTa(\eta^2\text{-}CH_2{=}CHR')H$ (where R' is methyl or phenyl). Both olefin-hydride complexes have been analyzed by Nuclear Overhauser difference NMR spectroscopy to determine the relative orientation of the bound olefin. These model systems have provided a more thorough understanding of stereocontrol with *ansa*-metallocene catalysts.

Introduction

Understanding mechanisms of stereocontrol in *ansa*-metallocene Ziegler-Natta polymerization catalysts has been an area of intense study since the infancy of these catalysts.[1] Brintzinger's report of isotactic polypropylene formation utilizing the C_2-symmetric, *rac*-ethylene bisindenyl zirconocene dichloride as a precatalyst[2] provided important insight into how metallocene symmetry affects polymer microstructure. Later work by Ewen suggested that C_s-symmetry may be necessary for the formation of syndiotactic polypropylene; he and others have employed C_s-symmetric, singly-linked cyclopentadienyl-fluorenyl zirconocenes for propylene polymerization.[3] Further studies in our group established additional requirements for syndiospecific polymerization catalysts; this work culminated in the introduction of a family of C_s-symmetric, doubly-silylene bridged *ansa*-zirconocenes ($RThpZrCl_2$) for production of highly syndiotactic polypropylene.[4] These zirconocene precatalysts and the polypropylene microstructures they provide are illustrated in Figure 1.

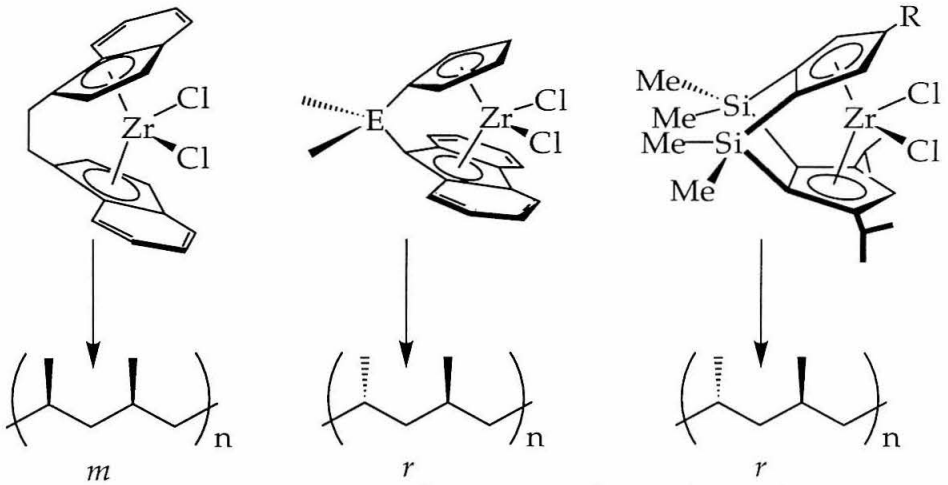

Figure 1: Metallocene symmetry exerts an influence on resulting polypropylene microstructure. Select C_2-symmetric zirconocenes may be used for the preparation of isotactic polymer (high *m* diad content). Select C_s-symmetric zirconocenes may be used for the preparation of syndiotactic polymer (high *r* diad content).

While the relationship between metallocene symmetry and polymer microstructure is becoming more well understood, the important stereodirecting interactions during olefin insertion that provide polymers with high stereospecificity and controlled molecular weight remain unclear. Prior studies

have established that prevalent 2,1-olefin insertions limit polymer molecular weight.[5] For example, RThp zirconocene catalysts can provide very high molecular weight polymers and exhibit negligible 2,1-olefin insertions (*exo* olefin coordination). This may be attributed to steric interactions between the incoming α-olefin and the dimethylsilyl methyl groups that orient themselves towards the metallocene wedge, as illustrated in Figure 2. This suggests the importance of ligand array in dictating olefin coordination preferences (*endo* versus *exo*). A systematic study of diastereomeric preferences for olefin coordination for a range of *ansa*-metallocenes has not been achieved to date.

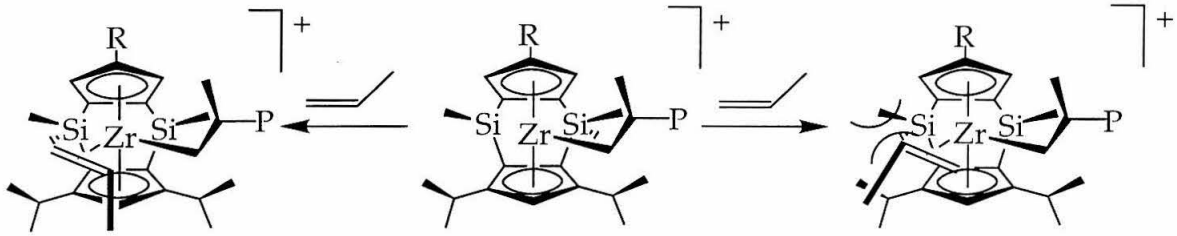

Figure 2: Doubly-silylene bridged zirconocenes favor 1,2-olefin insertion over 2,1-olefin insertion.

Prior studies have probed the important stereodirecting interactions that operate in the formation of isospecific poly(α-olefins). Pino *et al.* were the first to report the absolute enantioselectivity for α-olefin insertion into metal-hydride and metal-alkyl bonds of *ansa*-zirconocene polymerization catalysts.[6] Optically pure ethylene bis(4,5,6,7-tetrahydroindenyl) zirconocene dichloride was used to prepare low molecular weight hydrooligomers. Polarimetry measurements of select fractions suggest that olefin insertions into metal-hydride and metal-*n*-pentyl bonds proceed from opposite enantiotopic faces of 1-pentene. More recently, Gilchrist and Bercaw utilized an isotopically chiral olefin as a more sensitive probe for measurement of olefin insertion stereoselectivity.[7] An optically pure yttrocene, (R,S)-BnBpY-R (where R is H or *n*-pentyl), was employed to determine the absolute enantioselectivity for 1-pentene insertions into yttrocene-hydride and yttrocene-*n*-pentyl bonds. Insertions of 1-pentene into Y-H and Y-*n*-pentyl bonds were found to proceed with opposite olefin enantiofaces (as illustrated in Figure 3). In addition, while insertion into Y-H

exhibits low enantioselectivity (ee ≈ 33%), insertion into Y-*n*-pentyl is highly enantioselective (> 95% ee).

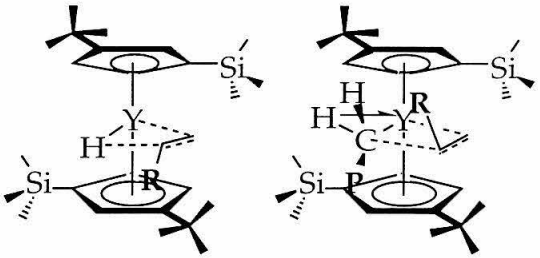

Figure 3: Proposed α-olefin insertion into yttrocene-hydride and yttrocene-polymer moieties.

These olefin insertion preferences with C_2-symmetric, isospecific metallocenes have been extended to predict preferences for C_s-symmetric, syndiospecific metallocenes. For example, the α-olefin insertion transition state for RThp zirconocene polymerization catalysts has been postulated (see Figure 4). It is presumed that the bulky diisopropyl-substituted cyclopentadienyl ring forces the polymer chain towards the R-substituted cyclopentadienyl ring, and the alkyl substituent of the incoming α-olefin is oriented *trans* with respect to the β-carbon of the polymer chain. In fact, the open region between the isopropyl substituents was designed to readily accommodate this alkyl substituent.

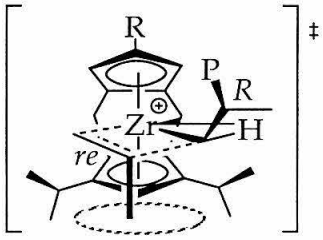

Figure 4: A proposed transition state for α-olefin insertion into a growing polymer chain for a C_s-symmetric, RThp metallocene.

While previous studies have demonstrated that enantiofacial preferences for olefin insertion into metal-hydride and metal-*n*-pentyl bonds of C_2-symmetric metallocenes differ, similar preferences for C_s-symmetric metallocenes (such as RThp metallocenes) have not been examined directly. If olefin insertions into metal-hydride and metal-alkyl bonds of RThp metallocenes proceed with opposite enantiofaces (as observed for C_2-symmetric metallocenes), intermediates such as those illustrated in Figure 5 may be operating. An understanding of olefin coordination and insertion for C_s-

symmetric metallocenes may further our understanding of the mechanism of syndiospecific α-olefin polymerization. More generally, examination of olefin coordination and insertion for a range of *ansa*-metallocenes may provide valuable insight into the origins of stereocontrol in Ziegler-Natta α-olefin polymerization.

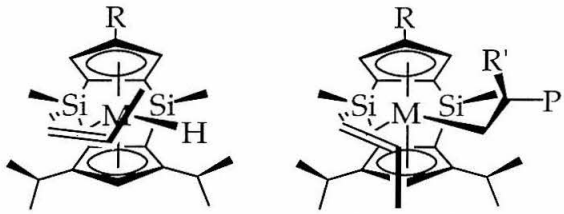

favored ? *favored ?*

Figure 5: Potential olefin insertion preferences into metal-hydride and metal-polymer bonds for C_s-symmetric, RThp metallocenes.

In order to probe these important stereocontrol issues, a family of *ansa*-tantalocene complexes has been prepared. Unlike neutral group 3 or cationic group 4 metallocenes, group 5 metallocenes may stabilize olefin adducts through π-backbonding. Isolation and characterization of these olefin adducts may allow an investigation of olefin coordination preferences for both metal-hydride and metal-alkyl complexes. Variation of ligand array (singly versus doubly-silylene bridged metallocenes with different substitution patterns, see Figure 6) may provide insight regarding the importance of ligand sterics and electronics in olefin coordination. This may furnish an understanding of diastereomeric

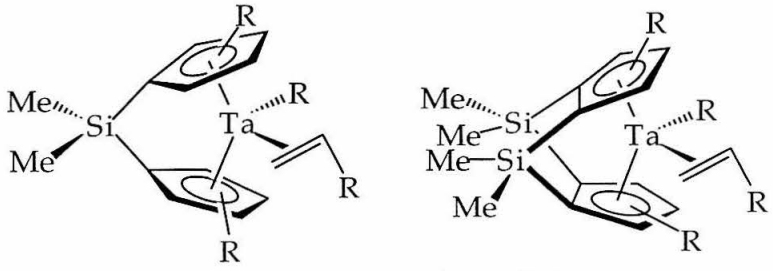

where R is hydride or alkyl

Figure 6: Singly- and doubly-silylene linked tantalocene olefin-hydride and olefin-alkyl complexes are desired as model complexes for Ziegler-Natta polymerization catalysts.

preferences for olefin coordination (*endo* versus *exo*, etc.). Also, olefin equilibration reactions may supply information regarding the relative ground

state energies of distinct tantalocene olefin adducts. Overall, it is hoped that these *ansa*-tantalocene olefin-hydride and olefin-alkyl complexes may serve as models for the olefin insertion transition state in Ziegler-Natta polymerization.

Few *ansa*-metallocenes incorporating group 5 transition metals have been reported to date. Green and coworkers have prepared a series of isopropylidene-linked niobocene dichloride complexes via reaction of deprotonated ligand salts with $NbCl_4(THF)_2$.[8] Select metallocenes may be converted to the corresponding borohydrides, yet subsequent conversion to niobocene olefin-hydride complexes has been unsuccessful to date. Dimethylsilyl-linked niobocene dichloride have been prepared similarly, and select alkyne-chloride complexes have also been reported.[9] More recently, Parkin has described the synthesis of the *ansa*-tantalocene, $Me_2Si(\eta^5\text{-}C_5Me_4)_2TaH_3$.[10] This tantalocene is prepared by metallation of the distannylated ligand with $TaCl_5$, reduction of the resulting trichloride complex with $LiAlH_4$, and subsequent hydrolysis. Addition of ethylene to the tantalocene trihydride complex and thermolysis (80°C, hours) affords the corresponding ethylene-hydride complex, $Me_2Si(\eta^5\text{-}C_5Me_4)_2Ta(\eta^2\text{-}CH_2{=}CH_2)H$. This is the first reported example of a group 5 *ansa*-metallocene olefin-hydride complex.

The use of $TaCl_2Me_3$ as a metal source for the preparation of *ansa*-tantalocenes has not been explored previously. This starting material has been utilized for the preparation of unlinked tantalocene trimethyl complexes; select metallocenes may serve as synthetic precursors to tantalocene olefin adducts. Moreover, the preparation of *ansa*-tantalocene complexes from distannylated ligands and $TaCl_5$ has some synthetic limitations (*vide infra*). Thus, our initial synthetic efforts directed towards the preparation of *ansa*-tantalocene olefin adducts have mirrored these prior investigations.

Schrock and coworkers have described the utility of $TaCl_2Me_3$ for the preparation of unlinked tantalocene trimethyl complexes, such as $(\eta^5\text{-}C_5H_5)_2Ta(CH_3)_3$ (Cp_2TaMe_3).[11] These complexes have been used as synthetic precursors to tantalocene ethylene-methyl complexes, as illustrated in Figure 7. Trityl tetrafluoroborate may be used to abstract a methyl group from the tantalocene trimethyl complex. Subsequent reaction of the cationic tantalocene dimethyl complex with base, such as methylidene trimethylphosphorane, affords

the corresponding tantalocene methylidene-methyl complex. The methylidene-methyl complex is unstable in solution at 25°C and undergoes facile bimolecular decomposition to afford one equivalent of [Cp_2TaMe] (not detected by ^1H NMR spectroscopy) and one equivalent of $Cp_2Ta(\eta^2\text{-}CH_2{=}CH_2)Me$. This bimolecular decomposition pathway has been supported by trapping experiments with donor ligands, such as ethylene, trimethylphosphine, dimethylphenylphosphine, and carbon monoxide; $Cp_2Ta(CH_3)L$ complexes are formed.

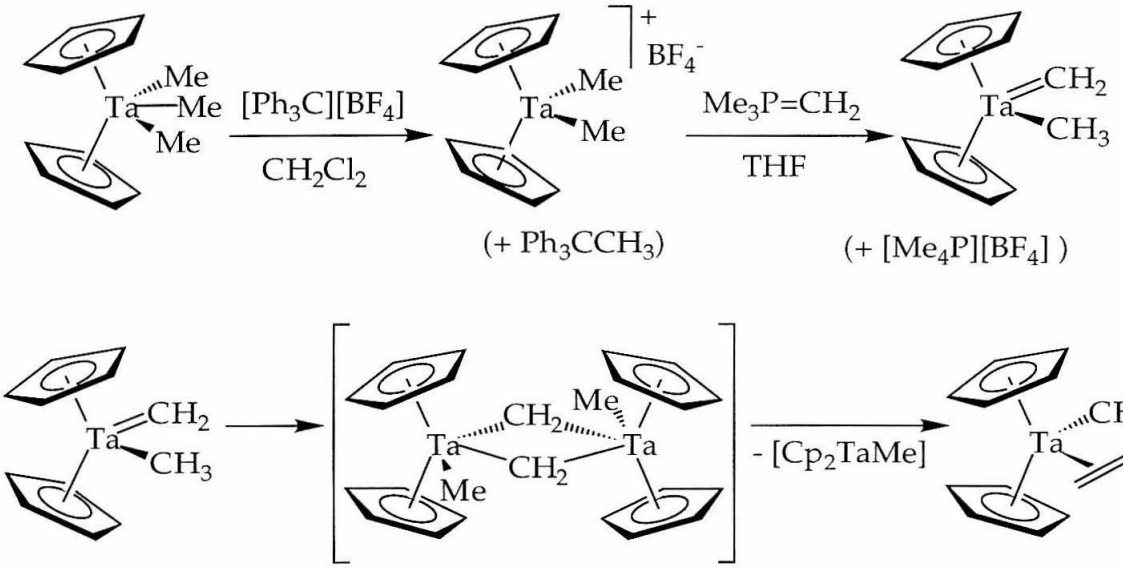

Figure 7: Cp_2TaMe_3 may be used as a synthetic precursor to the corresponding tantalocene ethylene-methyl complex.

In contrast, reaction of [$(\eta^5\text{-}C_5Me_5)_2Ta(CH_3)_2$][$BF_4$] ([$Cp^*_2TaMe_2$][$BF_4$]) with base, such as potassium hydride, affords the corresponding methylidene-methyl complex which is stable in solution at 25°C. Thermolysis (at 140°C) of this complex induces intramolecular α-migratory insertion to yield the ethylene-hydride complex, $(\eta^5\text{-}C_5Me_5)_2Ta(\eta^2\text{-}CH_2{=}CH_2)H$.[12] This reaction pathway is illustrated in Figure 8. The increased steric bulk of the bis-pentamethylcyclopentadienyl ligand framework appears to inhibit the bimolecular decomposition pathway observed for the bis-cyclopentadienyl tantalocene methylidene-methyl complex.

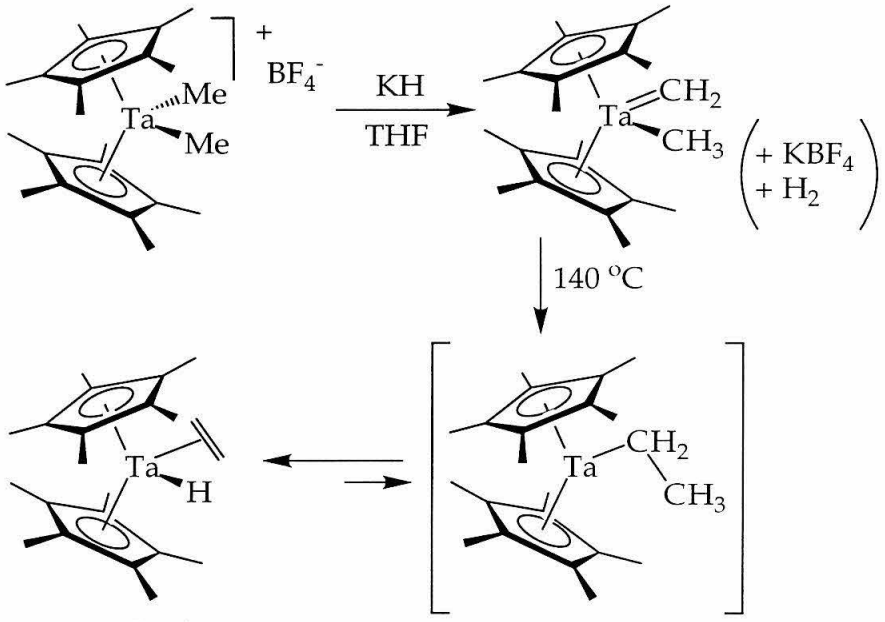

Figure 8: [Cp*$_2$TaMe$_2$][BF$_4$] may be used as a synthetic precursor to the corresponding tantalocene ethylene-hydride complex.

Results and Discussion

Singly-silylene bridged ansa-tantalocenes

Preparation of *ansa*-tantalocene complexes incorporating the singly-silylene linked ligand, $Me_2Si(C_5H_4)_2$, was an attractive initial synthetic target due to the simplicity of the ligand array. The *ansa*-tantalocene trihydride complex, $Me_2Si(\eta^5\text{-}C_5H_4)_2TaH_3$, has been prepared in our laboratories as a synthetic precursor to the corresponding ethylene-hydride complex.[13] In contrast to $Me_2Si(\eta^5\text{-}C_5Me_4)_2TaH_3$, thermolysis of $Me_2Si(\eta^5\text{-}C_5H_4)_2TaH_3$ in the presence of excess ethylene provides a mixture of ethylene-hydride and ethylene-ethyl complexes. This result provided additional motivation for the preparation of *ansa*-tantalocene trimethyl complexes as synthetic precursors for olefin adducts.

Reaction of the dilithio ligand salt, $Li_2[Me_2Si(C_5H_4)_2]$ (Li_2Sp), with $TaCl_2Me_3$ in benzene-d_6 provides a mixture of two products: $Me_2Si(\eta^5\text{-}C_5H_4)_2(TaMe_3Cl)_2$ [$Sp(TaMe_3Cl)_2$] and $Me_2Si(\eta^5\text{-}C_5H_4)_2TaMe_3$ ($SpTaMe_3$, **1**), as illustrated in eq. 1. These products have been identified by ^{1}H NMR spectroscopy; the tantalum-methyl resonances are diagnostic. The bridged

dinuclear complex, $Sp(TaMe_3Cl)_2$, comprises the majority of the product mixture. Preparative scale metallation of Li_2Sp with $TaCl_2Me_3$ in diethyl ether affords the bridged dinuclear complex as the sole isolable product.[14]

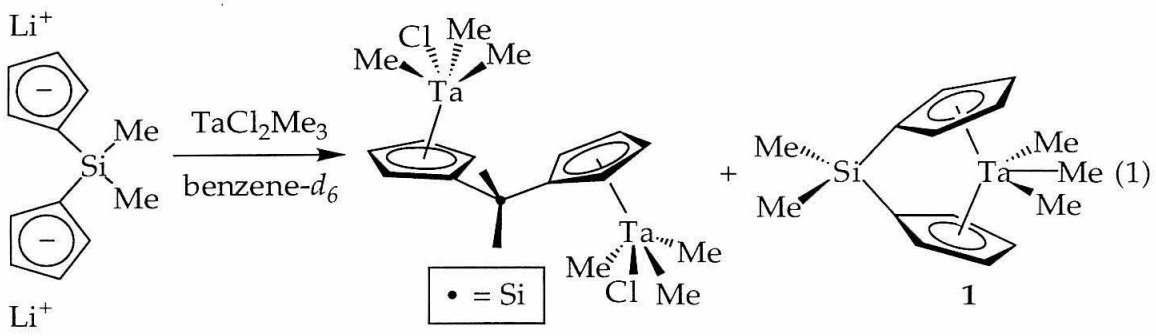

The desired tantalocene trimethyl complex (**1**) may be generated as the major product by use of the dipotassio ligand salt, $K_2[Me_2Si(C_5H_4)_2]$ (K_2Sp) for metallation. Dropwise addition of a dilute diethyl ether solution of $TaCl_2Me_3$ to a slurry of K_2Sp at 25°C was employed to maximize formation of the desired *ansa*-metallocene. Complex **1** may be isolated as an off-white powder in 19.8% yield.[15]

Slow cooling of a diethyl ether solution of **1** provides transparent crystals that are suitable for X-ray diffraction. Figure 9 contains the solid state structure of **1**; the space group is $P2(1)/n$. This structure does not contain any unusual features. The cyclopentadienyl rings display η^5, η^5 hapticity with 2.215 Å distances from tantalum to each cyclopentadienyl centroid. The tantalum-methyl bonds of 2.300 Å (Ta-C13), 2.277 Å (Ta-C14), and 2.310 Å (Ta-C15) are standard tantalum-alkyl bond lengths.

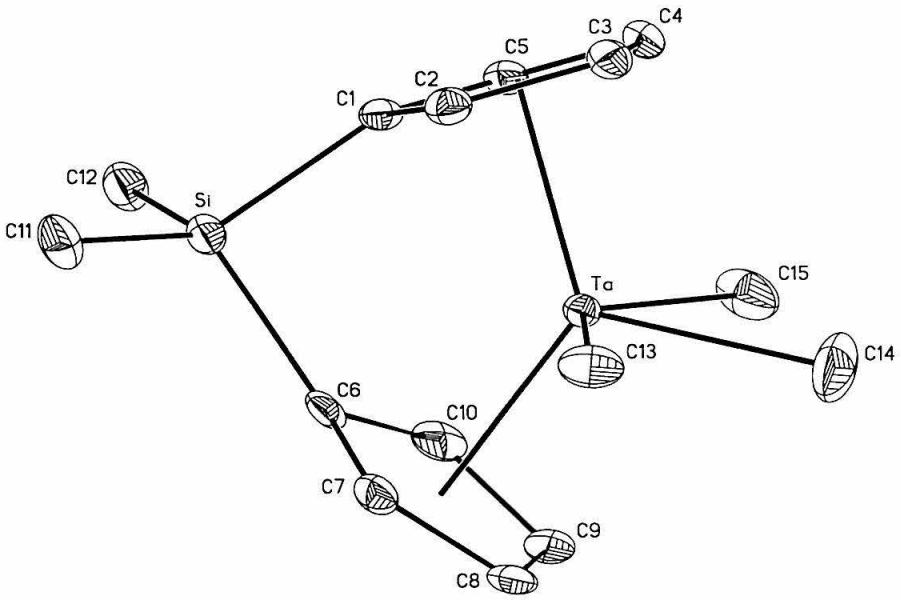

Figure 9: Molecular structure of **1** with selected atoms labeled (50% probability ellipsoids). Hydrogen atoms are omitted for clarity.

The lability of the tantalum-methyl ligands of **1** has been examined. Addition of 4 atm of dihydrogen to a benzene-d_6 solution of **1** provides no reaction. Since **1** is an 18 electron, coordinatively saturated complex, this lack of reactivity was not surprising. Combination of **1** with one equivalent $ZnCl_2$ in benzene-d_6 solution also provides no reaction, presumably due to the low solubility of $ZnCl_2$ in this solvent. Reaction of **1** with one equivalent HCl in methylene chloride-d_2 affords the tantalocene dimethyl-chloride complex, $Me_2Si(\eta^5\text{-}C_5H_4)_2TaMe(Cl)Me$ (SpTaMe(Cl)Me, **2**), where the central methyl group has been protonated to form the C_{2v}-symmetric product (eq. 2). Addition of one or two equivalents HCl to **2** does not provide the expected tantalocene methyl-dichloride and trichloride complexes, respectively; a mixture of products and decomposition are observed instead.

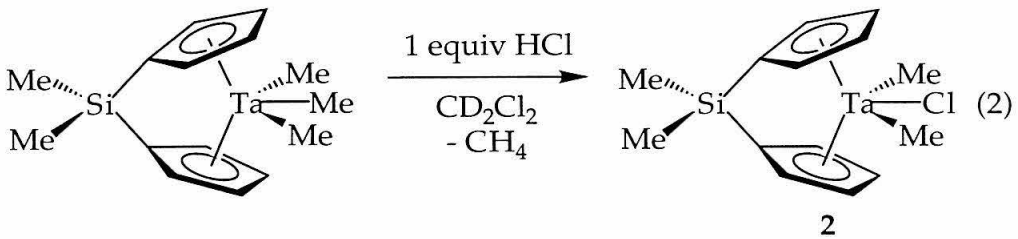

(2)

2

Addition of one equivalent of either trityl tetrafluoroborate or trityl hexafluorophosphate to **1** in methylene chloride liberates Ph_3CCH_3 and provides the corresponding cationic tantalocene dimethyl complex. Trityl tetrafluoroborate has been used to generate $[Me_2Si(\eta^5\text{-}C_5H_4)_2TaMe_2][BF_4]$ ($[SpTaMe_3][BF_4]$, **3**) on a preparative scale (eq. 3); **3** has been isolated as a bright yellow powder in high isolated yield (89.6%). Complex **3** is sparingly soluble in methylene chloride-d_2; consequently, only ^1H and ^{19}F NMR spectroscopy have been used for characterization purposes.

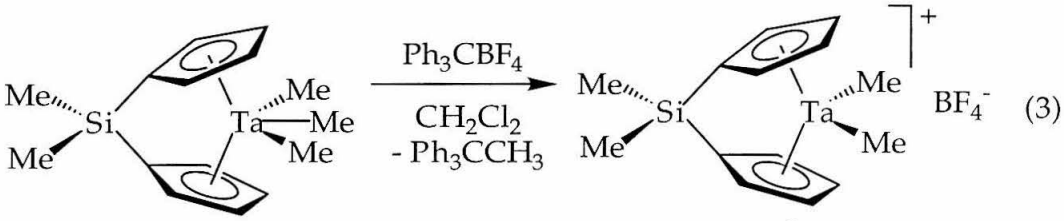

3 (3)

The reactivity of **3** towards various bases such as $LiCH(SiMe_3)_2$, $LiCH_2(SiMe_3)$, and $LiN(SiMe_3)_2$, has been examined. Reactions have been carried out in benzene-d_6 and monitored by ^1H NMR spectroscopy. At short reaction times the methylidene-methyl complex, $Me_2Si(\eta^5\text{-}C_5H_4)_2Ta(CH_2)CH_3$ (**4**), is observed. Over the course of 24 hours the ethylene-methyl complex, $Me_2Si(\eta^5\text{-}C_5H_4)_2Ta(\eta^2\text{-}CH_2{=}CH_2)CH_3$ (**4**), becomes the only metallocene product detected in the reaction mixture. Use of a sterically hindered base, such as $LiCH(SiMe_3)_2$ or $LiN(SiMe_3)_2$, minimizes formation of impurities. The reaction pathway for conversion of **3** to **5** is illustrated in eq. 4.

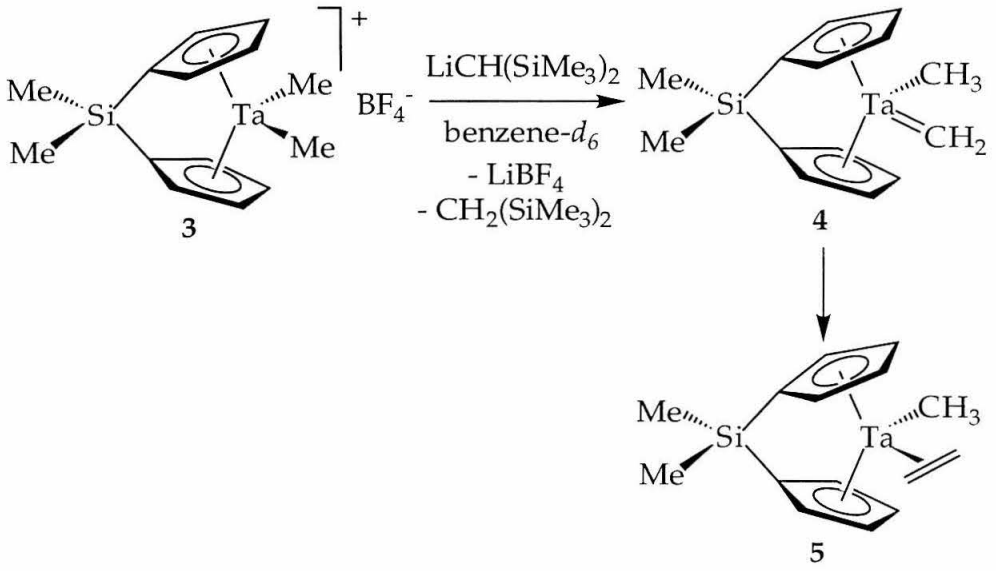

(4)

Diagnostic resonances for complexes **4** and **5** have been observed by ^{1}H and ^{13}C NMR spectroscopy. The methylidene-methyl complex displays a singlet at 10.30 ppm in the ^{1}H NMR spectrum for the methylidene hydrogens. The ^{1}H NMR spectrum of the ethylene-methyl complex contains two triplets at 1.23 and 0.96 ppm that correspond to the hydrogens of the bound ethylene. The carbons of the bound ethylene resonate at 26.53 and 18.89 ppm, and the tantalum-methyl carbon is observed at -4.54 ppm.

The proposed mechanism for formation of **5** is analogous to the bimolecular decomposition pathway illustrated in Figure 1. Two equivalents of the methylidene-methyl complex, **4**, may combine to form a bimolecular intermediate that disproportionates to generate one equivalent of **5** and one equivalent of a tantalum(III) methyl complex, $[Me_2Si(\eta^5\text{-}C_5H_4)_2TaCH_3]$, that is not observed by ^{1}H NMR spectroscopy.

This reaction pathway has been probed by addition of donor ligands, such as ethylene and propylene, to trap the putative tantalocene(III) methyl complex. Indeed, combination of **3** with $LiCH(SiMe_3)_2$ in the presence of 25 equivalents of ethylene produces greater than 50% conversion to **5**; the control experiment without added ethylene provides less than 50% conversion. Also, combination of **3** with $LiCH(SiMe_3)_2$ in the presence of 25 equivalents of propylene yields **5** with some evidence for tantalocene propylene-methyl complexes. These results

support a bimolecular decomposition mechanism for formation of **5**. Slower observed rates for conversion of the more sterically encumbered [$Me_2Si(\eta^5$-$C_5H_4)(\eta^5$-2,4-$(CHMe_2)_2$-$C_5H_2)$]$Ta(CH_2)CH_3$ to the corresponding ethylene-methyl complex also are in accord with a bimolecular decomposition mechanism.[13]

Consequently, complex **5** has been prepared on a preparative scale by combination of **3** with $LiCH(SiMe_3)_2$ under an atmosphere of ethylene; recrystallization from pentane affords **5** as a pale tan solid. Olefin exchange has been demonstrated with **5**; addition of excess propylene to **5** in benzene-d_6 solution affords two new olefin adducts (**6a, 6b**) in a 1.70 : 1 ratio, as evidenced by ^{1}H NMR spectroscopy. These propylene-methyl complexes exhibit characteristic ^{1}H NMR resonances for the propylene-methyl substituents (doublets at 2.04 and 1.92 ppm). NMR analysis is consistent with the formation of *endo* and *exo* propylene adducts, as illustrated in eq. 5.

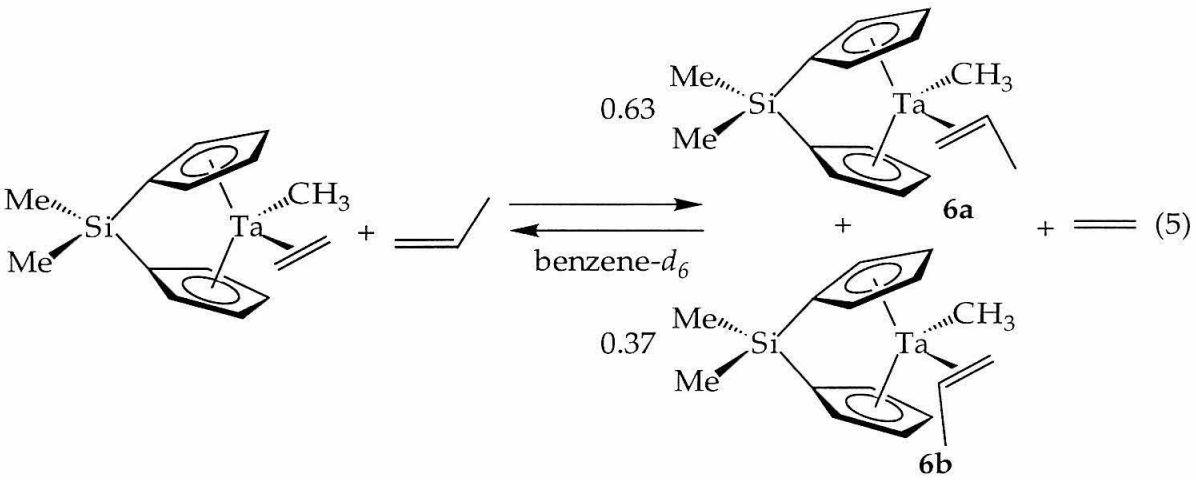

A preference for formation of the *endo* isomer may be attributed to unfavorable steric interactions in the *exo* isomer between the propylene-methyl substituent and a silyl-methyl substituent of the ligand. A comparison of the *endo* : *exo* ratio for **6** and other linked and unlinked niobocene and tantalocene propylene-hydride complexes is provided in Table 1.

molecular formula	% *endo*	% *exo*	reference
$Cp_2Nb(CH_2=CHCH_3)H$	50%	50%	16
$Cp^*_2Nb(CH_2=CHCH_3)H$	100%	0%	17
$Cp_2Ta(CH_2=CHCH_3)H$	50% (100%)	50% (0%)	18
$Cp^*_2Ta(CH_2=CHCH_3)H$	100%	0%	19
$iPrSpTa(CH_2=CHCH_3)H$	100%	0%	20
$tBuSpTa(CH_2=CHCH_3)H$	100%	0%	20
$SpTa(CH_2=CHCH_3)Me$	63%	37%	*

Table 1: Comparison of percent *endo* versus percent *exo* product for niobocene and tantalocene propylene adducts. * denotes data from this work.

Contrasting **6** with its unlinked, niobium counterpart $Cp_2Nb(\eta^2\text{-}CH_2=CHCH_3)H$ suggests that the *ansa*-bridge enforces a slight preference for the *endo* isomer. Two different *endo* to *exo* ratios have been reported for $Cp_2Ta(\eta^2\text{-}CH_2=CHCH_3)H$.[18] When $Cp_2Ta(\eta^2\text{-}CH_2=CHCH_3)H$ is generated by reaction of Cp_2TaCl_2 with two equivalents of *i*-PrMgCl, a 1 : 1 ratio of *endo* to *exo* isomers is observed. In contrast, when two equivalents of *n*-PrMgCl are employed, the endo isomer is the exclusive product.

The sterics towards the sides and back of the metallocene wedge of **6** appear to be less significant than those of $Cp^*_2M(\eta^2\text{-}CH_2=CHCH_3)H$ (where M = Nb, Ta), where exclusive *endo* olefin coordination is enforced. Similarly, *ansa*-tantalocenes of the form $[Me_2Si(\eta^5\text{-}C_5H_4)(\eta^5\text{-}3\text{-}R\text{-}C_5H_2)]Ta(\eta^2\text{-}CH_2=CHCH_3)H$ ($RSpTa(CH_2=CHCH_3)H$, where R = CMe_3, $CHMe_2$) display exclusive *endo* coordination of propylene. From this data, it appears that joining cyclopentadienyl ligands with a dimethylsilyl linker plays a small yet significant role in hindering *exo* propylene coordination.

The equilibrium described in equation 5 has been analyzed to determine the equilibrium constant, free energy change (at 298 K), and relative ground state energies (G.S.E.) for **5** and **6** (Table 2). When appropriate, the equilibrium constants in Table 2 were each calculated as an average of K_{eq}(endo) and K_{eq}(exo). Calculation of relative G.S.E. requires consideration of the contributions of free olefin to the equilibrium. Since coordination of an olefin to tantalum or niobium involves partial reduction of the double bond, olefin

hydrogenation may be used as a model reaction. Free energies of hydrogenation for ethylene and propylene[21] were used to determine the relative G.S.E. of **5** and **6**. This type of analysis has been used previously.[17,22] Equilibration between ethylene and propylene adducts is illustrated in Figure 10 in a more general fashion.

molecular formula	K_{eq}^{298}	ΔG° (kcal/mol)	relative G.S.E.	reference
$Cp_2Nb(\eta^2\text{-}CH_2{=}CHR')H$	3.0 (5) x 10^{-3}	3.4 (4)	3.7 (4)	16
$Cp^*_2Nb(\eta^2\text{-}CH_2{=}CHR')H$	6.9 x 10^{-4}	2.9 (2)	1.1	17
$SpTa(\eta^2\text{-}CH_2{=}CHR')Me$	9.2 x 10^{-4}	4.1	2.4	*

Table 2: Equilibrium data for ethylene (R' = H) and propylene (R' = Me) adducts, as described in Figure 10. * denotes signifies the data from this work.

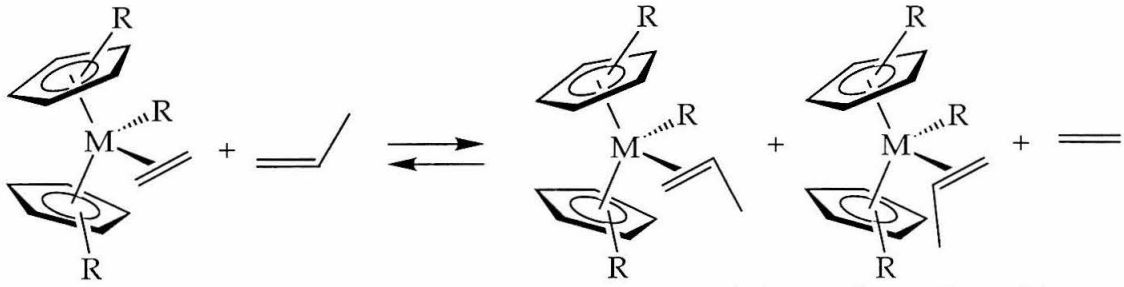

Figure 10: General equation for equilibration of metallocene ethylene and propylene adducts.

Development of a Ta(IV) starting material

Recently, *ansa*-tantalocene dichloride complexes of the form $[Me_2Si(\eta^5\text{-}C_5H_4)(\eta^5\text{-}3\text{-}R\text{-}C_5H_2)]TaCl_2$ ($RSpTaCl_2$, where R = CMe_3, $CHMe_2$) and $[Me_2Si(\eta^5\text{-}C_5H_4)(\eta^5\text{-}2,4\text{-}(CHMe_2)_2\text{-}C_5H_2)]TaCl_2$ ($iPr_2SpTaCl_2$) have been employed as synthetic precursors for olefin-hydride complexes.[20] These dichlorides have been synthesized using a multistep procedure, as illustrated in equation 6. Some notable aspects of this synthesis are the use of tri-*n*-butyl tin chloride for stannylation of the dilithio ligand salt and the zinc reduction of the tantalocene trichloride complex to generate the desired tantalocene dichlorides.

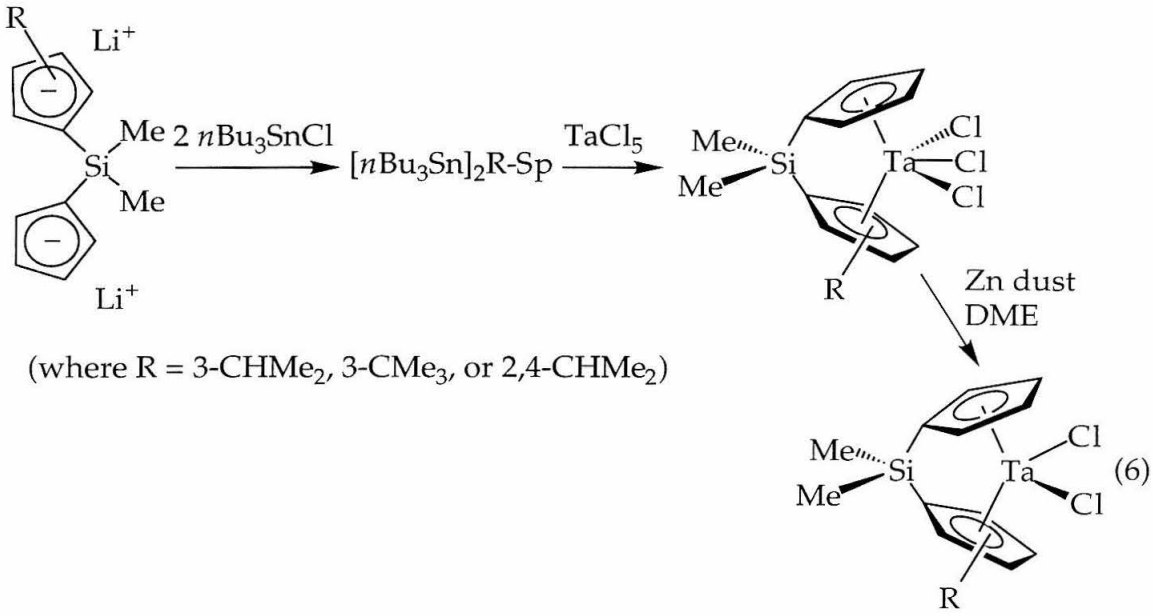

(where R = 3-$CHMe_2$, 3-CMe_3, or 2,4-$CHMe_2$)

Preparation of the analogous *ansa*-niobocene dichloride complexes may be achieved by combination of dilithio ligand salts and $NbCl_4(THF)_2$ (eq. 7).[20] The availability of a niobium (IV) starting material eliminates the need for a metallocene trichloride reduction and does not require use of stannylated ligand.

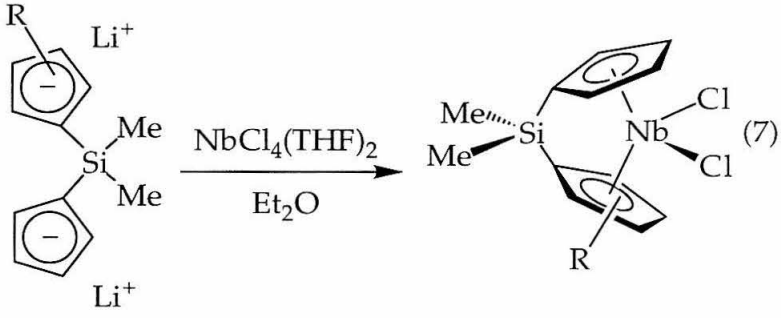

(where R = 3-$CHMe_2$, 3-CMe_3)

The synthesis of tantalocene dichloride complexes described in equation 15 has some synthetic limitations. Use of *n*-Bu_3SnCl is generally undesirable due to its toxicity. Also, stannylation of dilithio ligand salts is limited in ligand scope. Bulky ligand arrays such as tBuThp and Bp[14] are not amenable to distannylation. Moreover, the number of required reactions is greater than in preparation of the analogous niobocene complexes (eq. 7). This is due the lack of a suitable Ta(IV) precursor to date.

The number of Ta(IV) complexes in the literature are limited.[23] Some tantalum tetrachloride adducts have been reported, such as $TaCl_4(CH_3CN)_2$, $TaCl_4(pyridine)_2$,[24] $TaCl_4(PMe_3)_3$, and $TaCl_4(PEt_3)_2$.[25] The attempted preparation of $TaCl_4(THF)_2$ has also been described.[26] *In situ* generation of a Ta(IV) species for generation of dicyclopentadienyl tantalocene dichloride is also precedented; *i*-PrMgBr was used to reduce $TaCl_5$ to $TaCl_4$ (eq. 8).[27]

$$TaCl_5 + i\text{-PrMgBr} \xrightarrow[Et_2O]{} TaCl_4 + MgBrCl + [\text{i-Pr}\bullet] \quad \textit{green suspension}$$

$$TaCl_4 + 2\,CpNa \xrightarrow[Et_2O]{} Cp_2TaCl_2 + 2\,NaCl \qquad (8)$$

Both $TaCl_4(CH_3CN)_2$ and $TaCl_4(THF)_2$[28] were tested for metallation of the singly-bridged ligand, Li_2iPrSp {$Li_2[Me_2Si(3\text{-}CHMe_2\text{-}C_5H_3)(C_5H_4)]$}. These Ta(IV) sources did not afford the desired *ansa*-tantalocene dichloride complex. DME (1,2-dimethoxyethane) was examined in attempt to prepare a stabilized tantalum tetrachloride complex. Reduction of $TaCl_5$ with either Al or Zn in DME provided an olive-green solution over the course of hours. Attempts to concentrate the DME solution or isolate the reduction product as a solid resulted in decomposition or unexplained mixtures of products, as evidenced by EPR spectroscopy.

However, *in situ* reduction of $TaCl_5$ has been employed for preparation of the known complex, iPrSpTaCl_2 (eq. 9).[13] Reduction of $TaCl_5$ by 0.5 equivalents of zinc dust in DME affords an olive-green solution; dropwise addition of this solution to Li_2iPrSp (in DME) affords iPrSpTaCl_2 upon workup. This tantalocene dichloride was identified by ambient temperature EPR spectroscopy. Further reaction of this tantalocene dichloride complex with 2.2 equivalents of phenethylmagnesium chloride afforded the corresponding tantalocene styrene-hydride complexes, as reported previously. Similar reactions were attempted with a singly linked cyclopentadienyl-fluorenyl ligand, $Li_2[Ph_2C(C_5H_4)(C_{13}H_8)]$ (Li_2Ep), but the desired metallocenes were not isolated.

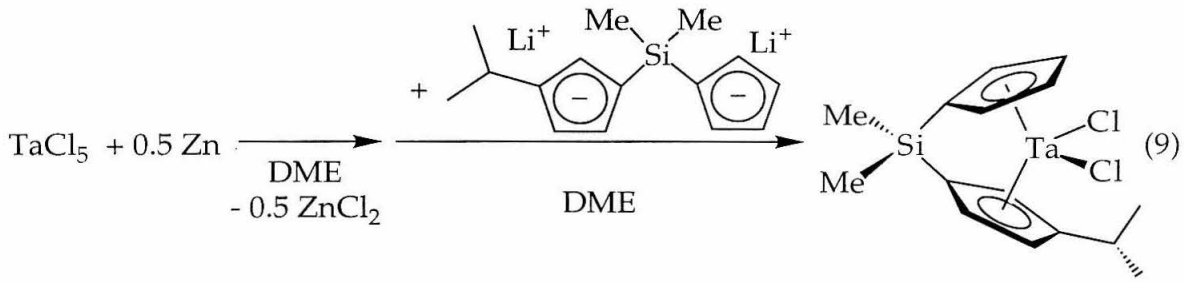

(9)

As noted above, tantalocene trichloride or dichloride complexes have not been prepared to date with the tBuThp ligand. Attempts to metallate M_2tBuThp (where M = Li, K) with $TaCl_5$ have been unsuccessful. Also, addition of two equivalents of *n*-Bu_3SnCl to M_2tBuThp does not yield the desired distannylated ligand, presumably due to the sterics of the diisopropyl substituted cyclopentadienyl ring. Therefore, $NbCl_4(THF)_2$ was examined as a starting material for the preparation of corresponding niobocene dichloride complex. Indeed, combination of Li_2tBuThp and $NbCl_4(THF)_2$ in diethyl ether affords tBuThpNbCl_2 over the course of days at 25°C (eq. 10). This niobium(IV) complex has been analyzed by ambient temperature EPR spectroscopy; in methylene chloride solution it exhibits a characteristic ten line spectrum (^{93}Nb = 100%, S = 9/2). Further manipulation of this complex to afford olefin adducts is currently in progress.

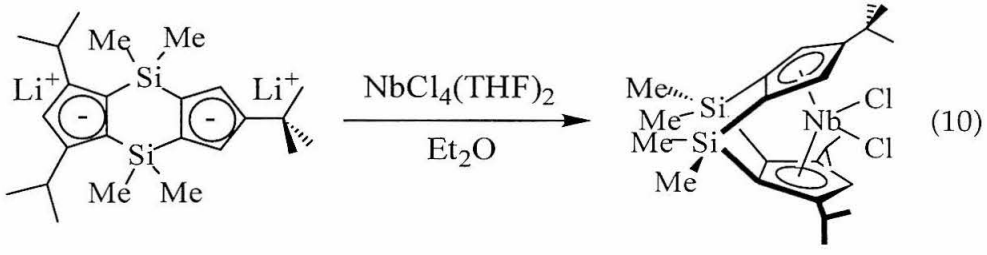

(10)

Doubly-silylene bridged ansa-tantalocenes

A variety of doubly-silylene bridged *ansa*-zirconocenes has been developed in recent years for use as α-olefin polymerization catalysts (see Figure 11). These catalysts display a range of polymerization activities and produce polymers with markedly different tacticities. Examination of these trends may provide a better understanding of the origin of stereocontrol for Ziegler-Natta

polymerization catalysts. In turn, this may facilitate the development of new poly(α-olefins).

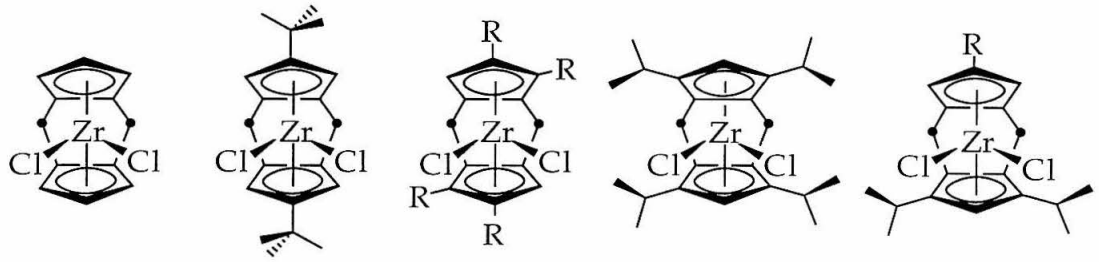

$RpZrCl_2$ $BsZrCl_2$ $BrZrCl_2$ $TIPZrCl_2$ $RThpZrCl_2$

Figure 11: $RpZrCl_2$[29,30], $BsZrCl_2$[31], $BrZrCl_2$[32], $TIPZrCl_2$[33], and $RThpZrCl_2$[4] are examples of previously reported doubly-silylene bridged *ansa*-zirconocene dichloride complexes.

Three types of doubly-silylene bridged ligands have been investigated for preparation of *ansa*-tantalocene complexes as models for Ziegler-Natta catalysts (see Figure 12). The unsubstituted, doubly-silylene bridged ligand, $(1,2\text{-}SiMe_2)_2(C_5H_3)_2$ (Rp), was chosen for comparison to the singly-silylene linked Sp ligand discussed above. The C_s-symmetric ligand array, $(1,2\text{-}SiMe_2)_2(4\text{-}R\text{-}C_5H_2)(C_5H_3)$ (RRp, where R = CMe_3, $CHMe_2$), has not been reported previously. This ligand was designed to further explore the importance of sterics in doubly-silylene bridged metallocenes. Also, it may provide some insight regarding the relationship between incoming monomer, polymer chain, and ligand array in α-olefin polymerization. *Ansa*-tantalocenes employing the RThp ligand, $(1,2\text{-}SiMe_2)_2(4\text{-}R\text{-}C_5H_2)(3,5\text{-}(CHMe_2)_2\text{-}C_5H)$ (RThp, where R = CMe_3), were also targeted. The mechanism for stereocontrol employed by RThp metallocene catalysts has received the most attention, primarily due to the high activity and syndiospecificity they can induce. While the mechanisms for propagation and stereoerror formation have been examined by polymerization studies with group 4[34] and group 3[35] RThp catalysts, the preparation of group 5 metallocenes may allow further investigation of olefin coordination preferences and the olefin insertion transition state in Ziegler-Natta polymerization.

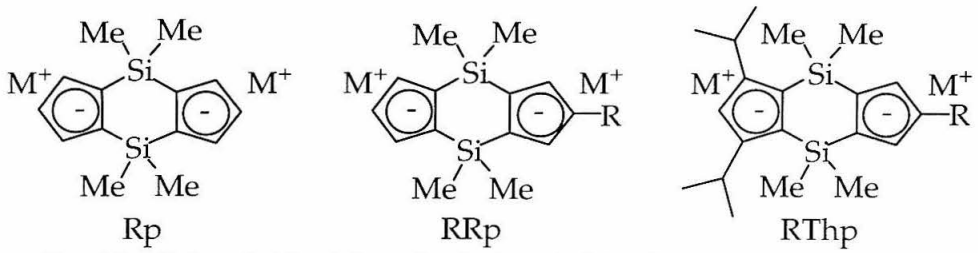

Figure 12: Doubly-silylene bridged ligand salts targeted for the synthesis of *ansa*-tantalocenes.

Rp ligand

Addition of a dilute solution of $TaCl_2Me_3$ (in THF) to a slurry of dipotassio ligand salt ($K_2[(1,2\text{-}SiMe_2)_2(C_5H_3)_2]$, K_2Rp) affords a bridged-dinuclear complex as the major reaction product (eq. 11) in addition to other decomposition products. Following the course of metallation in THF-d_8 by ^1H NMR spectroscopy reveals that the major product decomposes under the reaction conditions over the course of days. Use of the dilithio ligand salt (Li_2Rp) also provides this bridged-dinuclear complex as the predominant reaction product.[14] One hypothesis for the formation of this bridged-dinuclear complex is the low concentration of the ligand salt under reaction conditions due to poor solubility as compared to $TaCl_2Me_3$.

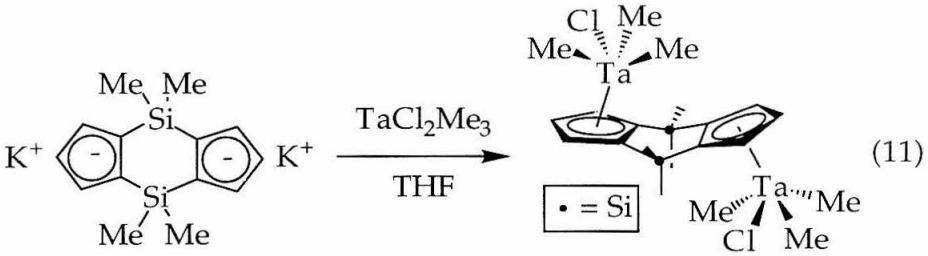

(11)

major product

To address the low solubility of the ligand salts, crown ethers (12-crown-4 or 18-crown-6) were added to the reaction mixture to complex Li^+ or K^+, respectively. However, in the presence of these crown ethers decomposition is accelerated and no metallocene products could be isolated.

A synthetic methodology analogous to that used for the preparation of the *ansa*-tantalocene, $Me_2Si(C_5Me_4)_2TaH_3$[10], was also attempted with the Rp

ligand. Transmetallation of Li_2Rp with *n*-Bu_3SnCl in diethyl ether affords (*n*-$Bu_3Sn)_2[(1,2\text{-}SiMe_2)_2(C_5H_3)_2]$ ((*n*-$Bu_3Sn)_2Rp$) as an orange oil. Subsequent reaction of the distannylated ligand with $TaCl_5$ affords a highly insoluble red-purple solid; ^1H NMR analysis of this product in THF-d_8 was inconclusive. Reduction of this red-purple solid with $LiAlH_4$, and subsequent hydrolysis (with aqueous ammonium chloride) did not provide the desired *ansa*-tantalocene trihydride complex. The very low solubility of the red-purple tantalocene product suggests the formation of bridged-dinuclear or higher oligomeric structures. Thus, the Rp ligand's lack of cyclopentadienyl substituents appears to favor spanning two tantalum centers. Since these methodologies have not allowed isolation of the desired η^5,η^5 *ansa*-tantalocenes, more substituted doubly-bridged ligand arrays were examined.

RRp ligand

The RRp ligand array, $[(1,2\text{-}SiMe_2)_2(4\text{-}R\text{-}C_5H_2)(C_5H_3)]$ (RRp, where R = iPr, tBu), was designed to probe its ability to direct olefin binding preferences. To provide a preliminary understanding of the stereodirecting ability of this ligand array, tBuRp zirconocene dichloride has been prepared and utilized for propylene polymerization. It is expected that bulky R substituent (iPr or tBu) will force the methyl substituent of an incoming propylene molecule towards the unsubstituted cyclopentadienyl ring (as illustrated in Figure 13). However, whether the propylene methyl substituent and β-carbon of the polymer chain exhibit a *trans* or *cis* relationship during olefin coordination and insertion is unclear. A *trans* relationship has been detected for select singly-bridged

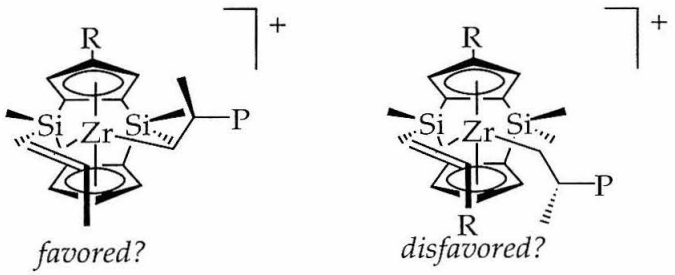

Figure 13: Both *trans* and *cis* relationships between the propylene methyl substituent and the β-carbon of the polymer chain may be possible for olefin coordination.

metallocenes[6,7] and postulated for other C_s-symmetric, doubly-silylene bridged metallocenes.[4] This relationship cannot be probed in a straightforward manner by employing RRp zirconocene polymerization catalysts. For these reasons, RRp tantalocene complexes were targeted.

The synthetic route employed for the preparation of RRp ligands is similar to that of other substituted doubly-silylene bridged ligands.[36] Preparation of the protio iPrRp ligand was attempted by the addition of Me_2SiCl_2 to a -78°C THF solution of Li_2iPrSp (eq. 12). The product of this reaction was isolated as a yellow oil; the ^{1}H NMR spectrum of the resulting product exhibited a large number of peaks and was difficult to interpret. Subsequent addition of *n*-BuLi to a diethyl ether solution of the reaction product affords a white solid. Analysis by ^{1}H NMR spectroscopy in THF-d_8 solvent reveals that the product is a mixture of two isomers, $Li_2[(1,2\text{-}SiMe_2)_2(4\text{-}CHMe_2\text{-}C_5H_2)(C_5H_3)]$ and $Li_2[(1,2\text{-}SiMe_2)_2(3\text{-}CHMe_2\text{-}C_5H_2)(C_5H_3)]$. A similar observation was made by Herzog in the preparation of $M_2[(1,2\text{-}SiMe_2)_2(4\text{-}CHMe_2\text{-}C_5H_2)(3,5\text{-}CHMe_2\text{-}C_5H)]$ (where M = Li, K); 10% of the undesired isomer, $Li_2[(1,2\text{-}SiMe_2)_2(3\text{-}CHMe_2\text{-}C_5H_2)(3,5\text{-}CHMe_2\text{-}C_5H)]$, was formed.[36] Metallation of Li_2iPrRp with $ZrCl_4$ in toluene provides a mixture of product isomers, as anticipated. Separation of $[(1,2\text{-}SiMe_2)_2(4\text{-}CHMe_2\text{-}C_5H_2)(C_5H_3)]ZrCl_2$ from $[(1,2\text{-}SiMe_2)_2(3\text{-}CHMe_2\text{-}C_5H_2)(C_5H_3)]ZrCl_2$ was not straightforward and thus not pursued further.

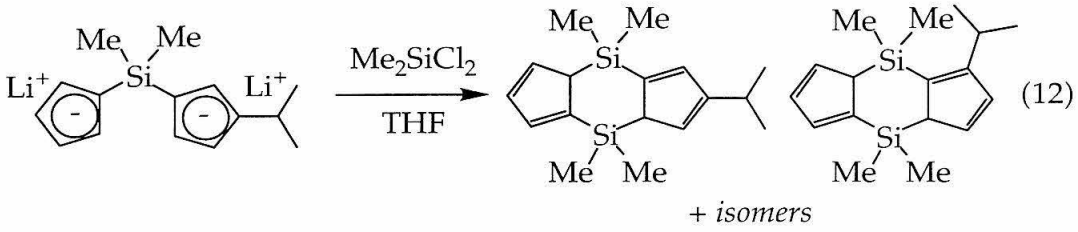

(12)

The tBuRp ligand was prepared in a similar fashion. Addition of Me_2SiCl_2 to a -78°C THF solution of Li_2tBuSp {$Li_2[Me_2Si(3\text{-}CMe_3\text{-}C_5H_3)(C_5H_4)$} affords $[(1,2\text{-}SiMe_2)_2(4\text{-}CMe_3\text{-}C_5H_2)(C_5H_3)]$ (**7**) as a yellow-white waxy solid (eq. 13). Subsequent deprotonation of **7** with either *n*-BuLi or KH provides the corresponding dilithio (Li_2tBuRp, **8**) or dipotassio (K_2tBuRp) ligand salts, respectively. Analysis by ^{1}H NMR spectroscopy reveals that only the desired 4-tBu substituted isomer is formed. The known propensity for *tert*-butyl

substituents to avoid occupying a position alpha to a dimethylsilyl linking substituent has been described previously.[37]

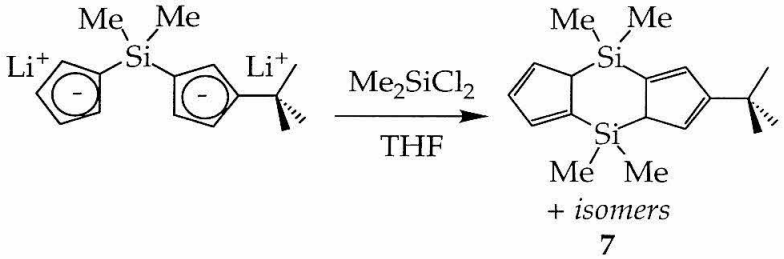

(13)

7

The corresponding zirconocene dichloride complex was prepared in a standard fashion by addition of toluene to a mixture of **8** and $ZrCl_4$ at -78°C and slow warming to 25°C (eq. 14). The reaction product was extracted away from lithium chloride using petroleum ether and isolated as a yellow-white solid. Examination of the ^1H NMR spectrum of the reaction product in benzene-d_6 indicates that only the desired 4-tBu substituted isomer, $[(1,2\text{-}SiMe_2)_2(4\text{-}CMe_3\text{-}C_5H_2)(C_5H_3)]ZrCl_2$ (tBuRpZrCl$_2$, **9**), is formed. Notably, use of refluxing toluene for metallation leads to extensive decomposition and **9** cannot be isolated.

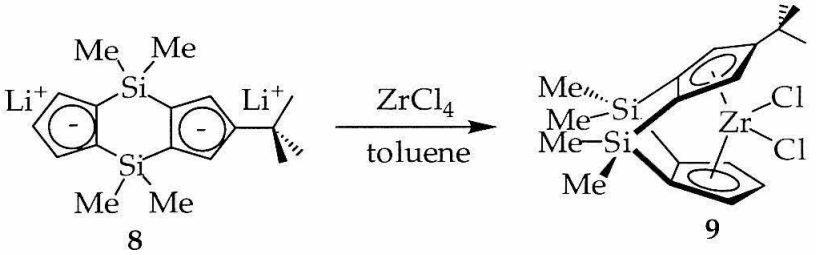

(14)

8 9

Complex **9** was targeted as an α-olefin polymerization precatalyst in order to assess the stereodirecting ability of the tBuRp ligand array. Towards this end, **9** was activated with 500 equivalents of MAO for propylene polymerization. The reaction was carried out in neat monomer at 0°C. Examination of the polymer tacticity by ^{13}C NMR spectroscopy indicates that the polymer is primarily atactic, with a slight syndiotactic preference ($[r] \approx 55.6\%$). The full pentad distribution for this sample is given in Table 3. Other polymerization conditions, such as dilute monomer concentration or higher polymerization temperature, have not been examined to date.

[*mmmm*]	[*mmmr*]	[*rmmr*]	[*mmrr*]	[*mrmm*] [*rmmr*]	[*mrmr*]	[*rrrr*]	[*mrrr*]	[*mrrm*]	[*r*]
7.23	8.59	7.96	5.21	23.86	12.26	13.92	14.78	6.19	55.6

Table 3: Pentad analysis for polypropylene produced using catalyst **9**.

The low syndiospecificity derived from the C_s-symmetric precatalyst, **9**, may be accounted for by a facile site epimerization mechanism. This phenomenon has been observed for other doubly-silylene bridged metallocene catalysts under various polymerization conditions.[34,35] Since *trans* and *cis* relationships between the propylene methyl substituent and the β-carbon of the polymer chain may be viable for olefin coordination (Figure 13), this adds another dimension to the operating polymerization mechanism. Assuming that the propylene methyl substituent will orient itself away from the *tert*-butyl group, the possibilities for olefin coordination are illustrated in Figure 14. The possibilities for olefin coordination with the propylene methyl substituent oriented towards the bulky *tert*-butyl group are omitted for steric reasons. The predicted preferences for olefin coordination and subsequent insertion in Figure 14 are based on presumed unfavorable steric interactions between certain polymer chain configurations and linking dimethylsilyl substituents. The relative energies of *trans* and *cis* conformers cannot be determined with this data.

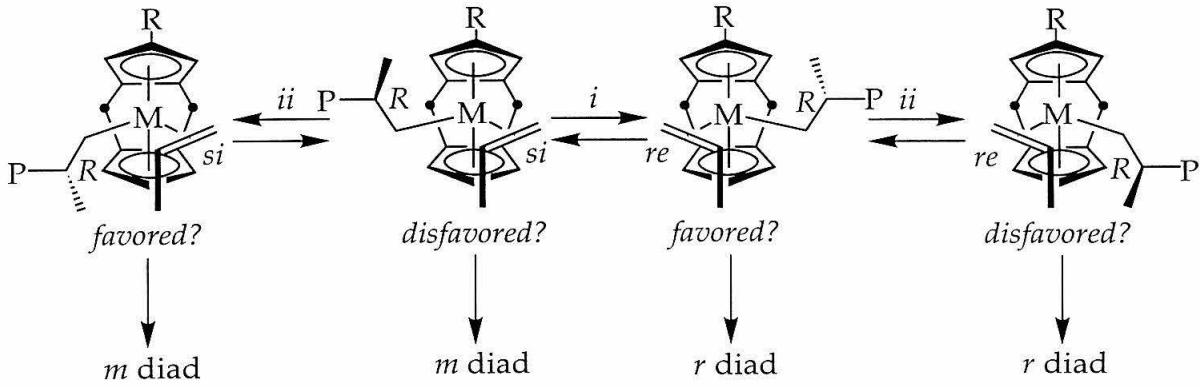

Figure 14: Invoking both a site epimerization mechanism and facile rotation about the α-carbon of the polymer chain may explain the atactic polymer formed using the RRp ligand array.

Tantalocenes employing the tBuRp ligand were targeted to ascertain how the sterics of this ligand array influence olefin coordination. Trimethyl complexes were sought as synthetic precursors for olefin adducts.

Dropwise addition of a THF solution of $TaCl_2Me_3$ to a -78°C THF solution of Li_2tBuRp and slow warming to 25°C provides an orange solution. Removal of THF *in vacuo* and extraction with toluene affords a brown oil that is primarily the methylidene-methyl complex, $[(1,2\text{-}SiMe_2)_2(4\text{-}CMe_3\text{-}C_5H_2)(C_5H_3)]Ta(CH_2)CH_3$ (tBuRpTa$(CH_2)CH_3$, **10**) (eq. 15). The methylidene protons appear as doublets at 9.43 and 9.74 ppm in the ^1H NMR spectrum; these resonances are characteristic of a tantalocene-methylidene complex. ^1H NMR analysis provides no evidence of the expected tantalocene trimethyl complex (see eq. 15). Subsequent dissolution of the brown oil in petroleum ether allows recrystallization of **10** as a tan solid in low yield.

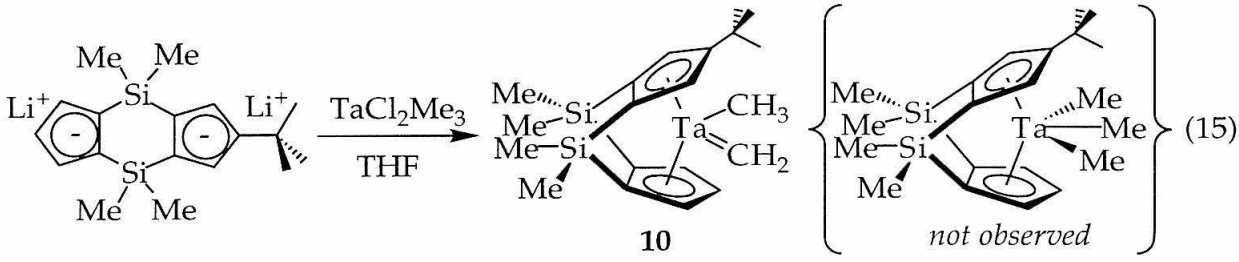

This metallation reaction was examined more closely by combination of the dilithio ligand salt, Li_2tBuRp, and $TaCl_2Me_3$ in benzene-d_6 in the absence of ambient light (eq. 16). Monitoring the reaction by ^1H NMR spectroscopy reveals that after 3.5 hours, the bridged dinuclear complex, $[(1,2\text{-}SiMe_2)_2(4\text{-}CMe_3\text{-}C_5H_2)(C_5H_3)](TaMe_3Cl)_2$ [tBuRp$(TaMe_3Cl)_2$] was present as the predominant reaction product. Two tantalum-methyl resonances of equal intensity at 1.06 ppm and 1.09 ppm are diagnostic for this type of ligand coordination. Fast rotation about the tantalum cyclopentadienyl bond equivalences the three methyl substituents bound to each tantalum center. The tantalocene methylidene-methyl complex (**10**) is also present yet it comprises only approximately 1.5% of the product mixture. Over time, the ratio of **10** to

tBuRp(TaMe$_3$Cl)$_2$ increases but decomposition also becomes more prevalent. Again, there is no evidence of the expected tantalocene trimethyl complex.

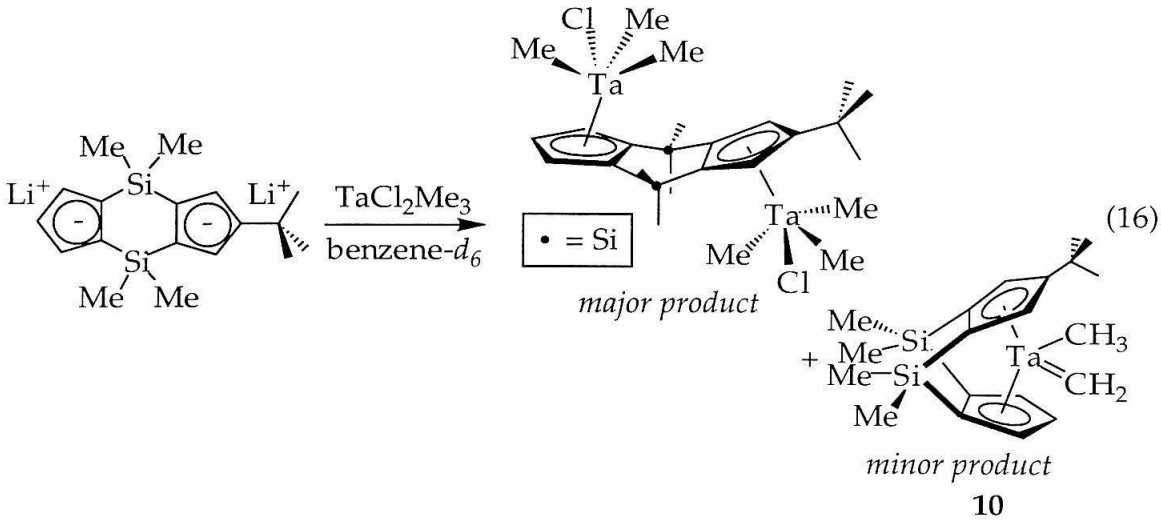

10

The mechanism for formation of **10** and the absence of the tantalocene trimethyl complex under these reaction conditions has not been investigated further. These issues will be addressed with reference to RThp tantalocenes.

Thermolysis of the methylidene methyl complex, **10**, in benzene-d_6 causes starting material resonances to diminish and other peaks to grow in the ^{1}H NMR spectrum. After four days at 100°C, a small resonance is present at -2.45 ppm that may be attributed to a tantalocene-hydride resonance but a variety of cyclopentadienyl and alkyl resonances are also present (too many to indicate sole formation of a tantalocene ethylene-hydride complex). Upon continued heating, extensive decomposition occurs providing no identifiable products. Some potential tantalocene products are illustrated in Figure 15.

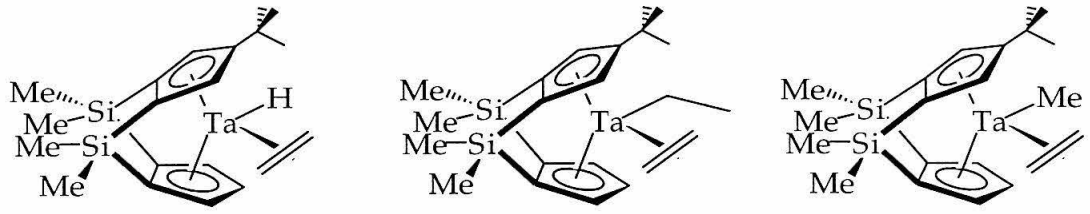

Figure 15: Potential products from thermolysis of **10**.

RThp ligand

Reaction of the dipotassio ligand salt, $K_2[(1,2\text{-}SiMe_2)_2\{4\text{-}CMe_3\text{-}C_5H_2\}\{3,5\text{-}(CHMe_2)_2\text{-}C_5H\}]$ (K_2tBuThp), with $TaCl_2Me_3$ in benzene-d_6 provides a mixture of two products: $[(1,2\text{-}SiMe_2)_2\{\eta^5\text{-}C_5H_2\text{-}4\text{-}CMe_3\}\{\eta^2\text{-}C_5H\text{-}3,5\text{-}(CHMe_2)_2\}]Ta(CH_3)_3$ (tBuThpTaMe$_3$, **11**) and $[(1,2\text{-}SiMe_2)_2\{\eta^5\text{-}C_5H_2\text{-}4\text{-}CMe_3\}\{\eta^5\text{-}C_5H\text{-}3,5\text{-}(CHMe_2)_2\}]Ta(CH_2)CH_3$ (tBuThpTa(CH$_2$)CH$_3$, **12**), as illustrated in eq. 17. The unusual η^2-cyclopentadienyl coordination observed for this tantalocene trimethyl complex (*vide infra*) and the formation of a tantalocene methylidene-methyl complex under these reaction conditions are notable.[38] The doubly-silylene bridged ligand array appears to induce this unexpected reactivity. Analogous reactivity is observed with K_2TMSThp as a ligand source.[13] In order to explore the course of this reaction, a variety of reaction conditions have been examined.

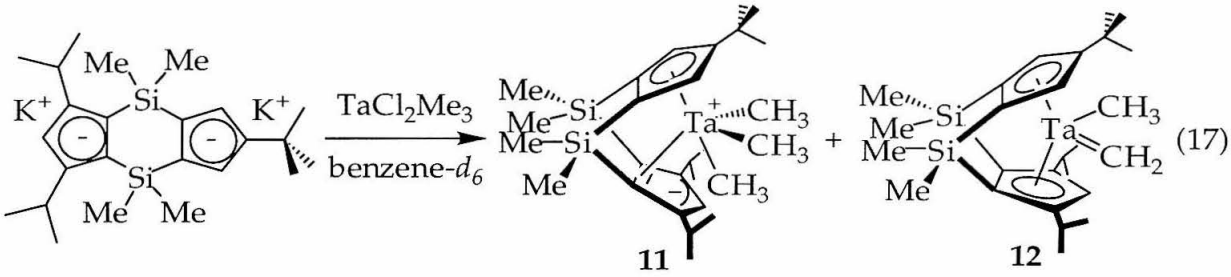

(17)

Order of addition does not alter the product distribution. Mild heating (60°C) also appears to exert little influence on the course of reaction. Addition of base, such as NEt_3, or excess ligand salt, K_2tBuThp, are other reaction modifications that do not affect metallation.

The product distribution was found to be highly dependent on the presence or absence of ambient light. If the metallation (eq. 17) is conducted in the presence of ambient light, **11** decomposes over the course of 24 hours. Compound **11** does not decompose to form **12**; these tantalocenes are formed at different rates under these reaction conditions. In the absence of ambient light, **12** is stable; compound **11** is also formed and is stable under these conditions. Hence, the tantalocene trimethyl and methylidene-methyl complexes may be isolated independently by selective recrystallization.

Following the course of metallation in benzene-d_6 by ^{1}H NMR spectroscopy (in the absence of ambient light) reveals that both **11** and **12** are formed in low yield (24% and 18%, respectively). This, in part, may be attributed to formation of a bridged dinuclear complex (see Figure 16) as an undesired byproduct.

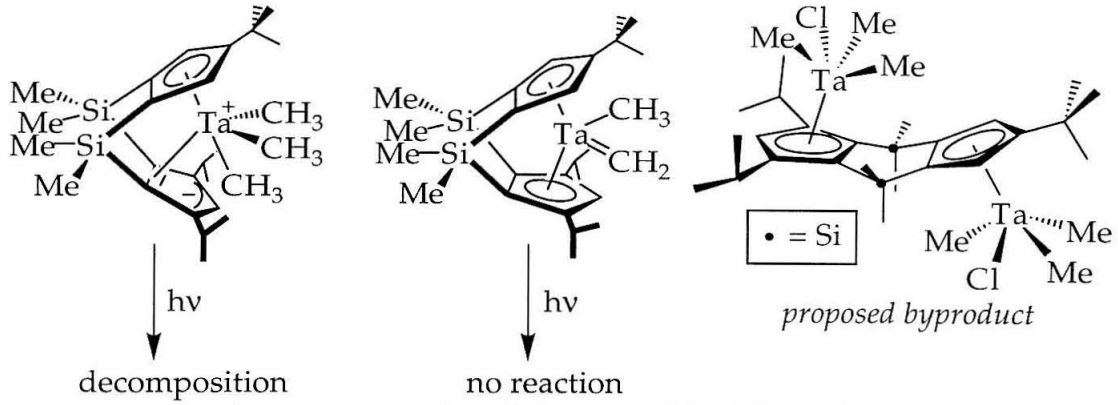

Figure 16: While **11** decomposes in ambient light, **12** is stable. A bridged dinuclear complex is formed as a byproduct under select metallation conditions.

The effect of solvent choice on metallation has been examined by monitoring metallation by ^{1}H NMR. Various deuterated solvents have been employed providing a range of product distributions. Generally, when tantalocene products are observed, the formation of the trimethyl complex is favored over the methylidene-methyl complex. The relative amount of the bridged dinuclear species (Figure 16) varies with solvent.

The use of polar solvents such as CD_3CN or THF-d_8 is unfavorable for metallation. The former leads to decomposition and the latter yields some of the bridged dinuclear species (as a result, K_2tBuThp is not completely consumed). When cyclohexane-d_{12} is used, the bridged dinuclear species is the major product. While metallation in Et_2O-d_{10} generates some of the bridged dinuclear species, formation of the methylidene-methyl complex is minimized (**11**/**12** ≈ 3.1). Thus, Et_2O is the preferred solvent for isolation of **11**. Metallation in benzene-d_6 minimizes formation of the bridged dinuclear species with a similar tantalocene product ratio (**11**/**12** ≈ 4). Since separation of **12** from the bridged dinuclear structure is difficult due to similar solubility properties, toluene has

been utilized for isolation of **12**. Recrystallization is crucial for the independent isolation of **11** and **12**.

The mechanism for formation of **12** is not well understood. Complex **11** does not appear to be a synthetic precursor to **12**; dissolution of isolated **11** in benzene-d_6 provides no evidence for production of **12** via methane loss over the course of months at 25°C. Also, thermolysis of isolated **11** in benzene-d_6 does not promote conversion to **12**; instead, decomposition ensues. Formation of **12** does not appear to be promoted by excess dipotassio ligand salt, K_2tBuThp. These results are consistent with two independent pathways for formation of **11** and **12**.

Complex **11** may be synthesized on a preparative scale by slow warming (from -78°C to 25°C) of a diethyl ether solution of K_2tBuThp and $TaCl_2Me_3$ in the absence of ambient light. Three hours after solvent addition, extraction of the product with diethyl ether and recrystallization affords **11** as an orange-yellow solid in reasonable yield (25.6%).

Complex **12** may be isolated preparatively by slow warming (-78°C to 25°C) of a toluene solution of K_2tBuThp and $TaCl_2Me_3$ in the presence of ambient light. After three days of reaction, extraction with diethyl ether and recrystallation from petroleum ether affords **12** as a mustard colored solid in modest isolated yield (20.9%).

Complexes **11** and **12** have been characterized by ^{1}H and ^{13}C NMR spectroscopy. The NMR spectra of **11** do not possess any unusual features. In benzene-d_6, two diagnostic downfield doublets are observed at 9.30 and 9.58 ppm in the ^{1}H NMR spectrum for the methylidene hydrogens of **12**. The methylidene carbon of **12** resonates at 211.26 ppm in the ^{13}C NMR spectrum. These NMR signals for **12** are consistent with other tantalocene methylidene-methyl complexes, such as $Cp_2Ta(CH_2)CH_3$[12] (^{1}H NMR: δ = 10.11 (s), Ta=CH_2; ^{13}C NMR: δ = 224, Ta=CH_2).

Slow cooling of a diethyl ether/petroleum ether solution of **11** affords tangerine colored crystals suitable for X-ray diffraction, as illustrated in Figure 17. Compound **11** crystallized in the space group *Pnma*. This metallocene sits on

a crystallographic mirror plane thus contributing to the disorder of the *tert*-butyl substituent. The η^5,η^2-cyclopentadienyl coordination of **11** was observed previously for the similar compound, TMSThpTaMe$_3$.[13] There are few examples of η^2-cyclopentadienyl coordination in the literature. Green and coworkers have characterized $(\eta^5\text{-}C_5H_5)_2Ti(\eta^2\text{-}C_5H_5)$ by X-ray crystallography.[39] Shapiro has examined Cp_2AlMe by X-ray diffraction and observed η^2-cyclopentadienyl coordination.[40] Select bond distances and angles are listed in Table 4.

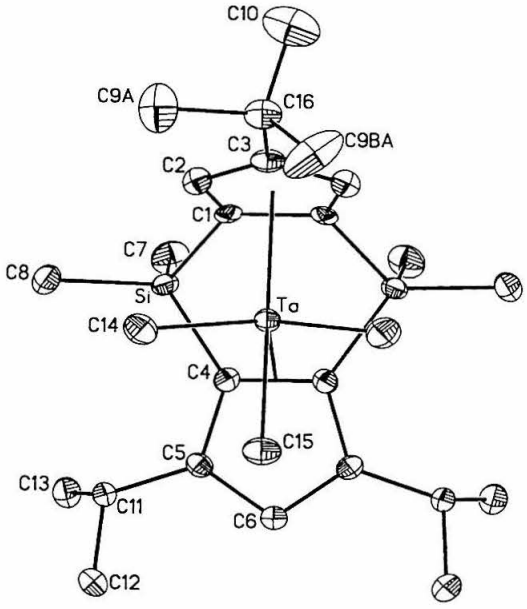

Figure 17: Molecular structure of **11** with selected atoms labeled (50% probability ellipsoids). Hydrogen atoms are omitted for clarity.

Slow cooling of a diethyl ether/pentane solution of **12** affords crystals suitable for X-ray diffraction, as illustrated in Figure 18. Compound **12** crystallized in the space group *P*2(1)/*m*. This metallocene sits on a crystallographic mirror plane and as a consequence the methylidene and methyl substituents in the metallocene wedge are indistinguishable. Importantly this structural analysis confirms η^5 coordination of both cyclopentadienyl ligands. Select bond distances and angles are provided in Table 4.

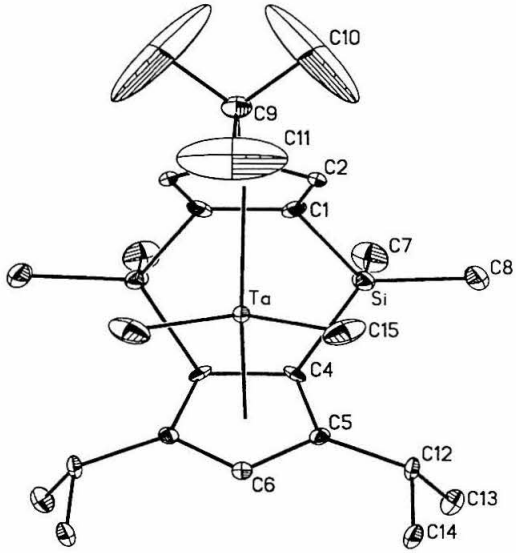

Figure 18: Molecular structure of **12** with selected atoms labeled (50% probability ellipsoids). Hydrogen atoms are omitted for clarity.

select bond distances (Å) *and bond angles* (°)	tBuThpTaMe$_3$ (**11**)	tBuThpTa(CH$_2$)CH$_3$ (**12**)
Ta-CpA	2.150	2.129
Ta-CpB	2.349	2.140
Ta-C14	2.215	—
Ta-C15	2.223	2.154
C15-Ta-C15A	—	99.3
C14-Ta-C14A	113.4	—
CpA-M-CpB	97.6	125.5
PlnA-PlnB	112.7(2)	67.0(3)

Table 4: Select bond distances and bond angles for **11** and **12**.

It appears that tantalocenes that employ the RThp ligand may not allow three substituents to occupy the metallocene wedge while maintaining standard η^5 coordination of both cyclopentadienyl ligands (Figure 20). This may be a consequence of the dimethylsilyl linking substituents that orient themselves towards the center of the metallocene wedge. The steric bulk of these methyl groups may hamper coordination of substituents in lateral positions of the metallocene wedge.

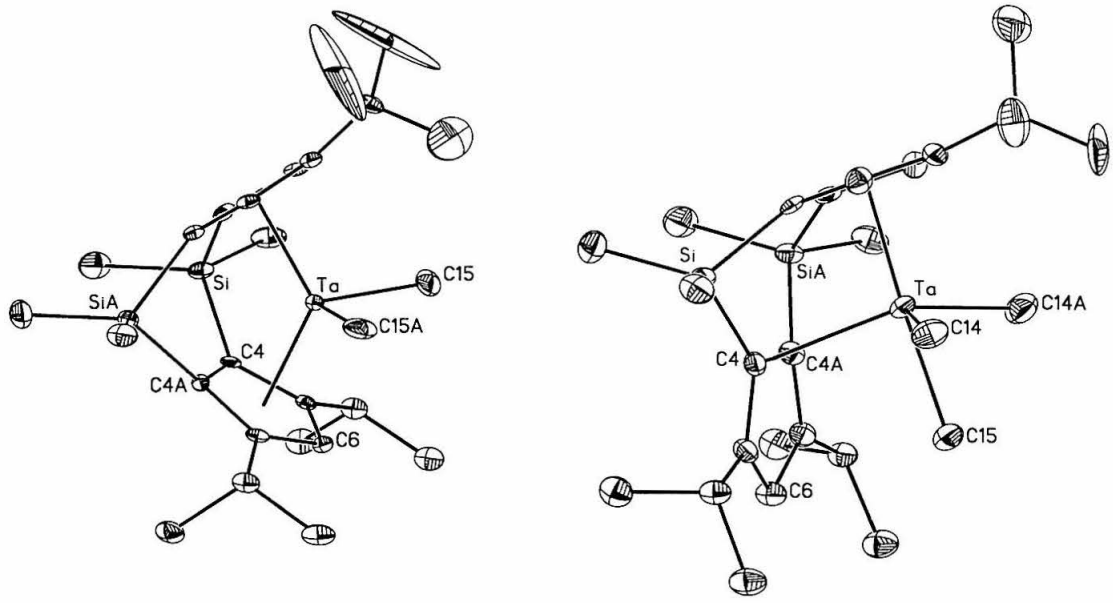

Figure 19: Comparison of molecular structures of **11** and **12** with selected atoms labeled (50% probability ellipsoids). Hydrogen atoms are omitted for clarity.

Conversion to olefin-hydride complexes

Thermolysis of **12** (at 100°C) in benzene-d_6 affords the *ansa*-tantalocene ethylene-hydride complex, tBuThpTa(η^2-CH_2CH_2)(H) (**13**), over the course of days; the yield of **13** is quantitative by ^{1}H NMR spectroscopy. This reaction may be carried out on a preparative scale; heating a toluene solution of **12** to 110°C for three days provides **13** in slightly diminished yields (eq. 18).

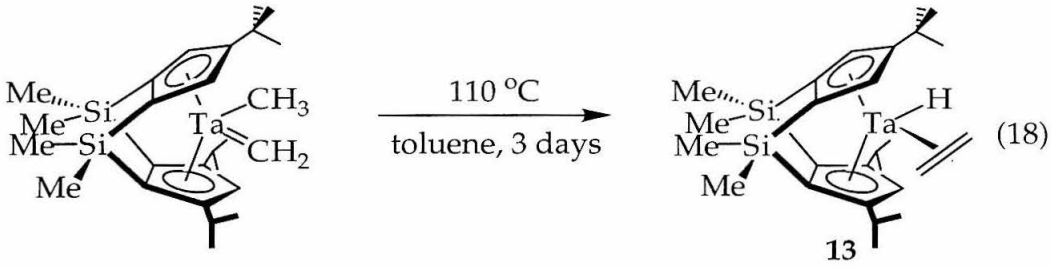

(18)

Complex **13** has been characterized by ^{1}H and ^{13}C NMR spectroscopy. The tantalocene hydride resonance at -2.05 ppm in the ^{1}H spectrum and the ethylene carbon resonances at 21.75 and 23.08 in the ^{13}C spectrum are diagnostic

for tantalocene ethylene-hydride complexes. For example, the tantalocene hydride resonance of $Cp^*_2Ta(\eta^2\text{-}CH_2{=}CH_2)H$ appears at -2.84 ppm in the ^1H NMR spectrum and the ethylene carbon resonances appear at 20.57 and 14.86 ppm in the ^{13}C spectrum.[19] A more thorough assignment of ^1H NMR resonances has been obtained by use of NOE difference NMR spectroscopy.

Presumably, complex **13** is formed via an α-methyl migration to the methylidene fragment and subsequent β-H elimination from the incipient tantalocene-ethyl complex (as illustrated in Figure 20). Formation of **13** from **12** is analogous to formation of $Cp^*_2Ta(\eta^2\text{-}CH_2{=}CH_2)H$ by thermolysis of the methylidene-methyl complex, $Cp^*_2Ta(=CH_2)(CH_3)$.[12] The latter thermal rearrangement requires more forcing conditions (heating to 140°C) than conversion of **12** to **13**. This rearrangement contrasts the solution behavior of $Cp_2Ta(=CH_2)(CH_3)$ which upon standing undergoes bimolecular decomposition forming one-half of an equivalent of the tantalocene ethylene-methyl complex, $Cp_2Ta(\eta^2\text{-}CH_2CH_2)(CH_3)$.[11] Similar to the sterically hindered bis-(C_5Me_5) ligand framework, it appears that cyclopentadienyl substitution serves to protect the metal center of **12** such that bimolecular decomposition is prevented. Instead, intramolecular α-migratory insertion affords **13**.

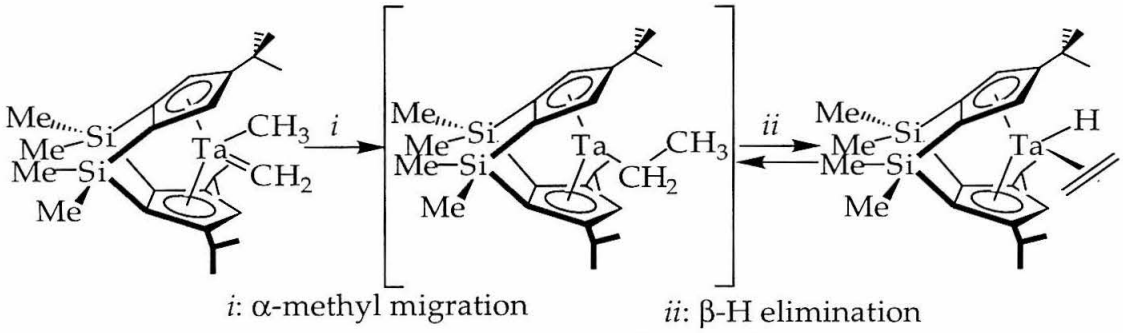

Figure 20: Conversion of **12** to **13** may involve a tantalocene-ethyl complex as an intermediate.

In attempt to capture the tantalocene-ethyl intermediate as a tantalocene-ethyl-(L) complex, trimethylphosphine was added to a benzene-d_6 solution of **13**. No reaction was observed, even upon heating to 100°C for days. Generation of alkyl-(L) complexes from olefin-hydrides has been reported when L may serve as a π-acid. For example, addition of CO or CNMe to $Cp^*_2Nb(\eta^2\text{-}CH_2{=}CHR')H$ provides the corresponding alkyl-(L) complexes;[17] addition of CO to $tBuSpTa(\eta^2\text{-}CH_2{=}CHPh)H$ affords the corresponding alkyl-(CO) compound.[13] The reactivity

of π-acid ligands such as CO or CNMe towards **13** has not been examined to date. Addition of excess ethylene to **13** was attempted to promote conversion to a tantalocene ethylene-ethyl complex. At 25°C, **13** remains intact; thermolysis of **13** (87°C) in the presence of excess ethylene also does not chemically modify **13**. Ethylene is not an effective trap for the proposed tantalocene-ethyl intermediate

Complex **13** undergoes olefin exchange with both propylene and styrene to afford the corresponding propylene-hydride and styrene-hydride complexes, respectively (eq. 19). Addition of excess propylene to a benzene-d_6 solution of **13** results in olefin equilibration over the course of weeks at 25°C. Notably, only one isomer of a propylene-hydride complex is detected in the equilibrium mixture; there are four possible isomers that may be detected (two endo and two exo).[41] Since both sides of the wedge are enantiotopic, two enantiomers of the tantalocene propylene-hydride may form. These enantiomers are indistinguishable by ^{1}H NMR analysis. In benzene-d_6, the ^{1}H NMR spectrum of **14a** displays a characteristic upfield resonance at -1.85 ppm for the tantalum hydride resonance as well as a doublet at 2.32 ppm for the methyl group of the coordinated propylene.

As with propylene, addition of excess styrene results in slow olefin exchange, forming one diastereomer of the tantalocene styrene-hydride complex (**14b**) (eq. 19). Two enantiomers of the tantalocene styrene-hydride may form that are indistinguishable by ^{1}H NMR analysis. The tantalocene-hydride resonance of **14b** appears at -1.10 ppm in the ^{1}H NMR spectrum, in benzene-d_6 solvent. Olefinic carbon resonances at 21.29 and 22.40 ppm in the ^{13}C NMR spectrum are also consistent with a styrene-hydride complex. The ortho, meta, and para styrene substituents are detected in the ^{1}H NMR spectrum at 7.47, 7.23, and 6.82 ppm, respectively. The equivalence of both ortho and meta hydrogens suggests that rotation of the phenyl ring is fast relative to the NMR time scale.

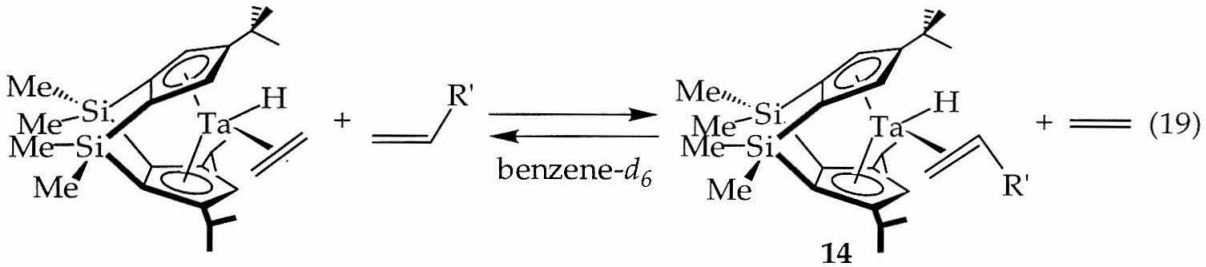

(19)

14

where R' = Me (**14a**)
where R' = Ph (**14b**)

Difference NOE experiments were used to establish the relative orientation of the bound propylene in **14a** in solution. Irradiation of the tantalocene-hydride, cyclopentadienyl resonances, and the propylene methyl substituent provide spectroscopic information that is consistent with the structures illustrated in Figure 21. These data indicate that the preferred diastereomer has the propylene coordinated in an *endo* fashion with the propylene methyl group directed away from the bulky *tert*-butyl substituent, nestled in the open region between the isopropyl groups. Unfavorable steric interactions between the propylene methyl group and the dimethylsilylene linkers appear to force coordination of the olefin in an *endo* arrangement. Formation of this diastereomer is consistent with the model previously proposed for this ligand array in the syndiospecific polymerization of propylene.[4]

Identification of the observed styrene-hydride complex, **14b**, has been accomplished by NOE difference NMR spectroscopy. Irradiation of the tantalocene-hydride, cyclopentadienyl resonances, and styrene resonances provides spectroscopic information that is consistent with the enantiomers illustrated in Figure 21. Irradiation of other ligand resonances (isopropyl, dimethylsilyl, and *tert*-butyl substituents) also corroborates this structural assignment. The preferred isomer is analogous to the isomer observed in the propylene-hydride case, namely where the olefin is coordinated in an *endo* arrangement with the phenyl substituent directed between the two isopropyl groups on the cyclopentadienyl ring. It is notable that complexes **14a** and **14b** exhibit the same thermodynamic preferences for olefin binding despite the increased sterics of bound styrene.

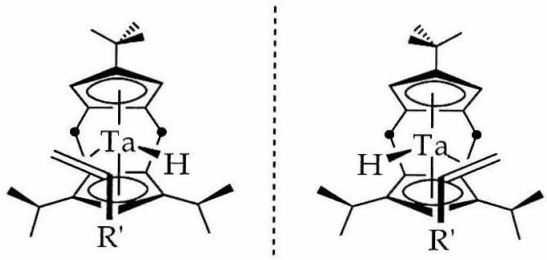

Figure 21: Difference NOE experiments indicate that (CH_2=CHR'), where R' is methyl or phenyl, coordinates in an *endo* fashion with the R' substituent directed between the two isopropyl groups of the cyclopentadienyl ring. Both possible enantiomers are shown; they are indistinguishable by ^{1}H NMR spectroscopy.

Olefin equilibration with **13** has also been achieved with fluorinated styrenes, such as 2,3,4,5,6-pentafluorostyrene and 4-trifluoromethylstyrene. Tantalocene-hydride resonances at -0.77 and -1.00 ppm in the ^{1}H NMR spectrum are typical for tantalocene olefin adducts. Isobutylene does not promote olefin exchange with **13**, even under forcing conditions (heating to 140°C). Further investigation of these olefin-hydride complexes is currently in progress.

This selectivity for CH_2=CHR' coordination in an olefin-hydride complex contrasts what has been observed previously for C_2-symmetric yttrocenes (*vide supra*). The selectivity for olefin coordination exerted by the C_s-symmetric tBuThp ligand and the C_2-symmetric Bp ligand is illustrated in cartoon fashion in Figure 22. The C_s-symmetric tBuThp ligand array displays some influence on olefin coordination by favoring two enantiotopic tantalocene olefin-hydride complexes. In contrast, the C_2-symmetric Bp yttrocene hydride compound exhibits a slight preference for coordination of one olefin enantioface. Two factors may contribute to these differences in olefin coordination. While isolated tantalocene olefin-hydrides are a measure of thermodynamic coordination preferences (ground states), prior measurements with group 3 and cationic group 4 metallocenes are based on kinetic coordination preferences (transition states). However, if the olefin insertion transition state is "early," it follows from the Hammond postulate that the olefin-hydride ground state may serve as a reasonable model for the olefin insertion transition state.[42] Metallocene symmetry is likely a more important factor for dictating stereocontrol; while **14a** and **14b** utilize the C_s-symmetric tBuThp ligand array, prior studies have employed C_2-symmetric metallocenes. It appears that metallocene symmetry

and disposition of ligand sterics may play a more substantial role in olefin coordination than previously postulated.

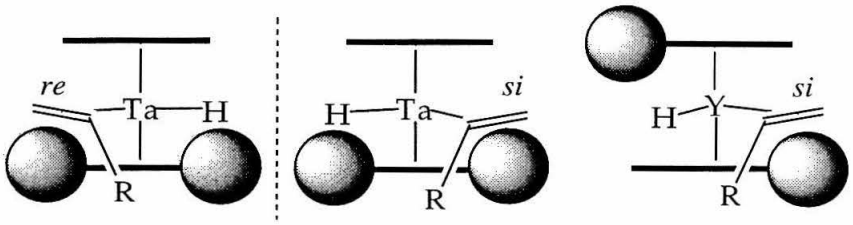

Figure 22: Selectivity for olefin coordination exerted by the C_s-symmetric tBuThp ligand and the C_2-symmetric Bp ligand.

Conclusions

A family of singly- and doubly-silylene linked tantalocene trimethyl and methylidene-methyl complexes have been synthesized and used as synthetic precursors for olefin adducts. These olefin complexes have been utilized as models for olefin coordination in Ziegler-Natta polymerization catalysts. A tantalocene trimethyl complex has been prepared that incorporates the singly-bridged [$Me_2Si(C_5H_4)_2$] (Sp) ligand. This compound has been characterized by X-ray crystallography and employed in the synthesis of the corresponding ethylene-methyl complex, SpTa(η^2-CH_2=CH_2)Me. Olefin exchange with propylene provides a mixture of *endo* and *exo* propylene-methyl isomers; the preference for *endo* isomer formation may be attributed to the *ansa*-bridge.

Doubly-silylene bridged ligands, [(1,2-$SiMe_2$)$_2$(C_5H_3)$_2$] (Rp), [(1,2-$SiMe_2$)$_2$(4-CMe_3-C_5H_2)(C_5H_3)] (tBuRp), and [(1,2-$SiMe_2$)$_2$(4-CMe_3-C_5H_2)(3,5-($CHMe_2$)$_2$-C_5H)] (tBuThp) have been targeted for the preparation of *ansa*-tantalocenes. While the Rp ligand affords bridged dinuclear and oligomeric complexes under the reaction conditions examined herein, the tBuRp ligand allows isolation of the methylidene-methyl complex, tBuRpTa(CH_2)CH_3, as a minor product. Thermolysis of this methylidene-methyl complex provides a mixture of products and decomposition, presumably due to the limited steric protection of the metal center. Metallation of the tBuThp ligand with $TaCl_2Me_3$ yields a mixture of [(1,2-$SiMe_2$)$_2$(η^5-4-CMe_3-C_5H_2)(η^2-3,5-($CHMe_2$)$_2$-C_5H)]$TaMe_3$ and [(1,2-$SiMe_2$)$_2$(η^5-4-CMe_3-C_5H_2)(η^5-3,5-($CHMe_2$)$_2$-C_5H)]Ta(CH_2)CH_3. Both complexes have been characterized by X-ray crystallography. Upon

thermolysis, the methylidene-methyl complex undergoes conversion to the corresponding ethylene-hydride complex, tBuThpTa(η^2-CH_2=CH_2)H. The ethylene-hydride complex undergoes olefin exchange with propylene and styrene to form the olefin-hydride complexes, tBuThpTa(η^2-CH_2=CHR')H (where R' is methyl or phenyl). Only one isomer is observed in each case, suggesting the importance of ligand array on olefin coordination. These models have provided an enhanced understanding of stereocontrol for *ansa*-metallocene catalysts.

Experimental

General Considerations. All air or moisture sensitive chemistry was performed using standard high vacuum line or Schlenk techniques, or in a dry box under a nitrogen atmosphere as described previously.[43] Dinitrogen, dihydrogen, and argon were purified by passage over MnO on vermiculite and activated molecular sieves. Petroleum ether and toluene were distilled from sodium and stored under vacuum over titanocene.[44] Tetrahydrofuran, diethyl ether, and dimethoxyethane were distilled from sodium benzophenone ketyl. Benzene-d_6 was distilled from $LiAlH_4$ and then distilled from sodium sand before use. Tetrahydrofuran-d_8 was distilled from sodium benzophenone ketyl and stored over 4Å molecular sieves. Methylene chloride-d_2 was distilled from calcium hydride. Anhydrous hydrochloric acid was purchased from Aldrich and used as received. Ethylene was purchased from Matheson and passed through a dry ice/acetone trap before use. In some cases, propylene was purchased from Aldrich and stored under vacuum over triisobutylaluminum. For polymerizations, propylene (99.5% polymer grade) was dried by passage through a Matheson 6110 drying system equipped with an OXISORB™ column. MAO (methylaluminoxane, Albemarle) was prepared by removing toluene *in vacuo*; the white MAO solid was dried at 25°C for 48 hours at high vacuum. $TaCl_2Me_3$ was prepared according to literature procedures[11] and sublimed under static vacuum at 50°C before use. Alkylchlorosilanes were distilled from CaH_2 immediately prior to use. $LiCH(TMS)_2$ was prepared by the method of Cowley.[45] Potassium bis(trimethylsilyl)amide ($KN(TMS)_2$) was sublimed before use. All dilithio and dipotassio ligand salts were prepared via standard procedures[36] unless otherwise noted. All other reagents were purchased from Aldrich and used as received or purified using standard methods.[46]

Instrumentation. NMR spectra were recorded on a Bruker AM500 (^{1}H, 500.13 MHz; ^{13}C, 125.77 MHz) spectrometer, a Joel GX-400 (^{1}H, 399.78 MHz; ^{13}C 100.53 MHz; ^{19}F, 376.1 MHz) spectrometer, a G.E. QE300 (^{1}H, 300.1 MHz) spectrometer, a Varian INOVA 500 (^{1}H, 500.13 MHz; ^{13}C, 125.77 MHz) spectrometer, or a Varian 300 (^{1}H , 300 MHz) spectrometer. All chemical shifts are relative to TMS for ^{1}H (residual) and ^{13}C NMR (solvent used as a secondary standard). Nuclear Overhauser (NOE) difference experiments were conducted using a Varian INOVA 500 MHz spectrometer. Elemental analysis was performed at the California Institute of Technology Elemental Analysis Facility by Fenton I. Harvey or at Midwest Microlab in Indianapolis, Indiana. X-ray crystallography was carried out by Dr. Michael W. Day and Lawrence M. Henling using either an Enraf-Nonius CAD-4 diffractometer or a Bruker Smart 1000 CCD diffractometer. Small crystalline fragments were cut under Paratone-N oil and mounted on the diffractometer under a stream of cold N_2 gas.

$Me_2Si(\eta^5\text{-}C_5H_4)_2Ta(CH_3)_3$ (1). (SpTaMe$_3$). In the dry box a 100 mL round bottom flask equipped with stir bar was charged with K_2Sp (1.35 g, 5.11 mmol) and Et_2O (60 mL) was added to provide an off-white slurry. A 25 mL round bottom flask was charged with $TaCl_2Me_3$ (1.52 g, 5.11 mmol) and Et_2O (15 mL) was added to provide a bright yellow solution. While rapidly stirring the slurry of K_2Sp, the solution of $TaCl_2Me_3$ was slowly added dropwise (over the course of 15 minutes). When the addition was complete, a fine swivel frit assembly was attached and the apparatus was connected to the vacuum line. An atmosphere of Ar was admitted to the reaction and it was left open to a mercury bubbler. After 11 hr of stirring at 25°C, a pale yellow solution was filtered away from a dark yellow precipitate. The solid was washed with Et_2O (6 x 15 mL), and solvent was removed *in vacuo* providing a pale yellow powder. This powder was transferred to a 50 mL round bottom flask equipped with stir bar and a fine swivel frit assembly was attached. On the vacuum line, Et_2O (25 mL) was added by vacuum transfer and then the frit was backfilled with Ar. The solution was cooled to -78°C to recrystallize the desired product; a yellow supernatent was filtered away from an off-white powder. After removal of solvent *in vacuo* **1** was isolated as an off-white powder; 417 mg (19.8%). Analysis for $C_{15}H_{23}Ta_1Si_1$: Calculated (Found) C: 43.69 (44.38); H: 5.62 (5.39). ^{1}H NMR (benzene-d_6): δ = -0.04 (s, 6H, $(CH_3)_2Si$), 0.47 (s, 3H, Ta-CH_3), 0.51 (s, 6H, Ta-CH_3), 4.76 (s, 4H, Cp-

H), 5.37 (s, 4H, Cp-*H*). ^{1}H NMR (CD_2Cl_2): δ = -0.24 (s, 3H, Ta-CH_3), 0.18 (s, 6H, $(CH_3)_2Si$), 0.53 (s, 6H, Ta-CH_3), 5.12 (s, 4H, Cp-*H*), 5.59 (s, 4H, Cp-*H*). ^{13}H NMR (benzene-d_6): δ = -5.37 ($(CH_3)_2Si$), 22.85, 24.89 (Ta-CH_3), 90.24, 105.11, 117.64 (Cp).
bridged-dinuclear byproduct $Sp(TaMe_3Cl)_2$ ^{1}H NMR (benzene-d_6): δ = 0.10 (s, 12H, $(CH_3)_2Si$), 0.87 (s, 9H, Ta-CH_3), 5.66 (s, 4H, Cp-*H*), 5.83 (s, 4H, Cp-*H*).

$Me_2Si(\eta^5\text{-}C_5H_4)_2Ta(CH_3)(Cl)(CH_3)$ (2). (SpTa(Me)(Cl)(Me)). A J-Young NMR tube was charged with **1** (10.6 mg, 0.0257 mmol) and on the vacuum line CD_2Cl_2 was added by vacuum transfer. The solution was cooled to -196°C and HCl (0.0257 mmol) was condensed into the NMR tube at this temperature, the tube was closed and warmed to 25°C. Immediately the solution turned bright yellow in color and **2** was observed by ^{1}H NMR spectroscopy. ^{1}H NMR (CD_2Cl_2): δ = 0.56 (s, 6H, $(CH_3)_2Si$), 0.62 (s, 6H, Ta-CH_3), 5.55 (s, 4H, Cp-*H*), 6.16 (s, 4H, Cp-*H*).

$[Me_2Si(\eta^5\text{-}C_5H_4)_2Ta(CH_3)_2][BF_4]$ (3). ($[SpTaMe_2][BF_4]$). A 50 mL round bottom flask equipped with stir bar was charged with **1** (508 mg, 1.23 mmol) and $(C_6H_5)_3CBF_4$ (406 mg, 1.23 mmol) and a medium swivel frit assembly was attached. On the vacuum line, 30 mL methylene chloride was added by vacuum transfer at -78°C. The solution immediately turned bright yellow in color and precipitate began to form. The reaction mixture was allowed to warm slowly to 25°C. After 19 hr of stirring, the solvent was removed *in vacuo* and Et_2O (25 mL) was added by vacuum transfer. After 2 hr of stirring, a pale yellow-orange solution was filtered away from a bright yellow precipitate. The solid was washed with Et_2O (4 x 10 mL) and then solvent was removed *in vacuo* to provide **3** as a bright yellow powder; 525 mg (89.6%). ^{1}H NMR (CD_2Cl_2): δ = 0.63 (s, 6H, $(CH_3)_2Si$), 0.72 (s, 6H, Ta-CH_3), 6.07 (s, 4H, Cp-*H*), 7.35 (s, 4H, Cp-*H*). ^{19}F NMR (CD_2Cl_2): δ = -75.5.

$Me_2Si(\eta^5\text{-}C_5H_4)_2Ta(CH_2)CH_3$ (4). ($SpTa(CH_2)CH_3$). (transient). ^{1}H NMR (CD_2Cl_2): δ = 4.59 (s, 2H, Cp-*H*), 5.67 (s, 2H, Cp-*H*), 5.75 (s, 2H, Cp-*H*), 5.90 (s, 2H, Cp-*H*), 10.28 (s, 2H, Ta-CH_2), *Me_2*Si and Ta-*Me* resonances not located.

$Me_2Si(\eta^5\text{-}C_5H_4)_2Ta(\eta^2\text{-}CH_2{=}CH_2)CH_3$ (5). ($SpTa(\eta^2\text{-}CH_2{=}CH_2)CH_3$). A 50 mL round bottom flask equipped with stir bar was charged with **3** (206 mg, 424 mmol) and $LiCH(SiMe_3)_2$ (70.2 mg, 424 mmol) and a fine swivel frit assembly

was attached. On the vacuum line, 25 mL methylene chloride was added by vacuum transfer at -78°C. The reaction solution was frozen to -196°C and 1 atm ethylene was admitted to the reaction apparatus. The -196°C bath was replaced with a -78°C bath and the reaction mixture was allowed to warm slowly to 25°C. After 43 hr stirring, solvent was removed *in vacuo* and 25 mL pentane was added by vacuum transfer. After 2 hr of vigorous stirring, a yellow solution was filtered away from a tan solid. The solid was washed with pentane (4 x 10 mL) and then the solvent was removed *in vacuo*. In the dry box, the collection flask was transferred to another fine swivel frit apparatus. On the vacuum line, 25 mL pentane was added by vacuum transfer, the swivel frit apparatus was backfilled with Ar and the solution was cooled to -78°C. A cold filtration was used to separate the yellow supernatent from the pale tan solid. Solvent was removed *in vacuo* to afford **5** as a pale tan solid; 24 mg (13.5%). ^{1}H NMR (benzene-d_6): δ = -0.02 (s, 3H, $(CH_3)_2Si$), 0.10 (s, 3H, $(CH_3)_2Si$), 0.48 (s, 3H, Ta-CH_3), 0.96 (t, 2H, CH_2=CH_2), 1.23 (t, 2H, CH_2=CH_2), 3.74 (s, 2H, Cp-*H*), 4.56 (s, 2H, Cp-*H*), 5.25 (s, 4H, Cp-*H*). ^{13}C NMR (benzene-d_6): δ = -8.89, -6.88 ($(CH_3)_2Si$), -4.54 (Ta-CH_3), 18.89, 26.53 (CH_2=CH_2), 78.74, 87.83, 94.81, 106.45, 123.37 (Cp).

$Me_2Si(\eta^5\text{-}C_5H_4)_2Ta(CH_2{=}CHCH_3)CH_3$ (6a (endo), 6b (exo)). (SpTa(CH_2=CHMe)Me).

$Me_2Si(\eta^5\text{-}C_5H_4)(\eta^5\text{-}3\text{-}CHMe_2\text{-}C_5H_3)_2TaCl_2$. (iPrSpTa$Cl_2$). In the dry box a 50 mL round bottom flask equipped with stir bar was charged with $TaCl_5$ (602 mg, 1.68 mmol) and Zn dust (55 mg, 0.84 mmol, 0.5 equiv) and a fine swivel frit assembly was attached. DME (25 mL) was added by vacuum transfer at -78°C, then the cold bath was removed to slowly warm the reaction mixture to 25°C. After 12 hr of stirring, an olive-green solution was filtered away from a gray precipitate and solid was washed with recycled solvent (2 x 15 mL). In the dry box, a 250 mL round bottom flask equipped with stir bar was charged with Li_2iPrSp (407 mg, 1.68 mmol) and DME (75 mL) was added to provide a pale yellow solution. While stirring this solution at 25°C, the olive-green solution was slowly added dropwise via a pipette. Upon addition the solution changed to red-brown in color. A fine swivel frit assembly was attached and the reaction mixture was stirred for 16 hr. DME was removed *in vacuo* and then diethyl ether (50 mL) was added by vacuum transfer. After stirring for 2 hr, solvent was removed *in vacuo* and petroleum ether (50 mL) was added by vacuum transfer.

The reaction mixture was stirred for 12 hr, and then solvent was removed *in vacuo*. Methylene chloride (70 mL) was added by vacuum transfer and then a red-brown solution was filtered from an off-white precipitate. The solid was washed with recycled solvent (3 x 30 mL) and then solvent was removed *in vacuo* to leave a red-black residue in the collection flask. Drying the product under high vacuum provides a black solid. Yield not determined. EPR spectrum consistent with the previously reported spectrum for this complex.[13]

[(1,2-SiMe$_2$)$_2${η^5-C$_5$H$_2$-4-CMe$_3$}{η^2-C$_5$H-3,5-(CHMe$_2$)$_2$}]NbCl$_2$. (tBuThpNbCl$_2$). In the dry box a 100 mL round bottom flask equipped with stir bar was charged with Li$_2$tBuThp (417 mg, 0.86 mmol) and NbCl$_4$(THF)$_2$ (327 mg, 1 equiv) and a fine swivel frit assembly was attached. Diethyl ether (50 mL) was added by vacuum transfer at -78°C, and with the cold bath intact the reaction mixture was left to slowly warm to 25°C. After 120 hr of stirring, solvent was removed *in vacuo* and petroleum ether (50 mL) was added by vacuum transfer. After stirring for 2 hr, solvent was removed *in vacuo* and methylene chloride (50 mL) was added by vacuum transfer. A red-brown solution was filtered away from a brown solid, and then the solid was washed with recycled solvent (4 x 30 mL). Solvent was removed *in vacuo* to leave a brown-black residue in the collection flask. Drying the product under high vacuum provides a black solid; 300 mg (73.9%). This product was analyzed by ambient temperature EPR spectroscopy in methylene chloride solvent; a characteristic ten line pattern was observed for the Nb(IV) nucleus (^{93}Nb = 100%, S = 9/2).

[(1,2-SiMe$_2$)$_2$(C$_5$H$_3$)$_2$](Ta(CH$_3$)$_3$Cl)$_2$ (Rp(TaMe$_3$Cl)$_2$). In the dry box a 100 mL round bottom flask equipped with stir bar was charged with K$_2$Rp (289 mg, 0.97 mmol) and tetrahydrofuran (60 mL) was added to provide an off-white slurry. In another flask, TaCl$_2$Me$_3$ was dissolved in tetrahydrofuran (10 mL). With rapid stirring in the absence of room light, the TaCl$_2$Me$_3$ solution was slowly added via pipette to the ligand slurry. A medium swivel frit assembly was attached to the reaction flask and reaction was continued for 12 hr in the absence of room light. Solvent was removed *in vacuo*, and petroleum ether (60 mL) was added by vacuum transfer. The petroleum ether slurry was stirred for 12 hr in the absence of room light. A yellow solution was filtered away from a yellow precipitate, and the solid was washed with recycled solvent (2 x 40 mL). Solvent was removed *in vacuo* to provide a yellow-orange residue in the collection flask and a

bright yellow solid above the frit. ^{1}H NMR analysis of the bright yellow solid reveals that the bridged-dinuclear complex, Rp($TaMe_3Cl)_2$, is the major product. No yield was determined. ^{1}H NMR (benzene-d_6): δ = 0.40 (s, 12H, $(CH_3)_2Si$), 1.09 (s, 9H, Ta-CH_3), 4.89 (d, 4H, Cp-*H*, J = 2.8), 6.29 (t, 2H, Cp-*H*, J = 2.8).

(*n*-$Bu_3Sn)_2$[(1,2-$SiMe_2)_2(C_5H_3)_2$] ((*n*-$Bu_3Sn)_2$Rp). In the dry box a 100 mL round bottom flask equipped with stir bar was charged with Li_2Rp (1.82 g, 5.53 mmol) and diethyl ether (50 mL). While stirring rapidly, *n*-Bu_3SnCl (3.0 mL, 11.1 mmol, 2 equiv) was slowly added dropwise via syringe. After the addition was complete, a fine swivel frit assembly was attached. After 96 hr stirring at 25°C, a viscous orange solution was filtered away from a white solid. The solid was washed with recycled solvent (3 x 30 mL) and then solvent was removed *in vacuo* to provide an orange oil in the collection flask. No yield determined. ^{1}H NMR (benzene-d_6): δ = 0.38 (s, 12 *H*, $(CH_3)_2Si$), 0.46-1.71 (*n*-Bu_3Sn, overlapping multiplets), 6.49 (s, 2H, Cp-*H*), 6.85 (s, 4H, Cp-*H*).

[(1,2-$SiMe_2)_2$(4-$CHMe_2$-C_5H_3)(C_5H_4)] and [(1,2-$SiMe_2)_2$(3-$CHMe_2$-C_5H_3)(C_5H_4)]. (iPrRpH_2). A 500 mL round bottom flask equipped with stir bar was charged with Li_2iPrSp (10.37 g, 42.81 mmol) and a fine swivel frit assembly was attached. On the vacuum line, 300 mL THF was added via cannula transfer. At -78°C, Me_2SiCl_2 (5.2 mL, 42.8 mmol) was added by vacuum transfer and the pale yellow reaction mixture was allowed to warm slowly to 25°C. The reaction mixture was stirred for 20 hr, and then the THF was removed *in vacuo*. Petroleum ether (150 mL) was added via cannula transfer, and the resulting yellow solution was filtered away from the white solid. The solid was washed with petroleum ether (3 x 50 mL) and then solvent was removed *in vacuo* to afford iPrRpH_2 as a pale yellow oil; 9.08g (74.0%).

Li_2[(1,2-$SiMe_2)_2$(4-$CHMe_2$-C_5H_2)(C_5H_3)] and Li_2[(1,2-$SiMe_2)_2$(3-$CHMe_2$-C_5H_2)(C_5H_3)]. (Li_2iPrRp). A 250 mL round-bottom flask equipped with stir bar was charged with iPrRpH_2 (3.88 g, 13.54 mmol) and a medium swivel frit assembly was attached. On the vacuum line, 125 mL Et_2O was added via cannula transfer. At 0°C, 1.6 M *n*-BuLi (18.6 mL, 29.8 mmol) solution was added via syringe against an Ar counterflow. The reaction mixture was allowed to warm slowly to 25°C. Upon stirring a white precipitate crashed out of the yellow solution. The reaction mixture was stirred for 40 hr, and then the yellow

supernatent was filtered away from the white solid. The white solid was washed with Et_2O (2 x 50 mL), and then the Et_2O was removed *in vacuo*. Petroleum ether (150 mL) was added to the apparatus via cannula transfer, and the white solid was washed with petroleum ether (2 x 50 mL). Petroleum ether was removed *in vacuo* and the white solid was dried under high vacuum for 4 hr affording Li_2iPrRp; 4.37g (86.8%). Both isomers are isolated in a 3 : 2 ratio. Major isomer ^{1}H NMR (THF-d_8): δ = 0.19 (s, 12H, $(CH_3)_2Si$), 1.12 (t, 6H, $((CH_3CH_2)_2O)$, 1.20 (d, 6H, $(CH_3)_2CH$, 6.4 Hz), 3.13 (s, 1H, $(CH_3)_2CH$, 8.3 Hz), 3.39 (q, 4H, $((CH_3CH_2)_2O)$, 5.95 - 6.20 (overlapping resonances, Cp-*H*). Minor isomer ^{1}H NMR (THF-d_8): δ = 0.27 (s, 12H, $(CH_3)_2Si$), 1.12 (t, 6H, $((CH_3CH_2)_2O)$, 1.20 (d, 6H, $(CH_3)_2CH$, 6.4 Hz), 2.89 (s, 1H, $(CH_3)_2CH$), 3.39 (q, 4H, $((CH_3CH_2)_2O)$, 5.95 - 6.20 (overlapping resonances, Cp-*H*).

[(1,2-SiMe$_2$)$_2$(4-CMe$_3$-C$_5$H$_3$)(C$_5$H$_4$)] (7). (tBuRpH$_2$). A 500 mL round bottom flask equipped with stir bar was charged with Li_2tBuSp (4.55 g, 17.76 mmol) and a fine swivel frit assembly was attached. On the vacuum line, 250 mL THF was added via cannula transfer. At -78°C, Me_2SiCl_2 (2.2 mL, 17.76 mmol) was added by vacuum transfer and the yellow reaction mixture was allowed to warm slowly to 25°C. The reaction mixture was stirred for 20 hr, and then the THF was removed *in vacuo*. Petroleum ether (150 mL) was added via cannula transfer, and the resulting yellow solution was filtered away from the white solid. The solid was washed with petroleum ether (4 x 50 mL) and then solvent was removed *in vacuo* leaving an orange-yellow oil. Under an Ar counterflow the collection flask was transferred to a Kügelrohr assembly and then the orange-yellow oil was Kügelrohr distilled at 100°C and <1 torr yielding **7** as a pale yellow-white waxy solid; 2.68 g (50.2%).

Li$_2$[(1,2-SiMe$_2$)$_2$(4-CMe$_3$-C$_5$H$_2$)(C$_5$H$_3$)] (8). (Li$_2$tBuRp). A 250 mL round-bottom flask equipped with stir bar was charged with $tBuRpH_2$ (3.32 g, 11.05 mmol) and a medium swivel frit assembly was attached. On the vacuum line, 100 mL Et_2O was added via cannula transfer. At 0°C, 1.6 M *n*-BuLi (15.2 mL, 24.3 mmol) solution was added via syringe against an Ar counterflow. The reaction mixture was allowed to warm slowly to 25°C. Upon stirring a white precipitate crashed out of the yellow solution. The reaction mixture was stirred for 48 hr, and then the yellow supernatent was filtered away from the white solid. The white solid was washed with Et_2O (4 x 50 mL), and then the Et_2O was removed

in vacuo. Petroleum ether (75 mL) was added to the apparatus via cannula transfer, and the white solid was washed with petroleum ether (2 x 50 mL). Petroleum ether was removed *in vacuo* and the white solid was dried under high vacuum for 4 hr affording **8** as a Et_2O adduct; 1.63 g (46.9%). ^1H NMR (THF-d_8): δ = 0.19 (s, 12H, $(CH_3)_2Si$), 1.12 (t, 6H, $((CH_3CH_2)_2O)$, 1.26 (s, 9H, $(CH_3)_3C$), 3.39 (q, 4H, $((CH_3CH_2)_2O)$, 6.03 (t, 1H, Cp-*H*), 6.11 (s, 2H, Cp-*H*), 6.14 (d, 2H, Cp-*H*).

[(1,2-$SiMe_2$)$_2$(4-CMe_3-C_5H_2)(C_5H_3)]$ZrCl_2$ (9). (tBuRpZrCl_2). A 25 mL round bottom flask equipped with stir bar was charged with **8** (282 mg, 0.726 mmol) and $ZrCl_4$ (169 mg, 1 equiv) and a fine swivel frit assembly was attached. On the vacuum line, 15 mL toluene was added by vacuum transfer at -78°C. The cold bath was removed to allow the solution to slowly warm to 25°C. After 18.5 hr, a yellow-orange solution was filtered away from a white solid. The solid was washed with toluene (3 x 10 mL) and solvent removed *in vacuo*. Petroleum ether (15 mL) was added by vacuum transfer, the reaction mixture stirred briefly, and solvent removed *in vacuo* to provide **9** as a pale yellow solid; 107 mg (32.0%). ^1H NMR (benzene-d_6): δ = 0.29 (s, 6H, $(CH_3)_2Si$), 0.52 (s, 6H, $(CH_3)_2Si$), 1.45 (s, 9H, $(CH_3)_3C$), 6.24 (t, 1H, Cp-*H*, 2.8 Hz), 6.82 (d, 2H, Cp-*H*, 1.4 Hz), 6.83 (d, 2H, Cp-*H*, 1.4 Hz). ^{13}C NMR (benzene-d_6): -4.33, 2.51 ($(CH_3)_2Si$), 31.99 ($(CH_3)_3C$), 33.27 ($(CH_3)_3C$), 114.67, 114.91, 115.60, 136.91, 140.30, 144.16 (Cp).

Propylene Polymerization Using 9 as catalyst (neat olefin, 0°C). A 6 oz. high pressure glass reactor equipped with a septum port, large stir bar, and pressure gauge (0-200 psig) was charged with MAO (500 mg, 8.6 mmol). The reactor was connected to a propylene line (120 psig), and the vessel purged with propylene for approximately 10 minutes. Next the vessel was placed in a 0°C ice water bath and propylene (~25 mL, ~0.6 mol) condensed inside. The propylene inlet valve was then closed, and a solution containing the zirconocene catalyst (2.5 mg, 0.0054 mmol) in toluene (0.25 mL) was added to the vigorously stirred MAO/ propylene suspension via a 1 mL Hamilton gas tight syringe through the septum. (The addition requires significant force since the pressure in the reactor is ~95 psig.) The reaction mixture was stirred for 25 minutes at 0°C, and then excess propylene was vented through an oil bubbler via a needle in the septum port. In the fume hood, the top was removed from the glass vessel and the reaction quenched with methanol (6 mL) and dilute methanol-HCl (10 mL. 3 :1, v/v). Addition of methanol (50 mL) and 20 minutes of stirring afforded a white

solid that was dried at high vacuum at 60°C for 3 hr. Activity: 769 g polymer/g catalyst/hr. Polymer tacticity was determined by ^{13}C NMR, using pentad level analysis as described by Bovey.[47] A small amount of the polymer sample was dissolved in a 9 : 7 (v/v) mixture of 1,2-dichlorobenzene and benzene-d_6, and ^{13}C NMR data was acquired at 306 K.

[(1,2-SiMe$_2$)$_2$(4-CMe$_3$-C$_5$H$_2$)(C$_5$H$_3$)]Ta(CH$_2$)CH$_3$ (10). (tBuRpTa(CH$_2$)CH$_3$). A 250 mL round bottom flask equipped with stir bar was charged with **8** (626 mg, 1.61 mmol). A 100 mL addition funnel with two Kontes was charged with $TaCl_2Me_3$ (478 mg, 1 equiv) and a small stir bar. The addition funnel was attached to the top of the reaction flask and a 180° needle valve was placed on top of the addition funnel. On the vacuum line, 125 mL THF was added to the reaction flask by vacuum transfer at -78°C and 25 mL THF was transferred to the addition funnel. While maintaining the reaction solution at -78°C, the apparatus was backfilled with Ar and left exposed to a mercury bubbler during the slow, dropwise addition of the $TaCl_2Me_3$ solution to the ligand solution. After 30 minutes, addition was complete and the reaction solution was orange in color. The cold bath (in a recrystallizing dish) was left intact to allow the solution to slowly warm to 25°C. After 1 day of stirring, THF was removed *in vacuo* and petroleum ether (75 mL) was added and the reaction mixture stirred briefly, and solvent then removed *in vacuo*. Inside the dry box a swivel frit assembly was attached to the reaction flask. On the vacuum line, toluene was added by vacuum transfer to provide a brown solution and off-white precipitate. The supernatent was filtered away from the solid and then the solid was washed with toluene (4 x 50 mL) and solvent removed *in vacuo*. Petroleum ether (50 mL) was added by vacuum transfer, the reaction mixture stirred briefly, and solvent removed *in vacuo* to provide a brown thick oil. In the dry box, the reaction product was dissolved in petroleum ether (4 mL) and cooled slowly to provide a tan precipitate. The supernatent was removed, the solid washed with chilled petroleum ether (2 x 1 mL), and then the solid was dried under high vacuum. **10** was isolated as a tan powder; 30 mg (3.7%). ^1H NMR (benzene-d_6): δ = 0.19 (s, 3H, (CH_3)$_2$Si), 0.21 (s, 3H, (CH_3)$_2$Si), 0.27 (s, 3H, Ta-CH_3), 0.31 (s, 3H, (CH_3)$_2$Si), 0.35 (s, 3H, (CH_3)$_2$Si), 1.41 (s, 9H, (CH_3)$_3$C), 5.50 (t, 1H, Cp-*H*, 2.4 Hz), 5.85 (s, 1H, Cp-*H*), 5.90 (d, 1H, Cp-*H*, 1.5 Hz), 6.46 (d, 1H, Cp-*H*, 1.8 Hz), 6.53 (s, 1H, Cp-*H*), 9.43 (d, 1H, Ta=CH_2, 9.3 Hz), 9.74 (d, 1H, Ta=CH_2, 9.3 Hz).

[(1,2-SiMe$_2$)$_2$(4-CMe$_3$-C$_5$H$_2$)(C$_5$H$_3$)](Ta(CH$_3$)$_3$Cl)$_2$. (tBuRp(TaMe$_3$Cl)$_2$)]. ^{1}H NMR (benzene-d_6): δ = 0.43 (s, 6H, (C*H*$_3$)$_2$Si), 0.47 (s, 6H, (C*H*$_3$)$_2$Si), 1.06 (s, 9H, Ta-C*H*$_3$), 1.09 (s, 9H, Ta-C*H*$_3$), 1.28 (s, 9H, (C*H*$_3$)$_3$C), 5.87 (d, 2H, Cp-*H*, 3.0 Hz), 6.24 (t, 1H, Cp-*H*), 6.42 (s, 2H, Cp-*H*).

[(1,2-SiMe$_2$)$_2${η^5-C$_5$H$_2$-4-CMe$_3$}{η^2-C$_5$H-3,5-(CHMe$_2$)$_2$}]Ta(CH$_3$)$_3$ (11). (tBuThpTaMe$_3$). All synthetic manipulations were carried out in the absence of ambient light. A 250 mL round bottom flask equipped with stir bar was charged with K$_2$tBuThp (1.05 g, 2.27 mmol) and a medium swivel frit assembly was attached. A 50 mL round bottom flask equipped with stir bar was charged with TaCl$_2$Me$_3$ (674 mg, 2.27 mmol) and a 180° needle valve was attached. On the vacuum line, Et$_2$O (250 mL) was added to the swivel frit assembly by vacuum transfer to provide an off-white slurry, and Et$_2$O (25 mL) was added to the latter assembly by vacuum transfer to provide a bright yellow solution. The K$_2$tBuThp slurry was cooled to -78°C and the solution of TaCl$_2$Me$_3$ was slowly added via cannula transfer. After 15 minutes of stirring at -78°C, the dry ice/acetone bath was replaced with a 0°C ice water bath and the reaction apparatus was covered in foil to exclude light. The reaction mixture was stirred for 3 hr, and then an orange solution was filtered away from an off-white solid. The solid was washed with Et$_2$O (3 x 25 mL), and solvent was removed *in vacuo* to provide **11** as an orange residue; 354.3 mg (25.6%). ^{1}H NMR (benzene-d_6): δ = 0.38 (s, 6H, (C*H*$_3$)$_2$Si), 0.48 (s, 6H, (C*H*$_3$)$_2$Si), 1.12 (s, 9H, (C*H*$_3$)$_3$C), 1.16 (d, 3H, (C*H*$_3$)$_2$CH, 6.6 Hz), 1.38 (d, 6H, (C*H*$_3$)$_2$CH, 6.9 Hz), 1.49 (s, 9H, Ta-C*H*$_3$), 2.72 (m, 2H, (CH$_3$)$_2$C*H*), 6.6 Hz), 6.51 (s, 1H, Cp-*H*), 6.59 (s, 1H, Cp-*H*). ^{13}C NMR (benzene-d_6): δ = -28.52 (Ta-CH$_3$), -0.60, 5.24 ((CH$_3$)$_2$Si), 21.61, 25.39, 31.63 ((CH$_3$)$_2$CH), 31.93 ((CH$_3$)$_3$C), 32.67 ((CH$_3$)$_3$*C*), 73.99, 74.05, 75.83, 75.88 (*C*$_5$H$_1$), 102.36, 118.32, 123.41, 129.63 (*C*$_5$H$_2$).

[(1,2-SiMe$_2$)$_2${η^5-C$_5$H$_2$-4-CMe$_3$}{η^5-C$_5$H-3,5-(CHMe$_2$)$_2$}]Ta(CH$_2$)CH$_3$ (12). (tBuThpTa(CH$_2$)CH$_3$). A 250 mL round bottom flask equipped with stir bar was charged with K$_2$tBuThp (2.68 g, 5.82 mmol) and TaCl$_2$Me$_3$ (1.73 g, 5.82 mmol) and a 180° needle valve was attached. On the vacuum line, 125 mL toluene was added to the reaction flask by vacuum transfer at -78°C. The dry ice/acetone bath cooling bath was removed and the reaction mixture was allowed to warm slowly to 25°C. The reaction mixture was stirred for 72 hr, and then the solvent was removed *in vacuo*. In the dry box, Et$_2$O (150 mL) was added to the reaction

mixture and then the contents were filtered through a bed of Celite and washed with Et_2O (5 x 25 mL). A 250 mL round bottom flask equipped with stir bar was charged with the brown mother liquor and a fine swivel frit assembly was attached. On the vacuum line the Et_2O was removed *in vacuo* and then 50 mL pentane was added by vacuum transfer. A brown supernatent was filtered away from a yellow precipitate, and the solid was washed with pentane (2 x 25 mL). Solvent was removed *in vacuo* to provide **12** as a yellow solid; 723 mg (20.9%). ^{1}H NMR (benzene-d_6): δ = 0.24 (s, 3H, $(CH_3)_2Si$), 0.36 (s, 3H, $(CH_3)_2Si$), 0.44 (s, 3H, $(CH_3)_2Si$), 0.45 (s, 3H, Ta-CH_3), 0.51 (s, 3H, $(CH_3)_2Si$), 1.10 (d, 3H, $(CH_3)_2CH$, 7.0 Hz), 1.12 (d, 3H, $(CH_3)_2CH$, 5.9 Hz), 1.16 (d, 3H, $(CH_3)_2CH$, 6.6 Hz), 1.39 (d, 3H, $(CH_3)_2CH$, 6.6 Hz), 1.49 (s, 9H, $(CH_3)_3C$), 2.55 (m, 1H, $(CH_3)_2CH$, 5.4 Hz), 3.38 (m, 1H, $(CH_3)_2CH$, 5.7 Hz), 5.91 (s, 2H, Cp-*H*), 6.57 (s, 1H, Cp-*H*), 9.30 (d, 1H, Ta=CH_2, 9.8 Hz), 9.58 (d, 1H, Ta=CH_2, 9.8 Hz). ^{13}C NMR (benzene-d_6): δ = -2.01 (Ta-CH_3), -1.82, -1.40, 3.78, 4.00 ($(CH_3)_2Si$), 21.61, 22.20, 28.04, 28.90, 30.18, 30.64 ($(CH_3)_2CH$), 31.16 ($(CH_3)_3C$), 33.05 ($(CH_3)_3C$), 102.71, 118.67, 123.74 (C_5H_3), 211.26 (Ta=CH_2).

[(1,2-SiMe$_2$)$_2${η^5-C$_5$H$_2$-4-CMe$_3$}{η^5-C$_5$H-3,5-(CHMe$_2$)$_2$}]Ta(η^2-CH$_2$=CH$_2$)H (13). (tBuThpTa(η^2-CH$_2$=CH$_2$)H). A 25 mL round bottom flask equipped with stir bar was charged with **12** (121 mg, 0.203 mmol) and a reflux condensor and 180° needle valve were attached. On the vacuum line, 15 mL toluene was added to the reaction flask by vacuum transfer providing a yellow-brown solution. The apparatus was backfilled with Ar and then heated to reflux. After 72 hr at reflux, the toluene was removed *in vacuo*, pentane (10 mL) was added by vacuum transfer and then removed *in vacuo* to provide a brown solid in 96.5% yield (116 mg). ^{1}H NMR (benzene-d_6): δ = -2.06 (s, 1 H, Ta-*H*), 0.43 (s, 3H, $(CH_3)_2Si$), 0.55 (s, 3H, $(CH_3)_2Si$), 0.63 (s, 3H, $(CH_3)_2Si$), 0.68 (s, 3H, $(CH_3)_2Si$), 0.78 (d, 3H, $(CH_3)_2CH$, 6.6 Hz), 0.97 (s, 9H, $(CH_3)_3C$), 1.10 (d, 3H, $(CH_3)_2CH$, 7.3 Hz), 1.11 (d, 3H, $(CH_3)_2CH$, 7.2 Hz), 1.37 (d, 3H, $(CH_3)_2CH$, 6.6 Hz), 2.97 (m, 1H, $(CH_3)_2CH$, 6.9 Hz), 3.40 (m, 1H, $(CH_3)_2CH$, 6.5 Hz), 4.13 (s, 1H, Cp-*H*), 5.81 (s, 1H, Cp-*H*), 6.35 (s, 1H, Cp-*H*). ^{13}C NMR (benzene-d_6): δ = -1.53, -0.78, 5.00, 6.14 ($(CH_3)_2Si$), 21.75, 23.08 (CH_2=CH_2), 28.67, 29.18, 29.63, 30.44, 31.93, 33.04, 30.83 ($(CH_3)_2CH$, $(CH_3)_3C$), 98.36, 110.66, 111.18, 137.72 (Cp).

[(1,2-SiMe$_2$)$_2${η^5-C$_5$H$_2$-4-CMe$_3$}{η^5-C$_5$H-3,5-(CHMe$_2$)$_2$}]Ta(η^2-CH$_2$=CH(CH$_3$))H (14a). (tBuThpTa(η^2-CH$_2$=CHMe)H). A J-Young NMR tube was charged with

13 (10.8 mg, 0.0182 mmol) and dissolved in benzene-d_6 to provide a red-brown solution. On the vacuum line, the solution was frozen at -196°C and the NMR tube was degassed. Propylene (0.182 mmol) was condensed into the NMR tube at this temperature, the tube was closed and warmed to 25°C. After 19 days at 25°C, a 10 : 1 ratio of **14a** : **13** was observed. ^{1}H NMR (benzene-d_6): δ = -1.86 (s, 1 H, Ta-*H*), -0.27 (br s, 1H, CH_2=C*H*(CH_3)), -0.19 (m, 2H, CH_2=CH(CH_3)), 0.42 (s, 3H, (CH_3)$_2$Si), 0.54 (s, 3H, (CH_3)$_2$Si), 0.61 (s, 3H, (CH_3)$_2$Si), 0.66 (s, 3H, (CH_3)$_2$Si), 0.97 (d, 3H, (CH_3)$_2$CH, 6.8 Hz), 1.01 (s, 9H, (CH_3)$_3$C), 1.11 (d, 3H, (CH_3)$_2$CH, 6.9 Hz), 1.16 (d, 3H, (CH_3)$_2$CH, 7.1 Hz), 1.35 (d, 3H, (CH_3)$_2$CH, 6.6 Hz), 2.32 (d, 3H, CH_2=CH(CH_3), 6.6 Hz), 3.10 (m, 1H, (CH_3)$_2$C*H*, 6.3 Hz), 3.38 (m, 1H, (CH_3)$_2$C*H*, 7.0 Hz), 4.19 (s, 1H, Cp-*H*), 5.55 (s, 1H, Cp-*H*), 6.32 (s, 1H, Cp-*H*). ^{13}C NMR (benzene-d_6): δ = -1.56, -0.91, 3.94, 4.17 ((*C*H_3)$_2$Si), 13.95, 21.77, 21.91 (CH_2=CH(*C*H_3)), 23.10, 28.68, 29.19, 29.40, 29.51, 30.67, 30.83, 32.03 ((*C*H_3)$_2$CH, (*C*H_3)$_3$C), 98.32, 110.14, 112.65, 126.66, 139.34, 147.42 (Cp).

[(1,2-SiMe$_2$)$_2${η^5-C$_5$H$_2$-4-C(CH$_3$)$_3$}{η^5-C$_5$H-3,5-(CHMe$_2$)$_2$}]Ta(η^2-CH$_2$=CH(C$_6$H$_5$))H (14b). (tBuThpTa(η^2-CH$_2$=CHPh)H). A J-Young NMR tube was charged with **13** (20.0 mg, 0.0337 mmol) and dissolved in benzene-d_6 to provide a red-brown solution. A small amount of a styrene/benzene-d_6 solution was added (0.4044 mmol, 12 equiv) and reaction was monitored at 25°C by ^{1}H NMR spectroscopy. After 79 days at 25°C, a 10 : 1 ratio of **14b** : **13** is observed. ^{1}H NMR (benzene-d_6): δ = -1.10 (s, 1 H, Ta-*H*), 0.35 (s, 3H, (CH_3)$_2$Si), 0.48 (s, 3H, (CH_3)$_2$Si), 0.56 (s, 3H, (CH_3)$_2$Si), 0.58 (s, 3H, (CH_3)$_2$Si), 0.60 (d, 3H, (CH_3)$_2$CH, 6.7 Hz), 0.95 (d, 3H, (CH_3)$_2$CH, 7.0 Hz), 1.08 (s, 9H, (CH_3)$_3$C), 1.14 (d, 3H, (CH_3)$_2$CH, 7.1 Hz), 1.18 (d, 3H, (CH_3)$_2$CH, 6.7 Hz), 1.29 (m, 2H overlapping, CH_2=CHPh), 2.80 (t, 1H, CH_2=C*H*Ph, 12.5 Hz), 3.19 (m, 2H overlapping, (CH_3)$_2$C*H*, 7.2 Hz), 3.63 (s, 1H, Cp-*H*), 5.62 (s, 1H, Cp-*H*), 6.43 (s, 1H, Cp-*H*), 6.82 (t, 1H, C_6H_5, *para*, 7.1 Hz), 7.23 (t, 2H, C_6H_5, *meta*, 8.0 Hz), 7.47 (d, 2H, C_6H_5, *ortho*, 7.9 Hz). ^{13}C NMR (benzene-d_6): δ = -1.84, -0.71, 3.89, 8.82 ((*C*H_3)$_2$Si), 21.29, 22.40 (CH_2=*C*HPh), 28.91, 29.42, 29.80, 31.26, 32.26, 33.13 ((*C*H_3)$_2$CH), 30.67 ((*C*H_3)$_3$C), 78.67, 81.34, 87.07, 102.93, 110.45, 112.08, 121.52, 126.31, *2 not located* (Cp), *not located* ((*C*H_3)$_3$C), 142.41, 148.40, 156.48, *1 not located* (C_6H_5).

References

1. Brintzinger, H.H.; Fischer, D.; Mülhaupt, R.; Rieger, B.; Waymouth, R.M. *Angew. Chem. Int. Ed. Engl.* **1995**, *34*, 1143.

2. (a) Kaminsky, W.; Kulper, K.; Brintzinger, H.H.; Wild, F.W.P. *Angew. Chem. Int. Ed. Engl.* **1985**, *24*, 507. (b) Roll, W.; Brintzinger, H.H.; Rieger, B.; Zolk, R. *Angew. Chem. Int. Ed. Engl.* **1990**, *29*, 279. (c) Wiesenfeldt, H.; Reinmuth, A.; Barsties, X.X.; Evertz, K.; Brintzinger, H.H. *J. Organomet. Chem.* **1989**, *369*, 359.

3. Ewen, J.A.; Jones, R.L.; Razavi, A.; Ferrara, J.D. *J. Am. Chem. Soc.*, **1988**, *110*, 6255.

4. Herzog, T.A.; Zubris, D.L.; Bercaw, J.E. *J. Am. Chem. Soc.*, **1996**, *118*, 11988.

5. (a) Ewen, J.A. *J. Am. Chem. Soc.* **1984**, *106*, 6355. (b) Grassi, A.; Zambelli, A.; Resconi, L.; Albizzati, E.; Mazzocchi, R. *Macromolecules* **1988**, *21*, 617.

6. Pino, P.; Galimberti, M. *J. Organomet. Chem.*, **1989**, *370*, 1.

7. Gilchrist, J.H.; Bercaw, J.E. *J. Am. Chem. Soc.*, **1996**, *118*, 12021.

8. a) Chernega, A.N.; Green, M.L.H.; Suárez, A.G. *Can. J. Chem.* **1995**, *73*, 1157. b) Bailey, N.J.; Cooper, J.A.; Gailus, H.; Green, M.L.H.; James, J.T.; Leech, M.A. *J. Chem. Soc. Dalton Trans.* **1997**, 3579. c) Bailey, N.J.; Green, M.L.H.; Leech, M.A.; Saunders, J.F.; Tidswell, H.M. *J. Organomet. Chem.* **1997**, *538*, 111. d) Conway, S.L; Doerrer, L.H.; Green, M.L.H.; Leech, M.A. *Organometallics* **2000**, *19*, 630.

9. Antinolo, A.; Martinez-Ripoll, M.; Mugnier, Y.; Otero, A.; Prashar, S.; Rodriguez, A.M. *Organometallics* **1996**, *15*, 3241.

10. Shin, J.H.; Parkin, G. *Chem. Comm.* **1999**, 887.

11. Schrock, R.R.; Sharp, P.R. *J. Am. Chem. Soc.* **1978**, *100*, 2389.

12. Parkin, G.; Bunel, E.; Burger, B.J.; Trimmer, M.S.; Asselt, A.V.; Bercaw, J.E. *J. Mol. Cat.*, **1987**, *41*, 21.

13. Chirik, P.J. *Ph.D. Thesis* California Institute of Technology, **2000**.

14. Chirik, P.J.; Bercaw, J.E., *unpublished results*.

15. A more efficient synthesis of **1** has been developed elsewhere; addition of a THF solution of Li_2Sp to a solution of $TaCl_2Me_3$ at -78°C permits isolation of **1** in 50-60% yield. Piers, W.E.; Cook, K.S.C., *personal communication*.

16. (a) Klazinga, A.H.; Teuben, J.H. *J. Organomet. Chem.* **1980**, *194*, 309. (b) Burger, B.J.; Santarsiero, B.D.; Trimmer, M.S.; Bercaw, J.E. *J. Am. Chem. Soc.* **1988**, *110*, 3134.

17. Doherty, N.M.; Bercaw, J.E. *J. Am. Chem. Soc.* **1985**, *107*, 2670.

18. Klazinga, A.H.; Teuben, J.H. *J. Organomet. Chem.* **1978**, *157*, 413.

19. Gibson, V.C.; Bercaw, J.E.; Bruton, W.J. Jr.; Sanner, R.D. *Organometallics* **1986**, *5*, 976.

20. Chirik, P.J.; Zubris, D.L.; Ackerman, L.J.; Bercaw, J.E. *manuscipt in preparation*.

21. Benson, S.W. *Thermochemical Kinetics* 2nd Ed.; Wiley and Sons, New York, 1976.

22. Burger, B.J.; Santarsiero, B.D.; Trimmer, M.S.; Bercaw, J.E. *J. Am. Chem. Soc.* **1988,** *110*, 3134.

23. Dictionary of Inorganic Compounds.

24. Fowles, G.W.A.; Tidmarsh, D.J.; Walton, R.A. *Inorg. Chem.* **1969**, *8*, 631.

25. Cotton, F.A.; Duraj, S.A.; Roth, R.J. *Inorg. Chem.* **1984**, *23*, 4046.

26. Fowles, G.W.A.; Tidmarsh, D.J.; Walton, R.A. *Inorg. Chem.* **1969**, *8*, 631.

27. Van Baalen, A.; Groenenboom, C.J.; De Liefde Meijer, H.J. *J. Organomet. Chem.* **1974**, *74*, 245.

28. $TaCl_4(CH_3CN)_2$ was prepared by reduction of $TaCl_5$ by Al in CH_3CN solvent for 96 hours at 25°C. $TaCl_4(THF)_2$ was isolated as a viscous red-brown oil, as described previously.

29. Siemeling, U.; Jutzi, P.; Neumann, B.; Stammler, H.G.; Hursthouse, M.B. *Organometallics* **1992**, *11*, 1328.

30. Cano, A.; Cuenca, T.; Gómez-Sal, P.; Royo, B.; Royo, P. *Organometallics* **1994**, *13*, 1688.

31. Bulls, A.R. *Ph.D. Thesis* California Institute of Technology, **1988**.

32. Mengele, W.; Diebold, J.; Troll, C.; Röll, W.; Brintzinger, H.-H. *Organometallics* **1993**, *12*, 1931.

33. Miyake, S.; Bercaw, J.E. *J. Mol. Cat. A Chem.* **1998**, *128*, 29.

34. Veghini, D.; Henling, L.M.; Burkhardt, T.J.; Bercaw, J.E. *J. Am. Chem. Soc.*, **1999**, *121*, 564.

35. Zubris, D.L., Chapter 1.

36. Herzog, T.A. *Ph.D. Thesis* California Institute of Technology, **1996**.

37. Coughlin, E.B. *Ph.D. Thesis* California Institute of Technology, **1994**.

38. Chirik, P.J.; Zubris, D.L.; Henling, L.M.; Bercaw, J.E. *manuscript in preparation.*

39. Lucas, C.R.; Green, M.L.H.; Forder, R.A.; Prout, K. *J. Chem. Soc. Chem. Comm.* **1973**, 97.

40. Fisher, J.D.; Wei, M.-Y.; Willett, R.; Shapiro, P. J. *Organometallics*, **1994**, *13*, 3324.

41. Enantiomeric forms are not considered in the total isomer count.

42. Lowry, T.H.; Richardson, K.S. *Mechanism and Theory in Organic Chemistry* 3rd Ed.; Harper Collins, New York, 1987.

43. Burger, B. J.; Bercaw, J. E. *New Developments in the Synthesis, Manipulation, and Characterization of Organometallic Compounds*, **1987**; Vol. 357. ACS Symposium Series.

44. Marvich, R. H.; Brintzinger, H. H. *J. Am. Chem. Soc.* **1971**, *93*, 203.

45. Cowley, A. H.; Kemp, R. A. *Synth. React. Inorg. Metal-Org. Chem.* **1981**, *11*, 591.

46. Perrin, D. D.; Armagrego, W. L. F. *Purification of Laboratory Chemicals*, 3rd ed.; Pergamon Press: New York, NY, 1988.

47. Zambelli, A.; Locatelli, P.; Bajo, G.; Bovey, F. A. *Macromolecules* **1975**, *8*, 687.

Appendix A: GPC Data

GPC data for select polypropylene and polypentene samples that appear in Table 8 of Chapter 1. This data was collected with the assistance of Dr. Steve A. Cohen at BP Amoco Chemical.

Two of the samples contain a higher molecular weight component: "Samples 20391-050-4 and 20391-050-8 exhibited a long, low amplitude shoulder on the high mol.wt. side of the peaks. This shoulder was verified by a rerun of 050-8 and all four measurements were averaged for the reported data."

TEST: GPC___0630: GPC - POLYPROPYLENE / POLYETHYLENE

COMPONENT NAME	RESULT VALUE	UNITS

==========

Entry 9 = 20391-050-1

No. Avg. Mol. Wt.	16.0	1000 g/mol
Wt. Avg. Mol. Wt.	32.1	1000 g/mol
Z Avg. Mol. Wt.	51.9	1000 g/mol
Z+1 Avg. Mol. Wt.	75.0	1000 g/mol
Wt. Avg./No. Avg. (PDI)	2.0	
Std. Dev. (No. Avg.)	0.1	
Std. Dev. (Wt. Avg.)	0.0	
Std. Dev. (Z Avg.)	0.3	
Std. Dev. (Z+1 Avg.)	1.0	
Std. Dev. (Wt./No. Avg) - (PDI)	0.0	

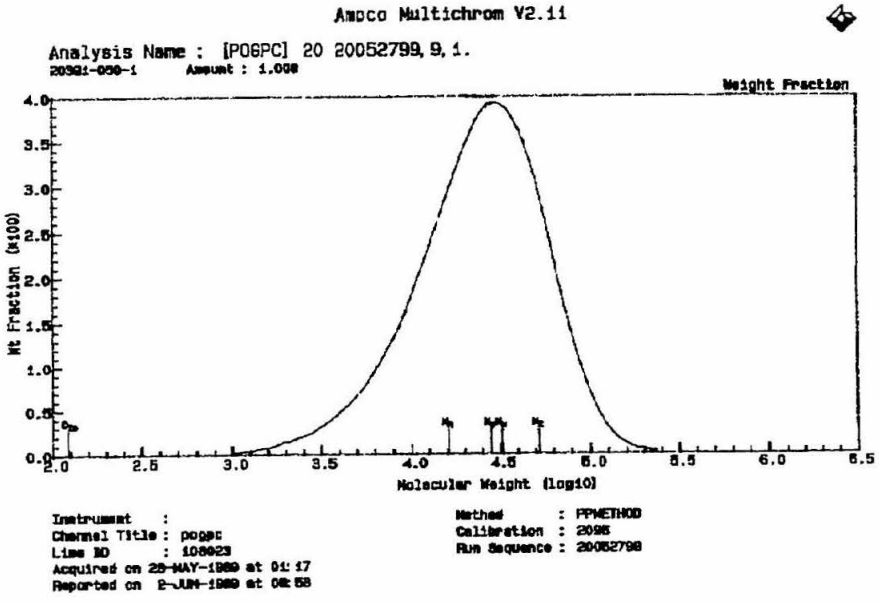

TEST: GPC___0630: GPC - POLYPROPYLENE / POLYETHYLENE

COMPONENT NAME	RESULT VALUE	UNITS
Entry 1 = 20391-050-2		
No. Avg. Mol. Wt.	86.0	1000 g/mol
Wt. Avg. Mol. Wt.	195	1000 g/mol
Z Avg. Mol. Wt.	356	1000 g/mol
Z+1 Avg. Mol. Wt.	562	1000 g/mol
Wt. Avg./No. Avg. (PDI)	2.3	
Std. Dev. (No. Avg.)	1.6	
Std. Dev. (Wt. Avg.)	0.4	
Std. Dev. (Z Avg.)	2.5	
Std. Dev. (Z+1 Avg.)	6.7	
Std. Dev. (Wt./No. Avg) - (PDI)	0.1	

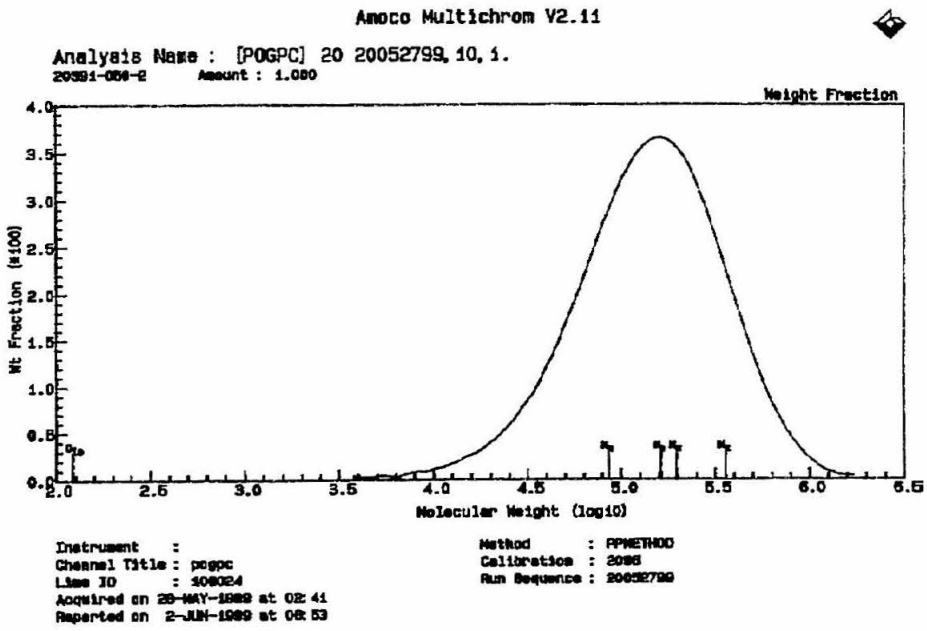

TEST: GPC___0630: GPC - POLYPROPYLENE / POLYETHYLENE

COMPONENT NAME	RESULT VALUE	UNITS
Entry 11 = 20391-050-3		
No. Avg. Mol. Wt.	3.9	1000 g/mol
Wt. Avg. Mol. Wt.	7.5	1000 g/mol
Z Avg. Mol. Wt.	12.0	1000 g/mol
Z+1 Avg. Mol. Wt.	16.9	1000 g/mol
Wt. Avg./No. Avg. (PDI)	1.9	
Std. Dev. (No. Avg.)	0.1	
Std. Dev. (Wt. Avg.)	0.0	
Std. Dev. (Z Avg.)	0.0	
Std. Dev. (Z+1 Avg.)	0.2	
Std. Dev. (Wt./No. Avg) - (PDI)	0.0	

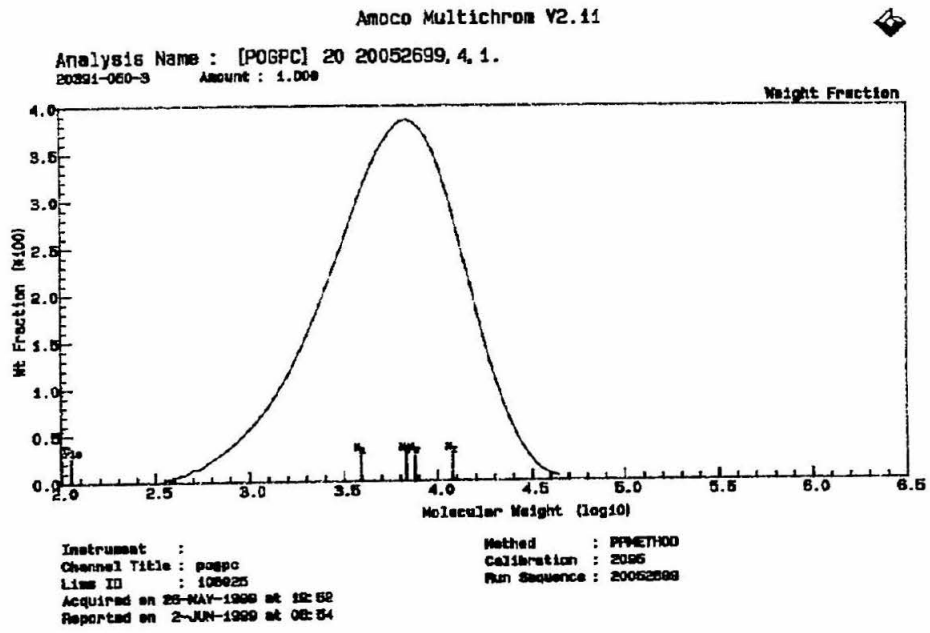

TEST: GPC___0630: GPC - POLYPROPYLENE / POLYETHYLENE

COMPONENT NAME	RESULT VALUE	UNITS
Entry 6 = 20391-050-4		
No. Avg. Mol. Wt.	9.3	1000 g/mol
Wt. Avg. Mol. Wt.	26.7	1000 g/mol
Z Avg. Mol. Wt.	133	1000 g/mol
Z+1 Avg. Mol. Wt.	501	1000 g/mol
Wt. Avg./No. Avg. (PDI)	2.9	
Std. Dev. (No. Avg.)	0.0	
Std. Dev. (Wt. Avg.)	0.1	
Std. Dev. (Z Avg.)	2.6	
Std. Dev. (Z+1 Avg.)	6.1	
Std. Dev. (Wt./No. Avg) - (PDI)	0.0	

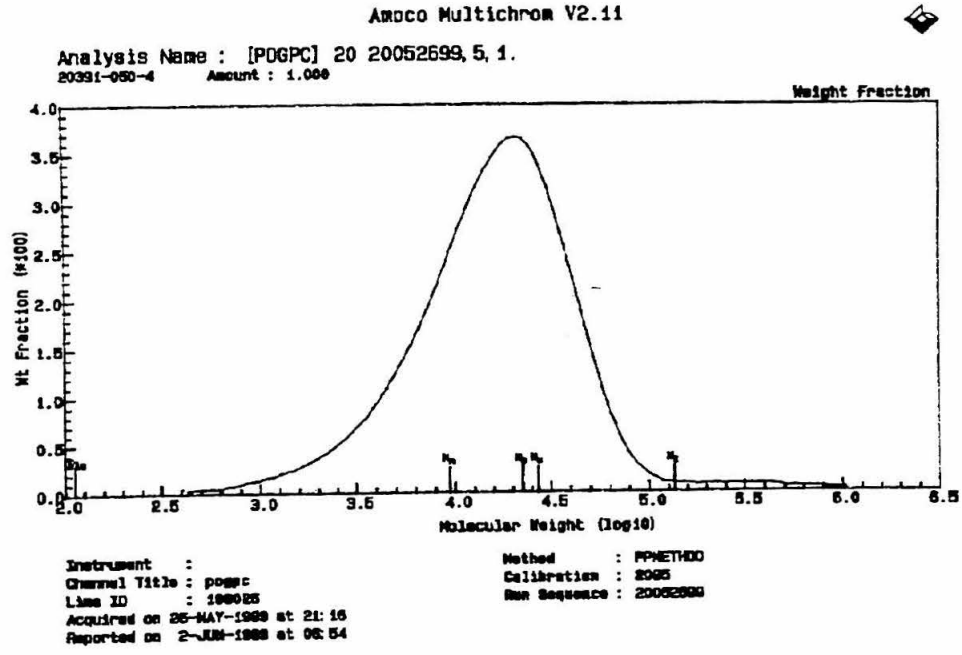

TEST: GPC___0630: GPC - POLYPROPYLENE / POLYETHYLENE

COMPONENT NAME	RESULT VALUE	UNITS

Entry 4 = 20391-050-5

No. Avg. Mol. Wt.	13.4	1000 g/mol
Wt. Avg. Mol. Wt.	34.0	1000 g/mol
Z Avg. Mol. Wt.	57.0	1000 g/mol
Z+1 Avg. Mol. Wt.	81.1	1000 g/mol
Wt. Avg./No. Avg. (PDI)	2.5	
Std. Dev. (No. Avg.)	0.6	
Std. Dev. (Wt. Avg.)	0.0	
Std. Dev. (Z Avg.)	0.4	
Std. Dev. (Z+1 Avg.)	1.0	
Std. Dev. (Wt./No. Avg) - (PDI)	0.1	

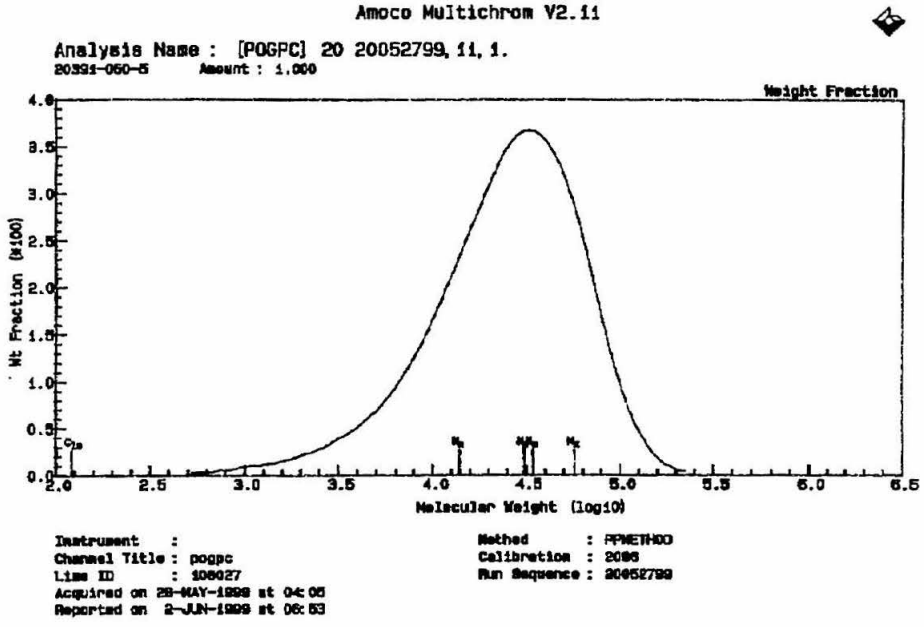

TEST: GPC___0630: GPC - POLYPROPYLENE / POLYETHYLENE

COMPONENT NAME	RESULT VALUE	UNITS

Entry 13 = 20391-050-6

No. Avg. Mol. Wt.	2.9	1000 g/mol
Wt. Avg. Mol. Wt.	5.5	1000 g/mol
Z Avg. Mol. Wt.	8.8	1000 g/mol
Z+1 Avg. Mol. Wt.	12.4	1000 g/mol
Wt. Avg./No. Avg. (PDI)	1.9	
Std. Dev. (No. Avg.)	0.1	
Std. Dev. (Wt. Avg.)	0.0	
Std. Dev. (Z Avg.)	0.2	
Std. Dev. (Z+1 Avg.)	0.5	
Std. Dev. (Wt./No. Avg) - (PDI)	0.1	

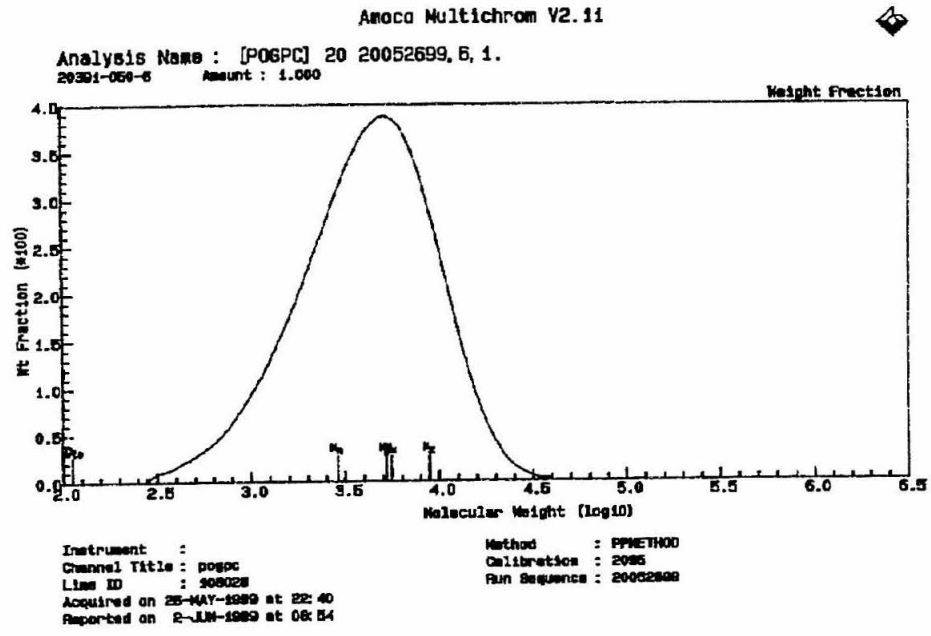

TEST: GPC___0630: GPC - POLYPROPYLENE / POLYETHYLENE

COMPONENT NAME	RESULT VALUE	UNITS

Entry 14 = 20391-050-7

No. Avg. Mol. Wt.	5.3	1000 g/mol
Wt. Avg. Mol. Wt.	10.5	1000 g/mol
Z Avg. Mol. Wt.	16.7	1000 g/mol
Z+1 Avg. Mol. Wt.	23.3	1000 g/mol
Wt. Avg./No. Avg. (PDI)	2.0	
Std. Dev. (No. Avg.)	0.2	
Std. Dev. (Wt. Avg.)	0.0	
Std. Dev. (Z Avg.)	0.2	
Std. Dev. (Z+1 Avg.)	0.5	
Std. Dev. (Wt./No. Avg) - (PDI)	0.1	

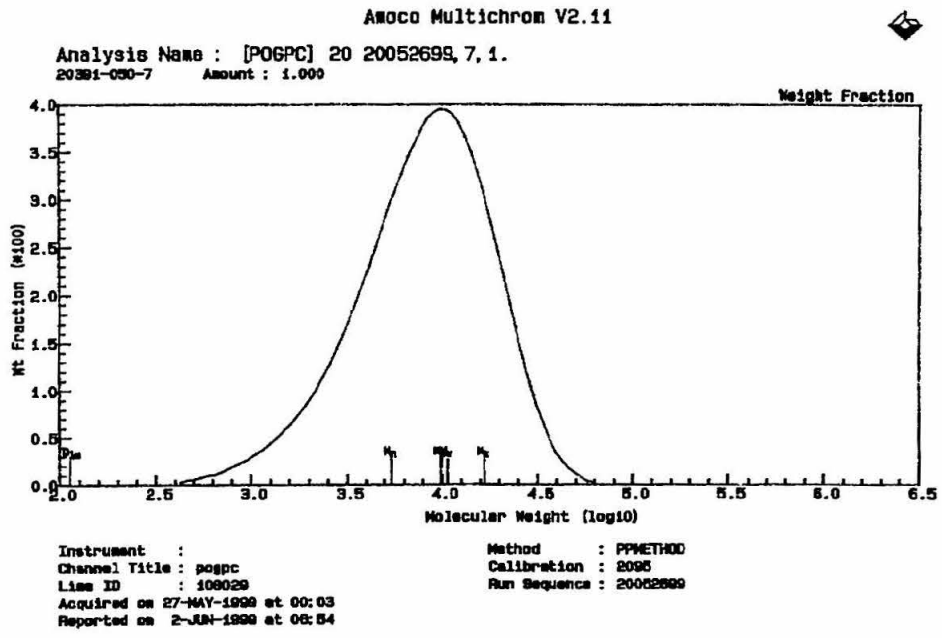

TEST: GPC___0630: GPC - POLYPROPYLENE / POLYETHYLENE

COMPONENT NAME	RESULT VALUE	UNITS
Entry 5 = 20391--050-8		
No. Avg. Mol. Wt.	4.5	1000 g/mol
Wt. Avg. Mol. Wt.	11.6	1000 g/mol
Z Avg. Mol. Wt.	69.0	1000 g/mol
Z+1 Avg. Mol. Wt.	285	1000 g/mol
Wt. Avg./No. Avg. (PDI)	2.6	
Std. Dev. (No. Avg.)	0.1	
Std. Dev. (Wt. Avg.)	0.3	
Std. Dev. (Z Avg.)	5.0	
Std. Dev. (Z+1 Avg.)	23.2	
Std. Dev. (Wt./No. Avg) - (PDI)	0.0	

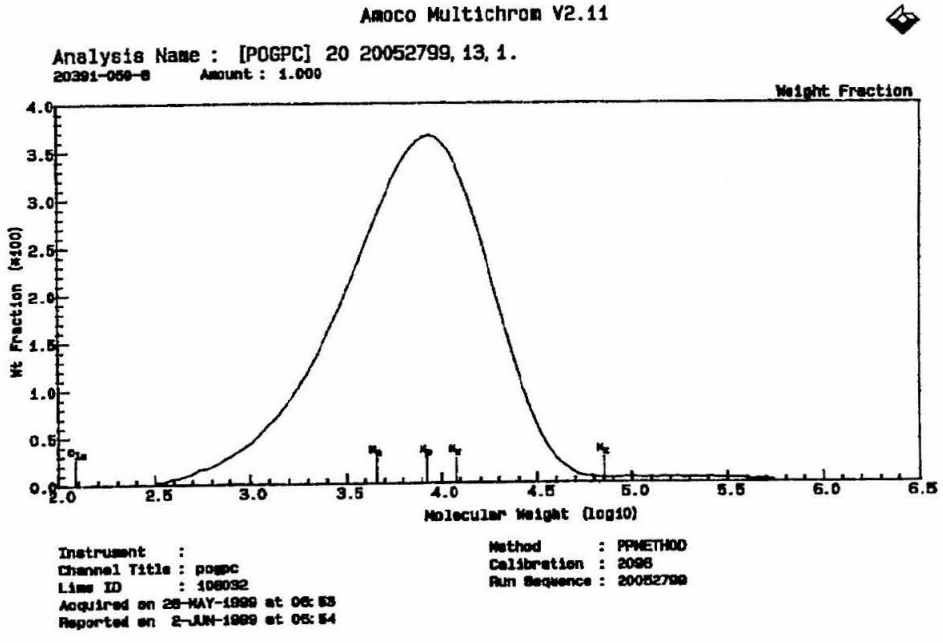

Appendix B: X-ray Crystallographic Data

Table 1. Crystal Data and Structure Analysis Details for dlz1 – $[(Me_2Si)_2(4\text{-}CMe_3\text{-}C_5H_2)(3,5\text{-}CMe_2H\text{-}C_5H_1)]Y(\mu\text{-}Cl)_2K(THF)_2$.

Empirical formula	$C_{32}H_{54}Cl_2K_1O_2Si_2Y_1$	
Formula weight	725.86	
Crystallization solvent	diethyl ether/tetrahydrofuran/pentane	
Crystal shape	irregular	
Crystal color	colorless	
Crystal size	0.190 x 0.200 x 0.330 mm	
Data Collection		
Preliminary photograph(s)	rotation	
Type of diffractometer	CAD-4	
Wavelength	0.7107 Å MoKα	
Data collection temperature	160 K	
Theta range for 25 reflections used in lattice determination	11 to 13°	
Unit cell dimensions	a = 10.204(2) Å b = 16.220(6) Å c = 23.074(7) Å	α= 90° β= 91.02(2)° γ = 90°
Volume	3818.3(20) $Å^3$	
Z	4	
Crystal system	monoclinic	
Space group	P $2_1/n$ (# 14)	
Density (calculated)	1.263 g/cm^3	
F(000)	1528	
Theta range for data collection	1.0 to 25.0°	
Index ranges	$0 \le h \le 12$, $-19 \le k \le 15$, $-27 \le l \le 27$	
Data collection scan type	ω scans	
Reflections collected	12148	
Independent reflections	6700 [R_{int}= 0.046; GOF_{merge}= 1.14]	
Reflections > 2σ(I)	6700	
Absorption coefficient	1.866 mm^{-1}	
Absorption correction	not applied	
Number of standards	3 reflections measured every 60 min	
Decay of standards	within counting statistics	

Structure Solution and Refinement

Primary solution method	direct methods
Secondary solution method	difference map
Hydrogen placement	calculated
Refinement method	full-matrix least-squares on F^2
Data / restraints / parameters	6700 / 0 / 330
Treatment of hydrogen atoms	not refined, U_{iso} fixed at 120% U_{eq} of attached atom
Goodness-of-fit on F^2	1.65
Final R indices [I>2σ(I), 6700 reflections]	R1 = 0.1099, wR2 = 0.1191
R indices (all data)	R1 = 0.1099, wR2 = 0.1191
Type of weighting scheme used	sigma
Weighting scheme used	$w=1/\sigma^2(Fo^2)$
Max shift/error	0.02
Largest diff. peak and hole	1.50 and -1.43 e·Å^{-3}

Programs Used

Cell refinement	CAD-4 Software (Enraf-Nonius, 1989)
Data collection	CAD-4 Software (Enraf-Nonius, 1989)
Data reduction	CRYM (Duchamp, 1964)
Structure solution	SHELXS-86 (Sheldrick, 1990)
Structure refinement	CRYM (Duchamp, 1964)

Special Refinement Details

A small, irregular, colorless crystal was mounted on a glass fiber with Paratone-N oil. Data were collected with 1.0° ω-scans. The GOF_{merge} was 1.14 (4027 multiples) in point group 2/m; R_{merge} was 0.046 for 2989 duplicates with $F_o > 0$. The individual backgrounds were replaced by a background function of 2θ derived from the backgrounds of weak reflections.

Weights w are calculated as $1/\sigma^2(F_o^2)$; variances ($\sigma^2(F_o^2)$) were derived from counting statistics plus an additional term, $(0.014I)^2$; variances of the merged data were obtained by propagation of error plus another additional term, $(0.014<I>)^2$. The refinement of F^2 is as always against all reflections. The weighted R-factor wR and goodness of fit S are based on F^2, conventional R-factors R are based on F, with F set to zero for negative F^2. The threshold expression of $F^2 > 2\sigma(F^2)$ is used only for calculating R-factors(gt) etc. and is not relevant to the choice of reflections for refinement.

The two tetrahydrofuran molecules are disordered and were not modeled

satisfactorily. One, modeled with only on position, has very large displacement parameters for two of the atoms. The other, modeled with two arrangements for the two outside carbon atoms, has a very unrealistic geometry for the minor site (C30B and C31B are 2.09(5)Å apart). In fact, it is not possible to rule out the presence of a small fraction of diethyl ether at this location.

There is also a much lesser disorder in one of the isopropyl groups.

The disorder of these groups should have little effect on the rest of the structure.

The K atom is coordinated to the two THF ligands, two chlorides (bridging to Y), and is also η^3 coordinated to the *t*-butyl cyclopentadienyl. This produces helical chains along the b-axis.

Table 2. Bond lengths [Å] and angles [°] for dlz1 – [$(Me_2Si)_2$(4-CMe_3-C_5H_2)(3,5-CMe_2H-C_5H_1)]Y(μ-Cl)$_2$K$(THF)_2$.

Y-Cl1	2.587(2)	C4-C15	1.504(9)
Y-Cl2	2.579(2)	C5-H5	0.95
Y-K	4.266(2)	C6-C7	1.480(9)
Y-Si1	3.281(2)	C6-C10	1.420(9)
Y-Si2	3.268(2)	C7-C8	1.422(9)
Y-C1	2.590(6)	C8-C9	1.397(9)
Y-C2	2.586(6)	C8-C19	1.518(9)
Y-C3	2.704(6)	C9-C10	1.402(9)
Y-C4	2.828(6)	C9-H9	0.95
Y-C5	2.735(6)	C10-C22	1.52(1)
Y-C6	2.545(6)	C11-H11a	0.95
Y-C7	2.548(6)	C11-H11b	0.95
Y-C8	2.750(6)	C11-H11c	0.95
Y-C9	2.815(7)	C12-H12a	0.95
Y-C10	2.737(7)	C12-H12b	0.95
Y-CpA [a]	2.403	C12-H12c	0.95
Y-CpB [b]	2.391	C13-H13a	0.95
Si1-C1	1.847(6)	C13-H13b	0.95
Si1-C6	1.856(7)	C13-H13c	0.95
Si1-C11	1.880(8)	C14-H14a	0.95
Si1-C12	1.856(9)	C14-H14b	0.95
Si2-C2	1.870(6)	C14-H14c	0.95
Si2-C7	1.873(6)	C15-C16	1.52(1)
Si2-C13	1.877(7)	C15-C17	1.53(1)
Si2-C14	1.865(7)	C15-C18	1.52(1)
C1-C2	1.438(8)	C16-H16a	0.95
C1-C5	1.428(9)	C16-H16b	0.95
C2-C3	1.426(9)	C16-H16c	0.95
C3-C4	1.423(9)	C17-H17a	0.95
C3-H3	0.95	C17-H17b	0.95
C4-C5	1.393(9)	C17-H17c	0.95

C18-H18a	0.95
C18-H18b	0.95
C18-H18c	0.95
C19-C20	1.525(9)
C19-C21	1.54(1)
C19-H19	0.95
C20-H20a	0.95
C20-H20b	0.95
C20-H20c	0.95
C21-H21a	0.95
C21-H21b	0.95
C21-H21c	0.95
C22-C23	1.51(1)
C22-C24	1.53(1)
C22-H22	0.95
C23-H23a	0.95
C23-H23b	0.95
C23-H23c	0.95
C24-H24a	0.95
C24-H24b	0.95
C24-H24c	0.95
K-Cl1	3.163(2)
K-Cl2	3.189(2)
K-O1	2.622(6)
K-O2	2.751(6)
K-C1	3.021(6)
K-C2	3.224(6)
K-C5	3.285(7)
O1-C25	1.52(2)
O1-C28	1.42(1)
C25-C26	1.33(2)
C25-H25a	0.95
C25-H25b	0.95
C26-C27	1.50(3)
C26-H26a	0.95
C26-H26b	0.95
C27-C28	1.45(2)
C27-H27a	0.95
C27-H27b	0.95
C28-H28a	0.95
C28-H28b	0.95
O2-C29	1.42(1)
O2-C32	1.43(1)
C29-C30A	1.47(2)
C29-C30B	1.48(3)
C29-H29a	0.95
C29-H29b	0.95
C29-H29c	0.95
C29-H29d	0.95
C30A-C31A	1.50(2)
C30A-C30B	0.97(4)
C30A-H30a	0.95
C30A-H30b	0.95
C31A-C31B	1.06(4)
C31A-C32	1.58(2)
C31A-H31a	0.95
C31A-H31b	0.95
C30B-H30c	0.95
C30B-H30d	0.95
C30B-C31B	2.09(5)
C31B-C32	1.26(4)
C31B-H31c	0.95
C31B-H31d	0.95
C32-H32a	0.95
C32-H32b	0.95
C32-H32c	0.95
C32-H32d	0.95

CpA-Y-CpB	115.0
CpA-Y-Cl1	113.1
CpA-Y-Cl2	111.0
CpB-Y-Cl1	109.3
CpB-Y-Cl2	111.1
Cl1-Y-Cl2	95.74(6)
C6-Si1-C1	96.1(3)
C11-Si1-C1	107.4(3)
C12-Si1-C1	116.3(3)
C11-Si1-C6	116.3(3)
C12-Si1-C6	113.5(3)
C12-Si1-C11	107.1(4)
C7-Si2-C2	95.7(3)
C13-Si2-C2	116.8(3)
C14-Si2-C2	107.3(3)
C13-Si2-C7	115.5(3)
C14-Si2-C7	115.3(3)
C14-Si2-C13	106.1(3)
C2-C1-Si1	122.2(4)
C5-C1-Si1	127.2(5)
C5-C1-C2	106.4(5)
C1-C2-Si2	123.8(4)
C3-C2-Si2	124.9(4)
C3-C2-C1	106.3(5)
C4-C3-C2	110.6(5)
H3-C3-C2	124.7
H3-C3-C4	124.7
C5-C4-C3	105.3(5)
C15-C4-C3	126.9(6)
C15-C4-C5	127.4(6)

C4-C5-C1	111.4(6)
H5-C5-C1	124.3
H5-C5-C4	124.3
C7-C6-Si1	122.3(5)
C10-C6-Si1	128.6(5)
C10-C6-C7	106.1(5)
C6-C7-Si2	121.9(4)
C8-C7-Si2	127.8(5)
C8-C7-C6	106.8(5)
C9-C8-C7	108.5(6)
C19-C8-C7	125.5(6)
C19-C8-C9	125.8(6)
C10-C9-C8	109.5(6)
H9-C9-C8	125.3
H9-C9-C10	125.3
C9-C10-C6	108.9(6)
C22-C10-C6	127.3(6)
C22-C10-C9	123.6(6)
H11a-C11-Si1	109.5
H11b-C11-Si1	109.5
H11c-C11-Si1	109.5
H11b-C11-H11a	109.5
H11c-C11-H11a	109.5
H11c-C11-H11b	109.5
H12a-C12-Si1	109.5
H12b-C12-Si1	109.5
H12c-C12-Si1	109.5
H12b-C12-H12a	109.5
H12c-C12-H12a	109.5
H12c-C12-H12b	109.5
H13a-C13-Si2	109.5
H13b-C13-Si2	109.5
H13c-C13-Si2	109.5
H13b-C13-H13a	109.5
H13c-C13-H13a	109.5
H13c-C13-H13b	109.5
H14a-C14-Si2	109.5
H14b-C14-Si2	109.5
H14c-C14-Si2	109.5
H14b-C14-H14a	109.5
H14c-C14-H14a	109.5
H14c-C14-H14b	109.5
C16-C15-C4	110.9(5)
C17-C15-C4	109.0(5)
C18-C15-C4	111.0(6)
C17-C15-C16	108.7(6)
C18-C15-C16	107.5(6)
C18-C15-C17	109.8(6)
H16a-C16-C15	109.5
H16b-C16-C15	109.5
H16c-C16-C15	109.5
H16b-C16-H16a	109.5
H16c-C16-H16a	109.5
H16c-C16-H16b	109.5
H17a-C17-C15	109.5
H17b-C17-C15	109.5
H17c-C17-C15	109.5
H17b-C17-H17a	109.5
H17c-C17-H17a	109.5
H17c-C17-H17b	109.5
H18a-C18-C15	109.5
H18b-C18-C15	109.5
H18c-C18-C15	109.5
H18b-C18-H18a	109.5
H18c-C18-H18a	109.5
H18c-C18-H18b	109.5
C20-C19-C8	110.4(5)
C21-C19-C8	113.2(5)
H19-C19-C8	106.5
C21-C19-C20	110.2(5)
H19-C19-C20	109.7
H19-C19-C21	106.7
H20a-C20-C19	109.5
H20b-C20-C19	109.5
H20c-C20-C19	109.5
H20b-C20-H20a	109.5
H20c-C20-H20a	109.5
H20c-C20-H20b	109.5
H21a-C21-C19	109.5
H21b-C21-C19	109.5
H21c-C21-C19	109.5
H21b-C21-H21a	109.5
H21c-C21-H21a	109.5
H21c-C21-H21b	109.5
C23-C22-C10	113.5(7)
C24-C22-C10	108.8(7)
H22-C22-C10	107.6
C24-C22-C23	110.7(7)
H22-C22-C23	105.6
H22-C22-C24	110.6
H23a-C23-C22	109.5
H23b-C23-C22	109.5
H23c-C23-C22	109.5
H23b-C23-H23a	109.5
H23c-C23-H23a	109.5
H23c-C23-H23b	109.5
H24a-C24-C22	109.5
H24b-C24-C22	109.5

H24c-C24-C22	109.5	H29a-C29-C30A	110.0
H24b-C24-H24a	109.5	H29b-C29-C30A	110.0
H24c-C24-H24a	109.5	H29c-C29-C30B	109.5
H24c-C24-H24b	109.5	H29d-C29-C30B	109.5
Cl1-K-Cl2	74.19(6)	H29b-C29-H29a	109.5
Cl1-K-O1	132.0(2)	H29d-C29-H29c	109.5
Cl1-K-O2	130.4(1)	C31A-C30A-C29	105(1)
Cl2-K-O1	87.5(1)	H30a-C30A-C29	110.5
K-Cl1-Y	95.26(6)	H30b-C30A-C29	110.5
K-Cl2-Y	94.81(6)	H30a-C30A-C31A	110.5
C28-O1-C25	116.1(8)	H30b-C30A-C31A	110.5
C26-C25-O1	96(1)	H30b-C30A-H30a	109.5
H25a-C25-O1	112.6	C32-C31A-C30A	98(1)
H25b-C25-O1	112.6	H31a-C31A-C30A	112.2
H25a-C25-C26	112.6	H31b-C31A-C30A	112.2
H25b-C25-C26	112.6	H31a-C31A-C32	112.2
H25b-C25-H25a	109.5	H31b-C31A-C32	112.2
C27-C26-C25	107(2)	H31b-C31A-H31a	109.5
H26a-C26-C25	110.1	H30c-C30B-C29	117.0
H26b-C26-C25	110.1	H30d-C30B-C29	117.0
H26a-C26-C27	110.1	H30d-C30B-H30c	109.5
H26b-C26-C27	110.1	C31B-C30B-C29	76(2)
H26b-C26-H26a	109.5	H30c-C30B-C31B	117.0
C28-C27-C26	103(1)	H30d-C30B-C31B	117.0
H27a-C27-C26	111.1	C32-C31B-C30B	92(2)
H27b-C27-C26	111.1	H31c-C31B-C32	113.5
H27a-C27-C28	111.1	H31d-C31B-C32	113.5
H27b-C27-C28	111.1	H31d-C31B-H31c	109.5
H27b-C27-H27a	109.5	H31c-C31B-C30B	113.5
C27-C28-O1	96(1)	H31d-C31B-C30B	113.5
H28a-C28-O1	112.7	C31A-C32-O2	105.9(9)
H28b-C28-O1	112.7	C31B-C32-O2	103(2)
H28a-C28-C27	112.7	H32a-C32-O2	110.3
H28b-C28-C27	112.7	H32b-C32-O2	110.3
H28b-C28-H28a	109.5	H32c-C32-O2	111.0
C32-O2-C29	108.7(8)	H32d-C32-O2	111.0
C30A-C29-O2	107(1)	H32a-C32-C31A	110.3
C30B-C29-O2	109(1)	H32b-C32-C31A	110.4
H29a-C29-O2	110.0	H32c-C32-C31B	111.0
H29b-C29-O2	110.0	H32d-C32-C31B	111.0
H29c-C29-O2	109.5	H32b-C32-H32a	109.5
H29d-C29-O2	109.5	H32d-C32-H32c	109.5

[a] CpA is the centroid of atoms C1, C2, C3, C4 and C5
[b] CpB is the centroid of atoms C6, C7, C8, C9 and C10

Table 3. Crystal Data and Structure Analysis Details for dlz2 – $[(Me_2Si)_2(4\text{-}CMe_3\text{-}C_5H_2)(3,5\text{-}CMe_2H\text{-}C_5H_1)]Sc(\mu\text{-}Cl)_2K(Et_2O)_2$.

Empirical formula	$C_{32}H_{32}Cl_2KO_2ScSi_2$
Formula weight	659.72
Crystallization solvent	diethyl ether/petroleum ether
Crystal shape	fragment
Crystal color	colorless
Crystal size	0.19 x 0.30 x 0.67 mm

Data Collection

Preliminary photograph(s)	rotation	
Type of diffractometer	CAD-4	
Wavelength	0.71073 Å MoKα	
Data collection temperature	160 K	
Theta range for 25 reflections used in lattice determination	10.6 to 12.2°	
Unit cell dimensions	a = 12.328(5) Å	α= 95.58(2)°
	b = 12.894(4) Å	β= 105.57(3)°
	c = 13.059(4) Å	γ = 100.41(3)°
Volume	1943.3(11) $Å^3$	
Z	2	
Crystal system	triclinic	
Space group	$P\bar{1}$ (# 2)	
Density (calculated)	1.127 g/cm^3	
F(000)	684	
Theta range for data collection	1.5 to 25.0°	
Index ranges	$-15 \le h \le 14$, $-15 \le k \le 15$, $-16 \le l \le 15$	
Data collection scan type	omega scans	
Reflections collected	15191	
Independent reflections	7609 [R_{int}= 0.034]	
Reflections > 2σ(I)	5720	
Average σ(I)/(net I)	0.0499	
Absorption coefficient	0.519 mm^{-1}	
Absorption correction	none	
Number of standards	3 reflections measured every 60 min	
Decay of standards	1.2%	

Structure Solution and Refinement

Primary solution method	direct methods
Secondary solution method	difference map
Hydrogen placement	calculated
Refinement method	full matrix least-squares on F^2
Data / restraints / parameters	7603 / 16 / 609
Treatment of hydrogen atoms	coordinates refined, U_{iso} fixed at 120% U_{eq} of attached atom
Goodness-of-fit on F^2	1.432
Final R indices [I>2σ(I), 5720 reflections]	R1 = 0.0421, wR2 = 0.0731
R indices (all data)	R1 = 0.0656, wR2 = 0.0806
Type of weighting scheme used	sigma
Weighting scheme used	$w=1/\sigma^2(Fo^2)$
Max shift/error	-0.562
Average shift/error	0.019
Largest diff. peak and hole	0.407 and -0.381 $e \cdot Å^{-3}$

Programs Used

Cell refinement	CAD-4 Software (Enraf-Nonius, 1989)
Data collection	CAD-4 Software (Enraf-Nonius, 1989)
Data reduction	CRYM (Duchamp, 1964)
Structure solution	SHELXS-86 (Sheldrick, 1990)
Structure refinement	SHELXL-93 (Sheldrick, 1993)

Special Refinement Details

A colorless crystal was mounted on a glass fiber with Paratone-N oil. Data were collected with ω-scans. Weights w are calculated as $1/\sigma^2(F_o^2)$; variances ($\sigma^2(F_o^2)$) were derived from counting statistics plus an additional term, $(0.014I)^2$; variances of the merged data were obtained by propagation of error plus another additional term, $(0.014<I>)^2$. The refinement of F^2 is as always against all reflections. The weighted R-factor wR and goodness of fit S are based on F^2, conventional R-factors R are based on F, with F set to zero for negative F^2. The threshold expression of $F^2 > 2\sigma(F^2)$ is used only for calculating R-factors(gt) etc. and is not relevant to the choice of reflections for refinement.

Table 4. Bond lengths [Å] and angles [°] for dlz2 – $[(Me_2Si)_2(4\text{-}CMe_3\text{-}C_5H_2)(3,5\text{-}CMe_2H\text{-}C_5H_1)]Sc(\mu\text{-}Cl)_2K(Et_2O)_2$.

Sc-CpA [a]	2.2351(8)	C34-H34B	0.98(3)
Sc-CpB [b]	2.2820(9)	C34-H34C	1.00(4)
Sc-C10	2.390(2)	C4-C5	1.420(3)
Sc-C6	2.399(3)	C4-H4A	0.87(2)
Sc-C5	2.436(2)	C6-C7	1.423(3)
Sc-C1	2.438(2)	C6-C10	1.472(3)
Sc-Cl1	2.4488(10)	C7-C8	1.407(3)
Sc-Cl2	2.5070(13)	C7-C71	1.511(3)
Sc-C4	2.567(3)	C71-C73	1.513(4)
Sc-C2	2.574(2)	C71-C72	1.534(4)
Sc-C9	2.650(2)	C71-H71A	0.97(2)
Sc-C7	2.679(3)	C72-H72A	0.99(3)
K-O1	2.62(2)	C72-H72B	0.98(3)
K-O2	2.704(4)	C72-H72C	0.96(3)
K-O3	2.762(12)	C73-H73A	0.94(3)
K-O4	2.952(9)	C73-H73B	0.98(3)
K-Cl1	3.082(2)	C73-H73C	1.00(3)
K-Cl2^{i}	3.1923(15)	C8-C9	1.400(3)
K-Cl2	3.2354(14)	C8-H8A	0.91(2)
K-K^{i}	4.735(2)	C9-C10	1.432(3)
Cl2-K^{i}	3.1923(15)	C9-C91	1.512(3)
Si1-C102	1.864(3)	C91-C93	1.529(4)
Si1-C101	1.866(3)	C91-C92	1.529(4)
Si1-C6	1.868(3)	C91-H91A	0.94(2)
Si1-C1	1.871(3)	C92-H92A	1.00(3)
Si2-C202	1.864(3)	C92-H92B	0.95(3)
Si2-C5	1.865(3)	C92-H92C	0.95(3)
Si2-C201	1.865(3)	C93-H93A	0.95(3)
Si2-C10	1.871(3)	C93-H93B	0.98(3)
C1-C2	1.418(3)	C93-H93C	0.93(3)
C1-C5	1.446(3)	C101-H10A	0.94(4)
C2-C3	1.410(3)	C101-H10B	0.92(4)
C2-H2A	0.92(2)	C101-H10C	0.92(4)
C3-C4	1.409(3)	C102-H10D	0.98(3)
C3-C31	1.520(3)	C102-H10E	0.96(3)
C31-C32	1.511(4)	C102-H10F	0.96(3)
C31-C34	1.529(4)	C201-H20A	0.87(4)
C31-C33	1.538(4)	C201-H20B	0.91(4)
C32-H32A	1.01(3)	C201-H20C	0.89(5)
C32-H32B	1.04(3)	C202-H20D	0.96(3)
C32-H32C	0.96(4)	C202-H20E	0.96(3)
C33-H33A	1.10(3)	C202-H20F	0.95(3)
C33-H33B	1.11(4)	O1-C112	1.494(10)
C33-H33C	1.05(3)	O1-C113	1.520(9)
C34-H34A	1.01(4)	C111-C112	1.531(10)

C111-H111	0.96
C111-H111	0.96
C111-H111	0.96
C112-H112	0.97
C112-H112	0.97
C113-C114	1.511(9)
C113-H113	0.97
C113-H113	0.97
C114-H114	0.96
C114-H114	0.96
C114-H114	0.96
O3-C312	1.469(8)
O3-C313	1.509(7)
C311-C312	1.519(8)
C311-H311	0.96
C311-H311	0.96
C311-H311	0.96
C312-H312	0.97
C312-H312	0.97
C313-C314	1.519(7)
C313-H313	0.97
C313-H313	0.97
C314-H314	0.96
C314-H314	0.96
C314-H314	0.96
O2-C212	1.445(6)
O2-C213	1.472(7)
C211-C212	1.529(8)
C211-H211	0.96
C211-H211	0.96
C211-H211	0.96
C212-H212	0.97
C212-H212	0.97
C213-C214	1.509(7)
C213-H213	0.97
C213-H213	0.97
C214-H214	0.96
C214-H214	0.96
C214-H214	0.96
O4-C413	1.484(8)
O4-C412	1.528(9)
C411-C412	1.547(9)
C411-H411	0.96
C411-H411	0.96
C411-H411	0.96
C412-H412	0.97
C412-H412	0.97
C413-C414	1.519(10)
C413-H413	0.97
C413-H413	0.97
C414-H414	0.96
C414-H414	0.96
C414-H414	0.96

CpA-Sc-CpB	122.71(3)
C10-Sc-C6	35.79(8)
C10-Sc-C5	69.34(9)
C6-Sc-C5	80.26(9)
C10-Sc-C1	79.78(9)
C6-Sc-C1	69.01(9)
C5-Sc-C1	34.52(8)
C10-Sc-Cl1	135.96(7)
C6-Sc-Cl1	105.30(7)
C5-Sc-Cl1	139.13(6)
C1-Sc-Cl1	108.68(7)
C10-Sc-Cl2	106.84(7)
C6-Sc-Cl2	137.49(7)
C5-Sc-Cl2	108.46(7)
C1-Sc-Cl2	138.78(6)
Cl1-Sc-Cl2	94.52(4)
C10-Sc-C4	97.29(9)
C6-Sc-C4	113.09(9)
C5-Sc-C4	32.85(8)
C1-Sc-C4	54.45(8)
Cl1-Sc-C4	123.29(6)
Cl2-Sc-C4	84.36(7)
C10-Sc-C2	112.50(9)
C6-Sc-C2	96.32(9)
C5-Sc-C2	54.51(8)
C1-Sc-C2	32.72(8)
Cl1-Sc-C2	84.66(7)
Cl2-Sc-C2	123.10(6)
C4-Sc-C2	51.93(8)
C10-Sc-C9	32.49(8)
C6-Sc-C9	54.56(8)
C5-Sc-C9	97.45(8)
C1-Sc-C9	112.24(8)
Cl1-Sc-C9	119.06(6)
Cl2-Sc-C9	82.94(6)
C4-Sc-C9	117.02(8)
C2-Sc-C9	144.95(8)
C10-Sc-C7	54.43(8)
C6-Sc-C7	31.95(8)
C5-Sc-C7	112.20(9)
C1-Sc-C7	96.57(9)
Cl1-Sc-C7	81.53(6)
Cl2-Sc-C7	120.78(6)
C4-Sc-C7	145.04(8)

C2-Sc-C7	115.34(8)	C2-C1-Si1	124.0(2)
C9-Sc-C7	51.14(8)	C5-C1-Si1	123.6(2)
O1-K-Cl1	109.2(3)	C2-C1-Sc	78.94(14)
O2-K-Cl1	89.21(10)	C5-C1-Sc	72.67(13)
O3-K-Cl1	102.7(2)	Si1-C1-Sc	93.08(10)
O4-K-Cl1	80.5(2)	C3-C2-C1	110.4(2)
O1-K-Cl2^{i}	106.9(3)	C3-C2-Sc	78.80(14)
O2-K-Cl2^{i}	92.18(14)	C1-C2-Sc	68.34(13)
O3-K-Cl2^{i}	113.9(2)	C3-C2-H2A	125.0(15)
O4-K-Cl2^{i}	108.0(2)	C1-C2-H2A	124.6(15)
Cl1-K-Cl2^{i}	142.36(3)	Sc-C2-H2A	117.8(14)
O1-K-Cl2	114.6(4)	C4-C3-C2	106.0(2)
O2-K-Cl2	139.90(11)	C4-C3-C31	127.1(2)
O3-K-Cl2	116.9(2)	C2-C3-C31	126.4(2)
O4-K-Cl2	144.5(2)	C4-C3-Sc	69.88(14)
Cl1-K-Cl2	70.32(3)	C2-C3-Sc	70.17(13)
Cl2^{i}-K-Cl2	85.12(4)	C31-C3-Sc	130.6(2)
O1-K-K^{i}	118.7(3)	C32-C31-C3	108.6(2)
O2-K-K^{i}	123.25(15)	C32-C31-C34	110.1(3)
O3-K-K^{i}	125.6(2)	C3-C31-C34	111.5(2)
O4-K-K^{i}	139.9(2)	C32-C31-C33	108.9(3)
Cl1-K-K^{i}	107.68(4)	C3-C31-C33	111.6(2)
Cl2^{i}-K-K^{i}	42.91(2)	C34-C31-C33	106.1(3)
Cl2-K-K^{i}	42.21(2)	C31-C32-H32A	100.3(15)
Sc-Cl1-K	99.58(4)	C31-C32-H32B	108.4(19)
Sc-Cl2-K^{i}	142.56(3)	H32A-C32-H32B	124.4(25)
Sc-Cl2-K	94.43(4)	C31-C32-H32C	112.1(21)
K^{i}-Cl2-K	94.88(4)	H32A-C32-H32C	102.3(25)
C102-Si1-C101	105.8(2)	H32B-C32-H32C	108.9(28)
C102-Si1-C6	115.99(14)	C31-C33-H33A	99.9(17)
C101-Si1-C6	114.53(14)	C31-C33-H33B	109.8(21)
C102-Si1-C1	106.95(13)	H33A-C33-H33B	119.9(26)
C101-Si1-C1	119.3(2)	C31-C33-H33C	111.6(17)
C6-Si1-C1	94.25(11)	H33A-C33-H33C	105.2(23)
C102-Si1-Sc	103.58(11)	H33B-C33-H33C	110.0(26)
C101-Si1-Sc	150.59(14)	C31-C34-H34A	106.1(25)
C6-Si1-Sc	49.38(7)	C31-C34-H34B	108.8(17)
C1-Si1-Sc	50.56(8)	H34A-C34-H34B	106.2(28)
C202-Si2-C5	108.85(14)	C31-C34-H34C	112.4(20)
C202-Si2-C201	106.5(2)	H34A-C34-H34C	112.3(31)
C5-Si2-C201	116.29(15)	H34B-C34-H34C	110.6(26)
C202-Si2-C10	114.98(13)	C3-C4-C5	110.6(2)
C5-Si2-C10	94.59(11)	C3-C4-Sc	79.09(14)
C201-Si2-C10	115.5(2)	C5-C4-Sc	68.49(14)
C202-Si2-Sc	105.05(12)	C3-C4-H4A	128.1(15)
C5-Si2-Sc	50.63(8)	C5-C4-H4A	121.3(15)
C201-Si2-Sc	148.46(14)	Sc-C4-H4A	120.2(15)
C10-Si2-Sc	49.25(7)	C4-C5-C1	106.3(2)
C2-C1-C5	106.7(2)	C4-C5-Si2	126.5(2)

C1-C5-Si2	121.6(2)
C4-C5-Sc	78.66(14)
C1-C5-Sc	72.81(13)
Si2-C5-Sc	93.08(10)
C7-C6-C10	107.4(2)
C7-C6-Si1	127.4(2)
C10-C6-Si1	122.3(2)
C7-C6-Sc	84.93(14)
C10-C6-Sc	71.77(13)
Si1-C6-Sc	94.41(10)
C8-C7-C6	107.8(2)
C8-C7-C71	125.7(2)
C6-C7-C71	126.4(2)
C8-C7-Sc	78.76(15)
C6-C7-Sc	63.12(13)
C71-C7-Sc	126.4(2)
C7-C71-C73	113.0(2)
C7-C71-C72	110.3(2)
C73-C71-C72	109.6(2)
C7-C71-H71A	109.1(13)
C73-C71-H71A	107.2(13)
C72-C71-H71A	107.5(14)
C71-C72-H72A	108.8(15)
C71-C72-H72B	110.8(16)
H72A-C72-H72B	111.6(22)
C71-C72-H72C	111.2(16)
H72A-C72-H72C	107.9(22)
H72B-C72-H72C	106.5(21)
C71-C73-H73A	109.2(17)
C71-C73-H73B	112.9(18)
H73A-C73-H73B	110.3(24)
C71-C73-H73C	109.6(14)
H73A-C73-H73C	107.4(21)
H73B-C73-H73C	107.4(23)
C9-C8-C7	110.1(2)
C9-C8-Sc	70.25(14)
C7-C8-Sc	71.39(14)
C9-C8-H8A	126.1(15)
C7-C8-H8A	123.7(16)
Sc-C8-H8A	126.5(15)
C8-C9-C10	108.3(2)
C8-C9-C91	125.2(2)
C10-C9-C91	126.3(2)
C8-C9-Sc	79.95(14)
C10-C9-Sc	63.71(13)
C91-C9-Sc	126.3(2)
C9-C91-C93	112.4(2)
C9-C91-C92	109.8(2)
C93-C91-C92	110.5(3)
C9-C91-H91A	110.0(15)
C93-C91-H91A	107.9(15)
C92-C91-H91A	106.0(15)
C91-C92-H92A	114.0(17)
C91-C92-H92B	106.5(17)
H92A-C92-H92B	113.2(25)
C91-C92-H92C	109.1(18)
H92A-C92-H92C	104.2(24)
H92B-C92-H92C	109.9(24)
C91-C93-H93A	114.0(19)
C91-C93-H93B	108.6(19)
H93A-C93-H93B	106.6(26)
C91-C93-H93C	109.2(19)
H93A-C93-H93C	110.0(26)
H93B-C93-H93C	108.3(26)
C9-C10-C6	106.4(2)
C9-C10-Si2	128.6(2)
C6-C10-Si2	122.0(2)
C9-C10-Sc	83.80(14)
C6-C10-Sc	72.44(13)
Si2-C10-Sc	94.37(10)
Si1-C101-H10A	111.4(21)
Si1-C101-H10B	108.7(22)
H10A-C101-H10B	113.4(29)
Si1-C101-H10C	119.3(25)
H10A-C101-H10C	103.4(30)
H10B-C101-H10C	100.3(30)
Si1-C102-H10D	111.0(17)
Si1-C102-H10E	107.6(19)
H10D-C102-H10E	108.8(25)
Si1-C102-H10F	111.9(16)
H10D-C102-H10F	104.5(23)
H10E-C102-H10F	113.0(24)
Si2-C201-H20A	111.0(27)
Si2-C201-H20B	113.7(26)
H20A-C201-H20B	99.6(34)
Si2-C201-H20C	116.0(29)
H20A-C201-H20C	103.7(36)
H20B-C201-H20C	111.2(37)
Si2-C202-H20D	112.5(17)
Si2-C202-H20E	110.1(17)
H20D-C202-H20E	107.5(23)
Si2-C202-H20F	109.2(17)
H20D-C202-H20F	111.1(24)
H20E-C202-H20F	106.3(23)
C112-O1-C113	91.7(12)
C112-O1-K	128.1(12)
C113-O1-K	132.4(12)
C112-C111-H111	109.4(14)

C112-C111-H111	109.4(12)
H111-C111-H111	109.5
C112-C111-H111	109.6(13)
H111-C111-H111	109.5
H111-C111-H111	109.5
O1-C112-C111	101.5(18)
O1-C112-H112	111.3(10)
C111-C112-H112	111.5(12)
O1-C112-H112	111.4(9)
C111-C112-H112	111.7(13)
H112-C112-H112	109.4
C114-C113-O1	100.5(11)
C114-C113-H113	111.7(6)
O1-C113-H113	111.7(9)
C114-C113-H113	111.7(7)
O1-C113-H113	111.7(7)
H113-C113-H113	109.4
C113-C114-H114	109.5(7)
C113-C114-H114	109.5(7)
H114-C114-H114	109.5
C113-C114-H114	109.5(7)
H114-C114-H114	109.5
H114-C114-H114	109.5
C312-O3-C313	116.5(11)
C312-O3-K	121.4(8)
C313-O3-K	109.9(7)
C312-C311-H311	109.4(10)
C312-C311-H311	109.6(10)
H311-C311-H311	109.5
C312-C311-H311	109.3(10)
H311-C311-H311	109.5
H311-C311-H311	109.5
O2-C212-H212	110.4(4)
C211-C212-H212	110.4(6)
H212-C212-H212	108.6
O2-C213-C214	110.9(6)
O2-C213-H213	109.5(3)
C214-C213-H213	109.4(5)
O2-C213-H213	109.5(3)
C214-C213-H213	109.5(4)
H213-C213-H213	108.0
C213-C214-H214	109.5(5)
C213-C214-H214	109.5(5)
H214-C214-H214	109.5
C213-C214-H214	109.5(4)
H214-C214-H214	109.5
H214-C214-H214	109.5
C413-O4-C412	106.4(9)
C413-O4-K	121.6(8)
O3-C312-C311	108.1(14)
O3-C312-H312	110.1(6)
C311-C312-H312	110.2(10)
O3-C312-H312	110.2(7)
C311-C312-H312	109.9(10)
H312-C312-H312	108.4
O3-C313-C314	103.2(7)
O3-C313-H313	111.1(6)
C314-C313-H313	111.1(5)
O3-C313-H313	111.1(6)
C314-C313-H313	111.1(5)
H313-C313-H313	109.1
C313-C314-H314	109.5(4)
C313-C314-H314	109.5(5)
H314-C314-H314	109.5
C313-C314-H314	109.5(5)
H314-C314-H314	109.5
H314-C314-H314	109.5
C212-O2-C213	112.3(6)
C212-O2-K	125.0(5)
C213-O2-K	117.6(4)
C212-C211-H211	109.5(5)
C212-C211-H211	109.5(6)
H211-C211-H211	109.5
C212-C211-H211	109.5(6)
H211-C211-H211	109.5
H211-C211-H211	109.5
O2-C212-C211	106.5(8)
O2-C212-H212	110.4(4)
C211-C212-H212	110.4(6)

C412-O4-K	118.0(8)
C412-C411-H411	109.5(9)
C412-C411-H411	109.5(13)
H411-C411-H411	109.5
C412-C411-H411	109.5(13)
H411-C411-H411	109.5
H411-C411-H411	109.5
O4-C412-C411	101.1(11)
O4-C412-H412	111.6(8)
C411-C412-H412	111.5(13)
O4-C412-H412	111.6(9)
C411-C412-H412	111.5(13)
H412-C412-H412	109.4
O4-C413-C414	104.3(12)
O4-C413-H413	110.9(5)
C414-C413-H413	110.9(8)
O4-C413-H413	110.9(7)

C414-C413-H413	110.9(10)	H414-C414-H414	109.5
H413-C413-H413	108.9	C413-C414-H414	109.5(10)
C413-C414-H414	109.5(9)	H414-C414-H414	109.5
C413-C414-H414	109.5(8)	H414-C414-H414	109.5

Symmetry transformations used to generate equivalent atoms:
(i), -x+1,-y+1,-z+1

[a] CpA is the centroid of atoms C1, C2, C3, C4 and C5
[b] CpB is the centroid of atoms C6, C7, C8, C9 and C10

Table 5. Crystal Data and Structure Analysis Details for dlz3 – Y{μ-[(Me_2Si)$_2$(4-CMe_3-C_5H_2)(3,5-CMe_2H-C_5H_1)]$_2$(μ-H)$_2$}Y.

Empirical formula	$[C_{24}H_{39}Si_2Y]_2[C_6H_6]_2$
Formula weight	[945.32][156.23]
Crystallization Solvent	benzene-d_6
Crystal Habit	square columns
Crystal size	0.48 x 0.22 x 0.17 mm^3
Crystal color	colorless
Data Collection	
Preliminary Photos	none
Type of diffractometer	CAD-4
Wavelength	0.71073 Å MoKα
Data Collection Temperature	85 K
Theta range for reflections used in lattice determination	16.6 to 20.3°
Unit cell dimensions	a = 10.477(6) Å b = 16.312(11) Å β= 105.12(6)° c = 17.341(13) Å
Volume	2861(3) $Å^3$
Z	2
Crystal system	monoclinic
Space group	$P2_1/c$
Density (calculated)	1.279 Mg/m^3
F(000)	1168
Theta range for data collection	1.75 to 25.0°
Completeness to θ = 25.00°	100.0 %
Index ranges	$-12 \le h \le 12$, $-19 \le k \le 19$, $0 \le l \le 20$
Data collection scan type	ω scans

Reflections collected	11228
Independent reflections	5031 [R_{int}= 0.031; GOF_{merge}= 1.11]
Absorption coefficient	2.138 mm^{-1}
Absorption correction	none
Number of standards	3 reflections measured every 75 min.
Variation of standards	within counting statistics, zero %.

Structure solution and Refinement

Structure solution program	SHELXS-97 (Sheldrick, 1990)
Primary solution method	Direct methods (See Special Refinement Details)
Secondary solution method	All non-H in initial solution
Hydrogen placement	Difference Fourier map
Structure refinement program	SHELXL-97 (Sheldrick, 1997)
Refinement method	Full matrix least-squares on F^2
Data / restraints / parameters	5031 / 0 / 478
Treatment of hydrogen atoms	unrestrained
Goodness-of-fit on F^2	1.392
Final R indices [I>2σ(I)]	R1 = 0.0324, wR2 = 0.0550
R indices (all data)	R1 = 0.0525, wR2 = 0.0588
Type of weighting scheme used	sigma
Weighting scheme used	$w=1/\sigma^2(Fo^2)$
Max shift/error	0.012
Average shift/error	0.000
Largest diff. peak and hole	0.413 and -0.280 e.$Å^{-3}$

Special Refinement Details

Direct methods and the Patterson method were unsuccessful at solving this structure in the true space group, $P2_1/c$, although fragments were discernable. The structure was solved by Direct methods in space group P1 using a triclinic expansion of the data, which revealed the positions of all the non-hydrogen atoms as well as the positions of the hydride. Since Z=2 for the dimer it was clear that the molecule must sit on a center of symmetry. The dimer was translated to the center at 0,0,0 and the unique atoms were retained for refinement. All other hydrogen atoms were visible in the Fourier map and were included in the refinement without restraints.

The variances [$\sigma^2(Fo^2)$] were derived from counting statistics plus an additional term, $(0.014I)^2$, and the variances of the merged data were obtained by propagation of error plus the addition of another term, $(0.014\langle I\rangle)^2$.

Refinement of F^2 against ALL reflections. The weighted R-factor (wR) and goodness of fit (S) are based on F^2, conventional R-factors (R) are based on F, with F set to zero for negative F^2. The threshold expression of $F^2 > 2\sigma(F^2)$ is used only for calculating R-factors(gt) etc. and is not relevant to the choice of reflections for refinement. R-factors based on F^2 are statistically about twice as large as those based on F, and R-factors based on ALL data will be even larger.

All esds (except the esd in the dihedral angle between two l.s. planes) are estimated using the full covariance matrix. The cell esds are taken into account individually in the estimation of esds in distances, angles and torsion angles; correlations between esds in cell parameters are only used when they are defined by crystal symmetry. An approximate (isotropic) treatment of cell esds is used for estimating esds involving l.s. planes.

Table 6. Bond lengths [Å] and angles [°] for dlz3 – $Y\{\mu\text{-}[(Me_2Si)_2(4\text{-}CMe_3\text{-}C_5H_2)(3,5\text{-}CMe_2H\text{-}C_5H_1)]_2(\mu\text{-}H)_2\}Y$.

Y-Cent2	2.3594(15)	C(4)-Si(2)^i	1.860(3)
Y-Cent1	2.3775(13)	C(5)-H(5)	0.94(2)
Y-Pln2	2.3576(27)	C(6)-C(10)	1.410(4)
Y-Pln1	2.3736(27)	C(6)-C(7)	1.416(4)
Y-C(9)	2.613(3)	C(6)-H(6)	0.89(2)
Y-C(3)	2.622(3)	C(7)-C(8)	1.426(4)
Y-C(8)	2.626(3)	C(7)-C(18)	1.517(3)
Y-C(4)	2.628(3)	C(8)-C(9)	1.455(3)
Y-C(2)	2.664(3)	C(9)-C(10)	1.422(4)
Y-C(10)	2.668(3)	C(9)-Si(1)^i	1.871(3)
Y-C(6)	2.676(3)	C(10)-C(15)	1.519(4)
Y-C(5)	2.679(3)	C(11)-C(13)	1.526(4)
Y-C(7)	2.680(3)	C(11)-C(14)	1.528(4)
Y-C(1)	2.744(3)	C(11)-C(12)	1.535(4)
Y-H	2.11(2)	C(12)-H(12A)	1.00(3)
Si(1)-C(3)	1.859(3)	C(12)-H(12B)	0.90(3)
Si(1)-C(9)^i	1.871(3)	C(12)-H(12C)	0.98(3)
Si(1)-C(21)	1.871(3)	C(13)-H(13A)	0.98(3)
Si(1)-C(22)	1.872(3)	C(13)-H(13B)	0.94(3)
Si(2)-C(4)^i	1.860(3)	C(13)-H(13C)	0.99(3)
Si(2)-C(24)	1.871(3)	C(14)-H(14A)	0.96(2)
Si(2)-C(8)	1.878(3)	C(14)-H(14B)	0.96(3)
Si(2)-C(23)	1.879(3)	C(14)-H(14C)	0.99(3)
C(1)-C(2)	1.416(4)	C(15)-C(16)	1.528(4)
C(1)-C(5)	1.422(4)	C(15)-C(17)	1.529(4)
C(1)-C(11)	1.523(4)	C(15)-H(15)	0.88(2)
C(2)-C(3)	1.415(4)	C(16)-H(16A)	0.96(3)
C(2)-H(2)	0.85(2)	C(16)-H(16B)	0.97(3)
C(3)-C(4)	1.438(3)	C(16)-H(16C)	0.95(3)
C(4)-C(5)	1.424(4)	C(17)-H(17A)	0.89(3)

C(17)-H(17B)	0.97(2)	C(4)-Y-C(2)	51.22(8)
C(17)-H(17C)	0.92(3)	C(9)-Y-C(10)	31.22(8)
C(18)-C(20)	1.527(4)	C(3)-Y-C(10)	159.28(8)
C(18)-C(19)	1.530(4)	C(8)-Y-C(10)	52.05(9)
C(18)-H(18)	0.95(2)	C(4)-Y-C(10)	134.18(9)
C(19)-H(19A)	0.97(3)	C(2)-Y-C(10)	133.93(9)
C(19)-H(19B)	0.94(2)	C(9)-Y-C(6)	51.27(9)
C(19)-H(19C)	0.97(3)	C(3)-Y-C(6)	140.08(8)
C(20)-H(20A)	0.89(3)	C(8)-Y-C(6)	51.35(9)
C(20)-H(20B)	0.99(3)	C(4)-Y-C(6)	139.68(9)
C(20)-H(20C)	0.94(3)	C(2)-Y-C(6)	109.08(9)
C(21)-H(21A)	0.98(3)	C(10)-Y-C(6)	30.60(8)
C(21)-H(21B)	0.98(3)	C(9)-Y-C(5)	134.75(8)
C(21)-H(21C)	1.02(3)	C(3)-Y-C(5)	51.44(8)
C(22)-H(22A)	0.91(3)	C(8)-Y-C(5)	159.41(8)
C(22)-H(22B)	0.96(3)	C(4)-Y-C(5)	31.12(8)
C(22)-H(22C)	0.88(3)	C(2)-Y-C(5)	50.02(9)
C(23)-H(23A)	0.95(3)	C(10)-Y-C(5)	108.92(9)
C(23)-H(23B)	0.93(3)	C(6)-Y-C(5)	108.58(9)
C(23)-H(23C)	0.92(3)	C(9)-Y-C(7)	51.90(8)
C(24)-H(24A)	0.93(3)	C(3)-Y-C(7)	134.36(8)
C(24)-H(24B)	0.96(3)	C(8)-Y-C(7)	31.16(8)
C(24)-H(24C)	0.94(3)	C(4)-Y-C(7)	158.97(8)
		C(2)-Y-C(7)	109.02(9)
C(61)-C(62)	1.380(4)	C(10)-Y-C(7)	51.10(8)
C(61)-C(66)	1.380(4)	C(6)-Y-C(7)	30.66(8)
C(61)-H(61)	0.91(3)	C(5)-Y-C(7)	133.29(8)
C(62)-C(63)	1.377(4)	C(9)-Y-C(1)	139.90(8)
C(62)-H(62)	0.90(3)	C(3)-Y-C(1)	51.42(8)
C(63)-C(64)	1.383(4)	C(8)-Y-C(1)	139.46(8)
C(63)-H(63)	0.86(3)	C(4)-Y-C(1)	51.37(8)
C(64)-C(65)	1.376(4)	C(2)-Y-C(1)	30.31(8)
C(64)-H(64)	0.92(3)	C(10)-Y-C(1)	108.72(9)
C(65)-C(66)	1.378(4)	C(6)-Y-C(1)	93.12(9)
C(65)-H(65)	0.91(3)	C(5)-Y-C(1)	30.36(8)
C(66)-H(66)	0.90(3)	C(7)-Y-C(1)	108.32(9)
		C(9)-Y-H	92.0(6)
		C(3)-Y-H	78.2(6)
Cent2-Y-Cent1	146.24(3)	C(8)-Y-H	74.0(6)
Pln2-Y-Pln1	151.7(1)	C(4)-Y-H	96.2(6)
C(9)-Y-C(3)	168.20(8)	C(2)-Y-H	96.5(6)
C(9)-Y-C(8)	32.24(8)	C(10)-Y-H	122.5(6)
C(3)-Y-C(8)	145.69(8)	C(6)-Y-H	122.8(6)
C(9)-Y-C(4)	145.98(8)	C(5)-Y-H	126.5(6)
C(3)-Y-C(4)	31.80(8)	C(7)-Y-H	93.1(6)
C(8)-Y-C(4)	168.58(8)	C(1)-Y-H	126.4(6)
C(9)-Y-C(2)	159.65(8)	C(3)-Si(1)-C(9)^{i}	105.27(12)
C(3)-Y-C(2)	31.03(8)	C(3)-Si(1)-C(21)	109.13(13)
C(8)-Y-C(2)	134.44(8)	C(9)^{i}-Si(1)-C(21)	117.71(13)

C(3)-Si(1)-C(22)	110.11(13)	C(8)-C(7)-Y	72.33(14)
C(9)^{i}-Si(1)-C(22)	107.79(13)	C(18)-C(7)-Y	123.34(16)
C(21)-Si(1)-C(22)	106.75(14)	C(7)-C(8)-C(9)	107.1(2)
C(4)^{i}-Si(2)-C(24)	109.88(13)	C(7)-C(8)-Si(2)	129.40(19)
C(4)^{i}-Si(2)-C(8)	105.75(12)	C(9)-C(8)-Si(2)	123.36(19)
C(24)-Si(2)-C(8)	117.07(13)	C(7)-C(8)-Y	76.52(14)
C(4)^{i}-Si(2)-C(23)	109.98(12)	C(9)-C(8)-Y	73.36(14)
C(24)-Si(2)-C(23)	104.61(15)	Si(2)-C(8)-Y	119.05(11)
C(8)-Si(2)-C(23)	109.52(12)	C(10)-C(9)-C(8)	107.7(2)
C(2)-C(1)-C(5)	105.5(2)	C(10)-C(9)-Si(1)^{i}	129.22(19)
C(2)-C(1)-C(11)	127.2(2)	C(8)-C(9)-Si(1)^{i}	122.70(19)
C(5)-C(1)-C(11)	126.3(2)	C(10)-C(9)-Y	76.55(14)
C(2)-C(1)-Y	71.73(15)	C(8)-C(9)-Y	74.40(14)
C(5)-C(1)-Y	72.28(15)	Si(1)^{i}-C(9)-Y	120.33(11)
C(11)-C(1)-Y	129.54(17)	C(6)-C(10)-C(9)	107.9(2)
C(3)-C(2)-C(1)	110.8(2)	C(6)-C(10)-C(15)	126.8(2)
C(3)-C(2)-Y	72.83(15)	C(9)-C(10)-C(15)	125.3(2)
C(1)-C(2)-Y	77.97(15)	C(6)-C(10)-Y	75.03(15)
C(3)-C(2)-H(2)	126.0(17)	C(9)-C(10)-Y	72.24(14)
C(1)-C(2)-H(2)	123.2(17)	C(15)-C(10)-Y	121.54(16)
Y-C(2)-H(2)	117.5(17)	C(1)-C(11)-C(13)	111.6(2)
C(2)-C(3)-C(4)	106.6(2)	C(1)-C(11)-C(14)	111.4(2)
C(2)-C(3)-Si(1)	129.41(19)	C(13)-C(11)-C(14)	108.9(2)
C(4)-C(3)-Si(1)	123.89(19)	C(1)-C(11)-C(12)	108.1(2)
C(2)-C(3)-Y	76.15(15)	C(13)-C(11)-C(12)	108.0(2)
C(4)-C(3)-Y	74.32(14)	C(14)-C(11)-C(12)	108.8(2)
Si(1)-C(3)-Y	117.66(11)	C(11)-C(12)-H(12A)	110.1(15)
C(5)-C(4)-C(3)	107.0(2)	C(11)-C(12)-H(12B)	107.6(16)
C(5)-C(4)-Si(2)^{i}	129.6(2)	H(12A)-C(12)-H(12B)	109(2)
C(3)-C(4)-Si(2)^{i}	123.37(19)	C(11)-C(12)-H(12C)	112.9(15)
C(5)-C(4)-Y	76.43(15)	H(12A)-C(12)-H(12C)	107(2)
C(3)-C(4)-Y	73.88(14)	H(12B)-C(12)-H(12C)	110(2)
Si(2)^{i}-C(4)-Y	116.23(11)	C(11)-C(13)-H(13A)	112.1(14)
C(1)-C(5)-C(4)	110.0(2)	C(11)-C(13)-H(13B)	111.2(15)
C(1)-C(5)-Y	77.36(15)	H(13A)-C(13)-H(13B)	109(2)
C(4)-C(5)-Y	72.46(15)	C(11)-C(13)-H(13C)	111.1(14)
C(1)-C(5)-H(5)	124.2(15)	H(13A)-C(13)-H(13C)	105(2)
C(4)-C(5)-H(5)	125.8(15)	H(13B)-C(13)-H(13C)	108(2)
Y-C(5)-H(5)	118.4(15)	C(11)-C(14)-H(14A)	109.2(15)
C(10)-C(6)-C(7)	109.4(2)	C(11)-C(14)-H(14B)	110.5(16)
C(10)-C(6)-Y	74.38(15)	H(14A)-C(14)-H(14B)	107(2)
C(7)-C(6)-Y	74.83(15)	C(11)-C(14)-H(14C)	113.2(14)
C(10)-C(6)-H(6)	126.5(15)	H(14A)-C(14)-H(14C)	107(2)
C(7)-C(6)-H(6)	123.8(15)	H(14B)-C(14)-H(14C)	110(2)
Y-C(6)-H(6)	122.2(15)	C(10)-C(15)-C(16)	112.5(2)
C(6)-C(7)-C(8)	107.9(2)	C(10)-C(15)-C(17)	113.1(2)
C(6)-C(7)-C(18)	126.8(2)	C(16)-C(15)-C(17)	110.1(2)
C(8)-C(7)-C(18)	125.1(2)	C(10)-C(15)-H(15)	106.6(15)
C(6)-C(7)-Y	74.51(14)	C(16)-C(15)-H(15)	106.1(15)

C(17)-C(15)-H(15)	108.0(15)	Si(1)-C(22)-H(22A)	110.2(17)
C(15)-C(16)-H(16A)	111.7(15)	Si(1)-C(22)-H(22B)	115.3(18)
C(15)-C(16)-H(16B)	115.4(15)	H(22A)-C(22)-H(22B)	104(2)
H(16A)-C(16)-H(16B)	109(2)	Si(1)-C(22)-H(22C)	115(2)
C(15)-C(16)-H(16C)	111.0(17)	H(22A)-C(22)-H(22C)	106(2)
H(16A)-C(16)-H(16C)	105(2)	H(22B)-C(22)-H(22C)	105(3)
H(16B)-C(16)-H(16C)	104(2)	Si(2)-C(23)-H(23A)	111.6(17)
C(15)-C(17)-H(17A)	112.3(18)	Si(2)-C(23)-H(23B)	106.8(19)
C(15)-C(17)-H(17B)	111.7(14)	H(23A)-C(23)-H(23B)	110(2)
H(17A)-C(17)-H(17B)	107(2)	Si(2)-C(23)-H(23C)	111.4(18)
C(15)-C(17)-H(17C)	113.3(17)	H(23A)-C(23)-H(23C)	107(2)
H(17A)-C(17)-H(17C)	105(2)	H(23B)-C(23)-H(23C)	111(2)
H(17B)-C(17)-H(17C)	107(2)	Si(2)-C(24)-H(24A)	105.8(17)
C(7)-C(18)-C(20)	113.1(2)	Si(2)-C(24)-H(24B)	114.1(16)
C(7)-C(18)-C(19)	111.8(2)	H(24A)-C(24)-H(24B)	109(2)
C(20)-C(18)-C(19)	110.5(2)	Si(2)-C(24)-H(24C)	109.8(18)
C(7)-C(18)-H(18)	106.6(15)	H(24A)-C(24)-H(24C)	110(2)
C(20)-C(18)-H(18)	107.5(15)	H(24B)-C(24)-H(24C)	108(2)
C(19)-C(18)-H(18)	106.9(15)		
C(18)-C(19)-H(19A)	111.0(15)	C(62)-C(61)-C(66)	119.8(3)
C(18)-C(19)-H(19B)	112.9(14)	C(62)-C(61)-H(61)	119.3(18)
H(19A)-C(19)-H(19B)	103(2)	C(66)-C(61)-H(61)	120.9(18)
C(18)-C(19)-H(19C)	109.2(15)	C(63)-C(62)-C(61)	120.0(3)
H(19A)-C(19)-H(19C)	112(2)	C(63)-C(62)-H(62)	121.4(19)
H(19B)-C(19)-H(19C)	108(2)	C(61)-C(62)-H(62)	118.6(19)
C(18)-C(20)-H(20A)	110.0(16)	C(62)-C(63)-C(64)	120.2(3)
C(18)-C(20)-H(20B)	111.6(15)	C(62)-C(63)-H(63)	122.3(19)
H(20A)-C(20)-H(20B)	107(2)	C(64)-C(63)-H(63)	117.5(19)
C(18)-C(20)-H(20C)	111.5(17)	C(65)-C(64)-C(63)	119.8(3)
H(20A)-C(20)-H(20C)	110(2)	C(65)-C(64)-H(64)	121.6(17)
H(20B)-C(20)-H(20C)	106(2)	C(63)-C(64)-H(64)	118.6(17)
Si(1)-C(21)-H(21A)	112.3(16)	C(64)-C(65)-C(66)	120.1(3)
Si(1)-C(21)-H(21B)	109.0(15)	C(64)-C(65)-H(65)	118.9(17)
H(21A)-C(21)-H(21B)	110(2)	C(66)-C(65)-H(65)	120.9(17)
Si(1)-C(21)-H(21C)	112.3(15)	C(65)-C(66)-C(61)	120.2(3)
H(21A)-C(21)-H(21C)	109(2)	C(65)-C(66)-H(66)	116.8(17)
H(21B)-C(21)-H(21C)	104(2)	C(61)-C(66)-H(66)	123.0(17)

Symmetry transformations used to generate equivalent atoms:
(i),-x,-y,-z

Cent1 is the centroid formed by C1, C2, C3, C4 and C5.
Cent2 is the centroid formed by C6, C7, C8, C9 and C10.
Pln1 is the plane formed by C1, C2, C3, C4 and C5.
Pln2 is the plane formed by C6, C7, C8, C9 and C10.

Table 7. Crystal Data and Structure Analysis Details for dlz4 – $[(Me_2Si)_2(4\text{-}CMe_3\text{-}C_5H_2)(3,5\text{-}CMe_2H\text{-}C_5H_1)]Sc(\mu\text{-}Me)_2AlMe_2$.

Empirical formula	$C_{28}H_{50}AlScSi_2$	
Formula weight	514.80	
Crystallization Solvent	toluene	
Crystal Habit	fragment	
Crystal size	0.41 x 0.28 x 0.09 mm^3	
Crystal color	colorless	
Data Collection		
Preliminary Photos	none	
Type of diffractometer	CAD-4	
Wavelength	0.71073 Å MoKα	
Data Collection Temperature	85 K	
Theta range for reflections used in lattice determination	10.9 to 16.8°	
Unit cell dimensions	a = 10.960(3) Å b = 11.033(5) Å c = 12.835(8) Å	α= 96.39(4)° β= 104.22(4)° γ = 94.01(3)°
Volume	1487.5(12) $Å^3$	
Z	2	
Crystal system	triclinic	
Space group	$P\bar{1}$	
Density (calculated)	1.149 mg/m^3	
F(000)	560	
Theta range for data collection	1.65 to 25.0°	
Completeness to θ = 25.00°	100.0 %	
Index ranges	$-13 \le h \le 12$, $-13 \le k \le 13$, $-15 \le l \le 14$	
Data collection scan type	ω scans	
Reflections collected	11200	
Independent reflections	5212 [R_{int}= 0.021; GOF_{merge}= 1.06]	
Absorption coefficient	0.371 mm^{-1}	
Absorption correction	none	
Number of standards	3 reflections measured every 75 min.	
Variation of standards	within counting statistics, zero %.	
Structure solution and Refinement		
Structure solution program	SHELXS-97 (Sheldrick, 1990)	

Primary solution method	Direct methods
Secondary solution method	All heavy atoms in initial solution
Hydrogen placement	Difference Fourier map
Structure refinement program	SHELXL-97 (Sheldrick, 1997)
Refinement method	Full matrix least-squares on F^2
Data / restraints / parameters	5212 / 0 / 489
Treatment of hydrogen atoms	unrestrained
Goodness-of-fit on F^2	1.725
Final R indices [I>2σ(I)]	R1 = 0.0305, wR2 = 0.0646
R indices (all data)	R1 = 0.0387, wR2 = 0.0664
Type of weighting scheme used	sigma
Weighting scheme used	$w=1/[\sigma^2(Fo^2)$
Max shift/error	0.001
Average shift/error	0.000
Largest diff. peak and hole	0.336 and -0.213 e.$Å^{-3}$

Special Refinement Details

Inspection of the structural geometry and the bond distances would suggest that the methyl groups (C25, C26, C27 & C28) are bonded to the aluminum atom. Methyl groups C(25) and C(26), those closest to scandium, are approximately 0.4Å further from the scandium than would be expected for a Sc-C single bond to an alkyl (See Table 3, Figures 5 and 6). This would suggest they are not strongly bond to scandium. However, the hydrogen atoms H(25C) and H(26C) are at a distance from scandium that would suggest a bonding interaction (See Table 3, Figures 5 and 6).

The variances [$\sigma^2(Fo^2)$] were derived from counting statistics plus an additional term, $(0.014I)^2$, and the variances of the merged data were obtained by propagation of error plus the addition of another term, $(0.014<I>)^2$.

Refinement of F^2 against ALL reflections. The weighted R-factor (wR) and goodness of fit (S) are based on F^2, conventional R-factors (R) are based on F, with F set to zero for negative F^2. The threshold expression of $F^2 > 2\sigma(F^2)$ is used only for calculating R-factors(gt) etc. and is not relevant to the choice of reflections for refinement. R-factors based on F^2 are statistically about twice as large as those based on F, and R-factors based on ALL data will be even larger.

All esds (except the esd in the dihedral angle between two l.s. planes) are estimated using the full covariance matrix. The cell esds are taken into account individually in the estimation of esds in distances, angles and torsion angles; correlations between esds in cell parameters are only used when they are defined

by crystal symmetry. An approximate (isotropic) treatment of cell esds is used for estimating esds involving l.s. planes.

Table 8. Selected bond lengths [Å] and angles [°] for dlz4 – $[(Me_2Si)_2(4\text{-}CMe_3\text{-}C_5H_2)(3,5\text{-}CMe_2H\text{-}C_5H_1)]Sc(\mu\text{-}Me)_2AlMe_2$.

Pln1-Sc	2.213(1)	Cent1-Sc	2.239(1)
Pln2-Sc	2.195(1)	Cent2-Sc	2.233(1)
Sc-Al	2.9179(14)	Al-C(27)	1.971(2)
Sc-C(26)	2.414(2)	Al-C(28)	1.970(2)
Sc-C(25)	2.442(2)	Al-C(25)	2.081(2)
Sc-H(26C)	2.21(2)	Al-C(26)	2.087(2)
Sc-H(25C)	2.19(2)		

Angles around Sc		Angles around Al	
Pln1-Sc-Pln2	104.32(7)	C(27)-Al-C(28)	111.13(10)
Cent1-Sc-Cent2	123.53(3)	C(27)-Al-C(25)	109.69(10)
C(26)-Sc-C(25)	88.48(8)	C(28)-Al-C(25)	110.14(9)
H(25C)-Sc-H(26C)	131.4(9)	C(27)-Al-C(26)	113.52(10)
		C(28)-Al-C(26)	103.45(10)
		C(25)-Al-C(26)	108.73(9)

Angles around C(25)

Al-C(25)-Sc	79.92(7)		
Al-C(25)-H(25A)	112(1)	Sc-C(25)-H(25A)	107(1)
Al-C(25)-H(25B)	90(1)	Sc-C(25)-H(25B)	146(2)
Al-C(25)-H(25C)	134(1)	Sc-C(25)-H(25C)	63(2)

Angles around C(26)

Al-C(26)-Sc	80.47(7)		
Al-C(26)-H(26A)	108(1)	Sc-C(26)-H(26A)	106(1)
Al-C(26)-H(26B)	90(1)	Sc-C(26)-H(26B)	145(1)
Al-C(26)-H(26C)	139(1)	Sc-C(26)-H(26C)	67(1)

Cent1 is the centroid formed by C1, C2, C3, C4 and C5.
Cent2 is the centroid formed by C6, C7, C8, C9 and C10.
Pln1 is the plane formed by C1, C2, C3, C4 and C5.
Pln2 is the plane formed by C6, C7, C8, C9 and C10.

Table 9. Bond lengths [Å] and angles [°] for dlz4 – $[(Me_2Si)_2(4\text{-}CMe_3\text{-}C_5H_2)(3,5\text{-}CMe_2H\text{-}C_5H_1)]Sc(\mu\text{-}Me)_2AlMe_2$.

Pln1-Sc	2.2134(1)	C(11)-C(12)	1.530(3)
Pln2-Sc	2.1950(14)	C(12)-H(12A)	0.96(2)
Cent1-Sc	2.2387(1)	C(12)-H(12B)	0.96(3)
Cent2-Sc	2.2331(10)	C(12)-H(12C)	0.91(2)
Sc-C(9)	2.3759(18)	C(13)-H(13A)	0.98(2)
Sc-C(8)	2.381(2)	C(13)-H(13B)	0.94(2)
Sc-C(26)	2.414(2)	C(13)-H(13C)	0.96(2)
Sc-C(3)	2.417(2)	C(14)-H(14A)	0.97(3)
Sc-C(4)	2.423(2)	C(14)-H(14B)	1.02(3)
Sc-C(25)	2.442(2)	C(14)-H(14C)	0.96(2)
Sc-C(2)	2.575(2)	C(15)-C(17)	1.522(3)
Sc-C(5)	2.583(2)	C(15)-C(16)	1.530(3)
Sc-C(10)	2.6117(19)	C(15)-H(15)	0.977(18)
Sc-C(7)	2.619(2)	C(16)-H(16A)	0.94(2)
Sc-C(6)	2.704(2)	C(16)-H(16B)	0.99(2)
Sc-C(1)	2.715(2)	C(16)-H(16C)	0.98(2)
Si(1)-C(22)	1.862(2)	C(17)-H(17A)	0.96(2)
Si(1)-C(3)	1.864(2)	C(17)-H(17B)	0.94(2)
Si(1)-C(21)	1.872(2)	C(17)-H(17C)	0.92(2)
Si(1)-C(8)	1.882(2)	C(18)-C(20)	1.523(3)
Si(2)-C(23)	1.852(2)	C(18)-C(19)	1.530(3)
Si(2)-C(24)	1.866(2)	C(18)-H(18)	0.971(18)
Si(2)-C(4)	1.8729(19)	C(19)-H(19A)	0.96(2)
Si(2)-C(9)	1.878(2)	C(19)-H(19B)	0.96(2)
Al-C(27)	1.971(2)	C(19)-H(19C)	0.95(2)
Al-C(28)	1.970(2)	C(20)-H(20A)	0.92(2)
Al-C(25)	2.081(2)	C(20)-H(20B)	0.95(2)
Al-C(26)	2.087(2)	C(20)-H(20C)	0.97(2)
C(1)-C(5)	1.414(2)	C(21)-H(21A)	1.01(2)
C(1)-C(2)	1.416(3)	C(21)-H(21B)	0.94(2)
C(1)-C(11)	1.528(2)	C(21)-H(21C)	0.93(2)
C(2)-C(3)	1.424(2)	C(22)-H(22A)	0.89(3)
C(2)-H(2)	0.969(19)	C(22)-H(22B)	0.94(3)
C(3)-C(4)	1.443(3)	C(22)-H(22C)	0.92(3)
C(4)-C(5)	1.420(3)	C(23)-H(23A)	0.95(3)
C(5)-H(5)	0.898(18)	C(23)-H(23B)	0.93(2)
C(6)-C(7)	1.407(3)	C(23)-H(23C)	0.89(2)
C(6)-C(10)	1.410(3)	C(24)-H(24A)	0.95(2)
C(6)-H(6)	0.903(18)	C(24)-H(24B)	0.96(2)
C(7)-C(8)	1.430(3)	C(24)-H(24C)	0.95(2)
C(7)-C(15)	1.519(3)	C(25)-H(25A)	0.99(2)
C(8)-C(9)	1.471(2)	C(25)-H(25B)	0.84(3)
C(9)-C(10)	1.419(2)	C(25)-H(25C)	0.92(3)
C(10)-C(18)	1.521(3)	C(26)-H(26A)	1.00(2)
C(11)-C(14)	1.517(3)	C(26)-H(26B)	0.93(2)
C(11)-C(13)	1.521(3)	C(26)-H(26C)	0.98(2)

C(27)-H(27A)	0.90(3)
C(27)-H(27B)	0.87(3)
C(27)-H(27C)	0.85(3)
C(28)-H(28A)	0.95(2)
C(28)-H(28B)	0.93(3)
C(28)-H(28C)	0.93(3)
Pln1-Sc-Pln2	104.32(7)
Cent1-Sc-Cent2	123.53(3)
C(9)-Sc-C(8)	36.02(6)
C(9)-Sc-C(26)	107.45(7)
C(8)-Sc-C(26)	138.07(7)
C(9)-Sc-C(3)	80.79(7)
C(8)-Sc-C(3)	69.51(7)
C(26)-Sc-C(3)	139.32(7)
C(9)-Sc-C(4)	69.24(7)
C(8)-Sc-C(4)	79.88(7)
C(26)-Sc-C(4)	109.71(7)
C(3)-Sc-C(4)	34.68(6)
C(9)-Sc-C(25)	139.82(7)
C(8)-Sc-C(25)	110.22(8)
C(26)-Sc-C(25)	88.48(8)
C(3)-Sc-C(25)	111.03(7)
C(4)-Sc-C(25)	140.31(7)
C(9)-Sc-C(2)	113.73(7)
C(8)-Sc-C(2)	97.55(7)
C(26)-Sc-C(2)	121.74(7)
C(3)-Sc-C(2)	32.95(6)
C(4)-Sc-C(2)	54.74(6)
C(25)-Sc-C(2)	85.61(7)
C(9)-Sc-C(5)	96.55(7)
C(8)-Sc-C(5)	112.65(7)
C(26)-Sc-C(5)	84.78(7)
C(3)-Sc-C(5)	54.55(7)
C(4)-Sc-C(5)	32.77(6)
C(25)-Sc-C(5)	121.98(7)
C(2)-Sc-C(5)	52.00(7)
C(9)-Sc-C(10)	32.63(6)
C(8)-Sc-C(10)	55.33(6)
C(26)-Sc-C(10)	82.76(7)
C(3)-Sc-C(10)	113.41(6)
C(4)-Sc-C(10)	97.33(7)
C(25)-Sc-C(10)	120.34(7)
C(2)-Sc-C(10)	146.36(6)
C(5)-Sc-C(10)	115.77(7)
C(9)-Sc-C(7)	55.27(7)
C(8)-Sc-C(7)	32.79(6)
C(26)-Sc-C(7)	120.28(7)
C(3)-Sc-C(7)	97.50(7)
C(4)-Sc-C(7)	112.66(7)
C(25)-Sc-C(7)	84.72(7)
C(2)-Sc-C(7)	116.74(7)
C(5)-Sc-C(7)	145.43(6)
C(10)-Sc-C(7)	52.21(6)
C(9)-Sc-C(6)	53.17(6)
C(8)-Sc-C(6)	53.27(6)
C(26)-Sc-C(6)	90.67(7)
C(3)-Sc-C(6)	122.77(6)
C(4)-Sc-C(6)	122.38(7)
C(25)-Sc-C(6)	91.13(7)
C(2)-Sc-C(6)	147.25(6)
C(5)-Sc-C(6)	146.33(6)
C(10)-Sc-C(6)	30.70(6)
C(7)-Sc-C(6)	30.61(6)
C(9)-Sc-C(1)	122.75(6)
C(8)-Sc-C(1)	123.04(6)
C(26)-Sc-C(1)	91.87(7)
C(3)-Sc-C(1)	53.54(6)
C(4)-Sc-C(1)	53.51(6)
C(25)-Sc-C(1)	92.31(7)
C(2)-Sc-C(1)	30.90(6)
C(5)-Sc-C(1)	30.83(6)
C(10)-Sc-C(1)	146.57(6)
C(7)-Sc-C(1)	147.53(6)
C(6)-Sc-C(1)	175.78(5)
C(9)-Sc-H(25C)	122.7(7)
C(8)-Sc-H(25C)	89.4(7)
C(26)-Sc-H(25C)	109.6(7)
C(3)-Sc-H(25C)	97.3(7)
C(4)-Sc-H(25C)	131.4(7)
C(25)-Sc-H(25C)	22.2(7)
C(2)-Sc-H(25C)	80.5(7)
C(5)-Sc-H(25C)	128.6(7)
C(10)-Sc-H(25C)	114.9(7)
C(7)-Sc-H(25C)	68.6(7)
C(6)-Sc-H(25C)	84.3(7)
C(1)-Sc-H(25C)	98.0(7)
C(9)-Sc-H(26C)	85.3(6)
C(8)-Sc-H(26C)	119.6(5)
C(26)-Sc-H(26C)	23.9(5)
C(3)-Sc-H(26C)	128.1(5)
C(4)-Sc-H(26C)	93.8(5)
C(25)-Sc-H(26C)	111.6(5)
C(2)-Sc-H(26C)	127.0(5)
C(5)-Sc-H(26C)	78.1(5)
C(10)-Sc-H(26C)	66.4(5)
C(7)-Sc-H(26C)	114.6(5)
C(6)-Sc-H(26C)	84.4(5)

C(1)-Sc-H(26C)	96.6(5)
H(25C)-Sc-H(26C)	131.4(9)
C(22)-Si(1)-C(3)	114.79(10)
C(22)-Si(1)-C(21)	107.25(11)
C(3)-Si(1)-C(21)	108.98(10)
C(22)-Si(1)-C(8)	116.43(10)
C(3)-Si(1)-C(8)	93.83(9)
C(21)-Si(1)-C(8)	115.12(10)
C(22)-Si(1)-Sc	146.90(8)
C(3)-Si(1)-Sc	49.92(6)
C(21)-Si(1)-Sc	105.74(8)
C(8)-Si(1)-Sc	48.85(6)
C(23)-Si(2)-C(24)	105.99(10)
C(23)-Si(2)-C(4)	120.56(9)
C(24)-Si(2)-C(4)	106.91(9)
C(23)-Si(2)-C(9)	114.15(9)
C(24)-Si(2)-C(9)	116.00(9)
C(4)-Si(2)-C(9)	93.26(8)
C(23)-Si(2)-Sc	149.60(7)
C(24)-Si(2)-Sc	104.36(8)
C(4)-Si(2)-Sc	49.91(6)
C(9)-Si(2)-Sc	48.48(6)
C(27)-Al-C(28)	111.13(10)
C(27)-Al-C(25)	109.69(10)
C(28)-Al-C(25)	110.14(9)
C(27)-Al-C(26)	113.52(10)
C(28)-Al-C(26)	103.45(10)
C(25)-Al-C(26)	108.73(9)
C(27)-Al-Sc	118.51(8)
C(28)-Al-Sc	130.29(7)
C(25)-Al-Sc	55.47(6)
C(26)-Al-Sc	54.67(6)
C(5)-C(1)-C(2)	106.06(16)
C(5)-C(1)-C(11)	126.35(16)
C(2)-C(1)-C(11)	126.50(16)
C(5)-C(1)-Sc	69.41(10)
C(2)-C(1)-Sc	69.05(10)
C(11)-C(1)-Sc	135.25(12)
C(1)-C(2)-C(3)	110.09(16)
C(1)-C(2)-Sc	80.05(11)
C(3)-C(2)-Sc	67.44(10)
C(1)-C(2)-H(2)	124.5(11)
C(3)-C(2)-H(2)	125.4(11)
Sc-C(2)-H(2)	121.3(11)
C(2)-C(3)-C(4)	106.80(15)
C(2)-C(3)-Si(1)	127.13(14)
C(4)-C(3)-Si(1)	121.31(13)
C(2)-C(3)-Sc	79.60(11)
C(4)-C(3)-Sc	72.87(10)
Si(1)-C(3)-Sc	93.92(8)
C(5)-C(4)-C(3)	106.63(15)
C(5)-C(4)-Si(2)	124.80(13)
C(3)-C(4)-Si(2)	123.62(13)
C(5)-C(4)-Sc	79.82(11)
C(3)-C(4)-Sc	72.45(10)
Si(2)-C(4)-Sc	93.83(8)
C(1)-C(5)-C(4)	110.41(16)
C(1)-C(5)-Sc	79.76(11)
C(4)-C(5)-Sc	67.41(10)
C(1)-C(5)-H(5)	125.2(11)
C(4)-C(5)-H(5)	124.4(11)
Sc-C(5)-H(5)	119.5(11)
C(7)-C(6)-C(10)	109.59(16)
C(7)-C(6)-Sc	71.38(10)
C(10)-C(6)-Sc	71.05(10)
C(7)-C(6)-H(6)	125.4(12)
C(10)-C(6)-H(6)	124.9(12)
Sc-C(6)-H(6)	127.4(11)
C(6)-C(7)-C(8)	108.16(16)
C(6)-C(7)-C(15)	125.34(16)
C(8)-C(7)-C(15)	126.10(16)
C(6)-C(7)-Sc	78.01(11)
C(8)-C(7)-Sc	64.41(10)
C(15)-C(7)-Sc	128.63(12)
C(7)-C(8)-C(9)	106.68(15)
C(7)-C(8)-Si(1)	127.79(13)
C(9)-C(8)-Si(1)	122.00(13)
C(7)-C(8)-Sc	82.80(11)
C(9)-C(8)-Sc	71.80(10)
Si(1)-C(8)-Sc	94.64(8)
C(10)-C(9)-C(8)	107.23(15)
C(10)-C(9)-Si(2)	128.14(13)
C(8)-C(9)-Si(2)	121.48(13)
C(10)-C(9)-Sc	82.86(10)
C(8)-C(9)-Sc	72.18(10)
Si(2)-C(9)-Sc	95.23(8)
C(6)-C(10)-C(9)	108.23(16)
C(6)-C(10)-C(18)	126.01(16)
C(9)-C(10)-C(18)	125.44(16)
C(6)-C(10)-Sc	78.25(11)
C(9)-C(10)-Sc	64.51(9)
C(18)-C(10)-Sc	127.67(12)
C(14)-C(11)-C(13)	108.91(18)
C(14)-C(11)-C(1)	111.47(16)
C(13)-C(11)-C(1)	111.52(16)
C(14)-C(11)-C(12)	108.89(19)
C(13)-C(11)-C(12)	108.18(19)
C(1)-C(11)-C(12)	107.78(16)

C(11)-C(12)-H(12A)	109.9(13)
C(11)-C(12)-H(12B)	111.7(15)
H(12A)-C(12)-H(12B)	111(2)
C(11)-C(12)-H(12C)	108.9(14)
H(12A)-C(12)-H(12C)	108.3(19)
H(12B)-C(12)-H(12C)	107(2)
C(11)-C(13)-H(13A)	111.1(13)
C(11)-C(13)-H(13B)	111.5(14)
H(13A)-C(13)-H(13B)	106.7(19)
C(11)-C(13)-H(13C)	109.2(12)
H(13A)-C(13)-H(13C)	110.3(18)
H(13B)-C(13)-H(13C)	108.1(18)
C(11)-C(14)-H(14A)	111.1(14)
C(11)-C(14)-H(14B)	112.7(14)
H(14A)-C(14)-H(14B)	107(2)
C(11)-C(14)-H(14C)	109.3(13)
H(14A)-C(14)-H(14C)	108.8(19)
H(14B)-C(14)-H(14C)	107.9(19)
C(7)-C(15)-C(17)	112.87(16)
C(7)-C(15)-C(16)	109.13(16)
C(17)-C(15)-C(16)	109.76(17)
C(7)-C(15)-H(15)	110.1(11)
C(17)-C(15)-H(15)	107.3(11)
C(16)-C(15)-H(15)	107.5(11)
C(15)-C(16)-H(16A)	111.7(12)
C(15)-C(16)-H(16B)	110.3(13)
H(16A)-C(16)-H(16B)	106.3(17)
C(15)-C(16)-H(16C)	108.5(13)
H(16A)-C(16)-H(16C)	111.1(18)
H(16B)-C(16)-H(16C)	108.9(18)
C(15)-C(17)-H(17A)	109.7(12)
C(15)-C(17)-H(17B)	112.4(12)
H(17A)-C(17)-H(17B)	107.9(16)
C(15)-C(17)-H(17C)	110.6(13)
H(17A)-C(17)-H(17C)	107.6(17)
H(17B)-C(17)-H(17C)	108.5(17)
C(10)-C(18)-C(20)	113.11(16)
C(10)-C(18)-C(19)	109.39(15)
C(20)-C(18)-C(19)	109.71(16)
C(10)-C(18)-H(18)	107.7(11)
C(20)-C(18)-H(18)	108.2(10)
C(19)-C(18)-H(18)	108.6(10)
C(18)-C(19)-H(19A)	109.2(12)
C(18)-C(19)-H(19B)	111.1(12)
H(19A)-C(19)-H(19B)	106.6(17)
C(18)-C(19)-H(19C)	110.4(12)
H(19A)-C(19)-H(19C)	108.5(16)
H(19B)-C(19)-H(19C)	111.0(17)
C(18)-C(20)-H(20A)	111.3(12)
C(18)-C(20)-H(20B)	111.5(12)
H(20A)-C(20)-H(20B)	104.6(16)
C(18)-C(20)-H(20C)	113.3(12)
H(20A)-C(20)-H(20C)	103.9(16)
H(20B)-C(20)-H(20C)	111.7(16)
Si(1)-C(21)-H(21A)	113.4(11)
Si(1)-C(21)-H(21B)	110.3(13)
H(21A)-C(21)-H(21B)	108.1(16)
Si(1)-C(21)-H(21C)	106.2(14)
H(21A)-C(21)-H(21C)	107.9(17)
H(21B)-C(21)-H(21C)	110.9(19)
Si(1)-C(22)-H(22A)	108.3(16)
Si(1)-C(22)-H(22B)	109.4(14)
H(22A)-C(22)-H(22B)	111(2)
Si(1)-C(22)-H(22C)	113.2(16)
H(22A)-C(22)-H(22C)	109(2)
H(22B)-C(22)-H(22C)	106(2)
Si(2)-C(23)-H(23A)	113.7(14)
Si(2)-C(23)-H(23B)	113.7(13)
H(23A)-C(23)-H(23B)	109.0(19)
Si(2)-C(23)-H(23C)	106.4(15)
H(23A)-C(23)-H(23C)	105(2)
H(23B)-C(23)-H(23C)	108.6(19)
Si(2)-C(24)-H(24A)	110.2(12)
Si(2)-C(24)-H(24B)	114.6(12)
H(24A)-C(24)-H(24B)	107.8(17)
Si(2)-C(24)-H(24C)	106.8(14)
H(24A)-C(24)-H(24C)	110.3(18)
H(24B)-C(24)-H(24C)	107.0(18)
Al-C(25)-Sc	79.92(7)
Al-C(25)-H(25A)	111.8(13)
Sc-C(25)-H(25A)	106.6(13)
Al-C(25)-H(25B)	90.6(17)
Sc-C(25)-H(25B)	145.9(17)
H(25A)-C(25)-H(25B)	107(2)
Al-C(25)-H(25C)	134.1(16)
Sc-C(25)-H(25C)	63.3(15)
H(25A)-C(25)-H(25C)	105(2)
H(25B)-C(25)-H(25C)	105(2)
Al-C(26)-Sc	80.47(7)
Al-C(26)-H(26A)	107.9(11)
Sc-C(26)-H(26A)	106.3(12)
Al-C(26)-H(26B)	90.2(12)
Sc-C(26)-H(26B)	145.1(12)
H(26A)-C(26)-H(26B)	108.6(17)
Al-C(26)-H(26C)	139.0(12)
Sc-C(26)-H(26C)	66.6(12)
H(26A)-C(26)-H(26C)	104.4(16)
H(26B)-C(26)-H(26C)	102.8(17)

Al-C(27)-H(27A)	117(2)	Al-C(28)-H(28A)	112.4(13)
Al-C(27)-H(27B)	114(2)	Al-C(28)-H(28B)	109.8(15)
H(27A)-C(27)-H(27B)	100(3)	H(28A)-C(28)-H(28B)	103.8(19)
Al-C(27)-H(27C)	113(2)	Al-C(28)-H(28C)	115.5(16)
H(27A)-C(27)-H(27C)	102(3)	H(28A)-C(28)-H(28C)	108(2)
H(27B)-C(27)-H(27C)	109(3)	H(28B)-C(28)-H(28C)	107(2)

Cent1 is the centroid formed by C1, C2, C3, C4 and C5.
Cent2 is the centroid formed by C6, C7, C8, C9 and C10.
Pln1 is the plane formed by C1, C2, C3, C4 and C5.
Pln2 is the plane formed by C6, C7, C8, C9 and C10.

Table 10. Crystal Data and Structure Analysis Details for dlz5 – $[(Me_2Si)_2(4\text{-}CMe_3\text{-}C_5H_2)(3,5\text{-}CMe_2H\text{-}C_5H_1)]YCH(SiMe_3)_2$.

Empirical formula	$C_{31}H_{57}Si_4Y$	
Formula weight	631.04	
Crystallization solvent	toluene-d_8	
Crystal shape	six-sided plate	
Crystal color	colorless	
Crystal size	0.22 x 0.37 x 0.37 mm	
Data Collection		
Type of diffractometer	CAD-4	
Wavelength	0.71073 Å MoKα	
Data collection temperature	84 K	
Theta range for 25 reflections used in lattice determination	13 to 15°	
Unit cell dimensions	a = 16.262(4) Å b = 11.833(6) Å c = 17.978(9) Å	α= 90° β= 92.94(3)° γ = 90°
Volume	3455(3) $Å^3$	
Z	4	
Crystal system	monoclinic	
Space group	$P2_1/n$ (#14)	
Density (calculated)	1.213 g/cm^3	
F(000)	1352	
Theta range for data collection	1.5 to 25.0°	
Completeness to theta = 25.0°	100.0 %	
Index ranges	$-15 \le h \le 19, -14 \le k \le 14, -21 \le l \le 21$	

Data collection scan type	ω-scan
Reflections collected	20178
Independent reflections	6067 [R_{int}= 0.057; GOF_{merge}= 1.07]
Reflections > 2σ(I)	4766
Average σ(I)/(net I)	0.0533
Absorption coefficient	1.845 mm^{-1}
Absorption correction	ψ-scan
Max. and min. transmission	1.08 and 0.91
Number of standards	3 reflections measured every 75 min
Decay of standards	0.6%

Structure Solution and Refinement

Primary solution method	direct methods
Secondary solution method	difference map
Hydrogen placement	calculated
Refinement method	full-matrix least-squares on F^2
Data / restraints / parameters	6067 / 0 / 492
Treatment of hydrogen atoms	coordinates refined, U_{iso} fixed at 120% U_{eq} of attached atom
Goodness-of-fit on F^2	1.456
Final R indices [I>2σ(I), 4766 reflections]	R1 = 0.0416, wR2 = 0.0598
R indices (all data)	R1 = 0.0665, wR2 = 0.0640
Type of weighting scheme used	sigma
Weighting scheme used	$w=1/\sigma^2(Fo^2)$
Max shift/error	0.032
Average shift/error	0.001
Largest diff. peak and hole	0.406 and -0.390 e·$Å^{-3}$

Programs Used

Cell refinement	CAD-4 Software (Enraf-Nonius, 1989)
Data collection	CAD-4 Software (Enraf-Nonius, 1989)
Data reduction	CRYM (Duchamp, 1964)
Structure solution	Bruker SHELXTL v5.1
Structure refinement	Bruker SHELXTL v5.1

Special Refinement Details

A small colorless six-sided plate was mounted on a glass fiber with Paratone-N oil. Data were collected with 1.0° ω-scans. Data that agreed poorly in a preliminary merging were recollected. The individual backgrounds were replaced by a background function of 2θ derived from those reflections with $I < 3\sigma(I)$. The GOF_{merge} was 1.07 (6067 multiples) in point group 2/m; R_{merge} was 0.061 for 2233 duplicates with $F_o > 0$. Ψ–scan data were used for the absorption correction. There was 0.6% linear decay. No outlier reflections were omitted from the refinement. A power failure occurred during the collection of reflection number 17290, shutting down the diffractometer and cooling unit; however, this event seems to have had no significant effect on the crystal or data set quality.

Weights w are calculated as $1/\sigma^2(F_o^2)$; variances ($\sigma^2(F_o^2)$) were derived from counting statistics plus an additional term, $(0.014I)^2$; variances of the merged data were obtained by propagation of error plus another additional term, $(0.014<I>)^2$. The refinement of F^2 is as always against all reflections. The weighted R-factor wR and goodness of fit S are based on F^2, conventional R-factors R are based on F, with F set to zero for negative F^2. The threshold expression of $F^2 > 2\sigma(F^2)$ is used only for calculating R-factors(gt) etc. and is not relevant to the choice of reflections for refinement.

There is one molecule in the asymmetric unit.

During refinement two atoms, C25 and C26, exhibited elongated displacement ellipsoids indicating disorder. The central carbon of the $CH(SiMe_3)_2$ moiety, C25, exists in either of two conformations, with the H up or with the H down with respect to the wedge of the cyclopentadienyl rings. The inversion of the carbon primarily affects C26, a terminal methyl group, which can also be correspondingly down or up. Various models were tried which attempted to split both atoms into two sites each, ~0.6Å apart. None were very successful. The final model leaves the methyl carbon C26 as a single anisotropic atom and C25 split into C25A with a population of 0.719(11) with the hydrogen atom pointed towards the t-butyl group and C25B with a population of 0.281(11). Both partial atoms were refined isotropically with a single U_{iso}.

A more interesting feature of the structure is the interaction between the Y atom and a Si-C bond (Si4-C29). The disordered coordinated carbon C25 of the $CH(SiMe_3)_2$ moiety is shifted to one side of the wedge to allow the Si-C bond access to the Y atom.

Table 11. Bond lengths [Å] and angles [°] for dlz5 – $[(Me_2Si)_2(4\text{-}CMe_3\text{-}C_5H_2)(3,5\text{-}CMe_2H\text{-}C_5H_1)]YCH(SiMe_3)_2$.

Y-CpA [a]	2.394	Y···PlnA [b]	2.371(2)
Y-CpB [c]	2.386	Y···PlnB [d]	2.356(2)
Y-Cen [e]	2.806	Y-C6	2.534(3)

Y-C7	2.535(3)	C11-H11B	0.94(3)
Y-C1	2.549(3)	C11-H11C	0.95(3)
Y-C2	2.591(3)	C12-H12A	0.94(3)
Y-C4	2.842(3)	C12-H12B	0.95(3)
Y-C5	2.681(3)	C12-H12C	0.95(3)
Y-C3	2.737(3)	C13-H13A	0.98(3)
Y-C10	2.742(3)	C13-H13B	0.91(3)
Y-C8	2.743(3)	C13-H13C	0.83(3)
Y-C9	2.821(3)	C14-H14A	0.97(3)
Y-C25B	2.377(10)	C14-H14B	0.92(3)
Y-C25A	2.437(4)	C14-H14C	0.89(3)
Y-C29	2.751(4)	C15-C16	1.518(4)
Y···Si4	3.1673(16)	C15-C18	1.523(4)
Y···H29C	2.58(3)	C15-C17	1.534(4)
Si1-C11	1.859(3)	C16-H16A	1.00(3)
Si1-C12	1.864(3)	C16-H16B	0.99(3)
Si1-C1	1.869(3)	C16-H16C	0.97(3)
Si1-C6	1.889(3)	C17-H17A	0.94(3)
Si2-C13	1.847(3)	C17-H17B	1.00(3)
Si2-C14	1.862(3)	C17-H17C	0.95(3)
Si2-C2	1.874(3)	C18-H18A	1.04(3)
Si2-C7	1.878(3)	C18-H18B	0.98(3)
Si3-C25A	1.859(4)	C18-H18C	0.93(3)
Si3-C27	1.860(4)	C19-C21	1.524(4)
Si3-C26	1.865(4)	C19-C20	1.529(4)
Si3-C28	1.876(4)	C19-H19A	0.97(3)
Si3-C25B	1.888(11)	C20-H20A	0.96(3)
Si4-C25A	1.828(4)	C20-H20B	0.96(3)
Si4-C31	1.858(4)	C20-H20C	0.91(3)
Si4-C30	1.860(4)	C21-H21A	0.97(3)
Si4-C25B	1.882(11)	C21-H21B	0.95(3)
Si4-C29	1.922(3)	C21-H21C	0.91(3)
C1-C5	1.429(4)	C22-C24	1.517(4)
C1-C2	1.440(4)	C22-C23	1.527(4)
C2-C3	1.419(4)	C22-H22	0.93(3)
C3-C4	1.415(4)	C23-H23A	1.00(3)
C3-H3	0.90(3)	C23-H23B	0.88(3)
C4-C5	1.405(4)	C23-H23C	0.97(3)
C4-C15	1.521(4)	C24-H24A	0.98(3)
C5-H5	0.91(3)	C24-H24B	1.00(3)
C6-C10	1.437(4)	C24-H24C	0.95(3)
C6-C7	1.457(4)	C25A···C25B	0.63(1)
C7-C8	1.424(4)	C25A-H25A	0.9800
C8-C9	1.414(4)	C25B-H25B	0.9800
C8-C19	1.518(4)	C26-H26A	0.99(4)
C9-C10	1.408(4)	C26-H26B	0.99(4)
C9-H9	0.91(3)	C26-H26C	0.89(4)
C10-C22	1.514(4)	C27-H27A	0.94(3)
C11-H11A	0.91(3)	C27-H27B	0.93(3)

C27-H27C	0.90(3)
C28-H28A	0.88(3)
C28-H28B	0.99(3)
C28-H28C	0.96(3)
C29-H29A	0.90(3)
C29-H29B	0.94(3)
C29-H29C	1.00(3)
C30-H30A	0.94(3)
C30-H30B	0.94(3)
C30-H30C	0.91(3)
C31-H31A	0.92(3)
C31-H31B	0.87(3)
C31-H31C	0.98(3)

CpA-Y-CpB	116.1
CpA-Y-C25A	127.5
CpA-Y-C25B	113.2
CpB-Y-C25A	109.1
CpB-Y-C25B	123.6
CpA-Y-Cen	121.5
CpB-Y-Cen	115.3
Cen-Y-C25A	52.3
Cen-Y-C25B	52.4
PlnA-PlnB	80.7(1)
C25B-Y-C29	71.6(3)
C25A-Y-C29	72.15(12)
C11-Si1-C12	107.32(15)
C11-Si1-C1	109.24(14)
C12-Si1-C1	113.44(14)
C11-Si1-C6	115.14(14)
C12-Si1-C6	115.72(14)
C1-Si1-C6	95.65(12)
C13-Si2-C14	107.51(16)
C13-Si2-C2	119.13(14)
C14-Si2-C2	106.47(14)
C13-Si2-C7	112.79(14)
C14-Si2-C7	115.34(14)
C2-Si2-C7	95.48(12)
C25A-Si3-C27	118.7(3)
C25A-Si3-C26	111.3(2)
C27-Si3-C26	105.47(19)
C25A-Si3-C28	107.9(2)
C27-Si3-C28	106.47(18)
C26-Si3-C28	106.4(2)
C27-Si3-C25B	99.8(6)
C26-Si3-C25B	116.2(4)
C28-Si3-C25B	120.8(5)
C25A-Si4-C31	118.6(3)
C25A-Si4-C30	110.4(3)
C31-Si4-C30	108.0(2)
C31-Si4-C25B	103.5(5)
C30-Si4-C25B	129.3(6)
C25A-Si4-C29	109.62(17)
C31-Si4-C29	105.70(16)
C30-Si4-C29	103.42(16)
C25B-Si4-C29	104.9(4)
C5-C1-C2	106.7(2)
C5-C1-Si1	129.8(2)
C2-C1-Si1	119.7(2)
C3-C2-C1	106.3(2)
C3-C2-Si2	124.7(2)
C1-C2-Si2	124.2(2)
C4-C3-C2	110.8(2)
C4-C3-H3	122.1(17)
C2-C3-H3	127.1(17)
C5-C4-C3	105.8(2)
C5-C4-C15	127.9(3)
C3-C4-C15	125.2(2)
C4-C5-C1	110.3(2)
C4-C5-H5	124.3(17)
C1-C5-H5	125.2(17)
C10-C6-C7	106.7(2)
C10-C6-Si1	127.4(2)
C7-C6-Si1	122.5(2)
C8-C7-C6	107.9(2)
C8-C7-Si2	129.0(2)
C6-C7-Si2	120.3(2)
C9-C8-C7	107.6(2)
C9-C8-C19	125.4(3)
C7-C8-C19	126.4(2)
C10-C9-C8	109.8(3)
C10-C9-H9	125.6(17)
C8-C9-H9	124.5(17)
C9-C10-C6	107.9(2)
C9-C10-C22	125.7(2)
C6-C10-C22	126.0(2)
Si1-C11-H11A	113.6(18)
Si1-C11-H11B	114.8(17)
H11A-C11-H11B	107(2)
Si1-C11-H11C	110.1(17)
H11A-C11-H11C	106(2)
H11B-C11-H11C	105(2)
Si1-C12-H12A	108.7(17)
Si1-C12-H12B	112.1(18)
H12A-C12-H12B	103(2)
Si1-C12-H12C	113.7(18)
H12A-C12-H12C	113(2)
H12B-C12-H12C	106(2)

Si2-C13-H13A	109.2(17)
Si2-C13-H13B	112.7(18)
H13A-C13-H13B	104(2)
Si2-C13-H13C	113(2)
H13A-C13-H13C	103(3)
H13B-C13-H13C	115(3)
Si2-C14-H14A	108.5(17)
Si2-C14-H14B	113.6(18)
H14A-C14-H14B	107(2)
Si2-C14-H14C	114.2(19)
H14A-C14-H14C	102(2)
H14B-C14-H14C	110(3)
C16-C15-C4	111.3(2)
C16-C15-C18	109.4(3)
C4-C15-C18	111.4(2)
C16-C15-C17	109.0(3)
C4-C15-C17	108.0(2)
C18-C15-C17	107.7(3)
C15-C16-H16A	111.4(18)
C15-C16-H16B	114.3(17)
H16A-C16-H16B	105(2)
C15-C16-H16C	111.0(18)
H16A-C16-H16C	109(3)
H16B-C16-H16C	106(3)
C15-C17-H17A	111.9(18)
C15-C17-H17B	111.5(16)
H17A-C17-H17B	108(2)
C15-C17-H17C	110.3(17)
H17A-C17-H17C	110(2)
H17B-C17-H17C	105(2)
C15-C18-H18A	111.5(17)
C15-C18-H18B	108.4(17)
H18A-C18-H18B	109(2)
C15-C18-H18C	111.3(19)
H18A-C18-H18C	111(2)
H18B-C18-H18C	106(2)
C8-C19-C21	113.7(3)
C8-C19-C20	109.1(3)
C21-C19-C20	110.2(3)
C8-C19-H19A	109.4(16)
C21-C19-H19A	105.9(17)
C20-C19-H19A	108.4(16)
C19-C20-H20A	112.9(17)
C19-C20-H20B	113.0(18)
H20A-C20-H20B	105(2)
C19-C20-H20C	108.5(19)
H20A-C20-H20C	112(3)
H20B-C20-H20C	105(3)
C19-C21-H21A	109.6(18)
C19-C21-H21B	108.8(19)
H21A-C21-H21B	109(2)
C19-C21-H21C	108.6(19)
H21A-C21-H21C	110(3)
H21B-C21-H21C	111(3)
C10-C22-C24	113.1(3)
C10-C22-C23	110.0(2)
C24-C22-C23	110.0(3)
C10-C22-H22	109.7(17)
C24-C22-H22	105.9(17)
C23-C22-H22	108.0(17)
C22-C23-H23A	109.7(16)
C22-C23-H23B	112.1(19)
H23A-C23-H23B	110(2)
C22-C23-H23C	109.9(17)
H23A-C23-H23C	109(2)
H23B-C23-H23C	105(2)
C22-C24-H24A	111.1(16)
C22-C24-H24B	112.6(16)
H24A-C24-H24B	105(2)
C22-C24-H24C	110.5(18)
H24A-C24-H24C	110(2)
H24B-C24-H24C	107(2)
Si4-C25A-Si3	118.5(2)
Si4-C25A-Y	94.83(18)
Si3-C25A-Y	139.3(3)
Si4-C25A-H25A	98.6
Si3-C25A-H25A	98.6
Y-C25A-H25A	98.6
Si4-C25B-Si3	114.4(6)
Si4-C25B-Y	95.4(4)
Si3-C25B-Y	141.8(6)
Si4-C25B-H25B	99.1
Si3-C25B-H25B	99.1
Y-C25B-H25B	99.1
Si3-C26-H26A	103(2)
Si3-C26-H26B	110(2)
H26A-C26-H26B	100(3)
Si3-C26-H26C	118(3)
H26A-C26-H26C	116(3)
H26B-C26-H26C	108(3)
Si3-C27-H27A	107.8(19)
Si3-C27-H27B	112.2(19)
H27A-C27-H27B	110(3)
Si3-C27-H27C	112(2)
H27A-C27-H27C	109(3)
H27B-C27-H27C	107(3)
Si3-C28-H28A	106(2)
Si3-C28-H28B	111.4(19)

H28A-C28-H28B	107(3)	Si4-C30-H30A	109(2)
Si3-C28-H28C	111(2)	Si4-C30-H30B	110(2)
H28A-C28-H28C	112(3)	H30A-C30-H30B	109(3)
H28B-C28-H28C	109(3)	Si4-C30-H30C	113(2)
Si4-C29-Y	83.34(11)	H30A-C30-H30C	118(3)
Si4-C29-H29A	114.6(18)	H30B-C30-H30C	97(3)
Y-C29-H29A	72.8(18)	Si4-C31-H31A	112(2)
Si4-C29-H29B	103.7(18)	Si4-C31-H31B	108(2)
Y-C29-H29B	172.3(18)	H31A-C31-H31B	113(3)
H29A-C29-H29B	106(2)	Si4-C31-H31C	112.8(19)
Si4-C29-H29C	115.6(16)	H31A-C31-H31C	103(3)
H29A-C29-H29C	111(2)	H31B-C31-H31C	109(3)
H29B-C29-H29C	104(2)		

[a] CpA is the centroid of atoms C1, C2, C3, C4 and C5
[b] PlnA is the best plane through atoms C1, C2, C3, C4 and C5
[c] CpB is the centroid of atoms C6, C7, C8, C9 and C10
[d] PlnB is the best plane through atoms C6, C7, C8, C9 and C10
[a] Cen is the centroid of atoms Si4 and C29

Table 12. Crystal Data and Structure Analysis Details for dlz6 – [$(Me_2Si)_2(\eta^5$-4-CMe_3-$C_5H_2)(\eta^5$-3,5-CMe_2H-$C_5H_1)$]$Ta(CH_2)CH_3$.

Empirical formula	$C_{26}H_{43}Si_2Ta$	
Formula weight	592.73	
Crystallization solvent	diethyl ether / pentane	
Crystal shape	twinned plate	
Crystal color	golden orange	
Crystal size	0.07 x 0.18 x 0.19 mm	
Data Collection		
Type of diffractometer	CAD-4	
Wavelength	0.71073 Å MoKα	
Data collection temperature	84 K	
Theta range for 25 reflections used in lattice determination	13 to 18°	
Unit cell dimensions	a = 8.508(3) Å	α= 90°
	b = 16.123(6) Å	β= 112.39(3)°
	c = 9.984(3) Å	γ = 90°
Volume	1266.3(8) $Å^3$	
Z	2	
Crystal system	monoclinic	
Space group	$P2_1/m$ (# 11)	

Density (calculated)	1.555 g/cm^3
F(000)	600
Theta range for data collection	2.21 to 25°
Completeness to theta = 25°	71.5 %
Index ranges	$-10 \leq h \leq 10, -19 \leq k \leq 19, -11 \leq l \leq 11$
Data collection scan type	ω-scan
Reflections collected	11978
Independent reflections	1651 [R_{int}= 0.050; GOF_{merge}= 1.58]
Reflections > 2σ(I)	1576
Average σ(I)/(net I)	0.0256
Absorption coefficient	4.445 mm^{-1}
Absorption correction	ψ-scan
Max. and min. transmission	1.16 and 0.84
Number of standards	3 reflections measured every 75 min
Decay of standards	0.5%

Structure Solution and Refinement

Primary solution method	direct methods
Secondary solution method	difference map
Hydrogen placement	calculated
Refinement method	full-matrix least-squares on F^2
Data / restraints / parameters	1651 / 0 / 140
Treatment of hydrogen atoms	not refined, U_{iso} fixed at 120% U_{eq} of attached atom
Goodness-of-fit on F^2	2.385
Final R indices [I>2σ(I), 1576 reflections]	R1 = 0.0274, wR2 = 0.0659
R indices (all data)	R1 = 0.0297, wR2 = 0.0664
Type of weighting scheme used	sigma
Weighting scheme used	$w=1/\sigma^2(Fo^2)$
Max shift/error	0.017
Average shift/error	0.001
Largest diff. peak and hole	1.577 and -0.823 $e \cdot Å^{-3}$

Programs Used

Cell refinement	CAD-4 Software (Enraf-Nonius, 1989)
Data collection	CAD-4 Software (Enraf-Nonius, 1989)
Data reduction	CRYM (Duchamp, 1964)
Structure solution	Bruker SHELXTL v5.1

Structure refinement Bruker SHELXTL v5.1

Special Refinement Details

The crystals grow as twinned, golden orange plates. Samples were mounted on a glass fibers with Paratone-N oil. Finally a crystal was found for which a unit cell could be determined. Although this crystal was also twinned, orientation matrixes were obtained for both twin components. The reflection indices (h k l) and (h' k' l') for the two twin components are related as:

$$(h' \quad k' \quad l') = \begin{pmatrix} 1 & 0 & 0.65 \\ 0 & -1 & 0 \\ 0 & 0 & -1 \end{pmatrix} \times \begin{pmatrix} h \\ k \\ l \end{pmatrix}$$

The twin may be described as a reflection twin across the [1 0 0] plane ; the corresponding reciprocal space description is a rotation twin about the $(1\ 0\ 0)^*$ axis as this axis is normal to the [1 0 0] plane. Since by the monoclinic symmetry, (h k l) is equivalent to (h k̄ l), Two interpretations of the reciprocal lattice overlap are shown as additional figures. Data were collected with 1.0° ω-scans. Data which agreed poorly in a preliminary merging were recollected. The individual backgrounds were replaced by a background function of 2θ derived from those reflections with $I < 3\sigma(I)$. The first attempts at refinement included all measured reflections; those reflections which presumably included overlap between the two twin components were given two sets of indices corresponding to the two twins. A twin parameter relating the relative contributions of the two components was included in the least squares matrix. Various criteria were used to identified overlapping reflections. However none of these approaches were particularly successful, presumably since most reflections do not perfectly coincide. The measured intensities of these reflections would then not reflect the true sum of the two contributing components. Finally, all reflections with $l = 3$, 6, 9 and 11 were removed from the dataset; these reflections transform with h' deviating from integral values by 0.05, 0.10, 0.15 and 0.15, respectively. Therefore only the $(h\ k\ 0)$ reflections, which overlap perfectly with the $(h\ -k\ 0)$ reflections of the twin, contain any twin contribution. The $(h\ -k\ 0)$ reflections were added as the symmetry equivalent $(h\ k\ 0)$ form. The GOF_{merge} was 1.58 (1651 multiples) in point group 2/m; due to the high redundancy of the data, there were no duplicates from which to calculate R_{merge}. Ψ–scan data were used for the absorption correction. There was 0.5% linear decay. No outlier reflections were omitted from the refinement.

Weights w are calculated as $1/\sigma^2(F_o^2)$; variances ($\sigma^2(F_o^2)$) were derived from counting statistics plus an additional term, $(0.014I)^2$; variances of the merged data were obtained by propagation of error plus another additional term, $(0.014\langle I\rangle)^2$. The refinement of F^2 is as always against all reflections. The weighted R-factor wR and goodness of fit S are based on F^2, conventional R-factors R are based on F, with F set to zero for negative F^2. The threshold expression of $F^2 > 2\sigma(F^2)$ is

used only for calculating R-factors(gt) etc. and is not relevant to the choice of reflections for refinement.

The molecule lies on a mirror plane containing the Ta and bisecting both Cp rings; there is 1/2 molecule in the asymmetric unit. The *t*-butyl group is disordered about the mirror plane, as is seen in similar compounds. Splitting the three methyl carbon atoms into two sites each did not improve the model, so these atoms were left at single sites with elongated displacement ellipsoids. Unfortunately, the mirror plane also confuses the $=CH_2$ and $-CH_3$ groups bound to the Ta. The principal axis of the displacement ellipsoid is perpendicular to the Ta to C bond. The hydrogen atoms on this C15 were modeled with three calculated sites, as a normal CH_3 group with one hydrogen atom pointing up with population one and the other two hydrogen atoms with population _. All hydrogen atoms were placed at calculated positions with U_{iso}'s fixed at 120% of the U_{eq} of the attached atom.

The minor twin component refined to a fractional population of 0.168(4). There are only two peaks greater than |1| $e{\cdot}Å^{-3}$ in the final difference map: 1.57 $e{\cdot}Å^{-3}$ (1.75Å from H6) and 1.07 $e{\cdot}Å^{-3}$ (0.79Å from H6).

Table 13. Bond lengths [Å] and angles [°] for dlz6 – $[(Me_2Si)_2(\eta^5\text{-}4\text{-}CMe_3\text{-}C_5H_2)(\eta^5\text{-}3,5\text{-}CMe_2H\text{-}C_5H_1)]Ta(CH_2)CH_3$.

Ta-CpA [a]	2.129	C7-H7A	0.9800
Ta-CpB [c]	2.139	C7-H7B	0.9800
Ta···PlnA [b]	2.117(4)	C7-H7C	0.9800
Ta···PlnB [d]	2.126(4)	C8-H8A	0.9800
Ta-C15	2.155(7)	C8-H8B	0.9800
Ta-C4	2.360(6)	C8-H8C	0.9800
Ta-C1	2.369(5)	C9-C10	1.440(10)
Ta-C2	2.464(5)	C9-C11	1.479(17)
Ta-C5	2.514(5)	C10-H10A	0.9800
Ta-C6	2.549(7)	C10-H10B	0.9800
Ta-C3	2.579(7)	C10-H10C	0.9800
Si-C8	1.856(6)	C11-H11A	0.9600
Si-C7	1.857(7)	C11-H11B	0.9601
Si-C1	1.874(6)	C12-C13	1.513(8)
Si-C4	1.891(5)	C12-C14	1.524(8)
C1-C2	1.418(8)	C12-H12	1.0000
C1-C1[(i)]	1.449(10)	C13-H13A	0.9800
C2-C3	1.422(7)	C13-H13B	0.9800
C2-H2	0.9500	C13-H13C	0.9800
C3-C9	1.513(12)	C14-H14A	0.9800
C4-C5	1.434(8)	C14-H14B	0.9800
C4-C4[(i)]	1.448(10)	C14-H14C	0.9800
C5-C6	1.416(7)	C15-H15A	0.9800
C5-C12	1.523(7)	C15-H15B	0.9800
C6-H6	0.9500	C15-H15C	0.9800

CpA-Ta-CpB	125.4
CpA-Ta-C15	107.1
CpB-Ta-C15	107.4
PlnA-PlnB	67.0(3)
C15-Ta-C15$^{(i)}$	99.3(4)
C8-Si-C7	106.9(3)
C8-Si-C1	108.1(3)
C7-Si-C1	116.5(3)
C8-Si-C4	116.4(3)
C7-Si-C4	116.7(3)
C1-Si-C4	91.9(2)
C2-C1-C1$^{(i)}$	106.8(3)
C2-C1-Si	124.8(4)
C1$^{(i)}$-C1-Si	122.55(17)
C1-C2-C3	110.1(5)
C1-C2-H2	124.9
C3-C2-H2	124.9
C2$^{(i)}$-C3-C2	106.0(7)
C2-C3-C9	126.5(4)
C5-C4-C4$^{(i)}$	107.5(3)
C5-C4-Si	125.4(4)
C4$^{(i)}$-C4-Si	122.23(16)
C6-C5-C4	107.7(5)
C6-C5-C12	125.2(5)
C4-C5-C12	126.7(5)
C5-C6-C5$^{(i)}$	109.4(7)
C5-C6-H6	125.3
Si-C7-H7A	109.5
Si-C7-H7B	109.5
H7A-C7-H7B	109.5
Si-C7-H7C	109.5
H7A-C7-H7C	109.5
H7B-C7-H7C	109.5
Si-C8-H8A	109.5
Si-C8-H8B	109.5
H8A-C8-H8B	109.5
Si-C8-H8C	109.5
H8A-C8-H8C	109.5
H8B-C8-H8C	109.5
C10-C9-C10$^{(i)}$	107.3(15)
C10-C9-C11	106.5(9)
C10-C9-C3	110.9(6)
C11-C9-C3	114.3(8)
C9-C10-H10A	109.5
C9-C10-H10B	109.5
H10A-C10-H10B	109.5
C9-C10-H10C	109.5
H10A-C10-H10C	109.5
H10B-C10-H10C	109.5
C9-C11-H11A	109.6
C9-C11-H11B	109.4
H11A-C11-H11B	109.5
C13-C12-C5	110.3(5)
C13-C12-C14	109.1(4)
C5-C12-C14	112.3(5)
C13-C12-H12	108.4
C5-C12-H12	108.4
C14-C12-H12	108.4
C12-C13-H13A	109.5
C12-C13-H13B	109.5
H13A-C13-H13B	109.5
C12-C13-H13C	109.5
H13A-C13-H13C	109.5
H13B-C13-H13C	109.5
C12-C14-H14A	109.5
C12-C14-H14B	109.5
H14A-C14-H14B	109.5
C12-C14-H14C	109.5
H14A-C14-H14C	109.5
H14B-C14-H14C	109.5
Ta-C15-H15A	109.5
Ta-C15-H15B	109.5
H15A-C15-H15B	109.5
Ta-C15-H15C	109.5
H15A-C15-H15C	109.5
H15B-C15-H15C	109.5

Symmetry transformations used to generate equivalent atoms:
(i) x,-y+1/2,z

[a] CpA is the centroid of atoms C1, C2, C3, C4 and C5
[b] PlnA is the best plane through atoms C1, C2, C3, C4 and C5
[c] CpB is the centroid of atoms C6, C7, C8, C9 and C10
[d] PlnB is the best plane through atoms C6, C7, C8, C9 and C10

Table 14. Crystal Data and Structure Analysis Details for dlz7 - $Me_2Si(C_5H_4)_2TaMe_3$.

Empirical formula	$C_{15}H_{23}SiTa$	
Formula weight	412.37	
Crystallization solvent	diethyl ether	
Crystal shape	irregular chunk	
Crystal color	colorless	
Crystal size	0.09 x 0.15 x 0.41 mm	
Data Collection		
Type of diffractometer	CAD-4	
Wavelength	0.71073 Å MoKα	
Data collection temperature	84 K	
Theta range for 25 reflections used in lattice determination	16 to 19°	
Unit cell dimensions	a = 7.722(3) Å b = 15.010(4) Å c = 12.620(4) Å	α= 90° β= 90.54(3)° γ = 90°
Volume	1462.7(8) $Å^3$	
Z	4	
Crystal system	monoclinic	
Space group	P $2_1/n$ (# 14)	
Density (calculated)	1.873 g/cm^3	
F(000)	800	
Theta range for data collection	1.5 to 30°	
Completeness to theta = 30°	100.0 %	
Index ranges	$-10 \le h \le 0, -21 \le k \le 21, -17 \le l \le 17$	
Data collection scan type	ω-scan	
Reflections collected	11938	
Independent reflections	4257 [R_{int}= 0.0234; GOF_{merge}= 1.73]	
Reflections > 2σ(I)	3974	
Average σ(I)/(net I)	0.0270	
Absorption coefficient	7.574 mm^{-1}	
Absorption correction	ψ-scan	
Max. and min. transmission	1.12 and 0.88	
Number of standards	3 reflections measured every 75 min	

Decay of standards	no correction applied

Structure Solution and Refinement

Primary solution method	direct methods
Secondary solution method	difference map
Hydrogen placement	calculated
Refinement method	full-matrix least-squares on F^2
Data / restraints / parameters	4257 / 0 / 224
Treatment of hydrogen atoms	coordinates refined, U_{iso} fixed at 120% U_{eq} of attached atom
Goodness-of-fit on F^2	2.555
Final R indices [I>2σ(I), 3974 reflections]	R1 = 0.0350, wR2 = 0.0819
R indices (all data)	R1 = 0.0377, wR2 = 0.0823
Type of weighting scheme used	sigma
Weighting scheme used	$w=1/\sigma^2(Fo^2)$
Max shift/error	0.051
Average shift/error	0.001
Extinction coefficient	0.00133(16)
Largest diff. peak and hole	3.186 and -3.035 e·Å^{-3}

Programs Used

Cell refinement	CAD-4 Software (Enraf-Nonius, 1989)
Data collection	CAD-4 Software (Enraf-Nonius, 1989)
Data reduction	CRYM (Duchamp, 1964)
Structure solution	Bruker SHELXTL v5.1
Structure refinement	Bruker SHELXTL v5.1

Special Refinement Details

An irregular chunk was cut from a colorless blob and mounted on a glass fiber with Paratone-N oil. Data were collected with 1.1° ω-scans. Data which agreed poorly in a preliminary merging were recollected. The crystal turned brown during irradiation. The individual backgrounds were replaced by a background function of 2θ derived from those reflections with $I < 8\sigma(I)$. The GOF_{merge} was 1.73 (3408 multiples) in point group 2/m; R_{merge} was 0.0207 for 3088 duplicates with $F_o > 0$. Ψ–scan data were used for the absorption correction. The three check reflections behaved erratically (or anisotrpically), showing changes of –2.6, -1.5 and 3.3% during data collection; accordingly, no correction was applied. Some reflections were lost due to a power failure (11589 – 12116). The last reflections collected merged poorly and so the range 8900 – 12466 was deleted from the data

file, leaving 8899 reflections. As these were redundant data or recollections of poorly merging multiples, there are no gaps in the data.

Weights w are calculated as $1/\sigma^2(F_o^2)$; variances ($\sigma^2(F_o^2)$) were derived from counting statistics plus an additional term, $(0.014I)^2$; variances of the merged data were obtained by propagation of error plus another additional term, $(0.014\langle I\rangle)^2$. The refinement of F^2 is as always against all reflections. The weighted R-factor wR and goodness of fit S are based on F^2, conventional R-factors R are based on F, with F set to zero for negative F^2. The threshold expression of $F^2 > 2\sigma(F^2)$ is used only for calculating R-factors(gt) etc. and is not relevant to the choice of reflections for refinement.

There is one molecule in the asymmetric unit. Although the β angle of 90.54(3)° is ~90° and the molecule possesses internal symmetry, the structure is clearly monoclinic. The 0 1 1 reflection was an outlier and omitted from the refinement. A SHELXL extinction coefficient refined to 0.00133(16). There are a number of large peaks in the final difference map; the three greater than |1.5| e·Å^{-3} are all near the Ta atom: 3.19 e·Å^{-3} at 0.70 Å from Ta, -3.04 e·Å^{-3} at 0.65 Å from Ta and 2.93 e·Å^{-3} at 0.71 Å from Ta.

Table 15. Bond lengths [Å] and angles [°] for dlz7 - $Me_2Si(C_5H_4)_2TaMe_3$.

Ta-CpA [a]	2.125	C8-C9	1.398(8)
Ta-CpB [c]	2.125	C8-H8	0.89(7)
Ta···PlnA [b]	2.124	C9-C10	1.407(7)
Ta···PlnB [d]	2.125	C9-H9	0.98(7)
Ta-C14	2.277(6)	C10-H10	0.90(7)
Ta-C13	2.300(6)	C11-H11A	0.95(7)
Ta-C15	2.310(6)	C11-H11B	0.92(7)
Si-C11	1.846(6)	C11-H11C	0.88(7)
Si-C12	1.856(6)	C12-H12A	0.97(7)
Si-C1	1.869(5)	C12-H12B	0.81(7)
Si-C6	1.874(5)	C12-H12C	1.00(6)
C1-C5	1.426(7)	C13-H13A	0.87(8)
C1-C2	1.432(7)	C13-H13B	0.95(7)
C2-C3	1.425(7)	C13-H13C	0.87(7)
C2-H2	0.82(7)	C14-H14A	0.86(8)
C3-C4	1.403(8)	C14-H14B	0.95(8)
C3-H3	0.90(7)	C14-H14C	0.94(8)
C4-C5	1.419(7)	C15-H15A	1.03(7)
C4-H4	0.93(7)	C15-H15B	1.00(8)
C5-H5	0.95(6)	C15-H15C	0.91(8)
C6-C7	1.420(7)		
C6-C10	1.436(7)	CpA-Ta-CpB	128.3
C7-C8	1.420(7)	CpA-Ta-C13	99.0
C7-H7	0.77(6)	CpA-Ta-C14	115.8
		CpA-Ta-C15	98.2

CpB-Ta-C13	98.2	C8-C9-C10	108.5(5)
CpB-Ta-C14	115.9	C8-C9-H9	122(4)
CpB-Ta-C15	98.6	C10-C9-H9	129(4)
PlnA-PlnB	55.0(2)	C9-C10-C6	108.9(5)
C14-Ta-C13	69.8(3)	C9-C10-H10	129(4)
C14-Ta-C15	70.6(3)	C6-C10-H10	122(4)
C13-Ta-C15	140.3(2)	Si-C11-H11A	112(4)
C11-Si-C12	115.7(3)	Si-C11-H11B	109(4)
C11-Si-C1	111.8(2)	H11A-C11-H11B	103(6)
C12-Si-C1	111.9(2)	Si-C11-H11C	106(4)
C11-Si-C6	111.9(3)	H11A-C11-H11C	112(6)
C12-Si-C6	110.0(2)	H11B-C11-H11C	115(6)
C1-Si-C6	93.4(2)	Si-C12-H12A	109(4)
C5-C1-C2	105.7(4)	Si-C12-H12B	113(5)
C5-C1-Si	124.5(4)	H12A-C12-H12B	115(6)
C2-C1-Si	124.2(4)	Si-C12-H12C	108(4)
C3-C2-C1	109.1(4)	H12A-C12-H12C	108(5)
C3-C2-H2	124(5)	H12B-C12-H12C	104(6)
C1-C2-H2	127(5)	Ta-C13-H13A	119(5)
C4-C3-C2	107.8(5)	Ta-C13-H13B	114(4)
C4-C3-H3	125(4)	H13A-C13-H13B	102(6)
C2-C3-H3	127(4)	Ta-C13-H13C	115(5)
C3-C4-C5	108.0(5)	H13A-C13-H13C	100(7)
C3-C4-H4	129(4)	H13B-C13-H13C	104(6)
C5-C4-H4	123(4)	Ta-C14-H14A	109(5)
C4-C5-C1	109.4(4)	Ta-C14-H14B	112(5)
C4-C5-H5	124(4)	H14A-C14-H14B	98(6)
C1-C5-H5	127(4)	Ta-C14-H14C	124(5)
C7-C6-C10	105.6(4)	H14A-C14-H14C	113(7)
C7-C6-Si	124.4(4)	H14B-C14-H14C	99(6)
C10-C6-Si	124.1(4)	Ta-C15-H15A	111(4)
C6-C7-C8	109.3(5)	Ta-C15-H15B	101(4)
C6-C7-H7	125(5)	H15A-C15-H15B	96(5)
C8-C7-H7	125(5)	Ta-C15-H15C	106(5)
C9-C8-C7	107.6(5)	H15A-C15-H15C	104(6)
C9-C8-H8	130(4)	H15B-C15-H15C	138(6)
C7-C8-H8	123(4)		

[a] CpA is the centroid of atoms C1, C2, C3, C4 and C5
[b] PlnA is the best plane through atoms C1, C2, C3, C4 and C5
[c] CpB is the centroid of atoms C6, C7, C8, C9 and C10
[d] PlnB is the best plane through atoms C6, C7, C8, C9 and C10

Table 16. Crystal Data and Structure Analysis Details for dlz8 - [$(Me_2Si)_2(\eta^5$-4-CMe_3-$C_5H_2)(\eta^2$-3,5-CMe_2H-$C_5H_1)$]$TaMe_3$.

Empirical formula	$C_{27}H_{46}Si_2Ta$
Formula weight	607.77
Crystallization solvent	diethyl ether / petroleum ether
Crystal shape	tapered block
Crystal color	tangerine
Crystal size	0.19 x 0.28 x 0.33 mm
Data Collection	
Preliminary photograph(s)	rotation
Type of diffractometer	Bruker SMART 1000 ccd
Wavelength	0.71073 Å MoKα
Data collection temperature	98 K
Theta range for 7898 reflections used in lattice determination	2.4 to 28.5°
Unit cell dimensions	a = 16.9762(8) Å α= 90° b = 16.2378(8) Å β= 90° c = 9.8844(5) Å γ = 90°
Volume	2724.7(2) $Å^3$
Z	4
Crystal system	orthorhombic
Space group	*Pnma* (# 62)
Density (calculated)	1.482 g/cm^3
F(000)	1236
Theta range for data collection	2.38 to 28.54°
Completeness to theta = 28.54°	96.6 %
Index ranges	$-22 \le h \le 22, -21 \le k \le 21, -13 \le l \le 12$
Data collection scan type	ω scans at 6 fixed φ values
Reflections collected	46479
Independent reflections	3468 [R_{int}= 0.0698]
Reflections > 2σ(I)	3219
Average σ(I)/(net I)	0.0216
Absorption coefficient	4.134 mm^{-1}
Absorption correction	none
Number of standards	first scans recollected at end of runs
Decay of standards	within counting statistics

Structure Solution and Refinement

Primary solution method	direct methods
Secondary solution method	difference map
Hydrogen placement	calculated
Refinement method	full-matrix least-squares on F^2
Data / restraints / parameters	3468 / 0 / 157
Treatment of hydrogen atoms	not refined, U_{iso} fixed at 120% U_{eq} of attached atom
Goodness-of-fit on F^2	2.547
Final R indices [I>2σ(I), 3219 reflections]	R1 = 0.0450, wR2 = 0.1515
R indices (all data)	R1 = 0.0479, wR2 = 0.1545
Type of weighting scheme used	sigma
Weighting scheme used	$w=1/[\sigma^2(F_o^2) + (0.05P)^2]$
Max shift/error	0.020
Average shift/error	0.001
Largest diff. peak and hole	10.876 and -4.558 e·Å^{-3}

Programs Used

Cell refinement	Bruker SAINT v6.02
Data collection	Bruker SMART v5.606
Data reduction	Bruker SAINT v6.02
Structure solution	Bruker SHELXTL v5.1
Structure refinement	Bruker SHELXTL v5.1

Special Refinement Details

A tapered block was cut from a large irregular lumpish tangerine-colored crystal and was mounted on a glass fiber with Paratone-N oil. Six runs of data were collected with 18 second long, –0.25° wide ω–scans at six values of φ (0, 120, 240, 60, 180, 90 and 300°) with the detector 5 cm (nominal) distant at a θ of -28°. The initial cell for data reduction was calculated from just under 1000 reflections chosen from throughout the data frames. For data processing with SAINT v6.02, all defaults were used, except: a fixed box size of 1.8 x 1.8 x 0.6 was used, profiles for the nine detector areas were blended, periodic orientation matrix updating was disabled, the instrument error was set to zero, no Laue class integration restraints were used, and for the post-integration global least squares refinement, no constraints were applied. No decay correction was needed. A data set corrected with SADABS v. 2.0 (beta) showed no improvement and consequently was not used. The data were intense and a weighting scheme of $w=1/[\sigma^2(F_o^2) + (0.05P)^2]$ was used, where $P = [2F_c^2 + \max(F_o^2,0)] / 3$.

There is 1/2 molecule in the asymmetric unit; the molecule lies on the mirror plane (Wyckoff site *c*). The mirror plane bisects both cyclopentadienyl rings and contains five atoms: Ta, C3 and C6 (cyclopentadienyl carbons), C15 (central tantalum methyl carbon), and C16 (*t*-butyl carbon).

The three methyl carbons on the *t*-butyl group are disordered about the mirror plane; consequently the population ratio is 50:50. This disorder is common in similar *t*-butyl substituted metallocenes. In particular this compound is essentially isostructural with the trimethysilyl-substituted analog, TMSThpTaMe$_3$ (PJC 22). These structures differ in the orientation of the 4-substituent on the cyclopentadienyl ring; in the latter case, one of the silyl-methyl bonds is oriented towards the center of the metallocene wedge. The orientation of this substituent is rotated 180° with respect to the *t*-butyl substituent of this structure.

No reflections were specifically omitted from the final processed dataset; 2369 reflections were rejected, with 50 space group-absence violations, 218 inconsistent equivalents and no reflections suppressed. Refinement of F^2 was against all reflections. The weighted R-factor (*w*R) and goodness of fit (S) are based on F^2, conventional R-factors (R) are based on F, with F set to zero for negative F^2. The threshold expression of $F^2 > 2\sigma(F^2)$ is used only for calculating R-factors(gt) etc. and is not relevant to the choice of reflections for refinement.

This dataset is typical for a tantalum containing compound on the CCD. There are many large peaks in the final difference map; the eight greater than |1| e·Å^{-3} are: 10.88, -4.56, -1.67, 1.61, -1.60 and 1.19 e·Å^{-3} at 0.55 to 1.37Å from Ta, 1.01 e·Å^{-3} at 0.47Å from C10 and 1.01 e·Å^{-3} at 0.84Å from C4.

Table 17. Bond lengths [Å] and angles [°] for dlz8 - [(Me$_2$Si)$_2$(η^5-4-CMe$_3$-C$_5$H$_2$)(η^2-3,5-CMe$_2$H-C$_5$H$_1$)]TaMe$_3$.

Ta-C1	2.392(4)	C1-C2	1.422(6)
Ta-C2	2.484(4)	C1-C1^i	1.458(9)
Ta-C3	2.593(7)	C2-C3	1.423(6)
Ta-C4	2.465(4)	C2-H2	0.9300
Ta-C14	2.215(6)	C3-C16	1.518(9)
Ta-C15	2.222(7)	C4-C5	1.423(6)
Ta···PlnA [a]	2.140(3)	C4-C4^i	1.499(9)
Ta···PlnB [b]	2.129(7)	C5-C6	1.408(5)
Ta-CpA [c]	2.150	C5-C11	1.518(6)
Ta···CpB [d]	2.895	C6-H6	0.9300
Ta-Cen [e]	2.349	C7-H7A	0.9600
Si-C1	1.862(4)	C7-H7B	0.9600
Si-C4	1.863(4)	C7-H7C	0.9600
Si-C7	1.870(6)	C8-H8A	0.9600
Si-C8	1.871(6)	C8-H8B	0.9600
		C8-H8C	0.9600

C9A-C16	1.663(12)
C9A-H9A	0.9600
C9A-H9B	0.9600
C9A-H9C	0.9600
C10-C16	1.493(14)
C10-H10A	0.9600
C10-H10B	0.9600
C10-H10C	0.9600
C9B-C16	1.447(13)
C9B-H9D	0.9600
C9B-H9E	0.9600
C9B-H9F	0.9600
C11-C13	1.532(6)
C11-C12	1.534(6)
C11-H11	0.9800
C12-H12A	0.9600
C12-H12B	0.9600
C12-H12C	0.9600
C13-H13A	0.9600
C13-H13B	0.9600
C13-H13C	0.9600
C14-H14A	0.9600
C14-H14B	0.9600
C14-H14C	0.9600
C15-H15A	0.9684
C15-H15B	0.9563

C14-Ta-C14^{i}	113.4(4)
C14-Ta-C15	75.15(16)
PlnA-PlnB	112.75(24)
CpA-Ta···CpB	115.7
CpA-Ta-Cen	97.6
CpA-Ta-C14	103.3
CpA-Ta-C15	176.8
Cen-Ta-C14	117.7
Cen-Ta-C15	85.6
C1-Si-C4	93.7(2)
C1-Si-C7	115.4(3)
C4-Si-C7	115.9(3)
C1-Si-C8	108.1(2)
C4-Si-C8	116.6(2)
C7-Si-C8	106.8(4)
C2-C1-C1^{i}	106.3(3)
C2-C1-Si	125.1(3)
C1^{i}-C1-Si	123.17(14)
C1-C2-C3	111.4(4)
C1-C2-H2	124.3
C3-C2-H2	124.3
C2^{i}-C3-C2	104.7(5)
C2-C3-C16	127.4(3)
C5-C4-C4^{i}	106.1(3)
C5-C4-Si	129.1(3)
C4^{i}-C4-Si	122.40(14)
C6-C5-C4	109.5(4)
C6-C5-C11	125.6(4)
C4-C5-C11	124.9(4)
C5-C6-C5^{i}	108.6(5)
C5-C6-H6	125.7
Si-C7-H7A	109.5
Si-C7-H7B	109.5
H7A-C7-H7B	109.5
Si-C7-H7C	109.5
H7A-C7-H7C	109.5
H7B-C7-H7C	109.5
Si-C8-H8A	109.5
Si-C8-H8B	109.5
H8A-C8-H8B	109.5
Si-C8-H8C	109.5
H8A-C8-H8C	109.5
H8B-C8-H8C	109.5
C16-C9A-H9A	109.5
C16-C9A-H9B	109.5
H9A-C9A-H9B	109.5
C16-C9A-H9C	109.5
H9A-C9A-H9C	109.5
H9B-C9A-H9C	109.5
C16-C10-H10A	109.5
C16-C10-H10B	109.5
H10A-C10-H10B	109.5
C16-C10-H10C	109.5
H10A-C10-H10C	109.5
H10B-C10-H10C	109.5
C16-C9B-H9D	109.5
C16-C9B-H9E	109.5
H9D-C9B-H9E	109.5
C16-C9B-H9F	109.5
H9D-C9B-H9F	109.5
H9E-C9B-H9F	109.5
C5-C11-C13	111.0(4)
C5-C11-C12	112.8(4)
C13-C11-C12	109.0(4)
C5-C11-H11	108.0
C13-C11-H11	108.0
C12-C11-H11	108.0
C11-C12-H12A	109.5
C11-C12-H12B	109.5
H12A-C12-H12B	109.5
C11-C12-H12C	109.5

H12A-C12-H12C	109.5	H14A-C14-H14C	109.5
H12B-C12-H12C	109.5	H14B-C14-H14C	109.5
C11-C13-H13A	109.5	Ta-C15-H15A	109.2
C11-C13-H13B	109.5	Ta-C15-H15B	109.7
H13A-C13-H13B	109.5	H15A-C15-H15B	109.1
C11-C13-H13C	109.5	C9B-C16-C10^{i}	111.3(10)
H13A-C13-H13C	109.5	C9B-C16-C3	113.6(6)
H13B-C13-H13C	109.5	C10-C16-C3	108.5(7)
Ta-C14-H14A	109.5	C9B-C16-C9A^{i}	108.5(11)
Ta-C14-H14B	109.5	C10-C16-C9A	105.2(9)
H14A-C14-H14B	109.5	C3-C16-C9A	109.4(5)
Ta-C14-H14C	109.5		

Symmetry transformations used to generate equivalent atoms:
(i) x,-y+1/2,z

[a] PlnA is the best plane through atoms C1, C2, C3, C1^{i} and C2^{i}
[b] PlnB is the best plane through atoms C4, C5, C6, C4^{i} and C5^{i}
[c] CpA is the centroid of atoms C1, C2, C3, C1^{i} and C2^{i}
[d] CpB is the centroid of atoms C4, C5, C6, C4^{i} and C5^{i}
[e] Cen is the centroid of atoms C4 and C4^{i}